The copyright of this thesis vests in the author. No quotation from it or information derived from it is to be published without full acknowledgement of the source. The thesis is to be used for private study or non-commercial research purposes only.

Published by the University of Cape Town (UCT) in terms of the non-exclusive license granted to UCT by the author.

University of Cape Town

CUT-OFF LOW PRESSURE SYSTEMS AND EXTREME RAINFALL OVER SOUTH AFRICA

Andrew Thomas Singleton

University of Cape Town

Dissertation submitted to the Faculty of Science,

University of Cape Town

for the Degree Doctor of Philosophy

UT 551.46 SING
77872S

University of Cape Town

Abstract

This thesis is an investigation of cut-off low pressure systems over South Africa. These weather systems have been responsible for many of the flooding disasters that have affected South Africa, particularly the coastal regions, over recent decades. The thesis has two main objectives, namely, to construct a 30-year climatology of cut-off lows over South Africa, and to further understanding of the evolution of the low-level flow that leads to these systems producing extreme quantities of rainfall.

The 30-year climatology is based on cut-off lows that occur over subtropical southern Africa and the surrounding oceans in the NCEP (National Center for Environmental Prediction) re-analysis 300 hPa geopotential height. The frequency, seasonality, interannual variability, location, duration and size of these systems is investigated. It is found that on average, 11 such systems occur over this region each year, and are most common in the austral autumn, with a relative peak in numbers in the austral spring over southwest South Africa. There is some indication of a relationship with ENSO (El Niño Southern Oscillation), with mature phase La Niña years being associated with above average occurrences. In addition a relationship with the SAO (Semi-Annual Oscillation) is proposed, with changes in the strength of the SAO resulting in winter becoming the most common season for these systems, and northeast South Africa becoming the most common location. Cut-off lows are found to typically last 2-4 days over the region. The most common size is 800-1200km in autumn/winter and 400-800km in spring/summer.

University of Cape Town

Two case studies of cut-off lows that resulted in extreme coastal rainfall are examined. The first occurred in August 2002 and resulted in four times the monthly climatological rainfall over 24 hours in East London, with a relatively small cut-off low over the Western Cape embedded in a cold trough aloft. The second case investigated is from March 2003, when a large, deep cut-off low over the south coast resulted in extreme rainfall in the coastal regions and more than nine times the monthly average fell in the town of Montagu in 24 hours resulting in flash flooding.

The cases were simulated using the limited area model, MM5. It is found that in both cases, a strong onshore low-level jet (LLJ) forms as a result of a steepening pressure gradient. Vigorous convection is found to be associated with the right-hand (looking downstream) and leading edges of the LLJ. At the leading edge, moist ascent is enhanced as the LLJ impinges on the coastal topography. Back trajectories indicate that low-level air originated from relatively high maritime latitudes to the south of South Africa, and that the warm SST of the Agulhas Current may have contributed low-level moisture to these events.

University of Cape Town

Sensitivity and factor separation studies done with MM5 show that warm SST (sea surface temperature) associated with the Agulhas Current influenced the moisture availability. In the case of the East London event, the warm SST of the Agulhas Current resulted in secondary cyclogensis, which strengthened the LLJ. The topography of South Africa was found to play an important role in enhancing moist ascent at the coast, as well as determining the location of

the LLJ, and therefore the rainfall. Surface heat fluxes are shown to be important in generating low-level instability, which leads to a trough extending down the eastern seaboard of South Africa. The strong pressure gradient that develops between this trough and a ridge of high pressure to the south of South Africa leads to the formation of the LLJ.

A conceptual model is proposed to describe the evolution of the low-level flow during cut-off low events that result in extreme rainfall. This conceptual model states that surface heat fluxes warm and destabilise the lower atmosphere, leading to the extension of a trough down the eastern seaboard of South Africa, and precipitation; at the same time the topography of South Africa blocks onshore flow resulting in a steep pressure gradient between a surface ridge to the south of South Africa and the aforementioned trough and the formation of the LLJ; this LLJ advects moist air onto the coastal topography of South Africa which enhances ascent.

University of Cape Town

I declare that this dissertation is my own, unaided work, and that it has not been submitted previously as a dissertation or thesis for any degree at any other University

University of Cape Town

Acknowledgements

I would like to thank A/ Professor Chris Reason for providing supervision, and much needed motivation throughout this PhD. Additionally, thanks are due to the South African Water Research Commission and the Benguela Current Large Marine Ecosystem project for funding this research, and to my parents for providing extra money. Further thanks are due to Tobias Öhgren for use of his laptop computer for writing this Thesis. Also the following for providing moral support at various times in working towards this PhD: Jens Hauser, Dougald Hine, Anthony Baxter, Tabitha Langford, Karen van Biljon, Juliet Hermes, Adrian Webb, Frank Colberg, Regan Janz, Christine Andhoey, Michael Kopf, Jacques DuPreez, Sabine Straßburg, Lucy Wincent-Dodd, Tobias Öhgren, Marc Kuhberg, Rebecca Giles, Sofia Svenssen, Jan Schenk, Ben Ludwig, Genevieve Dewar, Brian Stewart, Raeli Bronstein, Sam Challis, James Wiltshire, Maria-Grazia Galimberti, Clara Bubenzer, Bina Wansleben, Riashna Sithaldeen and Monique Carollisen.

University of Cape Town

University of Cape Town

CONTENTS

University of Cape Town

University of Cape Town

University of Cape Town

University of Cape Town

Chapter 1

Introduction

University of Cape Town

University of Cape Town

One of the challenges in issuing warnings of extreme weather is the difficulty in accurately predicting which areas will be worst affected. A bad forecast leads to a lack of trust from the end user in future forecasts. For example, if a flood warning is issued for a particular locale, but does not actually occur, the people of that area are not so likely to take future warnings seriously. On the other hand, if no extreme weather is predicted sufficiently long before it occurs, people do not have the time to take precautionary measures.

Cut-off lows are important systems bringing extreme weather to South Africa. These weather systems have been responsible for many of the flood disasters over South Africa, which have led to loss of life and serious damage to homes and infrastructure as a result of flash flooding and very high winds. In many cases, it has been difficult for the South African Weather Service to accurately predict which areas will be worst affected. However, an approaching cut-off low provides an indication that extreme weather may be on its way, and some general warnings may be issued.

University of Cape Town

Improving the understanding of cut-off lows over this region is therefore a priority. This thesis aims to address certain issues that will contribute to an improved understanding of these weather systems. An important aspect of any weather system is its seasonality. Improving understanding therein will give an indication as to the time of year such systems may be expected to occur. In addition, the interannual variability may give an insight into any long term cycles in the frequency of cut-off lows, or perhaps more importantly an association with large scale modes of the atmosphere, which will aid prediction. This thesis attempts to address these issues by developing a

30-year climatology of cut-off lows over subtropical southern Africa and the surrounding ocean areas.

On top of this, an improved comprehension of the processes that occur resulting in extreme rainfall during a cut-off low event is required. In particular, this will aid the forecaster in determining the rainfall potential of a cut-off low system, and will also assist in determining where the extreme rainfall will occur. Furthermore, an identification of the more important processes will point to areas that should be improved in a forecast model for better forecasting of rainfall during cut-off low events.

In order to address the identification of important processes, two recent cut-off low events that were characterised by extreme rainfall are examined. These case studies are from August 2002, when the Eastern Cape coastal city of East London received more than 300mm of rain in 24 hours, almost four times the climatological average for August; and March 2003, when the town of Montagu, in the Western Cape mountains some 80km north of the coast, received 178mm of rain in 24 hours, compared to the climatological average for March of just 17.5mm. These events differed in that the cut-off low in the East London case was relatively small compared to that in the Montagu case, yet both cases resulted in large amounts of rainfall.

University of Cape Town

Unfortunately, the observational network over southern Africa is relatively sparse, with only four daily coastal radiosonde ascents and relatively few in the interior of South Africa. This lack of observations makes the study of these important weather systems difficult. Options for diagnosing these systems include re-analysis data, analysis data from global forecasting models, or mesoscale modelling. The coastal topography of

South Africa is relatively complex, which is likely to have a modulating effect on passing weather systems. Moreover, the ocean around South Africa is characterised by the warm Agulhas current, which results in a complex mesoscale structure of SST with steep gradients, particularly near to the coast. Since South Africa and the surrounding ocean are rich in mesoscale detail, mesoscale modelling represents the best choice for studying the complexities of weather systems, particularly those which result in extreme weather over small areas.

An additional advantage of mesoscale modelling is that it is possible to evaluate the contributions of particular mechanisms to the forcing of regional circulations through model sensitivity studies. In essence, by including, excluding or altering the magnitude of particular mechanisms, their contribution to the system may be evaluated.

Therefore, for South African applications, mesoscale modelling represents the most suitable choice for examining cut-off low pressure systems, and in particular the forcing of the circulation and thermal evolution near to the surface. In this thesis, synoptic overviews of the aforementioned cut-off low events are presented using data from the MRF[1] global model, and more detailed analyses using the limited area model, MM5[2], are undertaken. In addition, the contrast between the two case studies represents a good test of MM5's ability to simulated different types of cut-off low events.

It is hoped that the results of this thesis will enable forecasting of extreme rainfall during cut-off low events to be improved. This thesis is separated into eight chapters.

[1] Medium Range Forecast model – see Chapter 3
[2] PSU/NCAR Mesoscale Model, version 5 – see Chapter 3

University of Cape Town

This introductory chapter is Chapter 1. Chapter 2 presents a background of cut-off lows and the processes that may be important in the South African context, culminating in a set of research objectives for this thesis. Chapter 3 describes the data and methods used in the thesis. Chapter 4 is devoted to developing a 30-year climatology of cut-off lows over subtropical southern Africa. Chapters 5-7 concern the case studies examined in this thesis. Specifically, Chapter 5 contains a synoptic overview of the case studies, and validation of the MM5 simulations. Chapter 6 discusses the MM5 simulations with a view to identifying reasons for the heavy rainfall. In Chapter 7, the relative importance of various factors are evaluated through sensitivity and factor separation studies. Finally, Chapter 8 details the conclusions of this thesis.

University of Cape Town

Chapter 2

Literature Review and Research Objectives

University of Cape Town

University of Cape Town

2.1. Introduction

This chapter presents a background to current knowledge of cut-off low pressure systems, and their importance to extreme weather over South Africa. Their characteristic development over South Africa is discussed and several previous case studies are mentioned. In addition, the forcing mechanisms unique to South Africa, such as the very high latent heat fluxes associated with the warm Agulhas Current and its retroflection in the South West Indian Ocean, are discussed, providing motivation for the present study. In addition, the relationship between LLJs and extreme rainfall is considered, as this thesis will show the importance of LLJs in cases of extreme rainfall embedded within a cut-off low system over South Africa.

This chapter is divided into four sections following this introduction. Section 2.2 gives an overview of current knowledge of cut-off low development and presents some discussion of previous cases in South Africa. Section 2.3 presents a discussion of the relationship between SST in the South West Indian Ocean and rainfall over South Africa. Section 2.4 discusses cases of severe rainfall associated with LLJs. Finally section 2.5 summarises the chapter and describes the motivation for the present study culminating in a set of research objectives.

University of Cape Town

2.2. Cut-off low pressure systems

The traditionally accepted process for the development of a cut-off low is described by Palmén and Newton (1969), based on the earlier work of Palmén (1949), Palmén and Nagler (1949), and Hsieh (1949), as "an upper low forms from a pre-existing cold trough that is ultimately cut-off from its connection with the polar source region in the upper troposphere." In addition, Palmén and Newton (1969) discuss the observed

structure of cut-off lows, such that they are characterised by raised isentropic surfaces below, and depressed isentropic surfaces above the cyclone centre. Furthermore, these systems are characterised by a lowering of the tropopause and strong jet streaks extending around their perimeter. Therefore, cut-off lows are identifiable by closed geopotential height contours and cyclonic circulation in the upper troposphere.

Following a statistical study of cut-off lows in the Northern Hemisphere, Price and Vaughan (1992) developed a classification of these systems depending on the nature of the jet streak that leads to their formation, and classified them as 'polar', 'subtropical' and 'polar vortex'. Polar type cut-off lows are formed as a result of equatorward extensions of a polar jet and tend to become situated polewards of the jet. Subtropical cut-off lows tend to be formed by equatorward extensions of a subtropical jet, or where a split in a zonal polar jet causes a weak equatorward branch. The polar vortex type cut-off low forms from an extension of the polar vortex itself, and tend not to be advected away from the main polar vortex. Since South Africa is situated in the Southern Hemisphere subtropics, this thesis concerns cut-off lows of the subtropical type classification.

University of Cape Town

Kleinschmidt (1950a,b) was the first to suggest that cut-off lows form as a result of an intrusion of polar stratospheric high potential vorticity air into the upper troposphere. This has led many researchers to investigate these systems from a potential vorticity perspective. Hoskins et al. (1985) provide an excellent summary to the details of thinking within the potential vorticity framework and the invertibility principle for potential vorticity. The invertibility principle enables the wind and temperature distribution of the atmosphere to be determined from a knowledge of the potential

vorticity distribution. The advantages of the potential vorticity approach have allowed more detailed investigations of cut-off low pressure systems to be undertaken.

Bell and Keyser (1993) investigated the interchanges between shear and curvature potential vorticity that lead to the detachment of a potential vorticity anomaly in the upper troposphere from what they term as the stratospheric reservoir polewards of the cut-off low over the United States. These authors suggest that in the formation phase of a cut-off low, the conversion from shear to curvature potential vorticity is maximised in the left exit region of a jet upstream of the trough axis, and the conversion from curvature to shear potential vorticity is maximised on the cyclonic shear side of a jet downstream of the trough axis. This leads to a relatively symmetric distribution of the cyclonic shear and cyclonic curvature maxima, resulting in a symmetric total potential vorticity anomaly in the troposphere, and therefore a cut-off low.

In a case study of a cut-off low over the eastern United States, Bell and Bosart (1993) showed that the advection of potential vorticity above 500 hPa in a northwesterly flow from the stratospheric reservoir, in combination with an intensifying jet streak in a long wave diffluent trough led to the formation of the cut-off low. Van Delden and Neggers (2003) suggest that unstable isentropic downgliding, whereby air parcels with baroclinic instability are advected downwards on sloping isentropic surfaces, is a necessary condition for cyclonic flow to develop in the upper troposphere.

Therefore, a set of theoretical ideas exist for the formation of cut-off lows in the upper troposphere. In the South African context, Taljaard (1985) investigated ten years of cut-off lows that existed over the area bounded by 20°-38°S latitude and lines drawn

University of Cape Town

approximately 5° longitude off the west and east coasts of the continent. The study was conducted for the years 1973-1982 in order to develop an "empirical" model for the formation of cut-off lows over this region, shown in Fig. 2.1 and described briefly below.

On day 1, a long-wave trough exists between Gough and Marion Islands. The upper wind at Gough Island is southwesterly, and at Marion Island is northwesterly. A cold front is located approximately half to three quarters of the distance from Gough Island to Cape Town. Warming is observed in the upper layers at Gough Island, and soon thereafter the surface wind veers to northwesterly and pressure starts falling.

On day 2, upper winds at Gough Island veer to northwesterly, leading to the formation of an 'S-shaped' wave, and warming continues. At Marion Island, the upper wind remains northwesterly, but surface pressure begins to fall ahead of the approaching cold front.

On day 3, northwesterly flow of warm air continues at Gough Island, while at Cape Town the wind backs rapidly to southerly after the passage of the coolest air. After the passage of the cold front at Marion Island, temperature there decreases and the wind begins to back. The wave in the upper air increases in amplitude and decreases in wavelength as warm air has been advected far to the southeast of Gough Island and recurves northwards towards Cape Town in a southerly flow.

University of Cape Town

Days 4 and 5 are the mature phase of the cut-off low. At this time a warm ridge exists south of Cape Town, cutting off cold air to its northeast leading to the formation of the cut-off low. A broad northwesterly flow exists in the upper air over the plateau of South Africa, and at the surface warm moist air flows southwards ahead of a surface low, which is typically situated well to the east of the upper low.

On days 6 and 7, a second cold front passes Gough Island followed by backing winds aloft, weakening the warm high ahead of it, and re-establishing normal westerly flow. The cut-off low gathers speed and moves off towards the Indian Ocean as it weakens.

This "empirical" model was based on more than 100 cut-off low occurrences, and is based on the most typical set of circumstances. However, the model predominantly relates to the evolution of the circulation in the upper air, and little emphasis is placed on the evolution of the flow near to the surface. In such baroclinic systems, it is likely that the circulation in low-levels of the troposphere is equally as important. It is therefore the aim of this thesis to determine a conceptual model of the development of the flow near to the surface for cut-off low pressure systems that result in extreme rainfall. In addition, the dynamical forcing of the evolution of the flow will be evaluated.

Taljaard (1985) also found that, on average, 11 cut-off lows occur over the South African region each year, most commonly in the spring and autumn months, and approximately one in five of these systems results in flood producing rainfall, mostly over the south and east coastal regions of South Africa.

University of Cape Town

There have been several well documented cases of flood producing cut-off lows over South Africa, which are briefly described here. In September 1968, more than 500 mm of rain fell over the city of Port Elizabeth in 24 hours due to a cut-off low over the southwest of South Africa (Haywood and van den Berg 1968), and a similar amount of rainfall was recorded over East London in August 1970 when a cut-off low was situated over central South Africa (Haywood and van den Berg 1970).

Additionally, in January 1981, a cut-off low off the west coast of South Africa led to flooding in the semi-desert town of Laingsburg some 150 km inland of the south coast (Estié 1981). Here, it was noted that a strengthening of the pressure gradient at the surface led to strong onshore flow of moist air into the system, and additionally, that the steep topography of the region was associated with heavy precipitation.

In September 1987, severe flooding affected the coastal areas of the KwaZulu Natal province when a cut-off low tracking east over the Northern Cape and Northwest Province led to accumulated rainfall in excess of 900mm over three days (Triegaardt et al. 1987). A strong positive correlation was found between the strength of the onshore flow and the rain rate. Furthermore, Tennant and van Heerden (1994), simulated this event using a GCM to investigate the response of the model to an SST increase in the South West Indian ocean, and to the topography of South Africa. They found that the topography of South Africa was important in generating the extreme quantities of precipitation observed, and the rate at which the cut-off low aloft travelled across the country. However, they were unable to identify any meaningful response to increased SST.

University of Cape Town

More recently, in August 2002, more than 300 mm of rain fell over East London in 24 hours (compared to the monthly average for August of 78mm), when a cut-off was situated over the western interior of South Africa; and in March 2003, a cut-off low tracking east along the south coast of South Africa led to flash flooding in the town of Montagu, some 80 km north of the coast, where close to 200 mm of rain was recorded over 24 hours compared to the climatological average for March of just 19.5mm. These latter examples are the subject of the present study.

This section has shown that considerable research has gone into developing an understanding of the processes that lead to the formation of a cut-off low in the upper air, and that over South Africa, these systems have been responsible for rainfall of flood producing quantities, mostly over southern and eastern coastal regions, and the adjacent interior of the country. A relationship between the rainfall, strong onshore flow and steep topography has been noted for these systems (Estié 1981; Triegaardt et al. 1988; Tennant and van Heerden 1994)

University of Cape Town

2.3. Air-sea interactions in the South African region

The SST to the south and east of South Africa is anomalously warm for its latitude. This is due to the presence of the Agulhas Current, which advects warm water polewards along the eastern seaboard of South Africa and along the south coast following the continental shelf (Stramma and Lutjeharms 1997). Between 16°-20°E, the Agulhas current retroflects (turns back on itself) and flows back towards the South Indian Ocean as the Agulhas Return Current (Lutjeharms and van Ballegooyen 1988). Steep SST gradients exist between the warm waters of the Agulhas Current and cold upwelled water on its inshore side (Darbyshire 1964; Schumann et al. 1982;

Lutjeharms et al. 1989; Lutjeharms et al. 2000). These steep SST gradients have naturally led researchers to investigate the atmospheric response to forcing from the ocean in this region.

Lutjeharms et al. (1986) noted persistent cloud lines over the Agulhas Current, particularly on the landward edge of the current, where the SST gradient is steeper. In addition, Jury and Walker (1988) and Mey et al. (1990), provide evidence of the modification of the marine atmospheric boundary layer (MABL) over the Agulhas Current retroflection region from aircraft and shipboard measurements during the summer season (late February 1987). Surface latent heat and sensible heat measurements showed an increase of more than double over the Agulhas Current compared to surrounding waters. Furthermore, over the course of three weeks, it was found that the average surface latent heat flux over the Agulhas Current was 20% greater than the climatological value, with a maximum heat loss of 828 $W.m^{-2}$ measured during strong wind conditions. In addition, it was found that a secondary sea-breeze like circulation existed across the SST front, and that the boundary layer was conducive to localised cyclogenesis with strong vertical shear in the zonal wind leading to enhanced baroclinicity.

University of Cape Town

Further research has been conducted over the Agulhas Current in the winter season (June 1989), when a SST front existed with a 7°C temperature difference over 10km (Jury and Courtney 1991; Jury 1993). A fivefold increase in the latent heat flux was observed on the warm side of the front. In addition, turbulent updrafts and downdrafts in excess of 1 $m.s^{-1}$ were measured in the MABL above the Agulhas Current leading

the authors to conclude that turbulent mixing in the MABL was achieved through convective eddies.

In April 1995, the ACASEX (Agulhas Current Air-Sea Exchange) cruise was undertaken to investigate air-sea interactions over the Agulhas Current south of Port Alfred (Rouault et al. 1995), a region which has been shown to exhibit particularly steep SST gradients (Lutjeharms et al. 2000). Lee-Thorpe et al. (1998) showed that the region over the Agulhas Current exhibited higher CAPE (Convective Available Potential Energy) than over the surrounding ocean. In addition, the MABL over the Agulhas Current was found to be unstable, contrasting with a stable MABL on both the seaward and landward sides of the current.

Lee-Thorp et al. (1999) present further results from the ACASEX cruise during onshore wind conditions. Surface latent heat flux estimates showed an approximate doubling from the seaward side to over the current, and a six times decrease over the shelf. In addition, an increase of approximately 25% in low-level atmospheric moisture was observed over the Agulhas Current, compared to the seaward side, coupled with a deepening of the high humidity humid mixed layer. A residual high humidity layer extending over the shelf was also evident. During along-current wind conditions on the same cruise (Rouault et al. 2000), a similarly large fivefold increase in the latent heat flux was observed between the continental shelf and the Agulhas Current leading to a transition in the stability of the MABL. The authors estimate that there is an increase in MABL height of approximately 40m.$^{o}C^{-1}$ SST, and an increase in moisture content of approximately 0.35g.kg^{-1}.$^{o}C^{-1}$ SST over the SST front.

University of Cape Town

Considering the above observations of boundary layer modification over the Agulhas Current, it seems logical to expect the increased latent heat fluxes over the current to have some impact on rainfall over the adjacent coast, particularly in the strong onshore flow typical in cut-off low situations where rainfall of flood producing quantities is observed (Estié 1981; Taljaard 1985; Triegaardt et al. 1988). Indeed, through a statistical analysis of summer rainfall at stations along the east coast of South Africa (Jury et al. 1993), it has been shown that a significant correlation between summer rainfall there and shelf width exists, i.e. the distance to the inshore edge of the Agulhas Current, with a shorter shelf width being associated with increased rainfall. These authors hypothesise that, during onshore wind conditions, high latent heat flux due to the warm SST of the Agulhas Current leads to increased moisture being advected onto the land and therefore increased rainfall.

Furthermore, many studies have been undertaken in order to establish the relationship between SST in the Agulhas Current region of the South West Indian Ocean and rainfall over South Africa. Walker (1990) was one of the first to identify a correlation between summer rainfall over South Africa and SST variability in the South West Indian Ocean. For non-ENSO seasons, it was found that warm (cold) events in the South West Indian Ocean were strongly correlated with increased (decreased) rainfall over the South African interior. The proposed mechanism for increased rainfall due to warm SST in the South West Indian Ocean is that these events are accompanied by strong easterly wind forcing and warmer moister airmasses around southern Africa increasing low-level moisture convergence over the interior. Additionally, an altering of latent heat flux distributions by the warm SST anomalies was proposed to enhance baroclinicity and increase instability of the lower troposphere favouring cyclogenesis.

University of Cape Town

Mason (1995) expanded on the work of Walker (1990) to identify principal components of SST variability in the South Indian and South Atlantic Oceans, and related these principal components to rainfall over South Africa. The South West Indian Ocean, including the Agulhas Current and the Mozambique Channel was found to be the second principal component (PC2) explaining 13% of the SST variability. Similar to Walker (1990), warm events in PC2 were associated with increased summer rainfall over South Africa. SST variability in this part of the ocean was further examined by Reason and Mulenga (1999) who ran an ensemble of integrations of a GCM with a warm anomaly imposed on the SST field roughly coinciding with the location of PC2 from Mason (1995). These experiments showed an increase in rainfall over the eastern part of South Africa and southern Africa, which the authors attributed to changes in moisture convergence and shifts in the local Walker-type circulation brought about by the imposed SST anomaly.

Further GCM experiments have been undertaken to assess the influence of SST in the Agulhas Current region on the surrounding atmosphere. Reason (1998) imposed an idealized warm anomaly on the monthly climatological SST, to simulate typical warm episodes in the South Atlantic / South Indian Oceans, roughly coinciding with the Agulhas Retroflection region, and repeated the simulation with a cold anomaly there. Changes in the model atmosphere were not reversed for the opposite anomalies, indicating that the atmospheric response to SST anomalies in this subtropical ocean region are, like many other areas, non-linear. The warm anomaly affected rainfall over much of southern Africa from intraseasonal through to interannual timescales. Over the south coast, it was proposed that these changes were due to increased evaporation from the ocean, whereas over the interior, changes

University of Cape Town

in low-level moisture convergence and a shift in the local Walker-type circulation were suggested as mechanisms that led to the summer rainfall anomalies in the model. The cold anomaly led to similar changes in rainfall, but only on intra- to interannual timescales.

In order to assess the influence of the presence of the Agulhas Current on regional atmospheric circulation patterns, Reason (2001) performed an ensemble of GCM experiments with the steep SST gradients smoothed over the South West Indian Ocean, effectively removing the Agulhas Current from the forcing. The model results showed a reduction in rainfall over southern Africa which was attributed to an anticyclonic anomaly over the ocean to the south of South Africa, with reduced cyclone density in the South East Atlantic region approaching South Africa, and cyclone tracks shifted to the south compared with the climatology. These results provide further evidence for the mechanisms suggested by Walker (1990) and Mason (1995), such that the warm SST of the Agulhas Current leads to high surface fluxes, low-level instability and enhanced baroclinicity, which lead to the increased rainfall observed during warm episodes. In addition, Reason (2001) states that the model response is stronger in winter, when there is a greater temperature difference between the atmosphere and the warm Agulhas Current.

The above studies were based on the influence of the warm SST of the Agulhas Current on seasonal and longer timescales. They show that warm episodes lead to increased rainfall over southern Africa due to enhanced moisture convergence, higher latent heat fluxes, reduced stability and increased baroclinicity. However, the influence

University of Cape Town

of the Agulhas Current on individual weather systems has been less thoroughly researched.

Using SST data and synoptic and upper air charts, Walker and Lindesay (1989) suggested that the anomalously warm SST of the Agulhas Current may have played a role in supplying moisture to two extratropical cyclones in February and March 1988, due to easterly onshore flow from the warm anomaly into the rainfall region.

Using a regional atmospheric model (RAMS), Crimp et al. (1998) investigated the atmospheric response to SST anomalies for a tropical temperate trough event, a weather system that contributes a large proportion of the summer rainfall over southern Africa (Preston-Whyte and Tyson 1988). They found that a warm SST anomaly in the southern Agulhas region led to increased surface heat fluxes, and therefore low-level instability, promoting the formation of westerly troughs favourable for tropical temperate trough formation.

University of Cape Town

Crimp and Mason (1999) used a similar regional model to simulate a heavy precipitation event in February 1996. Through a back trajectory analysis, they were able to show that low-level moisture was advected from the South West Indian Ocean to the south and southeast of South Africa where the Agulhas Current is situated.

Through an examination of NCEP reanalysis data, and back trajectories from ECMWF, Rouault et al. (2002) showed that the Agulhas Current region was the source of low-level moisture for an extreme precipitation event in December 1998.

These authors argued that large onshore moisture flux from this region suggests that the low-level moisture was predominantly due to evaporation from the ocean there.

This section has presented evidence that the warm SST in the South West Indian Ocean due to the presence of the Agulhas Current may have a sizeable influence on atmospheric circulations and rainfall over the southern African region. However, there is little evidence that the influence of the SST there has been thoroughly investigated for individual weather systems, and in particular those in which strong onshore flow over the Agulhas Current is a typical characteristic.

University of Cape Town

2.4. Low-level jets

The present study will show that the formation of an onshore low-level jet[3] (LLJ) is an important feature of extreme coastal rainfall in a cut-off low synoptic environment There are many documented examples of LLJ development across the globe. The formation of an LLJ, within an upper air environment exhibiting cut-off low characteristics, impinging on the coastal topography of France / Italy / Spain, and with a large fetch over the Mediterranean Sea has led to several flash flooding episodes (e.g. Binder and Rossa 1995; Buzzi et al. 1995; Fehlman et al. 2000; Romero et al. 2000). In these cases the LLJ was responsible for the advection of moist air into the rainfall region, where topographically forced ascent at its leading edge enhanced convection.

In addition, LLJs are important for heavy rainfall episodes in Taiwan (e.g. Chen and Yu 1988), eastern China (e.g. Chen et al. 1998) and Japan (e.g. Davidson et al. 1998) regions during the rainy Mei-Yu or Baiu season (early June-mid July). In these cases,

[3] For the purposes of this study, the LLJ is defined as a maximum in the low-level horizontal wind.

heavy precipitation tends to form on the left-hand side of the LLJ looking downstream (Matsuomo 1972, 1973; Ninomiya and Akiyama 1974). The formation of the LLJ has often been attributed to the Coriolis deflection of ageostrophic motion in the lower branch of a secondary mesoscale convective circulation through a mass-momentum adjustment process driven by diabatic heating (Chen 1982). Numerical modelling studies have shown that the LLJ forms as a result of an increasing pressure gradient due to the deepening of a lee cyclone and vertical motions associated with an upper level shortwave trough (Chen et al. 1997; Davidson et al. 1998). In addition, positive feedbacks due to latent release from convection have been shown to intensify the LLJ (Y.-L. Chen et al. 1997; C. Chen et al. 1998; Davidson et al. 1998; S.-J. Chen et al. 1998; Yeh and Chen 2002). In their MM5 numerical modelling experiments, Yeh and Chen (2002) showed that the topography of Taiwan is important for enhancing offshore convergence associated with the LLJ.

Further investigations of the mechanisms leading to the formation of a LLJ have been carried out in the United States, where a number of LLJ type phenomena occur. Over the Great Plains, a nocturnal LLJ forms, which has been attributed to inertial oscillation of the ageostrophic wind as, at sunset, the flow becomes decoupled from the surface frictional stress (Blackadar 1957). Furthermore, diurnal heating and cooling over sloping terrain has been shown to lead to an acceleration of the ageostrophic wind (Holton 1967; Peagle and Rasch 1973; Zeaman 1979; McNider and Pielke 1981).

In the coastal zone, enhanced low-level baroclinicity, due to cold upwelling creating large land-sea temperature contrasts, has been a mechanism shown to result in LLJ

University of Cape Town

formation (Dickinson and Neuman 1982; Mizzi and Pielke 1984; Doyle and Warner 1991). Doyle and Warner (1993a) found that a LLJ that formed parallel to the Carolina coast in the Genesis of Atlantic Lows Experiment (Dirks et al. 1988) was sensitive to SST distribution there. This SST distribution influenced the coastal baroclinic zone and therefore the intensity and exact location of the LLJ. Strong latent and sensible heating of the boundary layer due to the warm Gulf Stream was found by Doyle and Warner (1993b) to enhance the coastal baroclinic zone, and therefore the LLJ through increased pressure gradient forcing. In addition, Doyle (1997) showed that blocking due to steep coastal topography enhanced the strength of an alongshore LLJ off the California coast by as much as 45%.

A forcing of LLJs due to mass adjustment processes associated with upper level jet streaks has also been suggested. Uccellini (1980) found that mass adjustments in the exit region of upper level jet streaks resulted in the formation of LLJs over the Great Plains. Furthermore, Uccellini and Johnson (1979) and Uccellini et al. (1987) have shown that transverse circulations in upper-level jet streaks led to a mass adjustment process resulting in the development of a LLJ, as downward transport of momentum from the upper level jet accelerates the flow at low-levels.

Therefore, several mechanisms have been proposed in the literature which may lead to the formation and intensification of a LLJ. These mechanisms may be summarised as:

- Coriolis deflection of ageostrophic motion in the lower branch of a secondary convective circulation;
- Mass momentum adjustments driven by diabatic heating due to convection;

University of Cape Town

- Inertial oscillation of the ageostrophic flow within the boundary layer;
- Thermal wind due to nocturnal heating and cooling over sloping terrain;
- Enhanced baroclinicity due to strong air-sea temperature contrasts leading to increased pressure gradient forcing;
- Topographic blocking of onshore flow;
- Transverse circulations in upper-level jet streaks leading to mass adjustment processes.

Cut-off low pressure systems are characterised by upper-level jet streaks, suggesting that the mass adjustment processes proposed by Uccellini and co-workers (1979, 1980, 1987) may be responsible for the LLJ in these cases. In addition, the coastal region of South Africa is similar to the Carolina coast of the United States in that the SST there is characterised by a warm western boundary current. Therefore, enhanced baroclinicity due to strong air-sea temperature contrasts may also be important for LLJ formation in South African cut-off low events.

University of Cape Town

2.5. Summary and research objectives

Cut-off low pressure systems are an important weather system for South Africa since they have been shown to be the synoptic system associated with many flooding episodes that have led to substantial loss of life and damage to infrastructure. The processes leading to the formation of these systems is fairly well understood, and their characteristic development over South Africa has been investigated. However, no climatology for these systems currently exists for the South African region. Taljaard (1985) admits that the 10 years of data he investigated is not sufficiently long to draw any conclusions with regard to the frequency and variability of these systems. A

climatology of cut-off lows over South Africa would not only be of benefit to meteorologists, but also to those interested in the exchange of ozone and other reactive species between the stratosphere and the troposphere, which may have an effect on the radiative forcing of the global climate (Ramaswamy et al. 1992). Indeed, it has been shown that cut-off lows are an important system for stratosphere-troposphere exchange over South Africa (Barsby and Diab 1995). The above discussion therefore provides motivation for the first research objective of the present study:

To derive a climatology of cut-off low pressure systems over the southern African region and to investigate their frequency, variability and relationships with large scale modes in the Southern Hemisphere.

In cut-off low cases over South Africa that have led to flood producing rainfall, researchers have noted the presence of strong onshore flow into the region of highest rainfall. The ocean to the south and east of South Africa is characterised by warm SST due to the presence of the Agulhas Current. It has been shown that the MABL is destabilised by the warm SST of the Agulhas Current, and that variability of the SST in this region is related to rainfall over South Africa. However, few studies exist that investigate the influence the Agulhas Current may exert on weather systems involving extreme rainfall. Moreover, no attempt has been made to quantify the role of the Agulhas Current during the onshore flow conditions observed during cut-off low events with extreme coastal rainfall. Therefore, the second research objective of the present study is:

University of Cape Town

To investigate the influence of the Agulhas Current, and the associated mesoscale SST patterns, on extreme coastal rainfall events due to cut-off low pressure systems over South Africa.

Finally, the strong onshore wind in flood producing cut-off lows over South Africa suggests the presence of an onshore LLJ. These jets have been shown to form due to a number of mechanisms in different parts of the world. However, in the South African context, where steep coastal topography and SST are likely to exert some influence on the low-level flow, the mechanisms leading to the formation of LLJs has not been investigated. This gives rise to the final research objective:

To determine the relationship between an onshore LLJ and coastal rainfall in cut-off low situations, and to investigate the mechanisms responsible for the formation of the LLJ in these situations.

The following chapter details the data and methods used in the present study to address the above research objectives.

University of Cape Town

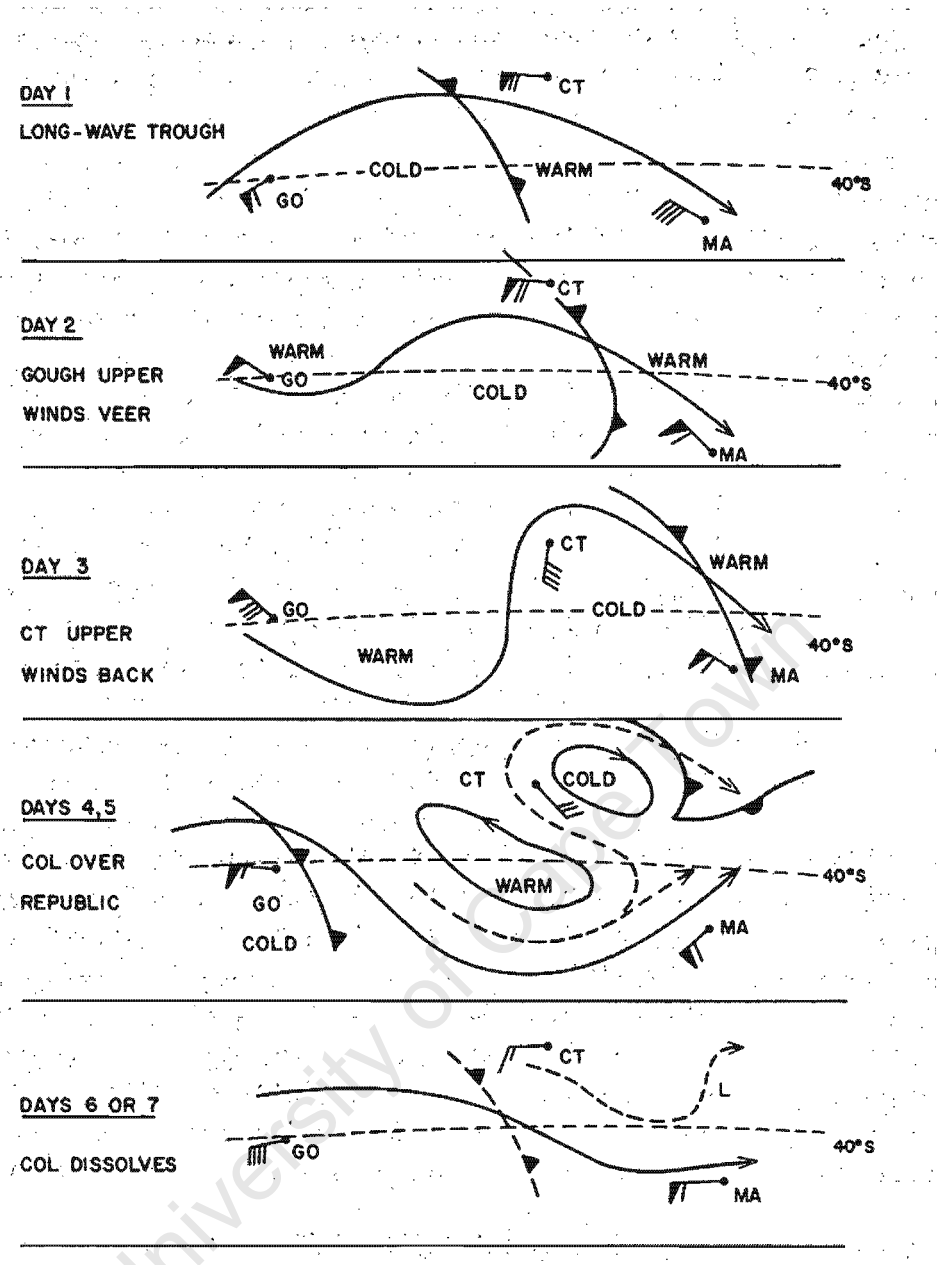

University of Cape Town

Figure 2.1 – Most common sequence of circulation patterns in the upper air in the Gough Island (GO) – Cape Town (CT) – Marion Island (MA) triangle during the development, maturity and decay of cut-off lows. Taken from Taljaard (1985).

Chapter 3

Data and Methodology

University of Cape Town

University of Cape Town

3.1. Introduction

In the previous chapter, the research objectives of the present study were identified. These objectives involve the investigation of phenomena occurring on climatological timescales as well as individual weather systems. Such wide-ranging objectives therefore require very different data and analysis techniques in order that the relevant processes may be properly examined. This chapter details the data used in the present study, and the techniques employed to analyse these data.

The first two sections of this chapter following this introduction describe the data used in this study. Section 3.2 describes the NCEP re-analysis data, and section 3.3 describes the data drawn from the MRF model. Following this, the tropopause mapping technique, which helps to identify cut-off low pressure systems, is explained in section 3.4.

From section 3.5 onwards, the chapter is dedicated to explaining the limited area model used in simulating the case studies (section 3.5), the techniques employed to analyse the model output (section 3.6), and sensitivity tests undertaken with the model (section 3.7).

University of Cape Town

3.2. NCEP re-analysis data

Recent efforts by the National Centers for Environmental Prediction (NCEP), together with the National Center for Atmospheric Research (NCAR), based in the United States of America, have led to a global analysis dataset covering the period from 1948 to the present day (Kalnay et al. 1996). These data contain all parameters that are contained in the equations of motion governing atmospheric circulations. In addition,

some data derived from these fields are also available. The data are available at a resolution of 2.5° x 2.5° in the horizontal at all standard pressure levels from 1000- to 10-hPa, and at a temporal resolution of six hours.

The data assimilation technique has been essentially constant throughout the period, leading to a near homogenous dataset for global climate applications. However, for Southern Hemisphere applications, certain caveats must be borne in mind. The Southern Hemisphere is dominated by the Southern Ocean, and therefore observations, particularly of the upper air, that are assimilated into the re-analysis data are relatively sparse. After 1978, satellite observations were introduced into the data assimilation routines. While this introduction of satellite data may lead to some discontinuities in the re-analysis fields, these are likely to be less pronounced over the land where observations already existed (Tennant 2004).

University of Cape Town

3.3. The MRF model

The Medium Range Forecast (MRF) model, developed by NCEP, is a global forecast model with 1°x1° resolution in the horizontal (Kanamitsu 1989; Kanamitsu et al. 1991; Kalnay et al. 1990). It is initialised daily at 0000 UTC and 1200 UTC using data objectively analysed onto the model grid from the global observation network. These initialisation fields are utilised to examine the synoptic environment of the case studies of the present study, and to provide initial and boundary conditions for the simulations using a limited area model. The MRF model was chosen due to the high spatial resolution and easy availability of the data.

3.4. Tropopause maps

In examining processes in the upper air, such as cut-off lows, the invertibility principle for potential vorticity (see Chapter 2) provides a useful framework. Hoskins et al. (1985) demonstrate the usefulness of isentropic potential vorticity maps in the analysis of midlatitude weather systems. Since potential vorticity is conserved on isentropic surfaces, the movement of particular systems in the upper air, as well as diabatic effects, can be easily identified. However, this requires an examination of potential vorticity on several isentropic surfaces.

Morgan and Nielsen-Gammon (1998) showed that, for an efficient description of the flow phenomena in the upper troposphere and lower stratosphere, an analysis of the potential temperature along the dynamic tropopause is sufficient. The dynamic tropopause is often defined as a constant potential vorticity surface equal to 1.5 PVU[4] (or -1.5 PVU in the Southern Hemisphere). Since potential vorticity is conservative on constant isentropic surfaces, it follows that the reverse association, such that potential temperature is conserved on a constant potential vorticity surface, is true.

University of Cape Town

The technique used to construct the tropopause map in the present study is the contour superposition technique (Bell and Bosart 1993; Morgan and Nielsen Gammon 1998), a description of which follows. Firstly, pressure level data is linearly interpolated onto isentropic surfaces. Secondly, the Ertel potential vorticity, Q, is calculated on isentropic surfaces, which with the hydrostatic approximation is defined by:

$$Q = g\frac{\zeta_{a\theta}}{\sigma}.$$

[4] 1 PVU = 1.0 x 10^{-6} $m^2.s^{-1}.K.kg^{-1}$

In the above expression, g represents the acceleration due to gravity, $\zeta_{a\theta}$ the component of absolute vorticity normal to an isentropic surface, and $\sigma = -\partial p / \partial \theta$ is the pseudo-density, inversely proportional to the static stability. The final stage of the process is to take contours of the Ertel potential vorticity equal to that defined as the dynamic tropopause (i.e. -1.5 PVU), and superpose them onto a new map, labelling them as the isentropic surface from which they were taken. In this way a single map of potential temperature on a constant potential vorticity surface may be constructed.

3.5. MM5

MM5 is the fifth generation of the Pennsylvania State University / National Center for Atmospheric Research (PSU/NCAR) mesoscale model. The version used in the present study is Version 3 (Grell et al. 1994). It is a limited area, non-hydrostatic, terrain-following sigma co-ordinate model designed to simulate mesoscale and regional scale atmospheric circulations. The model was chosen as it is freely available and has a large community of users. In addition, it has been shown to be an effective tool for diagnosing extreme rainfall cases in the Northern Hemisphere, in, for example USA (e.g. Colle and Mass 2000), Europe (e.g. Romero et al. 2000), and East Asia (e.g. Yeh and Chen 2002). However, little evidence exists that it has been widely applied to Southern Hemisphere extreme weather events. The present study therefore provides an opportunity to assess the usefulness of MM5 for South African extreme weather applications.

The model has both one and two-way nesting capabilities. For the purposes of the present study, the model was run with 27km resolution in the horizontal, with 10-minute resolution topography taken from the United States Geological Survey

University of Cape Town

(USGS), which is available for download as part of the MM5 suite of programs. For simulation in which nested grids are used, the horizontal resolution of the intermediate grid is 9km, using 2-minute resolution USGS topography, and the fine grid uses 3km resolution in the horizontal, and 30-second topography from USGS.

Many options exist for the parameterisation of sub-gridscale processes in MM5. In order to maintain consistency, the same parameterisations were chosen for both of the case studies. For all grids, 40 σ-levels were used in the vertical, with increased vertical resolution in the lowest kilometre (approximately 18 σ-levels) of the troposphere in order that boundary layer processes are adequately resolved.

Initial and boundary conditions were constructed by horizontal interpolation of global analyses of atmospheric variables and soil moisture and temperature from the $1^{\circ} \times 1^{\circ}$ resolution MRF model onto the MM5 grid, which were then vertically interpolated to the model σ-levels. Initial imbalances of the interpolated fields were reduced by removing the vertical integral of the horizontal divergence at each grid point through an iterative process (Grell et al. 1994). Boundary conditions from the MRF model were imposed every twelve hours (higher temporal resolution data are not available from the MRF model) for the outer grid, with a linear temporal interpolation between each MRF model time. The next four grid-points are relaxed towards the boundary values with a relaxation constant that decreases linearly away from the boundary. For the nested grids, boundary conditions were applied from the respective mother grids at each time step with two-way nesting applied to ensure that output from the higher resolution grids are fed back into the mother grids.

University of Cape Town

For the optimum simulations to be achieved, various tests were carried out (although not reported here) of different combinations of parameterisations for the case studies. In order to maintain consistency, the same parameterisations were used for each of the case studies in the final analysis. These are detailed below.

Planetary boundary layer physics were parameterised using the MRF scheme (Hong and Pan 1996). Surface temperature and moisture over land were calculated using the Noah land-surface model (Chen and Dudhia 2001a,b), which takes account of soil properties at depths up to 4m below the surface. The calculation of longwave and shortwave radiative effects on atmospheric temperature tendencies and surface fluxes included the effects of cloud cover. Moist convection was parameterised using the method of Grell (1993), whereby cloud properties are calculated using a single non-entraining updraft that detrains only at the cloud top, and a downdraft that begins at the level which has minimum moist static energy. For the 3km grid, this parameterisation was switched off to prevent conflict between explicitly resolved convection at this resolution and the parameterisation scheme. The explicit microphysics parameterization (Reisner et al. 1998), which uses predictive equations for cloud water and rain water below the freezing level and cloud ice and snow above the freezing level was employed. The effects of evaporation, condensation, hydrostatic water loading, melting, freezing, deposition, sublimation and supercooled liquid water were all included in this scheme.

University of Cape Town

3.6. Diagnosing the model output

Some of the techniques used in the diagnosis of the model output are detailed below. Some other techniques were also used, but are elaborated on in the relevant chapters of this thesis.

3.6.1. Identification of convection

One of the most important mesoscale processes contributing to events characterised by extreme regional rainfall, and in some cases flash-flooding, is deep moist convection (Doswell et al. 1996). For deep moist convection to occur, three criteria must be present, namely, upward motion, low-level moisture and instability. A useful diagnosis parameter here is integrated low-level moisture flux convergence, F_w, since it parameterises the first two criteria (i.e. upward motion in the presence of low-level moisture) (Barnes and Newton 1986). It is defined as

$$F_w = \int_{p_0}^{p} \nabla.(q\mathbf{V})\frac{dp}{g}.$$

In the above expression, q is the specific humidity, p_0 is 1000 hPa, and $\mathbf{V}$ is the horizontal wind.

In moist environments, equivalent potential temperature, θ_e, is the important parameter governing the stability of the atmosphere. Therefore an indication of instability can be gained by taking the difference in θ_e between the 1000 hPa and 500 hPa levels of the troposphere.

3.6.2. Orographic effects

In order to examine issues regarding the influence of mesoscale topography on the low-level flow impinging on it, two dimensionless parameters are important, namely

University of Cape Town

the Froude, Fr, and Rossby, Ro, numbers. Fr gives an indication of the preference of the flow to go over (Fr>1) or around (Fr<1) the topographic barrier (Smith 1979). However, it has been shown that some degree of blocking is likely for Fr<5 (Baines 1979; Smolarkiewicz and Rotunno 1990). Trüb and Davies (1995) found that as Ro decreases, the flow response to the topographic barrier changes from vertically propagating gravity waves (Ro>1), to a leeward train of near inertial waves (Ro~1), to a state dominated by the adjustment process associated with scale contraction (Ro<1). In the case of blocked flow, the Burger number (B=Ro/Fr) becomes important as it gives an indication of the timescales for which blocking will continue (Pierrehumbert and Wyman 1985). The expressions used to calculate Ro and Fr are shown below.

$$Fr = \frac{U}{Nh} \qquad Ro = \frac{U}{fL}.$$

In the above expressions, U is the incident wind speed, N is the Brunt-Väisälä frequency, which is a measure of buoyancy in the atmosphere, h is the height of the topographic barrier, L is its half width, and f is the Coriolis parameter. In this case N is calculated from

$$N^2 = \left(\frac{g}{\theta}\frac{\partial\theta}{\partial z}\right),$$

where g is the acceleration due to gravity, θ is the potential temperature and $\partial\theta/\partial z$ is the vertical gradient of potential temperature.

3.7. Sensitivity tests

Most of the sensitivity tests are detailed in Chapter 7. However, here an overview of the SST datasets used and a description of the factor separation technique are given.

University of Cape Town

3.7.1. Sea Surface Temperature

For the main part, the SST used in the simulations is taken from the NAVOCEONO (Naval Oceanographic Office, USA). This SST product is derived from the NOAA (National Oceanic and Atmospheric Administration)-Polar Orbiting Advanced Very High Resolution Radiometer (AVHRR) multi-channel sea surface temperature (MCSST) algorithm. Improved cloud detection algorithms applied by NAVOCEANO yield an increased number of retrievals compared to other MCSST datasets. The data are interpolated to an 18km grid and are available as weekly averages. Therefore the resolution is high enough that the mesoscale details of the SST in the Agulhas Current region are included, and the improved cloud detection algorithm allows more SST data to be available in areas such as over the Agulhas Current, where cloud is common (Lutjeharms et al. 1986).

For the lower resolution SST data, the data are taken from the NCEP Reynolds Optimally Interpolated (OI) SST dataset (Reynolds and Smith 1994). These data have a resolution of 1° latitude-longitude, and are derived from in-situ observations and the NOAA AVHRR satellite. The lower horizontal resolution of these data means that the warm core of the Agulhas Current and the steep mesoscale SST gradients are not well resolved (Rouault et al. 2003).

3.7.2. Factor separation

In sensitivity experiments in numerical modelling, the impact of one factor may be easily obtained by analysing the difference of simulations including that factor, and simulations excluding that factor. However, when more than one factor is to be considered, the evaluation of the influences of these factors is not so straight forward

University of Cape Town

due to non-linearities of the processes involved. In order to isolate the effects of these interacting processes, the factor separation of Stein and Alpert (1993) is used. These authors found that for investigations involving *n* factors, 2^n simulations are required. Therefore, for investigations, such as the present study, in which an evaluation of two factors is required, four simulations are necessary.

These four simulations are denoted f_0, in which neither of the factors are included; f_1, in which factor 1 is included, but not factor 2; f_2, in which factor 2 is included, but not factor 1; and f_{12}, in which both factors 1 and 2 are included. The *individual* contribution of factors 1 and 2, denoted by f_1^* and f_2^* respectively, are given by:

$$f_1^* = f_1 - f_0$$

$$f_2^* = f_2 - f_0,$$

and the *combined* contribution of factors 1 and 2, denoted by f_{12}^*, is given by:

$$f_{12}^* = f_{12} - (f_1 + f_2) + f_0$$

3.8. Summary

This chapter has provided details of the datasets, models and some of the analysis techniques used in this study. The following chapters use these data and techniques in order to address the research objectives set out in Chapter 2.

University of Cape Town

Chapter 4

A 30-year climatology of cut-off low pressure systems over subtropical southern Africa

University of Cape Town

University of Cape Town

4.1. Introduction

This chapter presents a 30-year climatology (1973-2002) of cut-off low pressure systems identified from 300 hPa geopotential height data for subtropical southern Africa. The area under investigation is the box bounded by 10–40°E longitude and 20–40°S latitude. The climatology was derived from 300 hPa reanalysis fields from NCEP (Chapter 3; Kalnay et al. 1996). Features of cut-off lows examined herein include their frequency, seasonality, interannual variability, geographical distribution, latitudinal width and duration. Possible relationships with large scale modes in the Southern Hemisphere are also investigated. This climatology represents a re-visiting of the 10 years of data examined by Taljaard (1985) using the more reliable NCEP re-analysis data, and an extension of the period to 30 years starting from the same year (1973).

Following this introduction, the chapter is divided into three main parts. Section 4.2 describes the methods used to identify cut-off lows, their size, duration and geographical distribution. Section 4.3 provides an analysis of these systems in terms of the methods described in section 4.2, and Section 4.4 concludes the chapter with a summary of the main findings.

University of Cape Town

4.2. Methodology

The cut-off lows were subjectively identified by a closed geopotential height contour lasting for more than 24 hours at the 300 hPa level within the southern African region bounded by 10–40°E longitude and 20–40°S latitude. Closed geopotential height contours that were not fully within this domain for at least 24 hours were discarded.

Over the period 1973–1982, a small number of the cut-off lows identified by Taljaard (1985) did not appear in the NCEP reanalysis data. In such cases, the geopotential height and winds at all standard pressure levels from 600–100 hPa were examined. However, in all these cases there appeared to be no evidence of cut-off lows in the NCEP data, although cold troughs were present. Additionally, a small number of cut-off lows were present in the NCEP reanalysis data that were not identified by Taljaard (1985), but were included in the construction of the present climatology. These discrepancies are likely a result of differences between the datasets used, although unfortunately it was not possible to access the raw data used by Taljaard (1985) to investigate further.

The duration of a cut-off low was defined as the time for which at least one closed geopotential height contour was within the area as described above. To analyse the duration of these systems, they were split into three categories, namely, those lasting 1–2 days over this region, those lasting 2–4 days and those existing >4 days.

The geographical location of a cut-off low was defined by separating the southern African domain into four regions, A in the southwest, B in the southeast, C in the northwest and D in the northeast (Fig. 4.1). A cut-off low was defined as being in a particular region by the location of its centre. These regions were divided in such a way as to minimise the number of systems that appeared in more than one region. In cases where a system tracked over more than one region, it was counted once for each region in which it was present.

University of Cape Town

The size of the cut-off was defined as the latitudinal width of the outer closed geopotential height contour of the system at 300 hPa. The cut-off lows were then split into four width categories, namely, 100–400 km, 400–800 km, 800–1200 km and >1200 km.

4.3. Analysis

4.3.1. Frequency and variability

A total of 323 cut-off lows were identified at 300 hPa over the 30-year 1973-2002 period (Appendix A), resulting in an annual average of around 11 systems, consistent with Taljaard (1985). The monthly frequency of cut-off lows aggregated over these 30 years is shown in Fig. 4.2. It is clear that April is the most common month for cut-off lows over subtropical southern Africa, accounting for 51 of these systems. March, May and June also show high occurrences, while cut-off lows are least common in December and January. This is consistent with the findings of Taljaard (1985) for 1973-1982. There also appears to be evidence of a semi-annual cycle with relative peaks in April and October. This suggests a possible association with the semi-annual oscillation (SAO), which is prominent in the Southern Hemisphere atmospheric circulation and rainfall between 35° and 65°S. Between these latitudes, the SAO is evident as sea-level pressure and geopotential height maxima during the spring and autumn, and minima in early winter and summer (van Loon 1967; van Loon and Rogers 1984; van Loon et al. 1993). Given that one of the characteristics of cut-off lows over southern Africa is a strong ridge of high pressure over the ocean to the south of South Africa, a strengthening of this ridge, or a shift in the longwave ridges and troughs due to the SAO may provide a mechanism for cyclonic systems becoming cut-off over this region.

University of Cape Town

Fig. 4.3 shows the annual frequency of cut-off lows over South Africa for the 30-year period 1973-2002. There appears to be no obvious trend in the number of these systems over this period. However, there is considerable interannual variability in the number of systems from year to year with noteworthy peaks and troughs. For example, in 1974 and 1983 there were 15 cut-off lows over southern Africa, while in 1991, 1998 and 1999 fewer than five cut-off lows occurred over the region.

Such interannual variability prompted an investigation of associations of cut-off lows with large scale interannual modes that are known to influence the climate of the region such as ENSO. ENSO is known to project strongly over the southern African and South Atlantic regions, particularly in JAS (July, August, September) of the onset year, and JFM (January, February, March) of the mature phase year (Lindesay 1988; Reason et al. 2000; Colberg et al. 2004). Fig. 4.3 shows that five of the seven strong mature phase La Niña years in the 30-year period (Table 4.1) correspond to above average frequencies (i.e. more than 11) of cut-off lows over southern Africa (1974, 1989, 1996, 2000, 2001). Only one of these years experienced a well below average cut-off low frequency (1999). The reverse El Niño association is not so robust, with only two years (1992, 1998) of the five strong El Niño mature phase years (Table 4.1) well below the average frequency. However, 1973 and 1987 experienced average numbers, and only 1983 was above average.

University of Cape Town

El Niño	La Niña
1973	1974
1983	1976
1987	1989
1992	1996
1998	1999
	2000
	2001

Table 4.1 – Strong mature phase years of ENSO

Further investigation of the variability of these systems was undertaken by dividing the occurrences of cut-off lows into seasons, namely, summer (December, January, February - DJF); autumn (March, April, May - MAM); winter (June, July, August - JJA); and spring (September, October, November - SON). For the DJF season (Fig. 4.4a), only 2-3 cut-off lows occurred in most years, with 5 in 1975 and 6 in 1990. In 1980, 1991, 1994 and 2002, no cut-off lows occurred over subtropical southern Africa in this season. As previously mentioned, cut-off lows are most abundant over this region in April, with March and May also experiencing high occurrences (Fig. 4.2). The frequency distribution for the MAM season (Fig. 4.4b) shows that 3-7 cut-off lows occurred in this season, and suggests that maxima occurred on an approximately 7-8 year cycle, with minima on an approximately 6-year cycle. Of the seven mature phase La Niña seasons, five experienced above average numbers. For the JJA season (Fig. 4.4c), there was considerable interannual variability in the frequency of cut-off lows, with 6 systems in 1983, and 7 in 1986, while there were none in 1976, 1990 and 1998. Additionally, all the La Niña onset years (1973, 1975, 1988, 1995, 1998, 1999, 2000) experienced below average numbers in this season. There was little interannual variability for the SON season (Fig. 4.4d), with many years experiencing three cut-off lows in this season. Significant peaks occurred in 2000 and 2001 when there were five cut-off lows in SON.

Although there seems to be an ENSO signal in the annual mean frequencies, there appears to be less evidence of an ENSO association in the seasonal frequencies, with no robust signal in the DJF frequency for mature phase years. However, there is some suggestion of a La Niña signal in the JJA frequency for onset years, and MAM for mature phase years. The frequency distributions for the JFM and JAS seasons were

University of Cape Town

also examined (not shown) for better comparison with the documented seasons of the projection of ENSO over the southern African and South Atlantic regions (Lindesay 1988; Reason et al. 2000; Colberg et al. 2004), but the results were similar to DJF and JJA.

The relative peaks in cut-off low frequencies noted in April and October indicate a potential relationship between cut-off low frequency and the SAO on annual timescales, possibly through alterations in the strength of the subtropical ridge. It seems logical, therefore, that interannual variability in the sea-level pressure and geopotential height maxima in mid-latitudes due to changes in the strength of the SAO, or shifts in the zonal wavenumber 3 pattern will affect the tendency for cold troughs becoming cut-off equatorwards of these pressure maxima.

It has been shown that there was a weakening of the SAO after 1979 (van Loon et al. 1993; Hurrell and van Loon 1994; van Loon and Tourpali 1995; Chen and Yen 1997; Meehl et al. 1998). This weakening was most prominent in the winter–spring half of the annual cycle over the mid-latitudes where the sea-level pressure maximum disappeared. These changes occurred mostly over the Southern Ocean between 40° and 60°S and were possibly related to shifts in the zonal wavenumber 3 pattern (van Loon et al. 1993). Through an examination of winter (JJA) circulation variability, Chen and Yen (1997) were able to show that an enhancement of zonal wavenumber 3 after 1980 led to sea-level pressure decreases over the three ocean sectors between 60° and 70°S and increases in the sea-level pressure of the subtropical ridges.

University of Cape Town

At the same time as the documented weakening of the SAO during the 1980's, cut-off low frequencies were average or above average every year in this decade (Fig. 4.3). Furthermore, there was a considerable increase in cut-off low frequencies in JJA at this time (Fig. 4.4c). Additionally, there was a considerable and sustained increase in the number of cut-off lows in the SON season after 1979 (Fig. 4d). The timing of these changes in cut-off low frequencies therefore appears to suggest an association with the weakening of the SAO, which was most pronounced in the winter-spring seasons. Further evidence for a relationship between cut-off lows over subtropical southern Africa is presented in section 4.3.3.

4.3.2. Duration

The duration of cut-off lows for each season is shown in Fig. 4.5. For all seasons, the distribution is broadly similar, with more than 50% of cut-off lows lasting only 1–2 days, and less than 10% lasting for more than four days. This is consistent with the findings of Price and Vaughan (1992), who found that at sub-tropical latitudes, cut-off lows tend to be relatively short-lived. In the MAM season, when the majority of cut-off lows occur over South Africa (Fig. 4.2), the number of cut-off lows lasting 2-4 days is closer to those lasting 1-2 days than in other seasons. However, it is also evident that in MAM there is a lower frequency of cut-off lows lasting for more than four days than in other seasons.

4.3.3. Regional distribution

The seasonal distribution of cut-off locations over subtropical southern Africa is shown in Fig. 4.6 (see Fig. 4.1 for regions). Region A is the preferred location for occurrences of cut-off lows over subtropical southern Africa with more than 35% in over this

University of Cape Town

southwestern region in all seasons. However, the relative frequency between the other regions changes from season to season. For example, in MAM, region B (southeast) is the second most common location, whereas in JJA and SON, region D (northeast) is the second most common location. Additionally, while SON shows the highest frequency of cut-off lows in region A, it has the lowest frequency in region B indicating that the southernmost regions do not necessarily have the highest frequency of events. A closer examination of the SON and MAM seasons (not shown) reveals that in MAM about 20% of the cut-off lows appearing in region A had tracked across to region B, whereas in SON only about 5% of the cut-off lows appearing in region A tracked across to region B. This suggests that in the MAM season, there is a stronger preference for cut-off lows to track east along the south coast compared to other seasons. The seasonal differences in the frequency of cut-off lows in the different regions described above may reflect shifts in the African sector of the zonal wavenumber 3 or 4 pattern of ridges and troughs in the Southern Hemisphere.

It was suggested in section 4.3.1 that the weakening of the SAO after 1979 and associated enhancement of the subtropical ridge, through a shift in the zonal wavenumber 3 pattern, may have been associated with the average or above average frequency of cut-off lows over South Africa throughout the 1980's. Van Loon and Tourpali (1995) showed that the weakening of the SAO was accompanied by an increase in the geopotential height gradient along 55°S at 500 hPa between 70° and 10°W in the Southwest Atlantic, suggestive of increased equatorward meridional flow in this region and therefore an increase in meridionally extensive trough development. In an attempt to investigate any relationship the weakening of the SAO may have had with the location of cut-off lows over southern Africa, time series of cut-off low

University of Cape Town

frequencies were constructed for each region (Fig. 4.7). Regions A and B (Fig. 4.7a-b) do not appear to display any coherent change in frequencies after 1980, although there is some evidence of a decrease in the number of systems in regions A and B after 1981 and 1983 respectively. Region D, however, shows a dramatic increase in the number of cut-off lows after 1982, which decreases again towards the end of the 1980's (Fig. 4.7d). Region C (Fig. 4.7c) shows a smaller increase after 1983, again with a decrease towards the end of the 1980s.

Region	A	B	C	D	TOTAL
73-82					
DJF	8	2	7	4	21
MAM	20	14	5	11	45
JJA	10	2	5	5	22
SON	13	5	4	2	22
TOTAL	**51**	**23**	**21**	**22**	**110**
83-92					
DJF	5	5	1	4	15
MAM	9	7	10	5	30
JJA	12	7	4	17	37
SON	12	3	4	10	26
TOTAL	**38**	**22**	**19**	**36**	**108**
93-02					
DJF	7	3	4	3	14
MAM	23	14	8	10	41
JJA	9	9	1	5	24
SON	12	4	6	8	26
TOTAL	**51**	**30**	**19**	**26**	**105**

Table 4.2 – Number of cut-off lows over Southern Africa in each season by the region in which they occur. Note that the right hand column is the total number of cut-off lows over the whole area, rather than the sum for each region, since some systems were present over more than one region.

University of Cape Town

The variability in the regional distribution of cut-off lows from decade to decade was investigated by splitting the climatology into three distinct ten-year portions (1973–1982, 1983–1992 and 1993–2002) based on Fig. 4.3. Table 4.2 shows the number of cut-off lows per season for these decades. For 1973–1982 and for 1993–2002, the southwestern region A was by far the most common region for cut-off low

occurrences. However, during the period 1983–1992, approximately 30% fewer cut-off lows were present over region A and close to 50% more over the northeastern region D. The decrease in the number of cut-off lows over region A was most pronounced in the MAM season, with 50% fewer systems, while region D experienced an approximately threefold increase in the JJA season. Additionally, for the 1983–1992 decade, the most common season for cut-off lows over the entire domain was JJA compared to MAM for the other two decades in the climatology. There was little appreciable change in the total number of systems over the northwestern region C between the decades, although many more were observed over this region in 1983–1992 and 1993–2002 in the MAM season than during 1973–1982. Region B (southeast) shows no major changes in the number of systems from 1973–1982 to 1983–1992, while there was a substantial increase in 1993–2002.

In order to investigate mechanisms potentially driving the changes in the regional and seasonal distribution from between decades, differences in the 500 hPa geopotential heights for the Southern Hemisphere between the decades were examined. On climatological timescales, the Southern Hemisphere shows an equivalent barotropic troposphere and thus changes in the 500 hPa geopotential height are reflected at other isobaric levels within the troposphere and in the sea-level pressure (Szeredi and Karoly 1987; Karoly 1995)

Fig. 4.8a shows the mean 500 hPa geopotential height difference between the 1983–1992 and the 1973–1982 periods, which roughly corresponds to the period when the SAO went from stronger to weaker conditions. During this period, there was a large pressure decrease to the south and southwest of South Africa and a pressure

University of Cape Town

increase between 35°-60°S to the southeast of South Africa. This dipolar pattern in pressure change in the South African region suggests an increase in the number of troughs approaching from the west, where pressure was decreased. The position of the pressure increase to the southeast of South Africa may have influenced these troughs becoming cut-off more to the east in region D compared to the more common region A for the previous decade, since it would tend to encourage large meridional displacements in the flow over eastern South Africa, and a strong contrast in the relatively tropical flow over eastern South Africa and the relatively polar flow over western South Africa.

A comparison of 1983–1992 with 1993–2002 (Fig. 4.8b) indicated that there was little change in the 500 hPa geopotential height distribution around South Africa, except for a small increase to the south and southeast of South Africa between 45° and 60°S. This pattern suggests a strengthening in the westward extent of the anticyclone south of South Africa and may have influenced region A becoming the more favoured region for cut-off lows (Table 4.2). Over the hemisphere as a whole, a Southern Annular Mode pattern (Kidson 1988) is apparent with a superimposed wave 3 structure in the midlatitudes.

Seasonal changes in 500 hPa geopotential height between the 1973-1982 and 1983-1992 decades are presented in Fig. 4.9. As has been discussed, the largest changes in cut-off low frequencies over this time period occurred in the MAM and JJA seasons. For the MAM season (Fig. 4.9b), there was a large decrease in geopotential height over the South Atlantic between 35°-60°S. The relatively zonal orientation of this decrease suggests that there was an increase in the zonal flow to the west of South

University of Cape Town

Africa. Thus, equatorwards meridional flow into the midlatitudes was likely decreased, reducing the likelihood of meridionally pronounced troughs forming, which is reflected in the reduction of the number of cut-off lows in this season from 45 in MAM of 1973-1982 to 30 in MAM of 1983-1992 (Table 4.2). In JJA, when there were 15 more cut-off lows during 1983–1992 than for 1973–1982 (Table 4.2), there was a reduction in the geopotential height south of South Africa (Fig. 4.9c). This area of geopotential height decrease extended to high latitudes, which suggests that there was an increase in the meridional flow, favouring the formation of meridionally extensive troughs and the potential for cut-off low formation. The increased geopotential height to the east of South Africa may have helped to promote the cutting-off process, while the location of the geopotential height decrease to the southeast of South Africa may have enhanced the likelihood of cut-off low formation over the northeast of South Africa as reflected in the large increase of cut-off lows in northeastern region D (Table 4.2). Additionally, the area to the west of South Africa showed increased baroclinicity in JJA as the lower troposphere warmed by 1.5°C and mid-levels became cooler by 0.5°C (not shown), suggesting greater numbers of baroclinic systems.

For the SON season, when there was also an increase in the number of cut-off lows in 1983–1992 compared to 1973–1982, particularly in northeastern region D (Table 4.2), there was a decrease in the geopotential height to the southwest of South Africa extending to 70°S (Fig. 4.9d). This reduction in geopotential height suggests an increase in the meridional flow to the west of South Africa, and thus the formation of troughs in that region. Additionally, there was a large increase in the geopotential height to the southeast of South Africa, which may

University of Cape Town

have favoured the cutting off process in region D, hence the increase in cut-off lows over that region (Table 4.2).

In the DJF season, there was a slight reduction in the total number of systems between 1973-1982 and 1983-1992 (Table 4.2), but the relationship to changes in geopotential height appears to be less robust. The change to the south of South Africa (Fig. 4.9a) was similar to that in the SON season (Fig. 4.9c), with a reduction in geopotential height to the southwest extending to high latitudes and an increase to the southeast. As discussed for the SON season, one would expect such a change in geopotential height to result in more cut-off lows, but for DJF the opposite is true. In the DJF season, however, the increase in geopotential height southeast of South Africa did not extend so far to the north, or to the south, and the magnitude was much less than in SON, which may have resulted in a weaker mechanism forcing troughs to become cut-off over South Africa. Additionally, Fig. 4.2 has shown that DJF is the season when the fewest cut-off lows formed, and therefore the seasonal signal likely obscures any relationship with the Southern Hemisphere geopotential height anomalies shown in Fig. 4.9a.

University of Cape Town

4.3.4.. Latitudinal width

The seasonal distribution of cut-off lows by latitudinal width is shown in Fig. 4.10. In the DJF season, the majority (about 36%) of cut-off lows have a latitudinal extent of 400 – 800 km, with 31% extending 800–1200 km, and 25%

being greater than 1200 km. Approximately 7.5% of cut-off lows in this season fell into the smallest category, with a latitudinal size of 100–400 km.

In the MAM season, when cut-off lows were most common over the 30-year climatology, the majority of cut-off lows (around 35%) had a latitudinal size of 800–1200 km. The 400–800 km and the greater than 1200 km categories each accounted for 30% of cut-off lows. Only 5% of cut-off lows fell into the 100–400 km category for this season.

Similar to the MAM season, the majority of cut-off lows (about 36%) in JJA had a latitudinal width of 800–1200 km. However, unlike the MAM season, a similar number of cut-off lows fell into the 400–800 km category, which accounted for 34% of the systems in the JJA season, as the 800–1200 km category. Accordingly, the number of systems larger than 1200 km in latitudinal size (25%) was much less in JJA compared MAM. Similar to MAM, only 5% of systems had a latitudinal size of 100–400 km.

In the SON season, there was a roughly equal distribution of systems between the 400–800 km (29%), 800–1200 km (29%), and greater than 1200 km (28%) categories. There was also a much larger proportion of small cut-off lows in SON compared to the other seasons, with the 100–400 km category accounting for 13% of the total for the season.

University of Cape Town

The interannual tendency in the average size of cut-off lows is presented in Fig. 4.11. It is clear from Fig. 4.11 that there was a tendency for the average size of cut-off lows to increase over subtropical southern Africa between 1984 and 1997. After 1997, the average decreased.

4.4. Summary

The purpose of this chapter was to develop a 30-year (1973-2002) climatology of cut-off low pressure systems over the subtropical southern Africa region from NCEP reanalysis data. The findings are consistent with a previous 10-year study, covering the period 1973-1982 (Taljaard 1985), with an average of approximately 11 cut-off lows per year and relative maxima in spring and autumn.

The interannual variability of cut-off lows over this region suggests that there may be some relationship between the frequency of cut-off lows and ENSO. Mature phase La Niña years were associated with increased occurrences of cut-off lows over subtropical southern Africa and, to some extent, the reverse was true for mature phase El Niño years.

In the 1980's, each year experienced an average or above average number of occurrences of cut-off lows, and there was a shift from MAM to JJA for the most favoured season for cut-off low occurrences over the region of the present study. Additionally, there was a change in the most common location for cut-off

University of Cape Town

lows from the southwest of the region to the northeast. This time period coincides with a weakening of the SAO, which has been shown to manifest itself in a strengthening of the subtropical ridge in winter due to a shift in zonal wavenumber 3 (Chen and Yen 1997). This strengthening of the subtropical ridge over, and to the east of South Africa, accompanied by a decrease in geopotential height over the South Atlantic, resulting in increased meridional flow, led to the increased number of cut-off lows in JJA. In MAM, however, there was an increase in the strength of the zonal flow to the west of South Africa creating less favourable conditions for troughs to extend equatorwards, and therefore fewer cut-off lows over the subtropical southern Africa region. These results suggest that there may be a strong relationship between the location and seasonality of cut-off lows over subtropical southern Africa, the SAO and zonal wavenumber 3.

Additionally, the latitudinal width and duration of cut-off lows has been discussed. In the MAM and JJA seasons, the majority of cut-off lows have a latitudinal width of 800-1200km, whereas in the SON and DJF seasons, smaller systems less than 800km in width account for a larger proportion of the total number of cut-off lows. From the mid-1980s, there was an increase in the average size of cut-off lows, which continued until the late 1990's. For all seasons, cut-off lows tended to be fairly short-lived at 1-2 days, which has been shown to be typical at subtropical latitudes (Price and Vaughan 1992). The

University of Cape Town

highest frequency of cut-off lows lasting for 2-4 days occurred in MAM, whereas those systems existing >4 days were most common in JJA.

This chapter has therefore established a climatology for cut-off low pressure systems over the subtropical southern Africa region, and proposed mechanisms for their interannual variability and changes in the most common seasons for occurrences over particular regions. Given that a high proportion of South Africa's flood disasters result from cut-off lows (Alexander 2000), better understanding of their seasonality and interannual variability should be a high priority. The following chapters present two case studies of cut-off lows that led to extreme quantities of rainfall over coastal regions of South Africa. In particular, the forcing mechanisms on the evolution of the low-level flow within the cut-off low environment are investigated using a mesoscale numerical model, with a view to establishing reasons for the extreme rainfall observed.

University of Cape Town

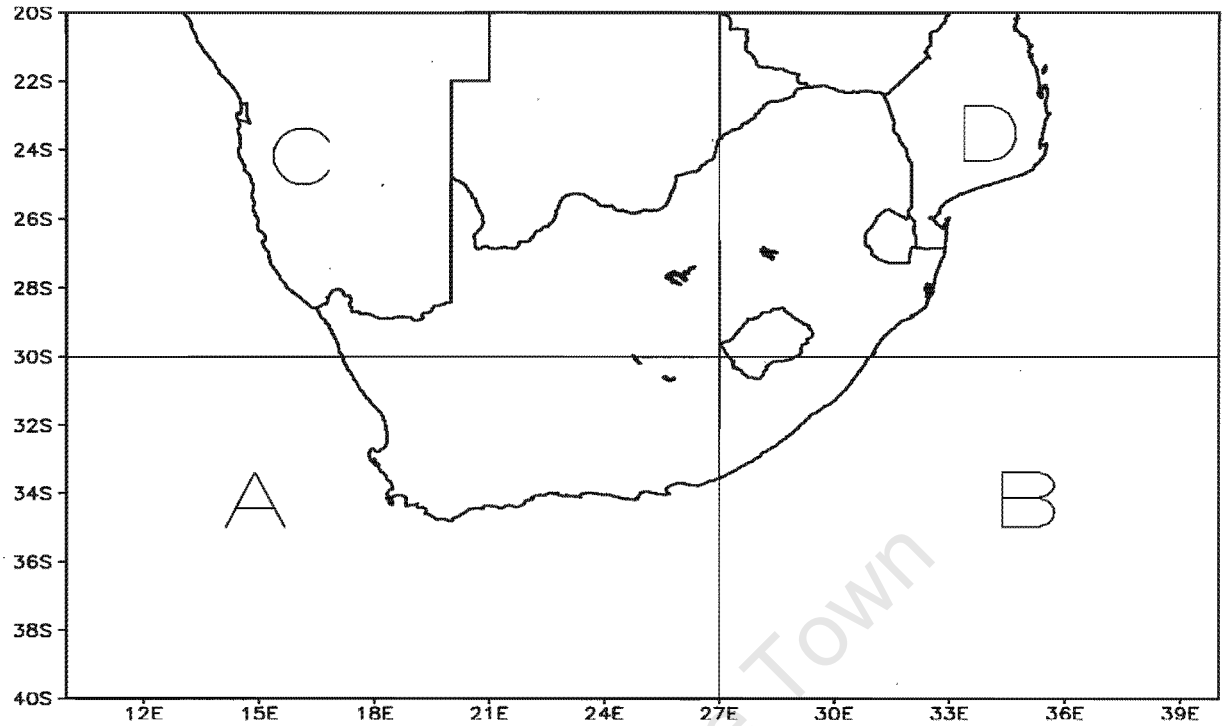

Figure 4.1 – Map of the domain covered by the cut-off low climatology divided into regions A, B, C, and D.

University of Cape Town

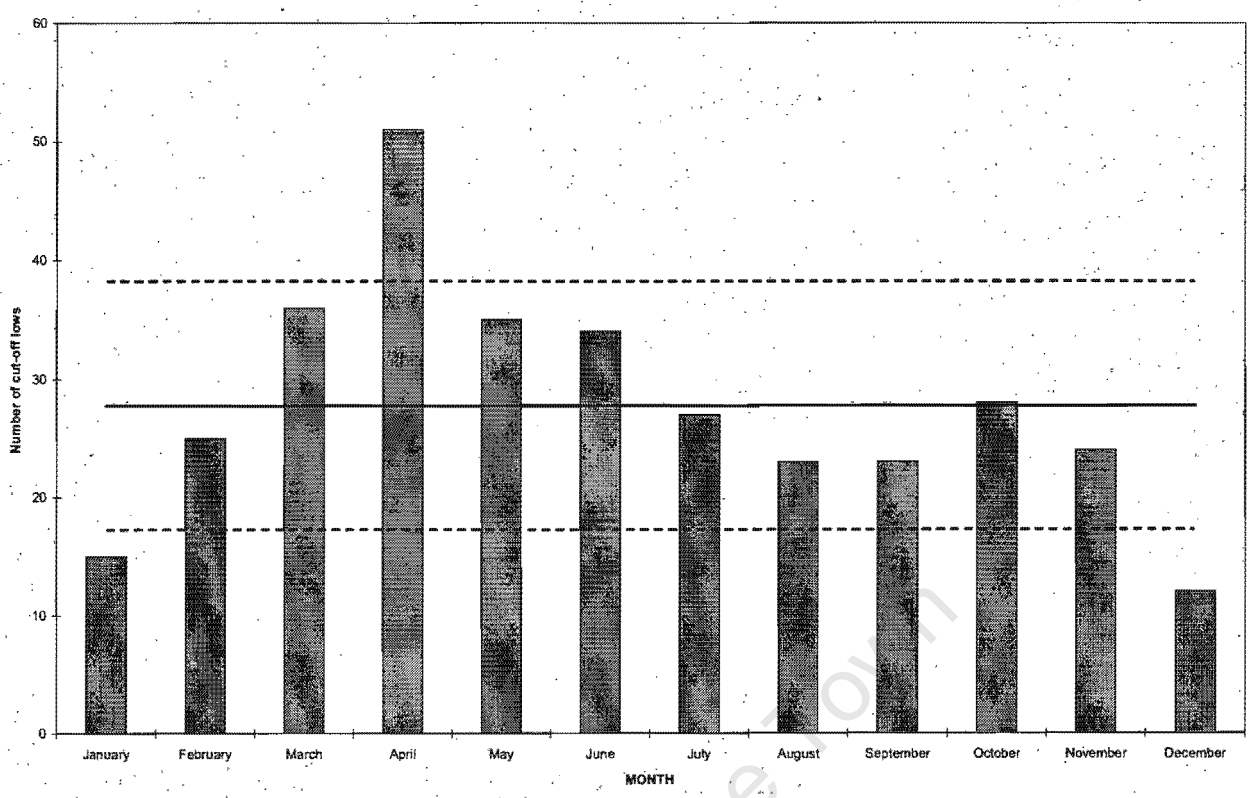

Figure 4.2 – Frequency distribution of occurrences of cut-off lows per month aggregated over the years 1973 – 2002. The solid horizontal line shows the mean, and the dashed lines one standard deviation either side of the mean.

University of Cape Town

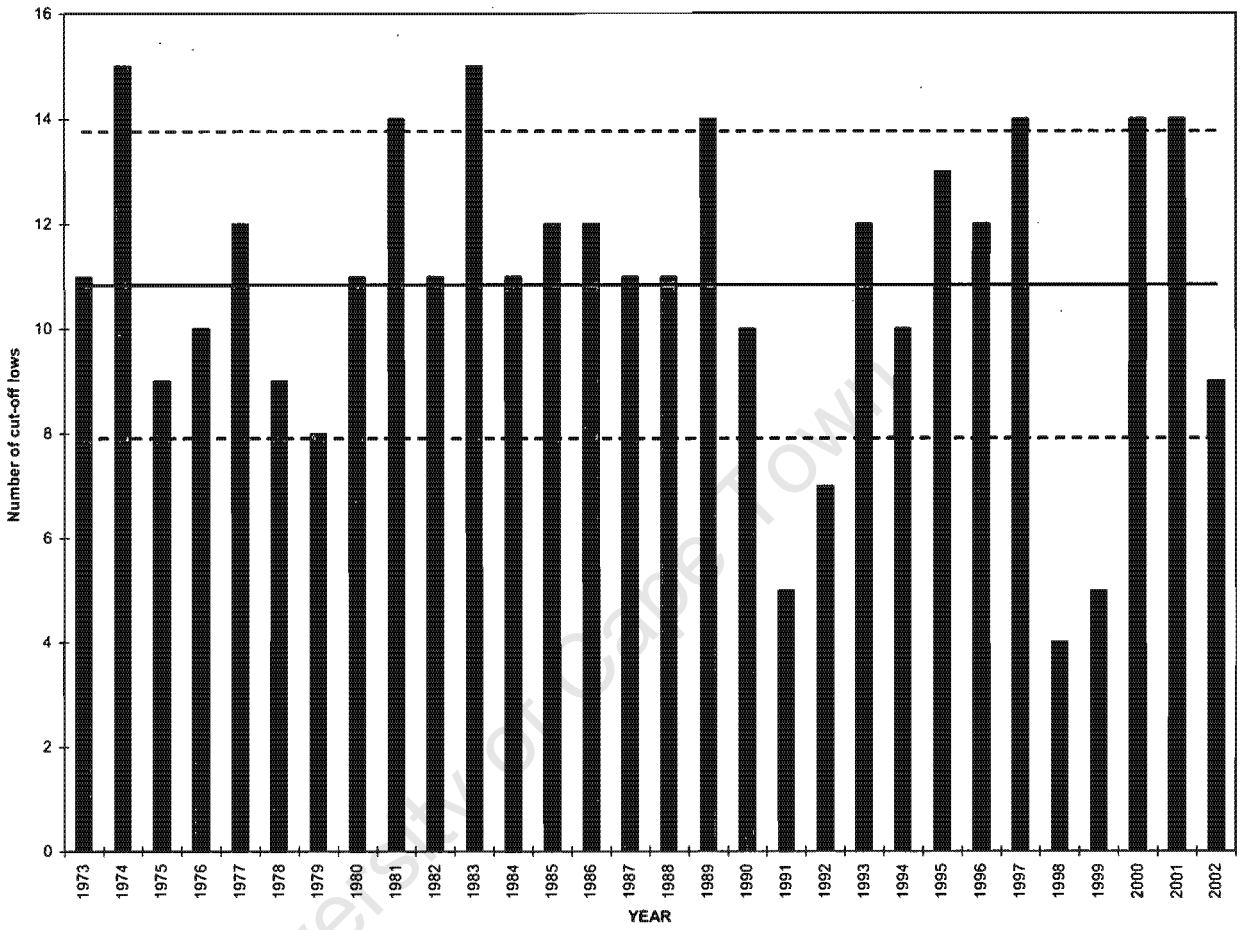

University of Cape Town

Figure 4.3 – Frequency distribution of cut-off lows per year from 1973 – 2002. The solid horizontal line shows the mean, and the dashed lines one standard deviation either side of the mean.

(a)

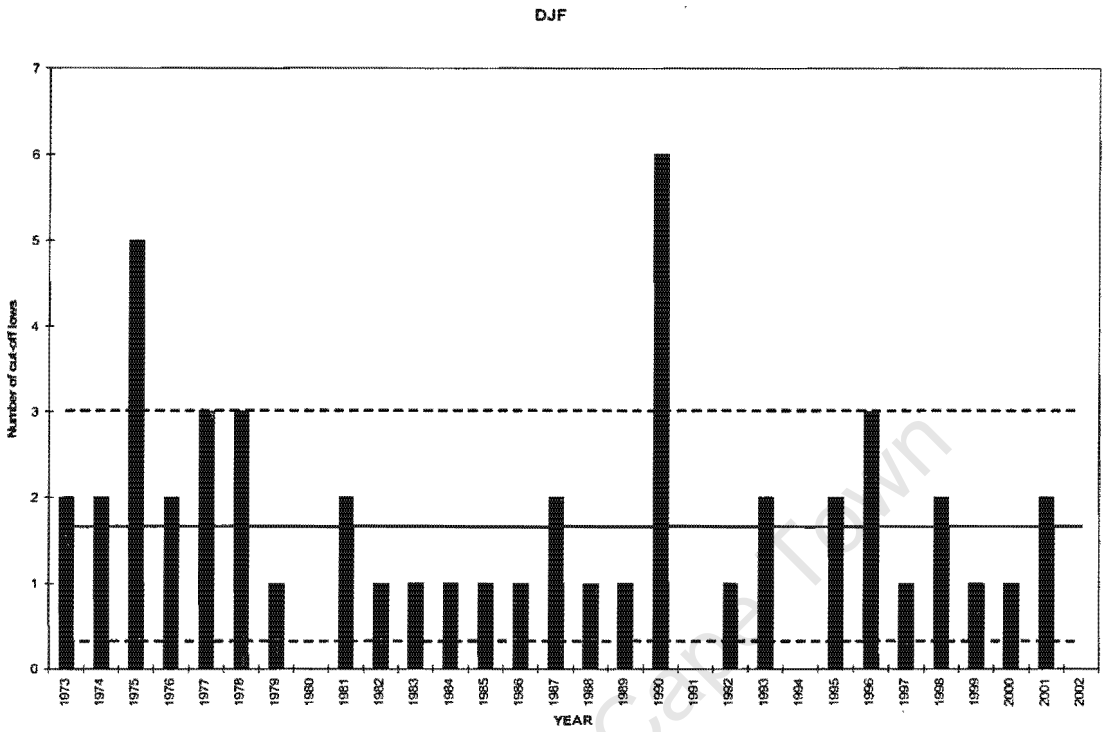

(b)

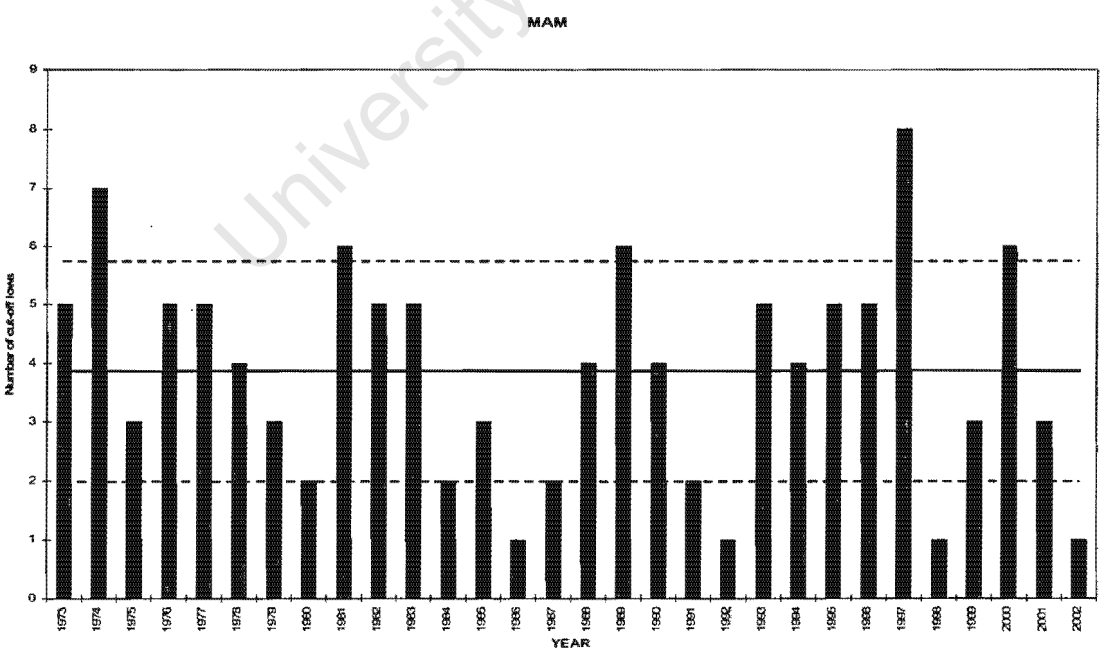

University of Cape Town

Figure 4.4 – Frequency distribution of cut-off lows for (a) DJF, (b) MAM, (c) JJA, and (d) SON for each year from 1973-2002. The solid horizontal line shows the mean, and the dashed lines one standard deviation either side of the mean.

(c)

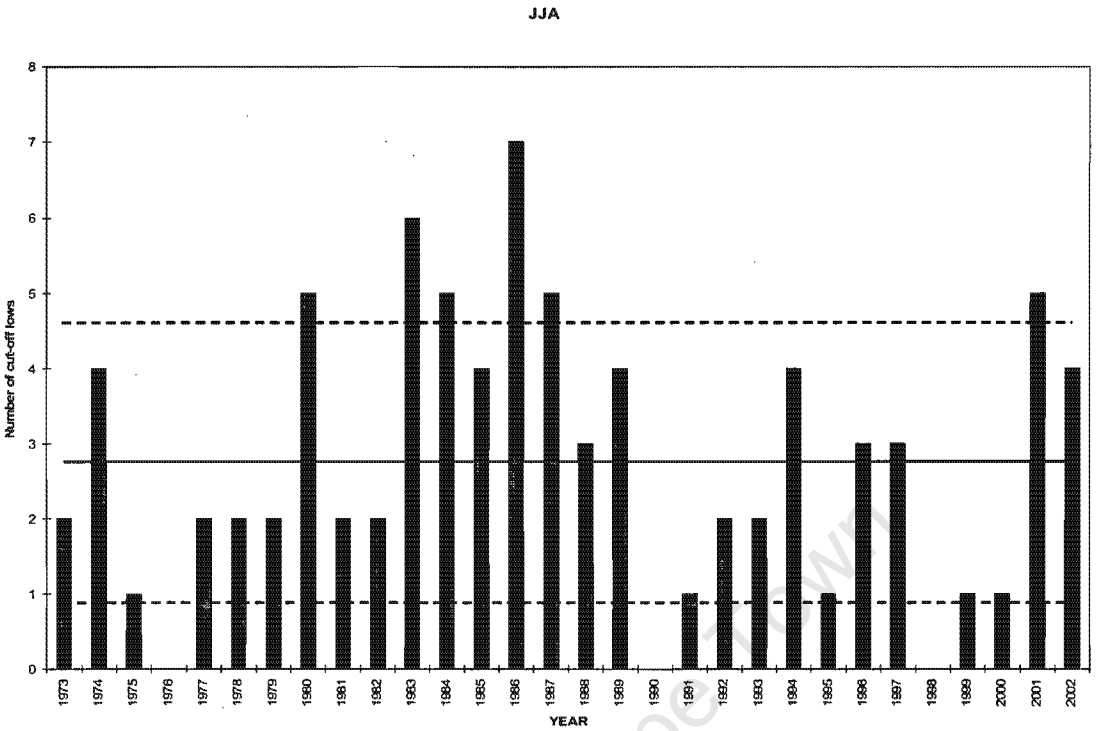

(d)

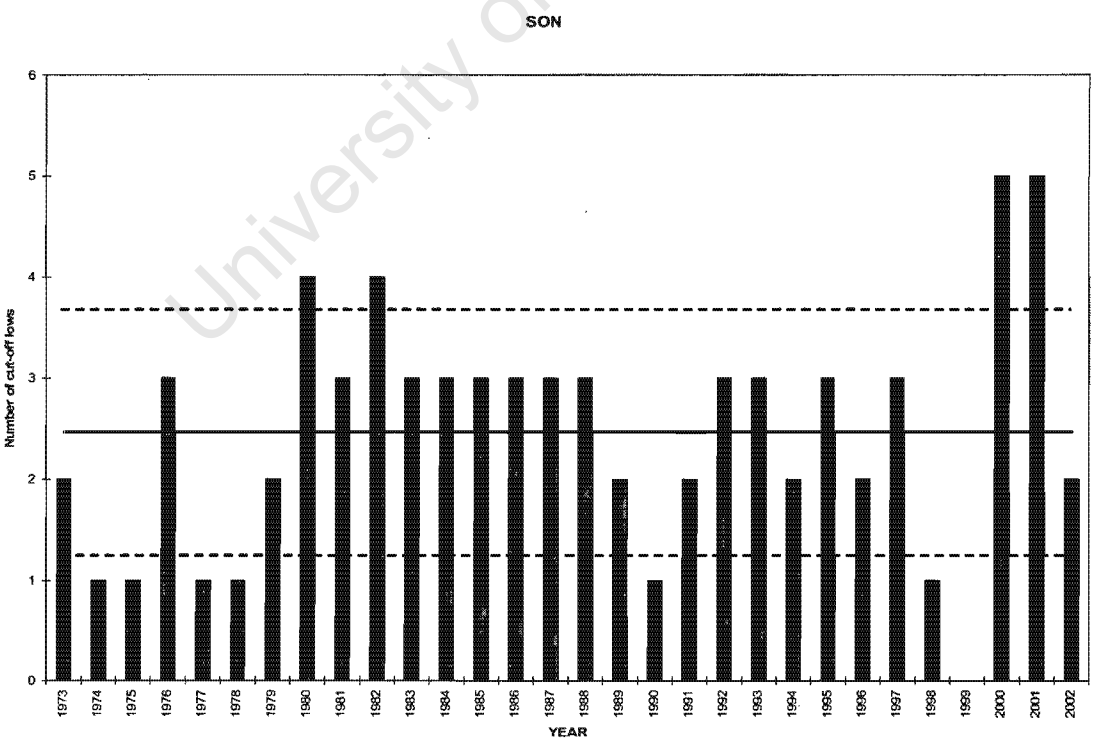

University of Cape Town

Figure 4.4 - *continued*

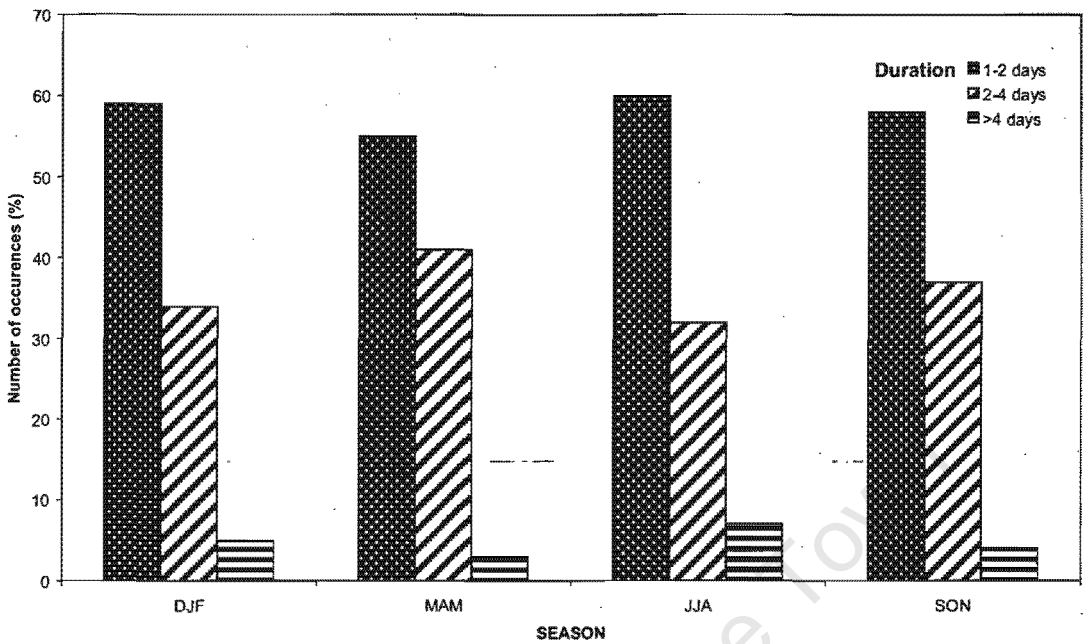

Figure 4.5 – Frequency distribution of the number of cut-off lows in three duration categories (as percentage of cut-off lows in each season) for the period 1973 – 2002.

University of Cape Town

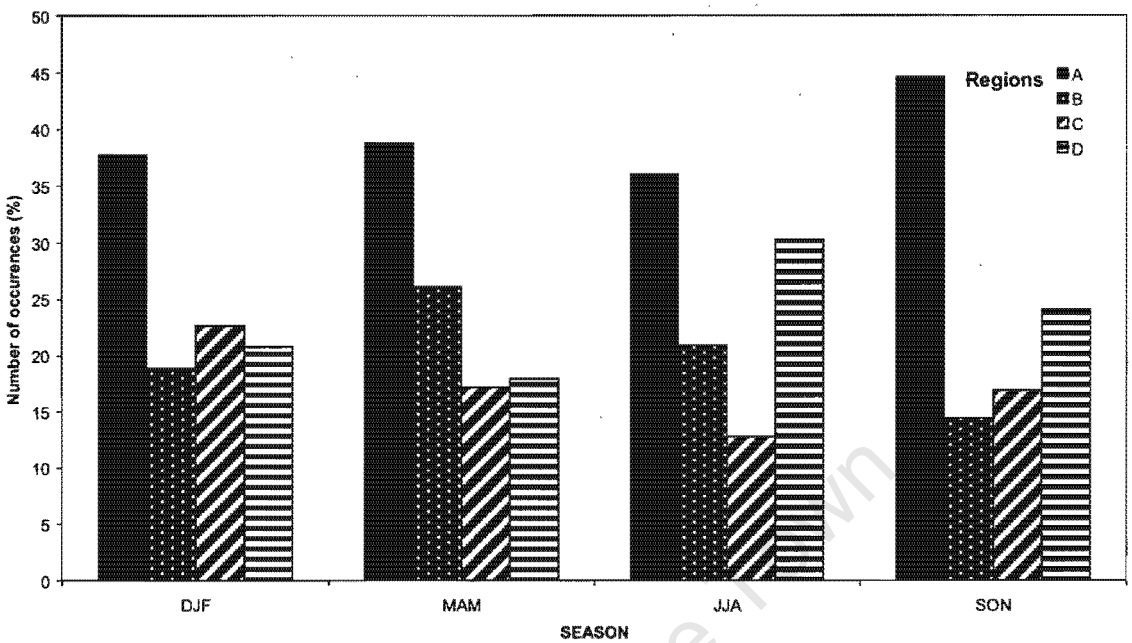

Figure 4.6 – Frequency distribution of the number of cut-off lows in regions A, B, C and D duration categories (as percentage of cut-off lows in each season) for the period 1973 – 2002.

University of Cape Town

(a)

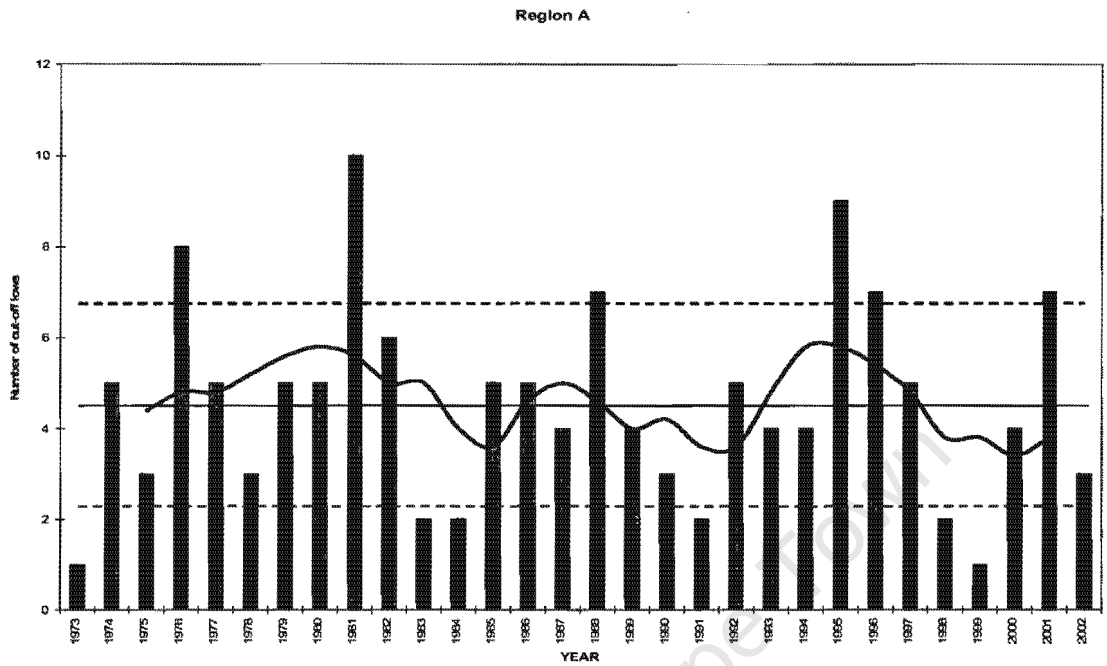

(b)

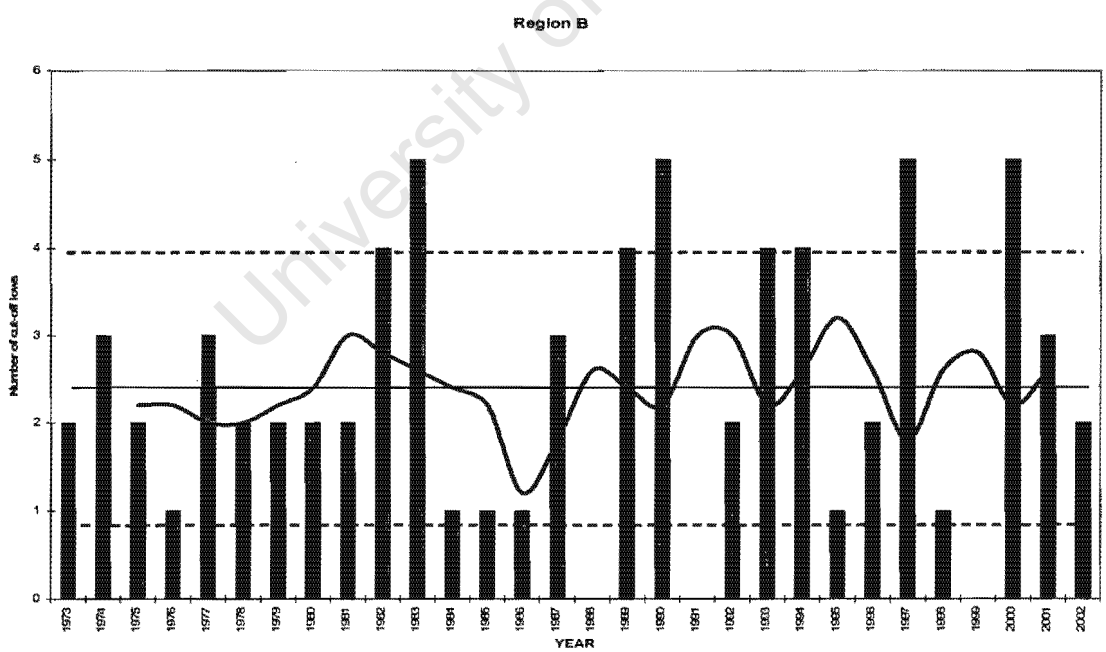

University of Cape Town

Figure 4.7 – Frequency distribution of the number of cut-off lows in (a) Region A, (b) Region B, (c) Region C and (d) Region D. The solid line represents a 5-year running mean. The solid horizontal line shows the mean, and the dashed lines one standard deviation either side of the mean.

(c)

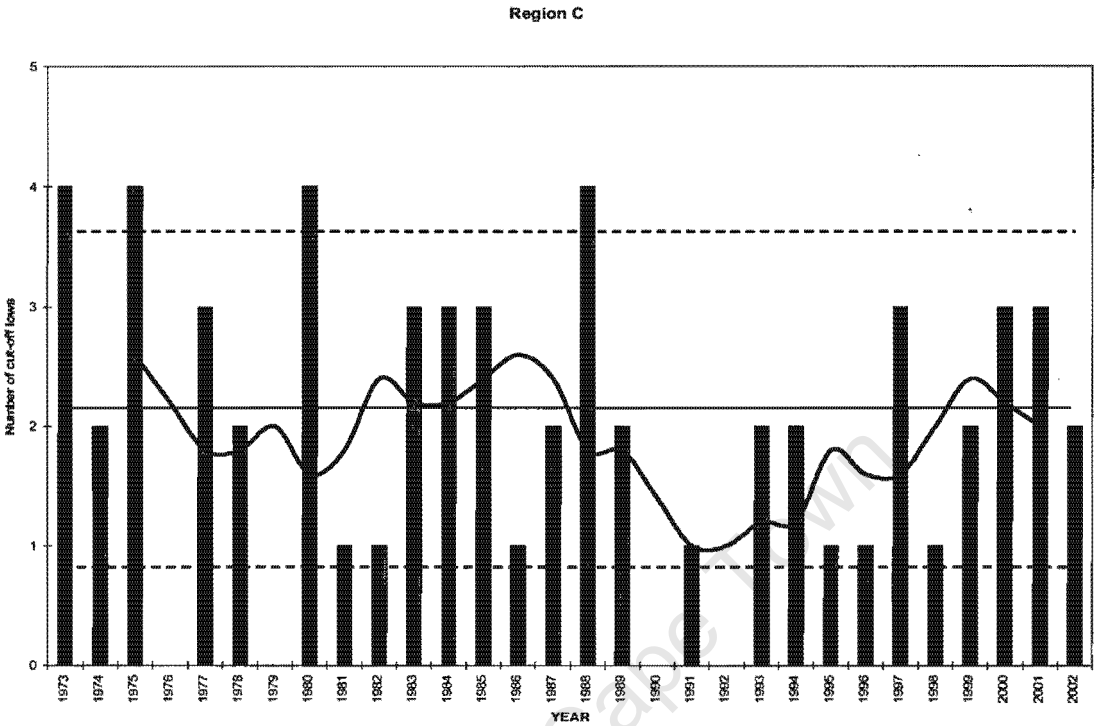

(d)

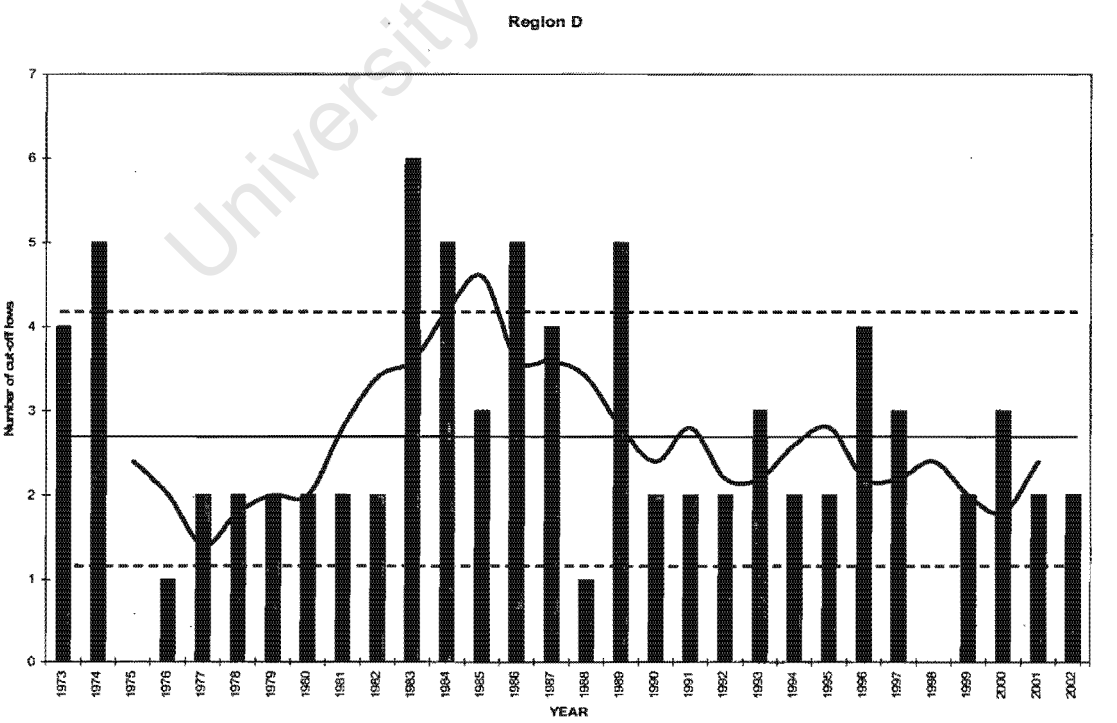

University of Cape Town

Figure 4.7 – *continued*

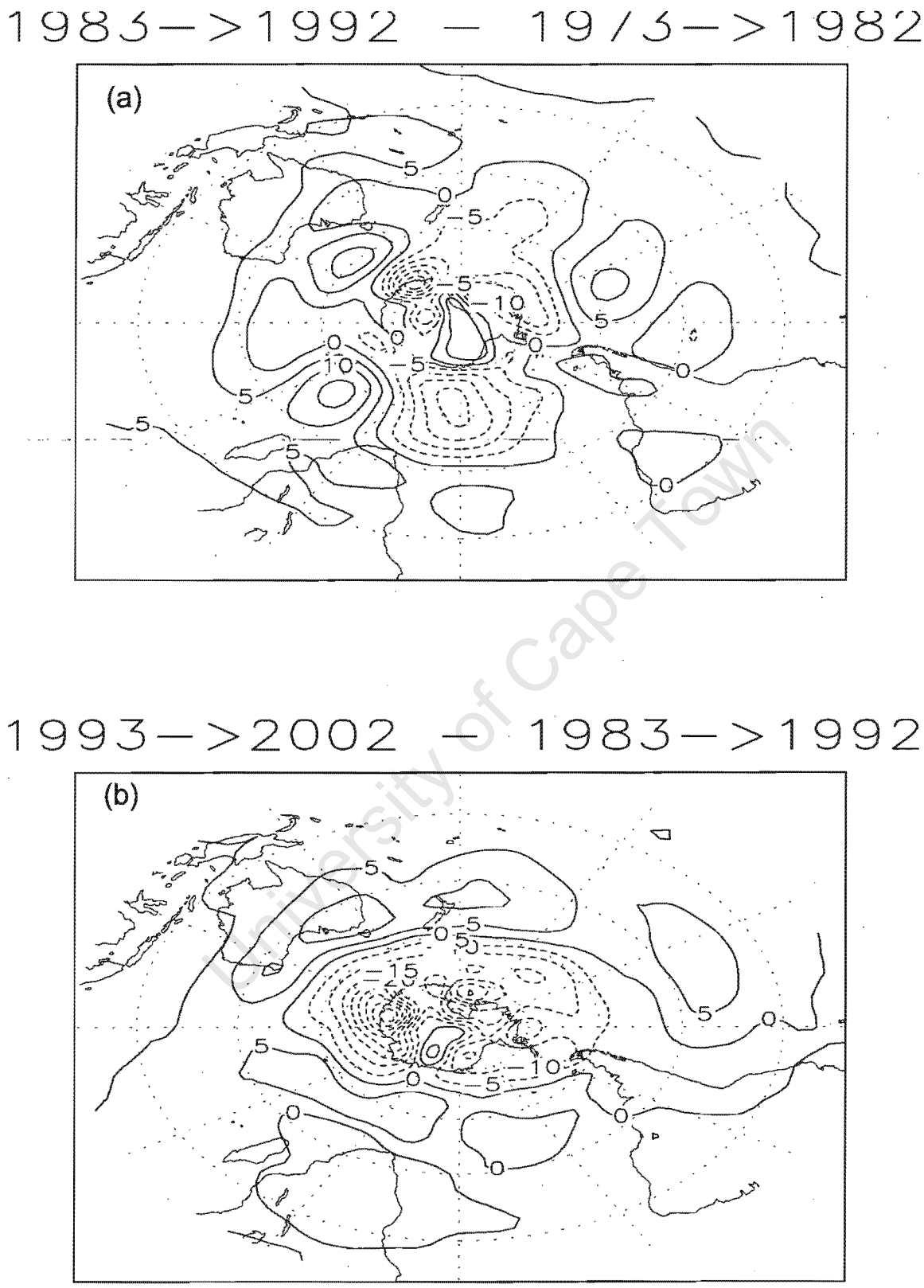

University of Cape Town

Figure 4.8 – Difference in the 500 hPa geopotential height: (a) 1983-1992 minus 1973-1982 and (b) 1993-2002 minus 1983-1992. Contour interval is 5m and solid (dashed) contours represent an increase (decrease).

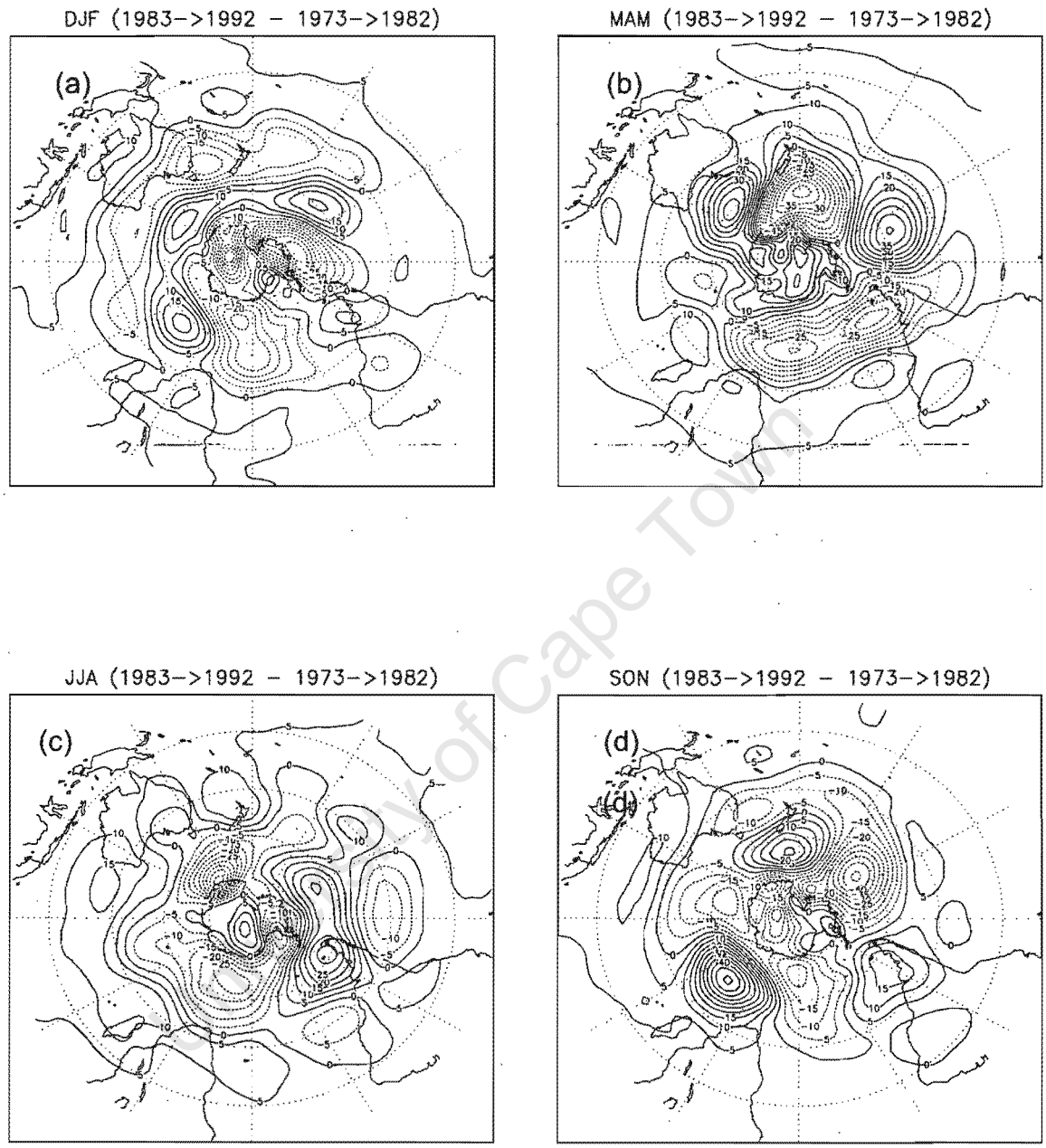

University of Cape Town

Figure 4.9 – Difference in the 500 hPa geopotential height: 1983-1992 minus 1973-1982; (a) DJF, (b) MAM, (c) JJA and (d) SON. Contour interval 5m, and solid (dashed) contours represent an increase (decrease).

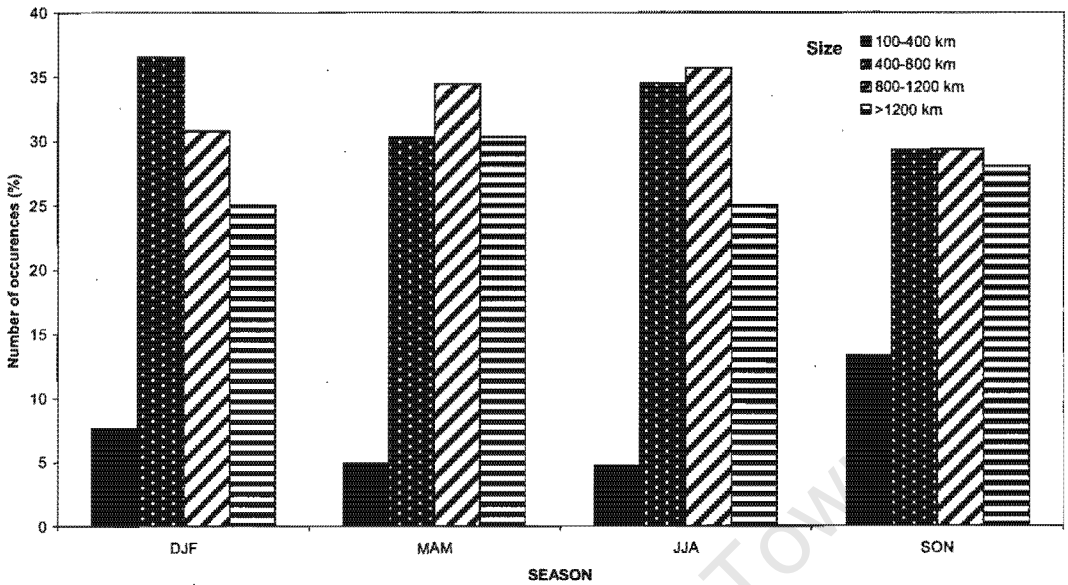

Figure 4.10 – Frequency distribution of the number of cut-off lows in four latitudinal width categories (as percentage of cut-off lows in each season) for the period 1973 – 2002.

University of Cape Town

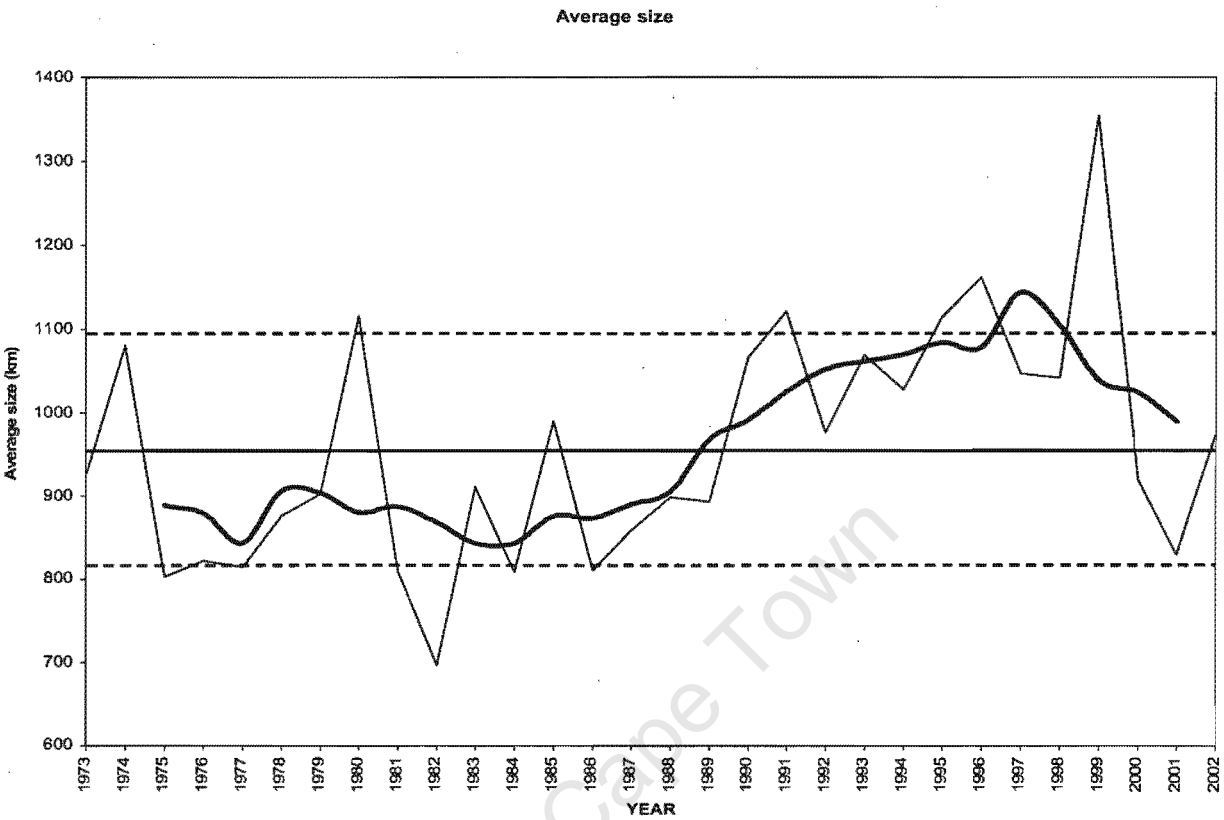

Figure 4.11 – Average size of cut-off lows from 1973 to 2002 (thin line), with a 5-year running mean (thick line). The solid horizontal line shows the long-term mean size, and the dashed lines show one standard deviation either side of the long-term mean.

University of Cape Town

Chapter 5

Synoptic Evolution and Model Validation

University of Cape Town

University of Cape Town

5.1. Introduction

The objective of this chapter is twofold. Firstly, an overview of the two case studies is presented. The quantity and location of the extreme rainfall for each of the case studies is discussed, and the evolution of the respective synoptic environments from the MRF model analyses is examined. Mechanisms which may have contributed to the extreme rainfall are identified. The second objective is to assess the ability of the mesoscale numerical model to simulate these events. Comparisons with observed precipitation, surface observations, MRF model analyses and satellite observations are made.

The chapter is set out as follows. In section 5.2, the East London case study is discussed in terms of the rainfall and synoptic evolution, and similarly in section 5.3 for the Montagu case study. Section 5.4 comprises a discussion of the validation of the MM5 output for the East London case study, with section 5.5 comprising the same for the Montagu case study. Section 5.6 concludes the chapter with a discussion of the similarities and differences between the two case studies.

University of Cape Town

5.2. The East London case: observations and synoptic overview

This event occurred in August 2002 and affected the coastal region of the Eastern Cape province. At least three lives were lost and there was considerable damage to homes, roads, bridges and infrastructure. Many storm drains were destroyed, and around 3000 people were left homeless due to flooding. The harbour at East London, which is of great importance to South Africa industry, was forced to close as water levels became too high to operate safely.

5.2.1. Observed precipitation

Figure 5.1a presents an objective analysis (Cressman 1959) of the observed rainfall over the Eastern Cape for the 24-hour period to 0800 LST 16 August 2002. (Note that LST = UTC + 2 hours). It is noted that caution should be observed in assuming that the spatial precipitation pattern is well resolved over this area since there are very few rainfall measuring stations, particularly near to the coast that can be included in the objective analysis. However, the spatial filtering implied by the analysis provides a slightly smoothed field which may be better suited to comparison with model results.

Heavy precipitation was mainly confined to the coastal region of the Eastern Cape of South Africa on 15-16 August, with a maximum at East London where 317 mm was measured at the SAWS recording station over the 24-hour period to 0600 UTC 16 August. This compares to the climatological average there for August of 78mm. Other precipitation peaks were observed at stations to the west of this, with 84mm at Grahamstown, and 81mm at Uitenhage, and there was little inland penetration of the rainfall (observed precipitation for all stations is included in Table B1, Appendix B at the end of this thesis). The maximum intensity of the precipitation occurred at the East London station between 2200 UTC 15 August and 0200 UTC 16 August, with a maximum rain rate of 84 mm.h-1 between 2300 UTC 15 August and 0000 UTC 16 August.

There appears to be little relationship between the individual rainfall peaks and topography in this region since the slope of the coastal topography here is relatively gentle, although it may be argued that the inland precipitation peaks are related to

University of Cape Town

the more complex topography there. However, it is possible that these precipitation peaks are an artefact of the paucity of available data in this region.

Rainfall over the ocean measured by the TMI sensor on the TRMM satellite showed an area of heavy precipitation to the southeast of the Eastern Cape coast centred at 37°E, 34°S, and a zonal band of precipitation just south of the Eastern Cape between 25°-35°S (Fig. 5.1b).

5.2.2. Synoptic evolution

A description of the synoptic structure and evolution of this case study follows, based mainly on analyses from the MRF model initialisation fields at 12-hour intervals.

The synoptic situation at 0000 UTC 15 August precedes the period of most intense precipitation over East London by 24 hours. The MRF model 500 hPa geopotential height, temperature and wind are shown in Fig. 5.2, with the corresponding fields at 925 hPa shown in Fig. 5.3. A cyclone centred at approximately 31°S, 20°E and embedded in a cold trough with a north-northwestward orientation, existed at 500 hPa over the west of South Africa, and a cold pool was present just to the south of the closed geopotential contour (Fig. 5.2a). An additional cold pool was also present over the ocean at 46°S, 22°E. A strong northwesterly jet flowing toward the South West Indian Ocean existed on the eastern side of the trough, while a warm ridge was present over Madagascar.

The low-level flow at this time was characterised by a ridge of high pressure over the ocean to the south of South Africa (Fig. 5.3a), a typical situation near the surface

University of Cape Town

during cut-off low events over South Africa (Taljaard 1985). Southeasterly onshore flow advected cold air from relatively high latitudes onto the Eastern Cape coast. Ahead of the ridge, an easterly trough advected warm, moist tropical air down the eastern seaboard of South Africa. Scatterometer surface winds derived from measurements from the QuikSCAT satellite show that the air being advected onto the Eastern Cape coast near to this time (~ 0500 UTC) originated from latitudes polewards of 45°S (Fig. 5.4a). As a result, a strong southwest – northeast air mass contrast existed in the lower levels of the atmosphere over the Eastern Cape coastal region.

The synoptic situation at 1200 UTC 15 August, at which time light precipitation had begun over coastal regions of the Eastern Cape, was similar to that seen twelve hours previously. The cyclone at 500 hPa had moved slightly to the east and was centred at approximately 31°S, 22.5°E, with strengthened cyclonic flow, while the northwesterly jet streak continued to exist on the eastern side of the trough (Fig. 5.2b). However, at this time, the cyclone did not appear to have any closed temperature contours associated with it as one would expect for a cut-off low. An inspection of the 700 hPa temperature distribution (not shown) revealed closed temperature contours around a cold pool approximately co-located with the cyclone at 500 hPa, suggesting that the centre of the cut-off low had penetrated lower into the troposphere.

At 1200 UTC 15 August (Fig. 5.3b), the near-surface ridge over the ocean had extended farther to the east, while the trough ahead of the ridge had extended over the ocean to the east of South Africa and farther to the south. As a result, the

University of Cape Town

strength of the onshore flow increased and led to the formation of an onshore LLJ impinging onto the coast at approximately 25.5–27°E. The flow in the vicinity of the entrance region of the LLJ had become more easterly suggesting that warmer, moister, lower latitude air than twelve hours previously was being advected onto the Eastern Cape coast by the LLJ, which is also confirmed by the QuikSCAT wind measurements near to this time (~1450 UTC) (Fig. 5.4b). However, it is unfortunate that at this time, some areas of interest for this event were obscured by the swathe of the satellite.

Twelve hours later, at 0000 UTC 16 August, during the period of most intense rainfall over East London, the gradient of the trough at 500 hPa had steepened towards its base to the northwest and at the head to the southeast. A closed geopotential height contour remained near 32°S, 24°E with a cold pool to its southwest (Fig. 5.2c). Towards the apex of the trough, a second cold pool had developed off the coast of Namibia, while the northwesterly jet streak continued to exist on the eastern side of the trough. At low-levels (Fig. 5.3c), the warm near surface trough to the east of South Africa extended farther to the south compared to twelve hours before, and the high pressure ridged farther to the east enhancing the pressure gradient over the ocean to the east of the Eastern Cape coast. As a result, the strength of the onshore LLJ increased further and remained at approximately the same location as twelve hours earlier (Fig. 5.3b). Towards the entrance region of the LLJ, the flow was northeasterly, suggesting that warmer, moister, subtropical air was being advected by the LLJ onto the Eastern Cape coast. Near this time (~0440 UTC), the QuikSCAT surface winds show that there was a considerable narrowing of the LLJ (Fig. 5.4c), and confirm the northeasterly flow into the LLJ. Additionally, the flow entering the

University of Cape Town

southern flank of the LLJ from the southeast did not originate from as far to the south compared to the previous measurement time (Fig. 5.4b).

Infrared images from the Meteosat satellite at the time of the heavy precipitation (0000 UTC 16 August) (Fig. 5.5) show a large area of cloud over the Eastern Cape coast, which extended to the east and appeared to be approximately co-located with the LLJ in Fig. 5.4c, indicating a possible association between the LLJ and the generation of cloud and precipitation in this region. A radiosonde ascent from Port Elizabeth at this time showed the atmosphere to be characterised by a deep layer of nearly saturated air, with evidence of the tropopause at 300 hPa (Fig. 5.6), above which the atmosphere was much less moist.

At 1200 UTC 16 August, the rainfall rate had reduced substantially over the Eastern Cape and the zonal extent of the trough at 500 hPa had contracted. A second closed geopotential height contour had formed towards the apex of the trough near 26°S, 16°E (Fig. 5.2d) associated with the cold pool that had existed there since 12 hours earlier. A cold pool remained over the Western Cape at 33°S, 20°E, with a closed geopotential height contour to its north at 30°S, 22°E. However, there was no evidence of closed cyclonic flow in the wind field there at this time. Near the surface, there was a weakening of the ridge of high pressure over the ocean to the south of the country, and the surface trough had moved to the east. The resulting pressure gradient weakened and led to weaker onshore flow and the disappearance of the LLJ (Fig. 4d). Shortly after this time (~ 1430 UTC), the surface winds derived from QuikSCAT show that the LLJ had moved to the east and no longer impinged onto the land (Fig. 5.4d). Although the swathe of the satellite obscured part of the region,

University of Cape Town

there was evidence of a depression at the surface over the ocean centred at approximately 35°E, 34°S, which appeared to provide the forcing for the LLJ on its western side.

Given that the cyclone that existed at 500 hPa was not accompanied by closed temperature contours around a cold pool at the same level at all times (e.g. 1200 UTC 15 August), as one would expect for a cut-off low, plus the observation that a secondary cut-off low appeared to develop as the trough extended to the northwest, an investigation of the system in terms of potential vorticity was undertaken in an attempt to clarify its evolution. For this purpose, dynamic tropopause maps of potential temperature were constructed. This was achieved by calculating the Ertel potential vorticity on isentropic surfaces and using the contour superposition method to construct the tropopause map. Briefly, the contour superposition method entails superposing the contour for the PV value defined as the dynamic tropopause from each isentropic surface onto a single map. On the new map, contours are labelled as the isentrope of the surface from which they came. Here, the dynamic tropopause is defined as the -1.5 PVU surface. This technique is discussed in detail by Morgan and Nielsen-Gammon (1998). Since PV is conserved on isentropic surfaces (Hoskins et al. 1985), it follows that potential temperature will be conserved on a constant PV surface, and thus pools of cold potential temperature at the dynamic tropopause reflect a PV anomaly in the troposphere due to a lowering of the dynamic tropopause (Morgan and Nielsen Gammon 1998).

At 0000 UTC 15 August, when a cut-off low was apparent in the geopotential height and temperature fields at 500 hPa over the west of South Africa (Fig. 5.2a), a cold

University of Cape Town

there was evidence of a depression at the surface over the ocean centred at approximately 35°E, 34°S, which appeared to provide the forcing for the LLJ on its western side.

Given that the cyclone that existed at 500 hPa was not accompanied by closed temperature contours around a cold pool at the same level at all times (e.g. 1200 UTC 15 August), as one would expect for a cut-off low, plus the observation that a secondary cut-off low appeared to develop as the trough extended to the northwest, an investigation of the system in terms of potential vorticity was undertaken in an attempt to clarify its evolution. For this purpose, dynamic tropopause maps of potential temperature were constructed. This was achieved by calculating the Ertel potential vorticity on isentropic surfaces and using the contour superposition method to construct the tropopause map. Briefly, the contour superposition method entails superposing the contour for the PV value defined as the dynamic tropopause from each isentropic surface onto a single map. On the new map, contours are labelled as the isentrope of the surface from which they came. Here, the dynamic tropopause is defined as the -1.5 PVU surface. This technique is discussed in detail by Morgan and Nielsen-Gammon (1998). Since PV is conserved on isentropic surfaces (Hoskins et al. 1985), it follows that potential temperature will be conserved on a constant PV surface, and thus pools of cold potential temperature at the dynamic tropopause reflect a PV anomaly in the troposphere due to a lowering of the dynamic tropopause (Morgan and Nielsen Gammon 1998).

University of Cape Town

At 0000 UTC 15 August, when a cut-off low was apparent in the geopotential height and temperature fields at 500 hPa over the west of South Africa (Fig. 5.2a), a cold

300K pool existed at the dynamic tropopause over the west coast of South Africa / Namibia, where there was also a small tropopause fold as the 300K pool crossed the 320K contour (Fig. 5.7a). By 1200 UTC 15 August, this cold pool at the tropopause had moved to the east and become located with the steep eastern flank of the dynamic tropopause (Fig. 5.7b), while at the same time the cut-off low in the 500 hPa geopotential height had moved a smaller distance eastwards, and the cold pool was situated lower in the troposphere at 700 hPa. At 0000 UTC 16 August, it appeared that the cold pool on the dynamic tropopause had split into two, with a 310K pool situated over the south coast of South Africa and a second 310K pool over the ocean to the west of Namibia (Fig. 5.7c). These two cold pools on the dynamic tropopause were reflected in both the geopotential height and temperature fields at 500 hPa (Fig. 3c). At 1200 UTC 16 August, a small cold pool remained on the dynamic tropopause over the Western Cape, while the northern cold pool became a narrow cold filament on the dynamic tropopause (Fig. 5.7d). At the same time, a large cold pool remained over the Western Cape at 500 hPa, while the cut-off low at the northern end of the trough appeared to strengthen.

The above discussion suggests that it is likely that the cut-off low observed in the geopotential height and temperature fields at 500 hPa was associated with an intrusion of high PV stratospheric air into the troposphere, while the formation of a second cut-off low appeared to be a result of a splitting of the PV anomaly in the troposphere into two separate anomalies. Additionally, the strengthening of the cut-off low that developed towards the apex of the trough on 16 August appeared to be related to the PV anomaly in the troposphere becoming a narrow filament.

University of Cape Town

5.2.3. Summary

This event was characterised by extreme rainfall over the coastal region of the Eastern Cape. East London received more than 300mm of rain over a 24-hour period, with the rain rate peaking at 84mm.h^{-1}, compared to the August climatological average of 78mm. The synoptic situation was characterised by the development of a cut-off low pressure system aloft over the Western Cape due to an intrusion of cold stratospheric air into the troposphere. In the lower troposphere, an LLJ developed due to a strong ridge of high pressure over the ocean to the south of South Africa and a trough to the east of the country creating a steep pressure gradient. This LLJ comprised warm moist tropical air from the northeast, which mixed with cooler drier air from the south, which was advected onto the coast of South Africa in the vicinity of East London. This strong air mass contrast was likely to have contributed to local instability and the heavy rainfall observed.

University of Cape Town

5.3. The Montagu case: observations and synoptic overview

This event occurred in March 2003 and affected the Western Cape coast and the adjoining hinterland. The town of Montagu, some 80km inland, was worst affected as the river there burst its banks leading to severe flooding. Several lives were lost in separate incidents due to high winds at the coast. There was also considerable damage to roads and property and a large amount of livestock was lost. This event received particular attention as the issued warnings were not sufficient for the appropriate precautionary action to be taken.

5.3.1. Observed precipitation

Over a ten day period from 21-31 March 2003, the south coast and adjoining hinterland received between 100mm and 200mm of rain (Fig. 5.8a), more than 200% of the climatological average for the whole month. The bulk of this rainfall occurred between 23-25 March, with the Heidelberg raingauge in the Western Cape recording 101mm of rainfall in the 24 hours to 0800 LST on 24 March alone, with a band of high rainfall extending inland from this station. Flash flooding affected the town of Montagu where 178mm of rain fell in the same 24-hour period (compared to the average for March of 19.5mm).

The 24-hour observed rainfall total objectively analysed (Cressman 1959) at 0600 UTC 24 March 2003 is shown in Fig. 5.8b. Over this region, rainfall measuring stations are less sparse than the in Eastern Cape, where the East London case study was centred. On this day, rain was heaviest near to the coast at 22.5°E, 34°S and inland at Montagu (See Table C1, Appendix C, at the back of this thesis for individual rainfall station data. The rainfall derived from the TMI sensor on the TRMM satellite shows that this rainfall at the coast extended over the ocean to the south of the Western Cape (Fig. 5.8c)

The coast of the Western Cape and the adjoining hinterland is characterised by steep topography, suggesting that observed peaks in the rainfall may have been influenced by topographic processes. However, the inland region in particular has a relatively sparse network of rainfall measuring stations and so some caution is needed in attributing extreme rainfall to the topography at this stage.

University of Cape Town

5.3.2. Synoptic evolution

The sequence of satellite images over the night of 23-24 March (Fig. 5.9), shows a circular area of cloud over the southwest of South Africa, indicative of cyclonic circulation, and a band of frontal cloud over the east of the country. This 'comma' type cloud formation is typical of well developed, highly baroclinic disturbances in the midlatitude Southern Hemisphere westerlies (Preston-Whyte and Tyson 1988). As the region of circular cloud appeared to weaken, a band of cloud persisted to the south of the Western Cape, suggestive of continued convection in this region.

Data taken from the MRF model analysis fields at twelve hour intervals show the evolution of this system as it developed from a cold trough at 500 hPa into a severe cut-off low system (Fig. 5.10). At 0000 UTC 23 March, there was a cold trough oriented equatorwards towards the northwest, with its apex to the west of South Africa (Fig. 5.10a). A jet streak was apparent on the western side and around the apex of the trough, which was an equatorward extension of the subtropical jet, a scenario typical for the formation of a subtropical type cut-off low (Price and Vaughan 1992). The near surface flow at this time was characterised by a LLJ off the southwest coast of South Africa, with a steep temperature gradient across the land and high pressure ridging in from the northwest over the ocean to the south of the country (Fig. 5.11a). This ridge of near surface high pressure extending to the south of South Africa is a characteristic typical for cut-off lows in this region and aids the advection of warm, moist tropical air into the system from the northeast (Taljaard 1985). Surface winds derived from QuikSCAT around this time (~ 0600 UTC) show that strong southeasterly winds existed over the ocean to the south of South Africa, which were advecting air from higher latitudes towards the Western Cape coast (Fig

University of Cape Town

5.12a). Additionally, there was some evidence of alongshore westerly flow off the south coast of South Africa, indicative of topographic blocking of the onshore flow.

By 1200 UTC 23 March, a steep temperature gradient had developed at 500 hPa to the south of the Western Cape (Fig. 5.10b) indicative of the cold, relatively high latitude air in the trough becoming cut-off from its source region, and a closed contour had formed in the geopotential height. Near the surface, the axis of the ridge of high pressure to the south of South Africa had moved slightly to the north, while a tongue of cool air extended from the ocean over the Western Cape (Fig. 5.11b). Note that average daytime temperatures for this region in March are of the order 25-32°C whereas Fig. 5.11b shows much a cooler air temperature of 11°C at 925 hPa and observed maximum surface temperatures were record lows at several stations (e.g. Beaufort West had a maximum temperature of 17°C, compared to the previous lowest recorded daytime maximum there of 18.5°C). The winds derived from QuikSCAT near to this time (~ 1600 UTC) show continued southeasterly flow from high latitudes that becomes westerly at the coast (Fig. 5.12b).

University of Cape Town

At 0000 UTC 24 March, the nearest available MRF data to the time of the most intense rainfall, the 500 hPa analysis showed closed contours in the geopotential height, indicative of a cyclonic vortex, with a jet streak extending around its flanks and a relatively steep temperature gradient to the cold air at its centre (Fig. 5.10c). Near the surface, a depression had formed over the south coast of South Africa, below the cut-off low at 500 hPa. On the western side of this low, there was an onshore LLJ with wind speeds in excess of 24 $m.s^{-1}$, and a well developed cold front to the east (Fig. 5.11c), as seen in the satellite imagery (Fig. 5.9). The LLJ appeared

to extend up to at least the 500 hPa level (Fig. 5.10c), and to be advecting warm air of lower latitude origin out over the ocean and back onto the Western Cape coast near the surface. Close to this time (~ 0600 UTC), the QuikSCAT derived surface wind shows very strong southerly wind over the ocean to the south of the Western Cape coast (Fig. 5.12c). The wind speed maximum was located just off the coast near 20°E, 35°S. The QuikSCAT winds suggest that the air being advected onto the coast originated from latitudes around 45°S. At this time there was little evidence of the surface depression in the QuikSCAT winds, although part of the ocean in this region was obscured by the swathe of the satellite.

The nearest available upper air observations were from Cape Town, and the sounding taken there at 0000 UTC 24 March (Fig. 5.13) exhibited the signature of the LLJ, and the jet streak near 500 hPa, with a layer of stable air capping the moist air at around 800 hPa. The static lapse rate at low levels, taken from the difference in temperature from the MRF model between the 1000 hPa and 800 hPa levels at this time, reveals an area of steep static lapse rate, indicative of low-level instability, over the ocean areas to the west and south of South Africa (Fig. 5.14). Over the Western Cape, the low-level lapse rate was generally between 6 $K.km^{-1}$ and 7 $K.km^{-1}$, with some areas in excess of 7 $K.km^{-1}$ in the west, suggesting that convection may have occurred to return the stratification of the lower troposphere towards that of a moist adiabat (typically around 6.5 $K.km^{-1}$).

By 1200 UTC 24 March, the jet streak on the western flank of the cut-off low had weakened and the temperature and geopotential height gradients on its southern side had become less steep (Fig. 5.10d). However, the jet streak on the eastern flank

University of Cape Town

of the cut-off low remained. The depression near the surface had weakened considerably, but the onshore LLJ persisted on its western flank, with a tongue of warm air extending onto the landmass to its east, while the ridge of high pressure to the south had weakened (Fig. 5.11d). During 25 March, when the intensity of the rainfall had reduced considerably, the cut-off low moved to the east with the jet streaks on its flanks weakening (Fig. 5.10e-f), and the LLJ disappeared as the surface pressure filled (Fig. 5e-f). Near to this time (~1600 UTC), the QuikSCAT surface winds (Fig. 5.12d) showed that the LLJ was slightly weaker than at the previous measurement time (Fig. 5.12c), with the onshore flow coming from latitudes around 45°S.

A clarification of the upper air evolution from a PV perspective follows. Tropopause maps were constructed using the same contour superposition method as in the East London case. At 0000 UTC 23 March, when a cold trough existed over the west of South Africa at 500 hPa (Fig. 5.10a), there was an equatorward extension of high PV air in the troposphere over the same region (Fig. 5.15a). At this time, the tropopause was steep on its western side indicative of a strong upper level jet streak there (Hoskins et al. 1985; Morgan and Nielsen-Gammon 1998). At 1200 UTC, a steep temperature gradient had developed (Fig. 5.10b), perhaps in response to the 310K contour on the dynamic tropopause becoming more zonal (Fig. 5.15b). There was a steepening of the tropopause at the northern edge of the trough near to 20°E, 28°S indicative of an increase in the wind speed there. It is also evident that at this time, the high PV aloft was passing over a baroclinic zone near the surface over the Western Cape (Fig. 5.11b). This is a typical situation for surface cyclogenesis (Hoskins et al. 1985), and it is therefore likely that the PV anomaly in the upper

University of Cape Town

troposphere in association with a baroclinic zone near the surface led to the development of the surface depression.

By 0000 UTC 24 March, a severe, cold-cored cut-off low had developed at 500 hPa (Fig. 5.10c) as a result of the high PV air in the troposphere becoming cut-off from its high latitude source region (Fig. 5.15c). The PV anomaly in the troposphere included a narrow filament of 310K air towards the eastern side of the trough where the dynamic tropopause had become steeper. At 1200 UTC 24 March, the cut-off low at 500 hPa had moved to the east (Fig. 5.10d), and this was reflected in an eastward movement of the cold air on the dynamic tropopause (5.15d). Additionally, the gradient on the eastern flank of the trough had weakened as the 310K contour was located farther to the west of the eastern flank of the trough. Over the following 24 hours, as the cut-off low continued to track east (Fig. 5.10e-f), the PV anomaly in the troposphere moved to the east (Fig. 5.15e-f). By this time, the 310K contour had disappeared, indicative of a slight warming of the dynamic tropopause, likely as a result of latent heat release due to convection (Hoskins et al. 1985).

University of Cape Town

5.3.3. Summary

This event was characterised by heavy rainfall over the Western Cape south coast and the adjacent hinterland. The town of Montagu received nearly 200mm over a 24-hour period and suffered severe flash-flooding. The synoptic environment was characterised by a severe cut-off low pressure system aloft, which formed as a result of high PV air in the troposphere becoming cut-off from its high latitude source region. The cut-off low aloft was reflected in a depression at the surface, where a strong onshore LLJ developed on its western flank, with wind speeds in excess of 25

$m.s^{-1}$. This LLJ appeared to be advecting moist maritime air onto the south coast of the Western Cape.

5.4. The East London case: model validation

For this case study, MM5 was initialised at 0000 UTC 14 August 2002 with the initialisation fields from the MRF model at this time. A 27km horizontal resolution grid with 142 x 112 grid points, centred at 36°S, 26°E, and 40 σ-levels in the vertical was used. Topography was taken from the 5-minute resolution USGS dataset. In addition, nested grids with horizontal resolutions of 9km and 3km were tested, and are discussed later in this chapter. The parameterisations that deal with sub-gridscale processes are described in Chapter 3. A timestep of 40 seconds was used and output from the model was saved every hour. Subsequently, the saved output was vertically interpolated from the model σ-levels onto standard pressure levels.

The precipitation field in MM5 for the 24 hours to 0700 UTC 16 August (Fig. 5.16a) corresponds to the observed rainfall plot in Fig. 5.1a. While comparison here may be flawed due to the relative paucity of rainfall stations in this region and observations over the ocean are only inferred from two satellite passes, it gives some indication of how well the model performed in simulating the rainfall for this case study. Unfortunately, MM5 was unable to capture the observed extreme rainfall maximum of 317mm over East London (33°S, 27.5°E), simulating a precipitation maximum of 190mm just off the south coast of the Eastern Cape at 34°S, 26°E. However, the timing of the most intense precipitation in MM5 compared well with that observed at East London, suggesting that the precipitation maximum in the model corresponds to the maximum observed at East London. Over the ocean, MM5 simulated a zonal

University of Cape Town

band of precipitation to the east of the Eastern Cape, which is approximately co-located with the cloud observed in the Meteosat infra-red image at 0000 UTC 16 August (Fig. 5.5), and was also reflected in rainfall derived from TMI sensor on the TRMM satellite (Fig. 5.1b).

Therefore MM5 had some difficulty in correctly locating the precipitation, particularly over the coast. The maximum was also underestimated, which is a flaw often associated with mesoscale models. However, the overall structure of the precipitation field in MM5 appeared to be in agreement with the location of thick cloud in the infra-red satellite imagery.

For validation of the large scale flow, MM5 fields were compared with the MRF analyses at 0000 UTC 16 August 2002, since this was the time at which precipitation was most intense (see Fig. B1, Appendix B, for other times). A comparison of the large scale flow at 925 hPa at this time from MM5 (Fig. 5.16b) with the MRF analysis at this time (Fig. 5.3c) shows that MM5 was unable to accurately resolve the position of the onshore LLJ. MM5 shows the LLJ impinging on the Eastern Cape coast at approximately 150 km to the west of that suggested by the MRF model analysis at this time. However, many other aspects of the large scale flow were adequately resolved in MM5, suggesting that its main difficulty was in correctly simulating the mesoscale processes contributing to the event around the area of the extreme precipitation near East London. MM5 suggests that a meso-beta scale low pressure system formed off the Eastern Cape coast with cyclonic circulation over the coast between 26°-27.5°E. There is some evidence of a cyclonic flow at this time in the MRF model analysis on the northern flank of the LLJ over the Eastern Cape coast

University of Cape Town

(i.e. weak offshore flow at 33°S, 29°E in Fig. 5.3c), although this is farther to the east compared with MM5, consistent with the erroneous location of the precipitation maximum and the LLJ in the MM5 simulation. Further experiments were undertaken with different parameterisations for boundary layer processes and sub-gridscale convection, but the combination of parameterisations described in Chapter 3 appeared to produce the results that were most comparable with the MRF analyses.

The model was re-run with two nested grids centred over East London using two-way nesting at 9km and 3km resolution. For these higher resolution grids, topography was taken from the 2-minute and 30-second resolution USGS datasets respectively. The results from the three grids are hereafter referred to as EL1, EL2 and EL3 for the 27km, 9km and 3km grids respectively. Since two-way nesting was used, the outer 27km resolution grid, EL1, was affected by the inner grids, EL2 and EL3, over East London. In EL1 (Fig. 5.17a), the precipitation maximum was moved inshore and approximately 0.4° to the east compared to the run with the single 27km grid (Fig 5.16a). However, the quantity of this maximum was reduced from 190mm to 130mm. The inland penetration of the precipitation was forecast farther to the east, and appeared to be associated with the topography. It is difficult to confirm whether this topographic precipitation was real or an artefact of the model, since rainfall measuring stations were particularly sparse over the Eastern Cape interior. In EL2 (Fig. 5.17b), the overall structure of the simulated precipitation was similar to that in EL1 (Fig. 5.17a), but the quantity of the precipitation maximum was increased to 178mm. A second maximum was forecast to the west of this, which may correspond to the peak observed at Bathurst (Fig. 5.1a). In EL3 (Fig. 5.17c), the overall structure

University of Cape Town

of the precipitation was largely the same as that in EL2 (Fig. 5.17b), but the precipitation maximum was increased to 234mm.

At 500 hPa (Fig. B2Appendix B), the simulation with the single 27km grid compared very favourably with the MRF model analysis suggesting that inaccuracies were due to problems in adequately simulating processes in the lower troposphere. While the single 27km grid simulation had some difficulties in accurately simulating the location of the precipitation maxima and the LLJ, little advantage was gained by increasing the grid resolution at great computational expense. Therefore, it was decided that an analysis of this event from the single 27km grid simulation would be adequate. However, the higher resolution grids are able to provide some extra validation of the MM5 simulation by comparison with station data time series.

Eight automatic weather stations exist in the area covered by EL3: Queenstown (26.88°E, 31.92°S); Fort Beaufort (26.63°E, 32.78°S); Bisho (27.28°E, 32.90°S); East London (27.83°E, 33.03°S); Grahamstown (26.50°E, 33.28°S); Port Alfred (26.88°E, 33.60°S); Uitenhage (25.43°E, 33.70°S) and Port Elizabeth (25.52°E, 33.98°S). Time series from EL3 of surface temperature and pressure were constructed by bi-linearly interpolating to the station locations from the four surrounding grid points. These time series were compared with observations at these stations (Fig. 5.18).

There appeared to be a bias at all stations in simulating too cool a temperature overnight on 14-15 August, and too warm a temperature during the day on 15 August (Fig. 5.18). This suggests that EL3 was not producing enough cloud at this time leading to excessive outgoing longwave radiation overnight, and too much incoming

University of Cape Town

shortwave radiation during the day. At East London (Fig. 5.18d), the daytime temperature was too warm in EL3 by up to 7°C, suggesting that the hypothesis of a lack of cloud there in the simulation appears to be confirmed in that more than 300mm of precipitation was observed there, but in EL3 there was no precipitation simulated at East London. The same argument can also be assumed to be valid at Uitenhage, since precipitation was also greatly underestimated in EL3 there. For the other stations, however, this argument is not so robust, but it seems logical to assume that too cold a night-time temperature followed by too warm a daytime temperature is related to an underestimation of the amount of cloud produced by the simulation. (Cloud cover from the model is shown in Fig. B3, Appendix B cf Fig. 5.5)

The time series of surface pressure (Fig. 5.19) indicate that the low pressure that developed over the Eastern Cape coast in the simulation (Fig. 5.16b) was sustained for too long in the simulation. There was an overestimation in the magnitude of the pressure decrease at Port Alfred, which is consistent with the LLJ and rainfall being simulated too far to the west. However, the lack of pressure decrease in EL3 at Port Elizabeth and Uitenhage indicates that the base of the trough that extended down the eastern seaboard of South Africa (Fig. 5.3) did not extend far enough to the west in the simulation.

To summarise, MM5 was able to simulate the large scale flow for this event, but had some difficulty in accurately simulating the mesoscale aspects near the surface near to the location of the most intense rainfall. The precipitation maximum and the LLJ were simulated to be approximately 150km to the west in the MM5 simulation compared the position suggested by the MRF model analyses. Increasing the

University of Cape Town

horizontal grid resolution to 3km reduced the discrepancy in the location of these features by approximately 40km. Additionally, comparison of surface parameters from the 3km grid with station observations suggest that MM5 did not generate sufficient cloud in the simulation.

Given that little improvement was achieved by increasing the grid resolution, it was decided that the analysis of this event presented in Chapters 6 and 7 could be based on the simulation with a single 27km grid. This is especially relevant to the sensitivity studies presented in Chapter 7, where it was felt that the minor improvements in the simulation achieved by increasing the grid resolution were not sufficient to warrant the massive increase in computational expense and storage a suite of high resolution sensitivity experiments would require.

University of Cape Town

5.5. The Montagu case: model validation

For this case study, MM5 was initialised at 0000 UTC 22 March 2003 with the initialisation fields from the MRF model at this time. A 27km horizontal resolution grid with 122 x 122 grid points, centred at 36°S, 26°E, and 40 σ-levels in the vertical was used. Topography was taken from the 5-minute resolution USGS dataset. The parameterisations that deal with sub-gridscale processes are described in Chapter 3. As with the East London case, a timestep of 40 seconds was utilised and output from the model was saved every hour, and this saved output was then vertically interpolated from the model σ-levels onto standard pressure levels.

The MM5 simulated precipitation for the 24-hour period to 0600 UTC 24 March 2003 is shown in Fig. 5.20, which corresponds to the observed precipitation field for this

event in Fig. 5.8b. The simulated precipitation compares reasonably well with the observed, with a maximum of 100mm over the south coast of the Western Cape. However, this maximum was located at 21.5°E, 34°S, approximately 100 km to the west of the observed maximum (22.5°E, 34°S). Additionally, the rainfall maximum observed at Montagu was not simulated by MM5. South of the precipitation maximum over land, the rainfall extended over the ocean, which compares well with the band of rainfall from TRMM (Fig. 5.8c). MM5 also simulated an area of lighter rainfall over the ocean off the Eastern Cape coast, which also compares favourably with the TRMM rainfall.

The large scale flow was validated against the MRF model analyses at 0000 UTC 24 March 2003. This time corresponds with the closest available MRF model analysis to the time of the most intense precipitation over the coastal regions of the Western Cape (~ 0400 UTC 24 March). A comparison of the large-scale flow from MM5 at 500 hPa (Fig. 5.21a) with the MRF model analysis (Fig. 5.11c) at 0000 UTC 24 March (see Fig. C1, Appendix C, for other times) shows that MM5 was able to simulate most aspects of the large scale flow with a fair degree of accuracy. However, the cut-off low simulated in MM5 (Fig. 5.21a) appeared to be less severe than that suggested by the MRF model (Fig. 5.10c), with less steep gradients in geopotential height and temperature on its southern side (see Fig. C2, Appendix C for other times). For example, in the MM5 simulation, a temperature gradient of 6K existed from the centre of the system to the last closed contour, whereas the corresponding difference in the MRF model was 10K. Similarly, a geopotential height difference of 100m existed from the centre of the cut-off low to the southernmost closed contour in the MM5 simulation compared to 200m for the MRF model at this time. This weaker gradient in

University of Cape Town

geopotential height from the MM5 simulation is due to the cut-off low not being so deep at its centre, with a central geopotential height of 5550m compared to 5500m in the MRF model. Although the temperature of the cold core was 252K in both the MRF model and the MM5 simulation, the cold core was situated farther to the north, at approximately 32°S in the MM5 simulation, compared to approximately 34°S in the MRF model.

Radiosonde observations from Cape Town at this time had a 500 hPa temperature of 256K (Fig. 5.13), compared with 257K for the MRF model (Fig. 5.10c) and 258K for the MM5 simulation (Fig. 5.21a), while the radiosonde from Port Elizabeth (not shown) observed a temperature of 251K at 500 hPa, compared to approximately 252K from the MRF model (Fig. 5.10c) and approximately 255K from the MM5 simulation. These differences suggest that the MM5 simulation had some difficulty in properly calculating the position of the cold core of the cut-off low, which observations and the MRF model suggest was around the Port Elizabeth area, while it was more successful in calculating the temperature around its extremities at Cape Town. A possible reason for the superior accuracy in the MRF temperature field is the assimilation of these upper air observations into these analyses. Experimentation was undertaken with upper observations objectively analysed into the initialisation of the MM5 simulation, but the relative paucity of these observations in this region meant that no appreciable improvement in the accuracy of the simulation was achieved.

University of Cape Town

Near the surface, MM5 simulated the position of the depression over the south coast and the LLJ impinging onto the coast on its western flank quite accurately at 0000 UTC 24 March (Fig. 5.21b), but the central geopotential height of the depression at 925 hPa of 690m was not as deep as the 630m suggested by the MRF model. The maximum wind speed in the LLJ at 925 hPa was also slightly lower in the MM5 simulation at 25 $m.s^{-1}$, compared to 27 $m.s^{-1}$ from the MRF model and QuikSCAT surface winds, probably due to slightly weaker pressure gradient forcing in MM5.

Similar to the East London case, the model was re-run with two nested grids, centred over the area of most intense precipitation over the land, with 9km and 3km horizontal resolution and 2-minute and 30-second resolution topography respectively. Again, two-way nesting was utilised so the processes simulated in the higher resolution grids were fed back into the lower resolution outer grids. The outputs of these grids, shown in Fig. 5.22, are hereafter referred to as M1, M2, and M3 for the 27km, 9km, and 3km resolution grids respectively. The main effect of running the model with nested grids was a narrowing of the band of rainfall extending onto the land and an increase in the amount of precipitation produced. Indeed, the precipitation was overestimated in M3. Additionally, this band of precipitation was moved approximately 50km to the east.

At 500 hPa (not shown), the effect of increasing the model resolution was minimal, indicating that the model was only sensitive to increased horizontal resolution near to the surface. Since one of the aims of this study was to perform various sensitivity tests with MM5, it was decided that the huge increase in computational expense and data storage requirements of increasing the model resolution was not justified for

University of Cape Town

only a small improvement in the simulation. Therefore, the analyses presented in Chapters 6 and 7 are based on simulations with a single 27km horizontal resolution grid.

However, the output of M3 is useful in validating the simulation against weather station observations since errors associated with the interpolation of model data to the station locations will be small. Nine weather stations exist in M3: Beaufort West (22.55°E, 33.32°S); Knysna (23.05°E, 34.05°S); George (22.45°E, 33.97°S); Ladismith (21.21°E; 33.48°S); Laingsburg (20.62°E, 32.90°S); Plettenberg Bay (23.32°E, 34.08°S); Riviersonderend (19.9°E, 34.15°S); Stilbaai (21.42°E, 34.37°S) and Struisbaai (20.07°E, 34.8°S). Time series of 2m temperature and surface pressure from M3 were constructed by bi-linearly interpolating to these locations and comparing with the corresponding observations.

Overall, the output from M3 compared reasonably well with the observed time series of 2m temperature at all stations (Fig. 5.23), although errors are more obvious at the coastal stations of George, Knysna and Plettenberg Bay, where M3 simulated a peak in temperature at around 0600 LST (0400 UTC) on 24 March. This is the time at which precipitation was most intense at these stations. As previously discussed, the simulated precipitation was located slightly to the west of the observed suggesting that these temperature peaks in M3 were related to a lack of cloud at these locations at the appropriate time (cloud cover from M3 is shown in Fig. C3, Appendix C).

At most stations, there was a sizeable fall in the surface pressure at around 0000 LST of up to 15hPa (Fig. 5.24). This was due to the development of the depression at

University of Cape Town

the surface (Fig. 5.11c) at this time. M3 was able to simulate the timing of this pressure decrease reasonably well at stations in the eastern part of the domain (Beaufort West, George, Knysna, Plettenberg Bay), but approximately two hours after the observed time. Additionally, at these stations, the magnitude of the decrease was not so pronounced in M3 as the observations suggest. This confirms the difficulty MM5 had in accurately simulating the severity of the surface depression (Fig. 5.21b). At the stations in the western portion of M3 (Ladismith, Laingsburg, Stilbaai, Struisbaai), M3 did not simulate the fall in surface pressure that was observed. This suggests that the surface depression did not extend so far to the west in M3 as in reality. At Riviersonderend, which is located very near to the western boundary of M3, the simulation of surface pressure was not so accurate, with M3 suggesting continually increasing pressure from 0000 UTC 23 March. This may be due to inaccuracies towards the boundary of M3 as the boundary conditions are applied from M2.

In summary, MM5 was reasonably successful in simulating this event. However, there was an apparent weakness in simulating the location and quantity of the most intense rainfall and the depth of the surface depression. There was an improvement in the location of precipitation when the horizontal resolution was increased to 3km, but there was also an overestimation of the quantity. Comparison with station data from the 3km resolution grid suggests that MM5 was able to accurately simulate the temperature trend during this event, but the magnitude of the pressure decrease due to the development of a surface depression was underestimated. Additionally, the westward extent of this depression was also underestimated by MM5.

University of Cape Town

5.6. Discussion and summary

This chapter described the synoptic evolution and the ability of the MM5 model to simulate two cut-off low events over South Africa in August 2002 and March 2003. These months are fairly typical times of year for cut-off lows to occur over subtropical southern Africa (see Chapter 4).

The August 2002 event, referred to as the East London case, featured a small cut-off that developed in a deep trough over the Western Cape province of South Africa, followed by the development of a second cut-off low within the same trough, with the second cut-off low located over the coast of Namibia. These locations correspond to regions A and C in the climatology discussed in Chapter 4. In addition, this system was in the 400-800km size and 2-4 days duration category. An analysis from a potential vorticity perspective suggests that a single cut-off low split into two separate systems. More than 300mm of rain fell in 24 hours over the city of East London on the Eastern Cape coast. The low-level flow was characterised by a ridge of high pressure over the ocean to the south of South Africa, and a trough over the ocean to the east of southern Africa. A LLJ formed where there was a strong pressure gradient between the ridge and the trough, and advected air rapidly onto the coast where the rainfall was intense. The trough to the east of South Africa advected air from tropical latitudes in the LLJ, and the ridge was responsible for advecting cooler air from higher latitudes into the LLJ.

The qualitative validation and assessment of this event shows that MM5 was able to simulate this event reasonably well, but had some difficulty in simulating the location and quantity of the heaviest precipitation, and the location of the LLJ. However, it

University of Cape Town

was able to simulate the salient features of the event allowing a more detailed analysis (Chapters 6 and 7) to be undertaken.

In contrast, the event in March 2003, referred to as the Montagu case, featured a deep cut-off low aloft, which extended down to the surface where a deep depression formed. The cut-off low aloft developed over the Western Cape and subsequently tracked east over the south coast of South Africa. This is an example of a cut-off low over region A that tracked across to region B (see Chapter 4). Additionally, following the categories in Chapter 4, the size of this cut-off low was >1200km and the duration was 2-4 days. Heavy rainfall fell over the south coastal region of the Western Cape leading to flash flooding in the town of Montagu, some 50km inland. The low-level flow was characterised by a LLJ that formed on the western side of the surface depression and advected air onto the Western Cape coast. A ridge extended eastwards to the south of the depression and advected high latitude air into the LLJ, and a trough ahead of the surface depression advected warmer moister tropical air into the LLJ.

University of Cape Town

The present study is concerned with case studies in which there was a cut-off low aloft, and the formation of an onshore LLJ which advected air towards the regions of heaviest rain over land. However, in the East London case, the cut-off low was considerably smaller and less severe than in the Montagu case, and there was little evidence of surface cyclogenesis in the East London case. Additionally, in the East London case, the onshore LLJ formed below offshore flow aloft, whereas in the Montagu case the flow above the onshore LLJ was in the same direction throughout the atmosphere. The quantity of rainfall observed in the East London case was

greater in the East London case compared to the Montagu case, which may have been due to the onshore LLJ having a much larger fetch over high latent heat fluxes from the surface due to the warm SST of the Agulhas Current. This is investigated further in Chapter 7.

In both cases, MM5 was able to simulate the salient features of the event, but it had difficulty in simulating the location and quantity of the heavy precipitation. Increasing the horizontal resolution in both cases only led to small improvements in the simulations. Therefore, for both cases, the analysis of the MM5 simulations in the following chapter is based on the single 27km grid runs.

University of Cape Town

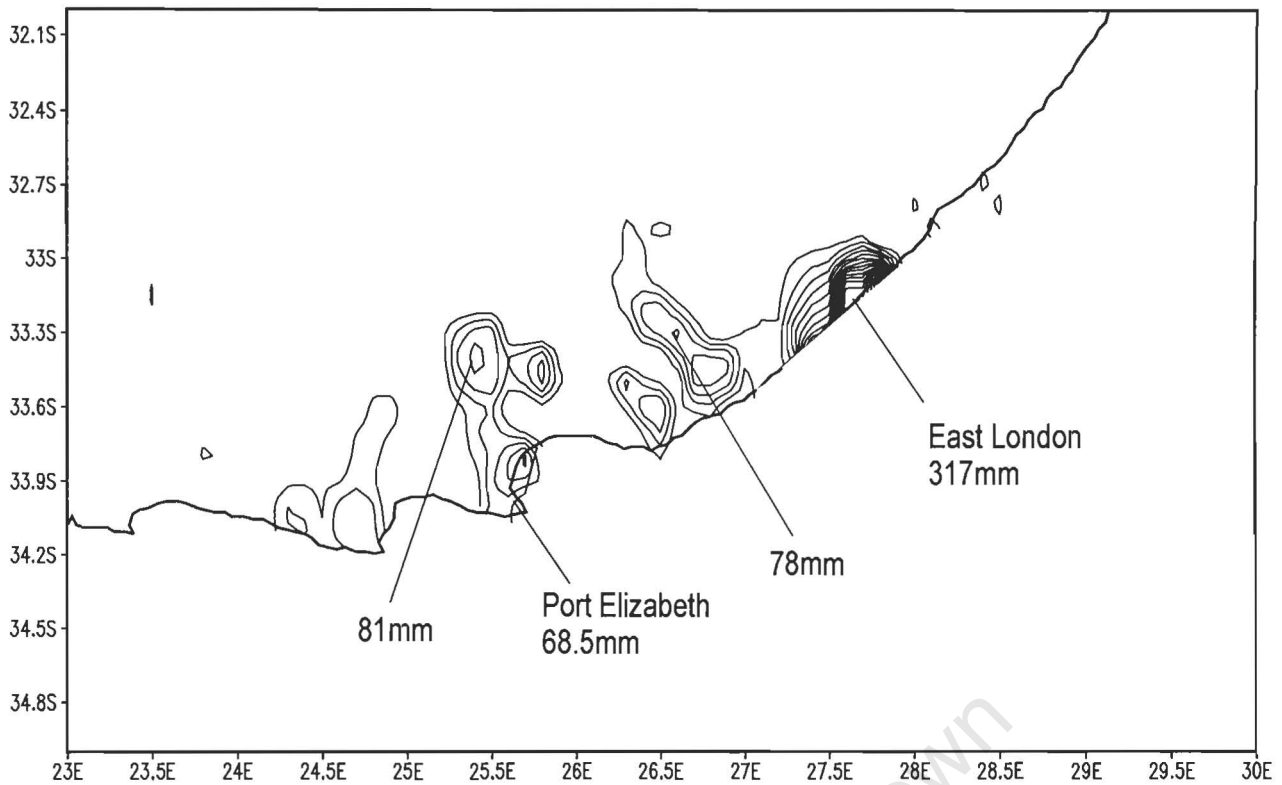

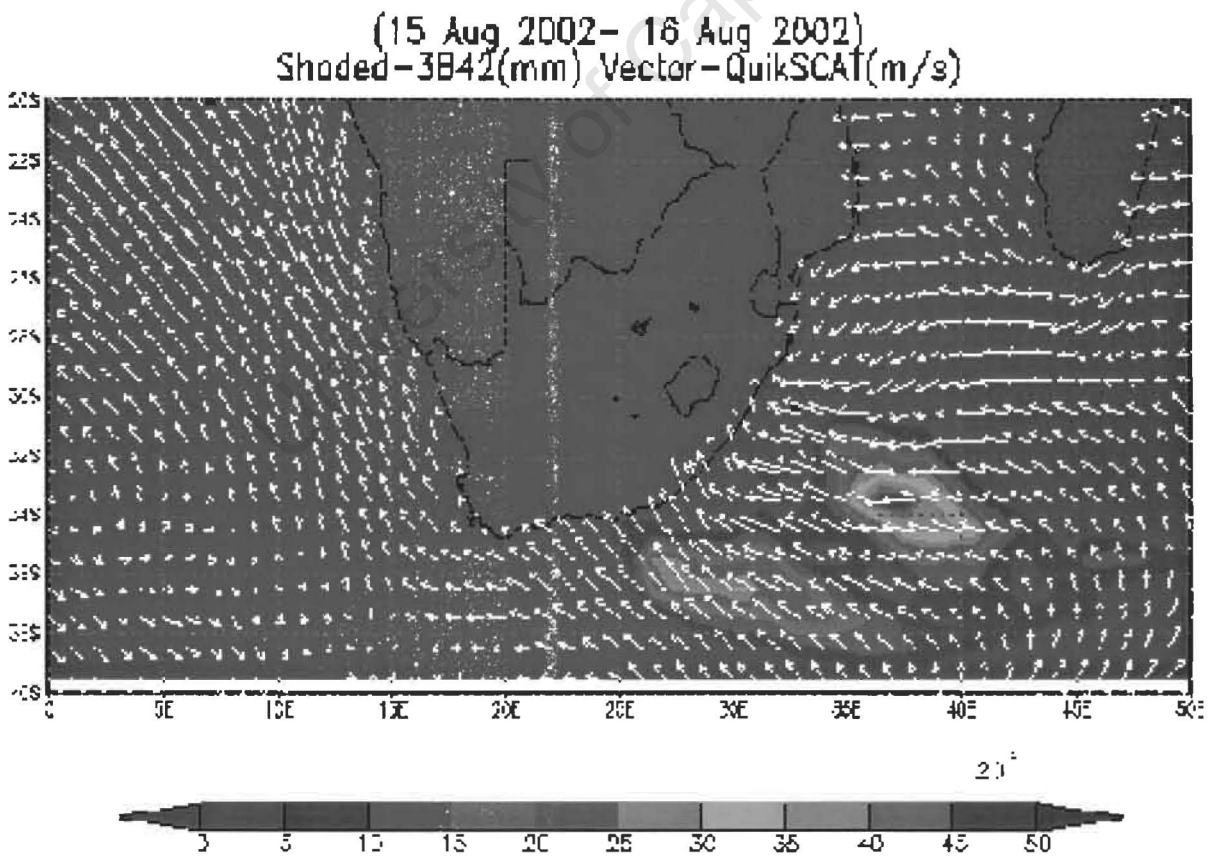

Figure 5.1 - (a) Objectively analysed observed rainfall from SAWS stations for the 24-hour period to 0700 UTC 16 August 2002.Contour interval is 20mm, starting at 20mm; (b) Rainfall from TRMM and mean surface winds from QuikSCAT for 15-16 August 2002. A colour scale is given for the rainfall, and a vector scale for the surface winds.

University of Cape Town

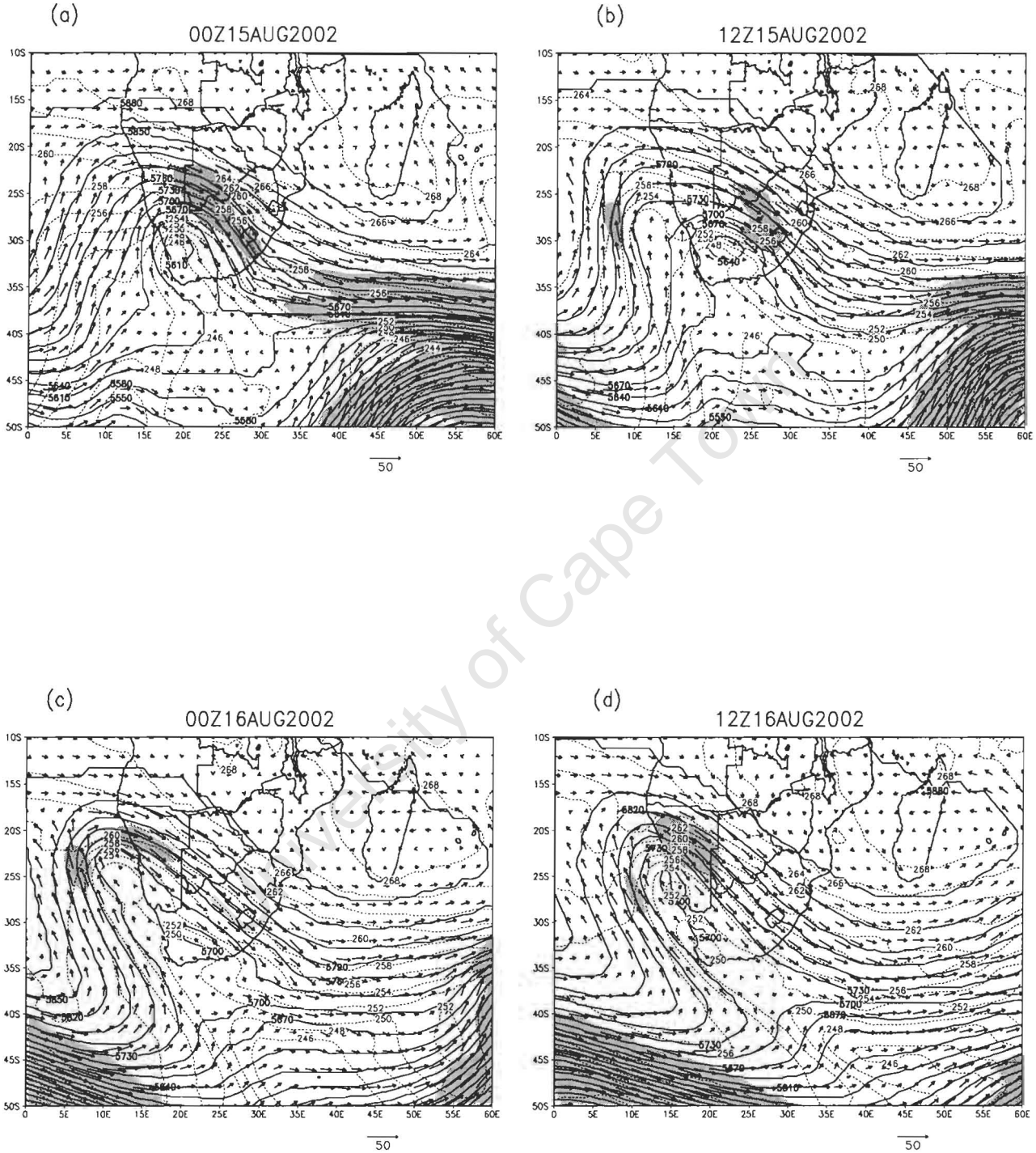

University of Cape Town

Figure 5.2 – 500 hPa geopotential height (solid contours, interval 30m), temperature (dashed contours, interval 2K), wind vectors (with a vector scale given to the bottom right of each panel in $m.s^{-1}$), and wind speed greater than $30m.s^{-1}$ (shading), from MRF model analyses at 12 hour intervals from (a) 0000 UTC 15 August to (d) 1200 UTC 16 August 2002

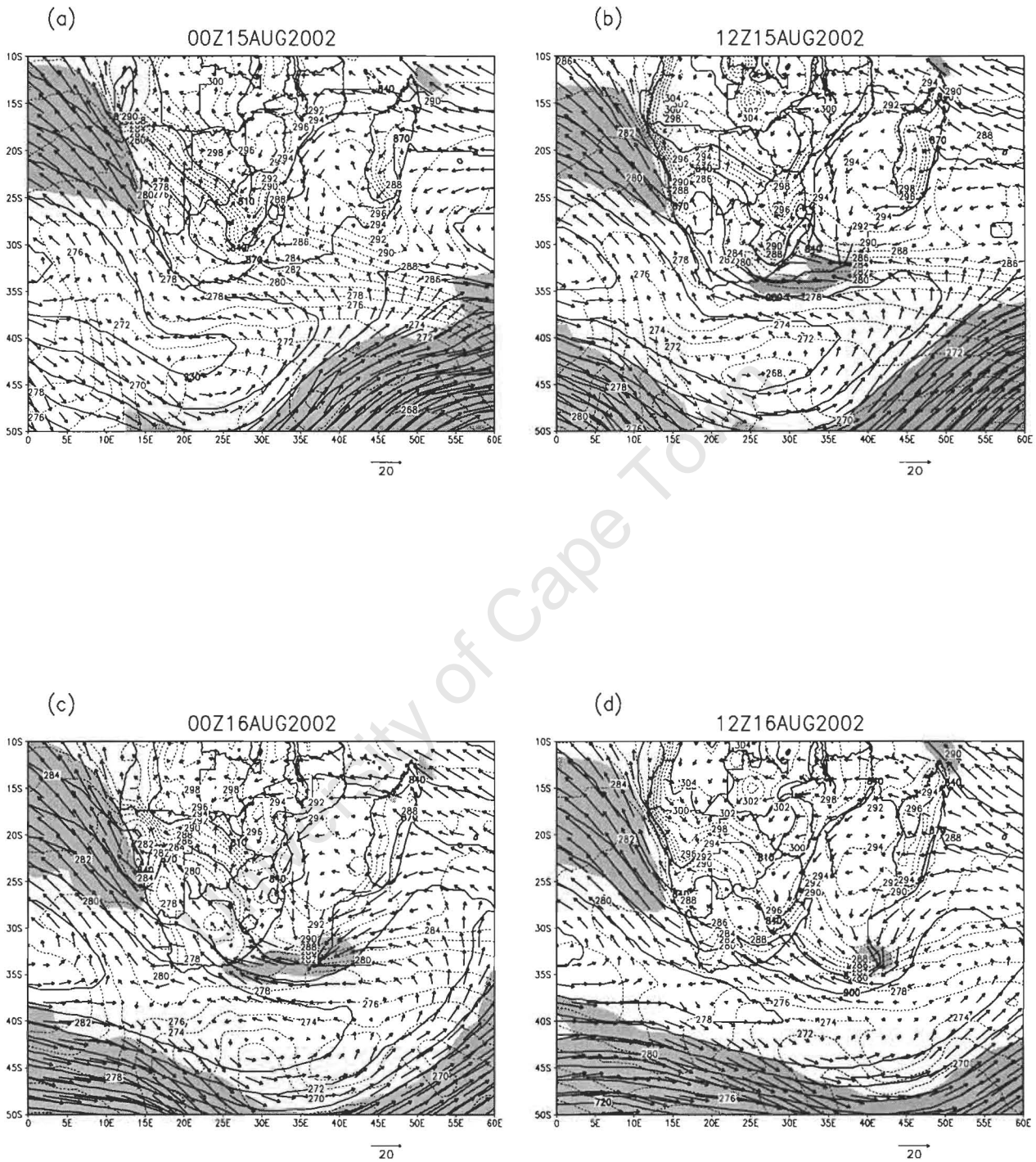

University of Cape Town

Figure 5.3 – As in Fig. 5.2 except at 925 hPa and wind speed greater than 15 $m.s^{-1}$ shaded

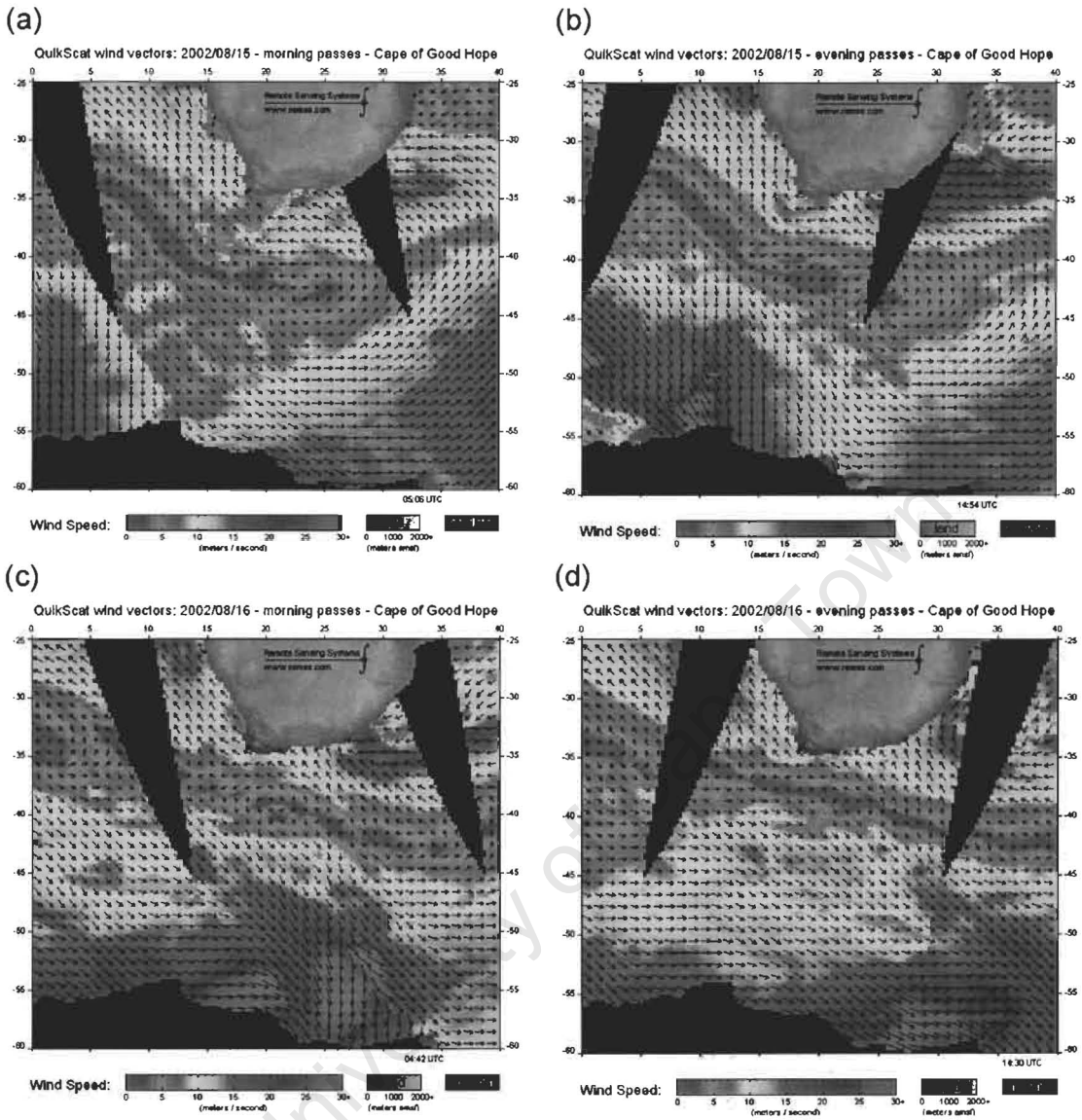

Figure 5.4 – Surface wind speed derived from QuikSCAT scatterometer measurements for (a) 15 August 2002 morning pass; (b) 15 August 2002 evening pass; (c) 16 August 2002 morning pass; (d) 16 August 2002 evening pass. A colour scale for wind speed in $m.s^{-1}$ is given below each panel

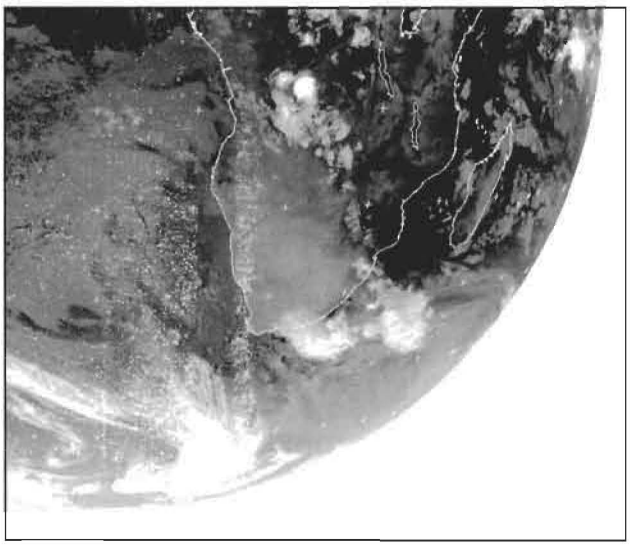

Figure 5.5. – Meteosat infrared image for 0000 UTC 16 August 2002.

University of Cape Town

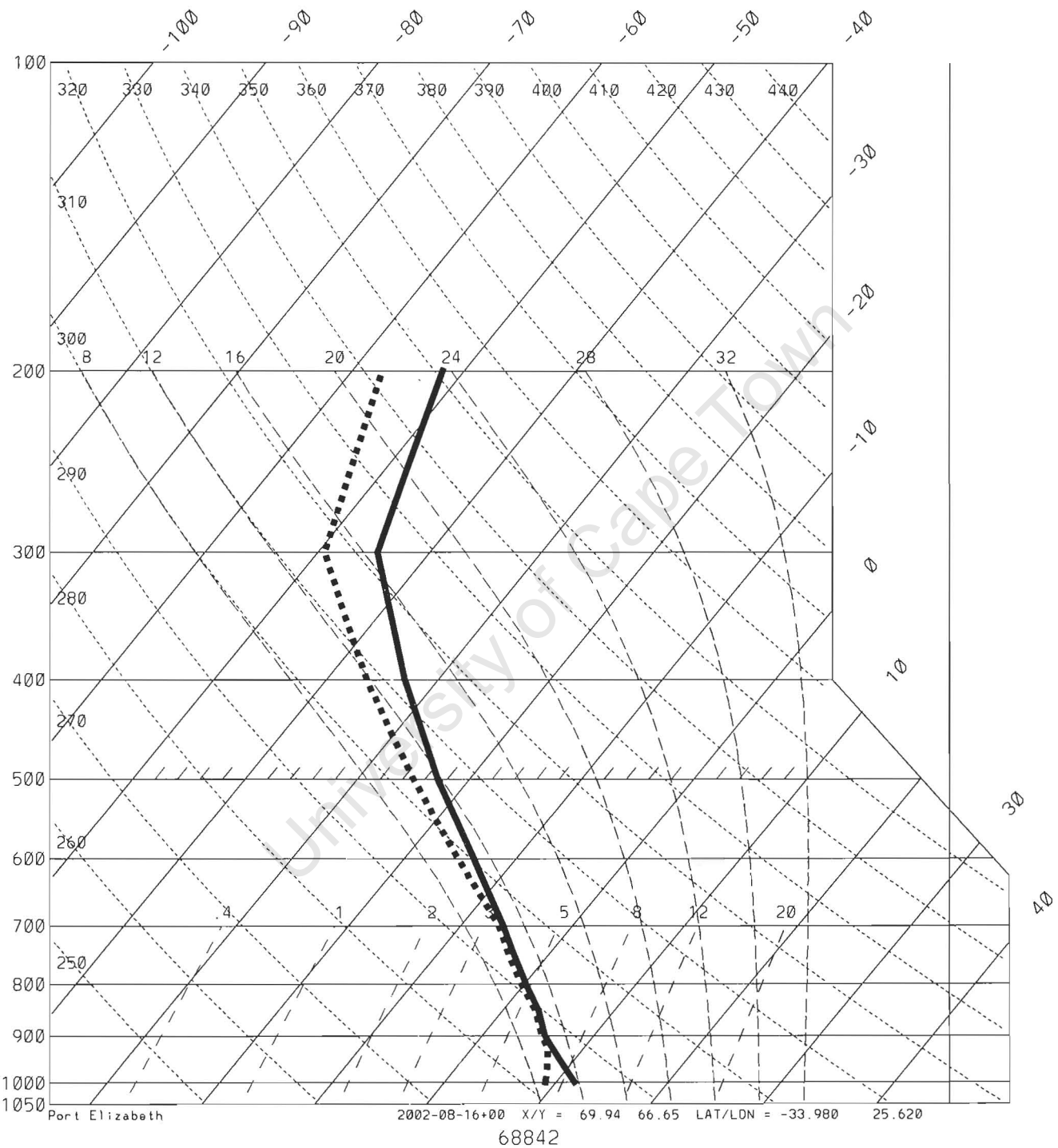

University of Cape Town

Figure 5.6 - Radiosonde ascent from Port Elizabeth at 0000 UTC 16 August.

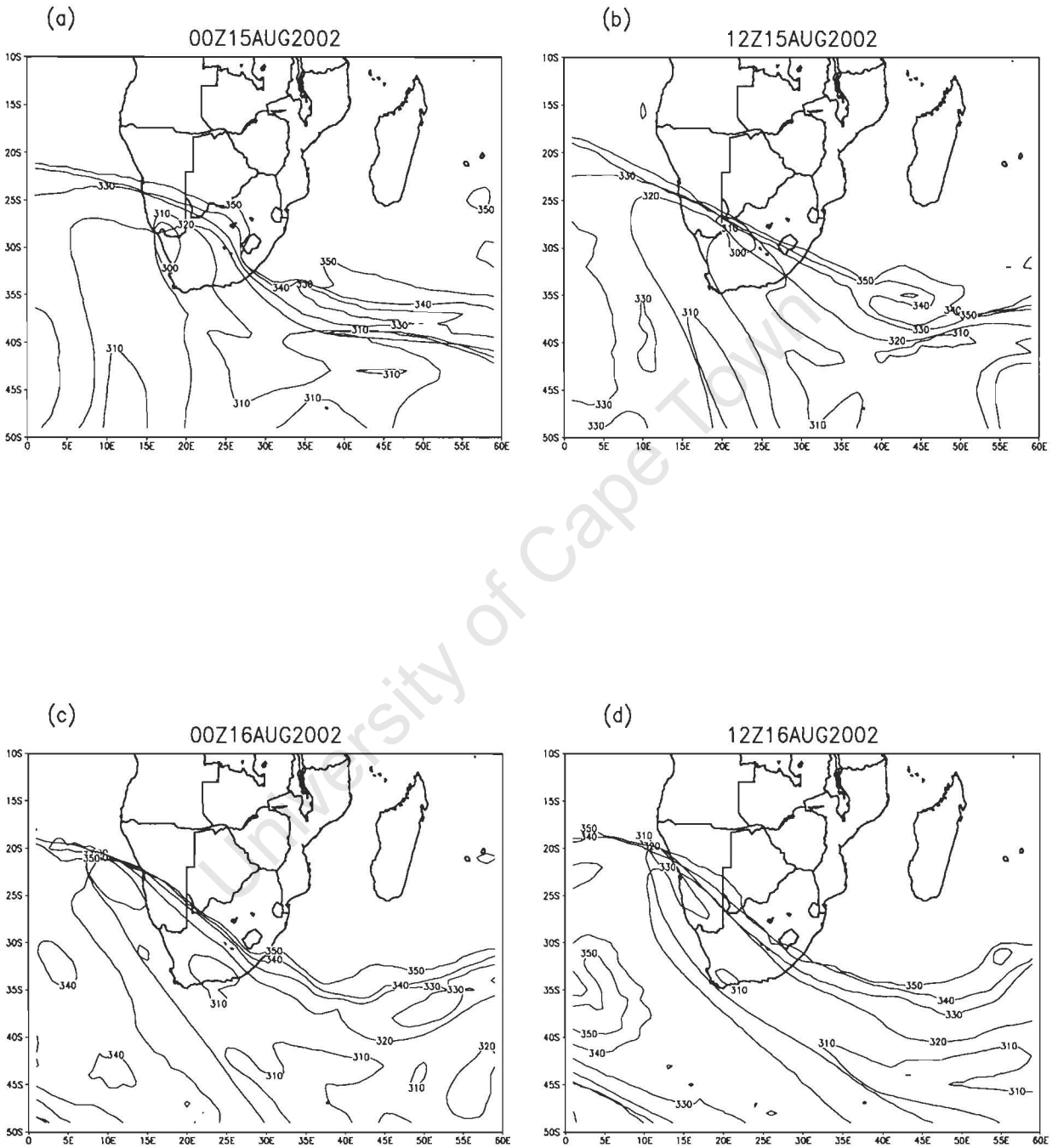

Figure 5.7 – Potential temperature superimposed onto the dynamic tropopause, defined as the -1.5 PVU surface, from the MRF model analyses at 12 hour intervals from (a) 0000 UTC 15 August to (d) 1200 UTC 16 August 2002. Contour interval is 10K.

University of Cape Town

(a)

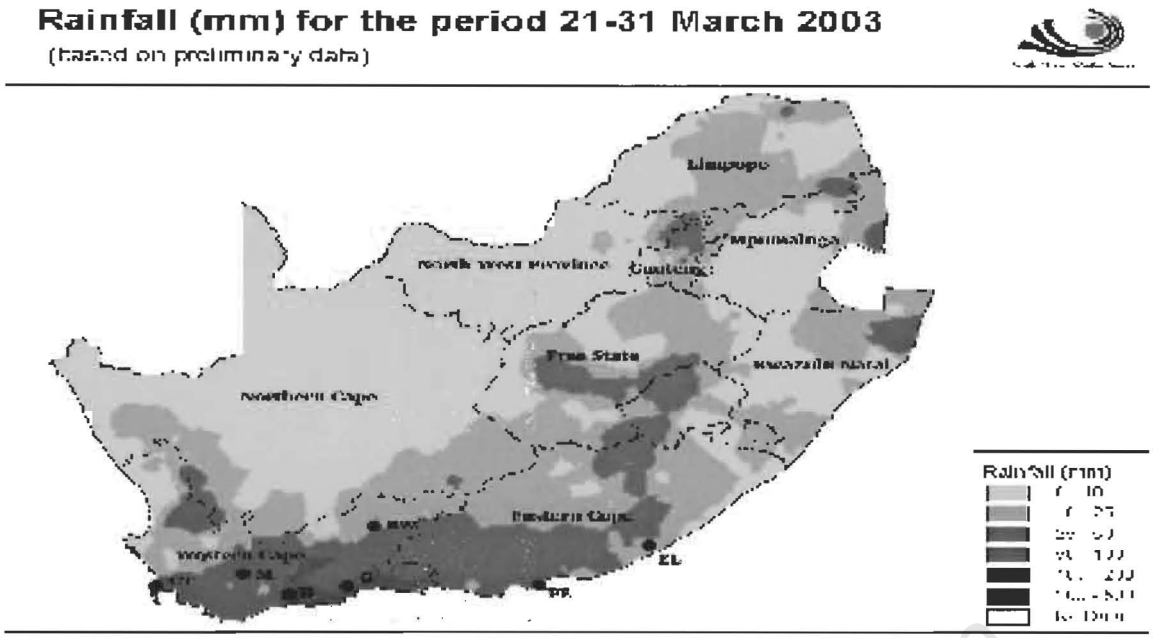

(b)

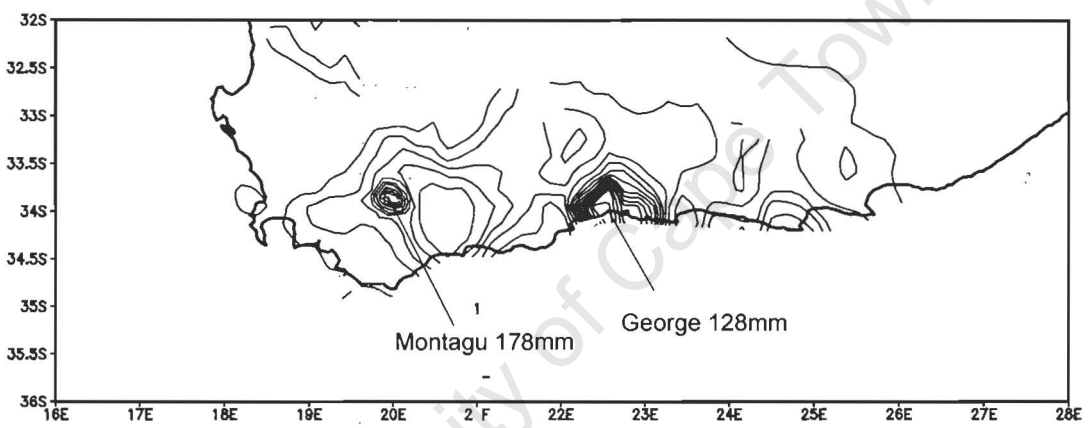

(c)

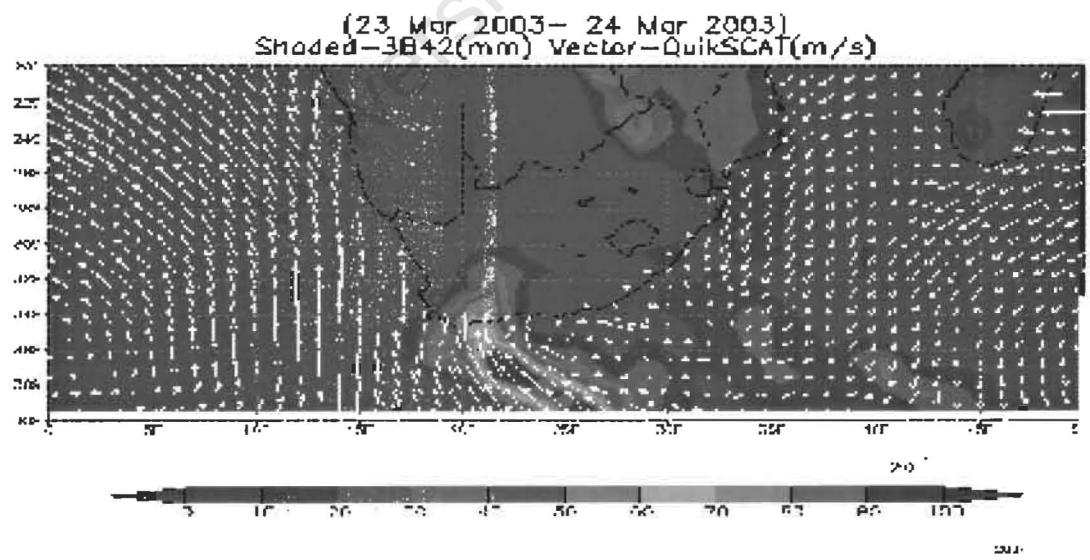

Figure 5.8 - (a) 10-day rainfall for the period 21-31 March 2003 from SAWS, with a colour scale given in the bottom right of the panel. (b) Objectively analysed rainfall from SAWS for the 24-hour period to 0600 UTC 24 March 2003. (c) Rainfall from TRMM and mean surface winds from QuikSCAT for 23-24 March 2003. A colour scale for rainfall and a vector scale for surface winds are given below the panel.

University of Cape Town

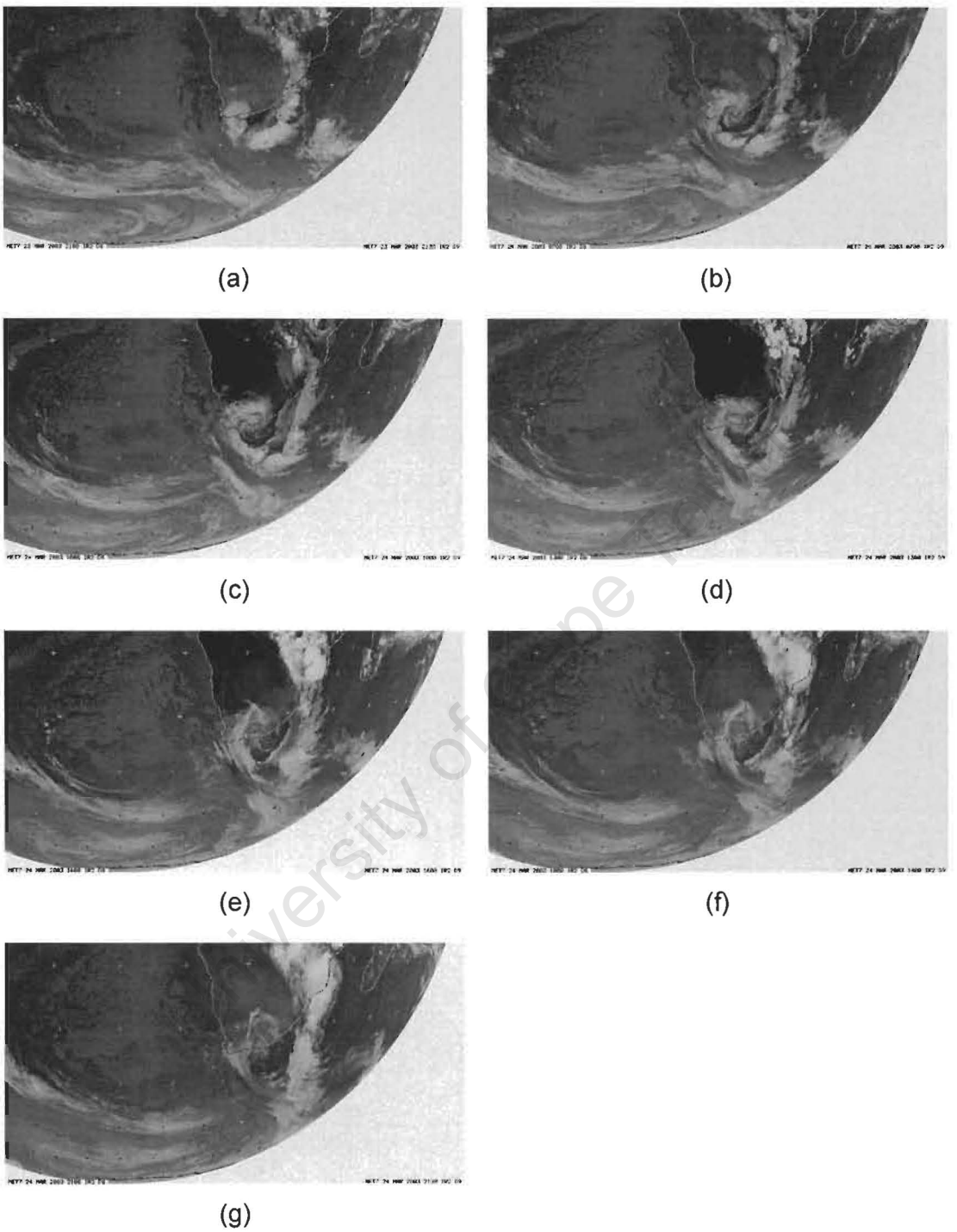

Figure 5.9 - Meteosat infrared images on (a) 23 March 2003 at 2100 UTC, and on 24 March 2003 at (b) 0700, (c) 1000, (d) 1300, (e) 1600, (f) 1800 and (g) 2100 UTC.

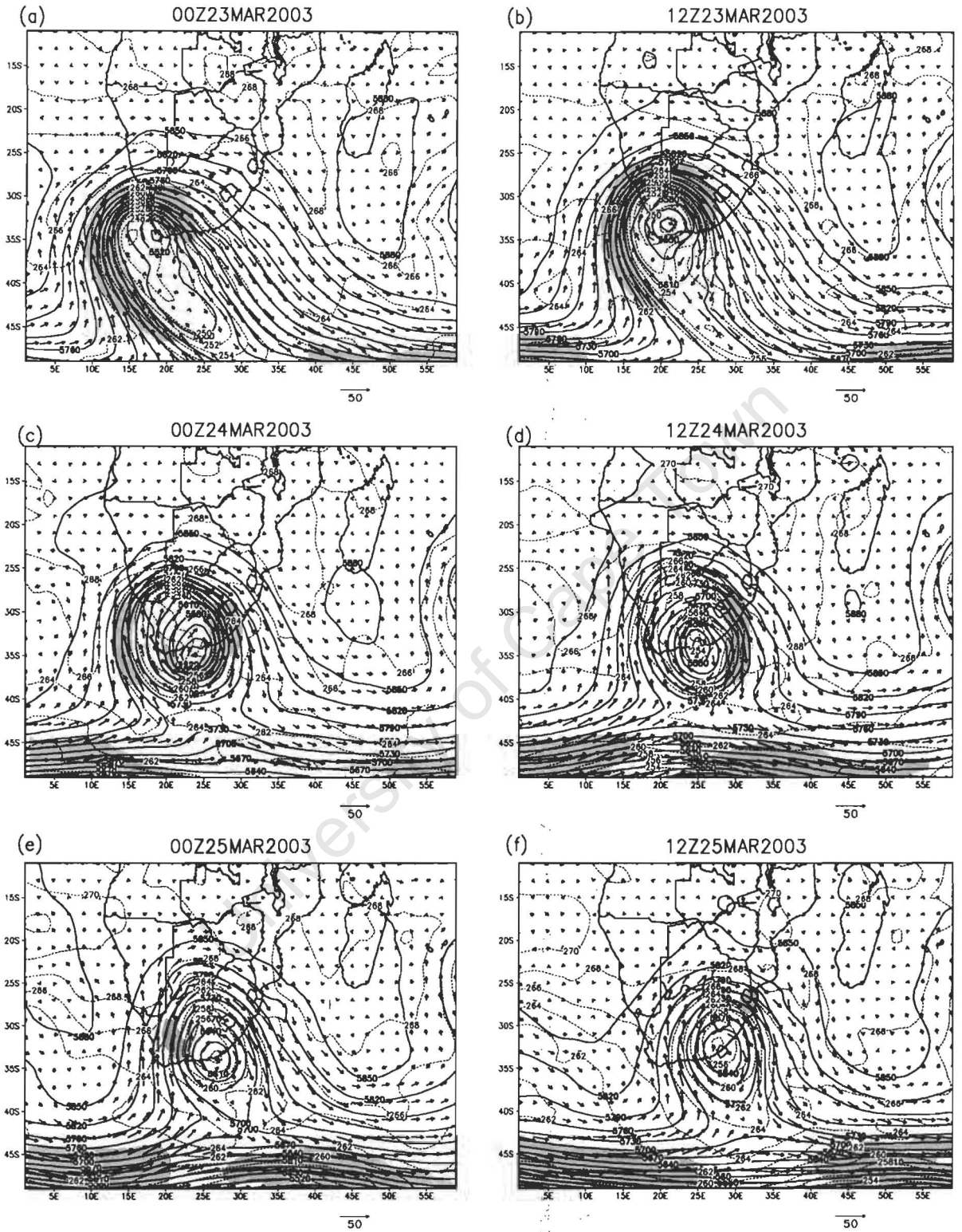

Figure 5.10 – 500 hPa geopotential height (solid contours, interval 30m), temperature (dashed contours, interval 2K), wind vectors (with a vector scale given to the bottom right of each panel in $m.s^{-1}$), and wind speed greater than $30m.s^{-1}$ (shading), from MRF model analyses at 12 hour intervals from (a) 0000 UTC 23 March to (f) 1200 UTC 25 March 2003

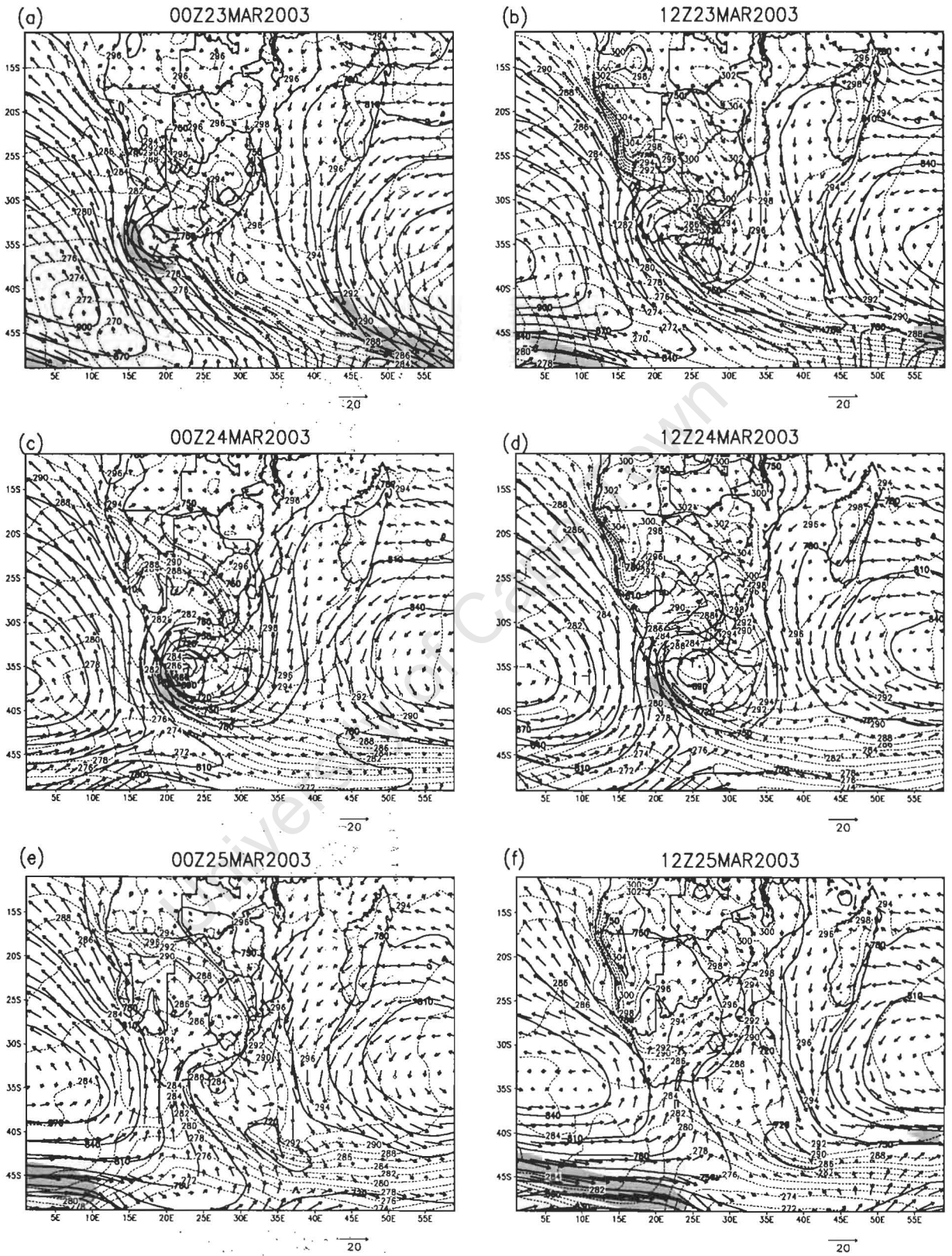

Figure 5.11 – As in Fig. 5.10 except at 925 hPa and wind speed greater than 20 $m.s^{-1}$ shaded.

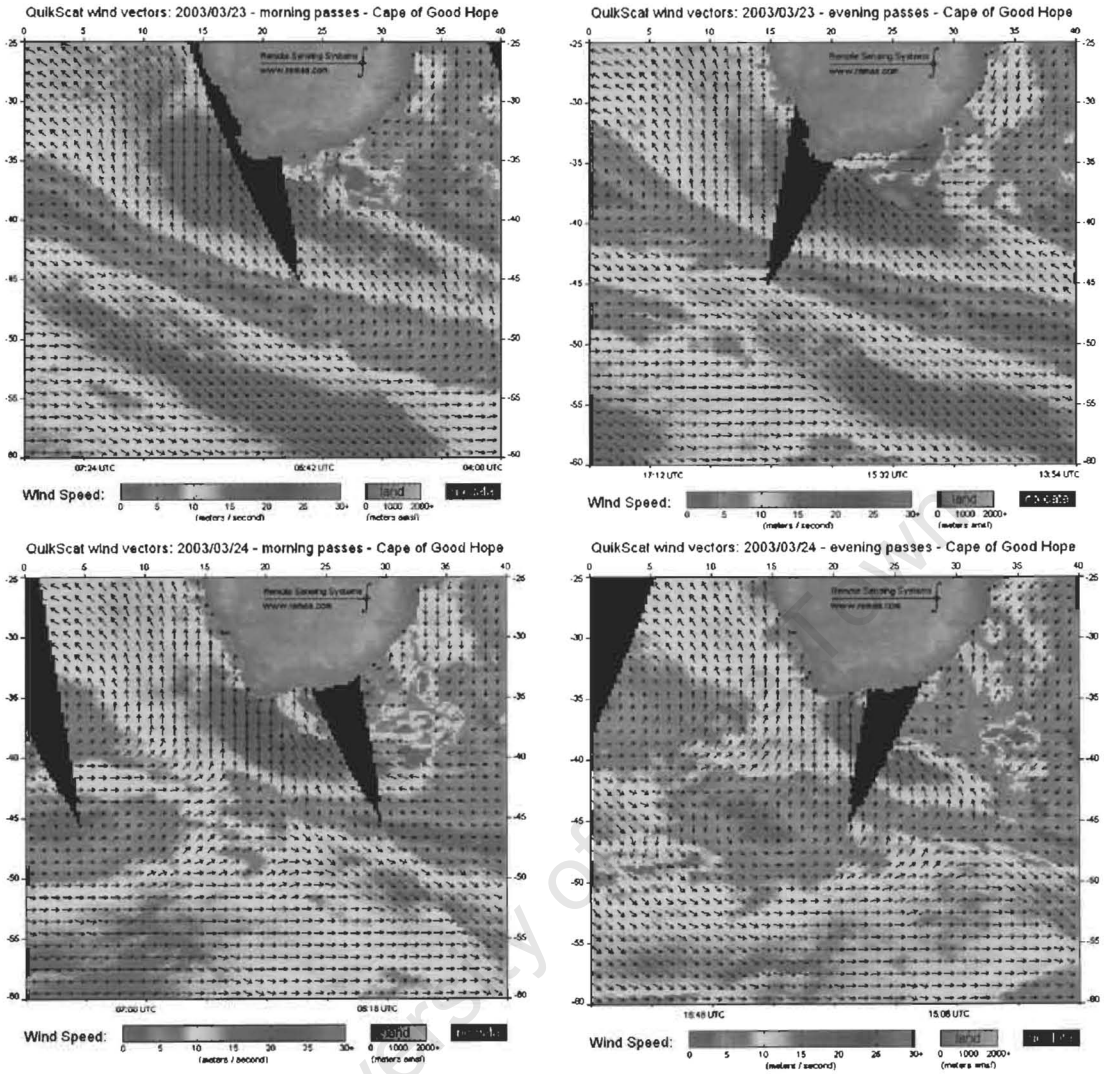

Figure 5.12 – Surface winds from derived from QuikSCAT scatterometer measurements for (a) 23 March 2003 morning pass; (b) 23 March 2003 evening pass; (c) 24 March 2003 morning pass; (d) 24 March 2003 evening pass.

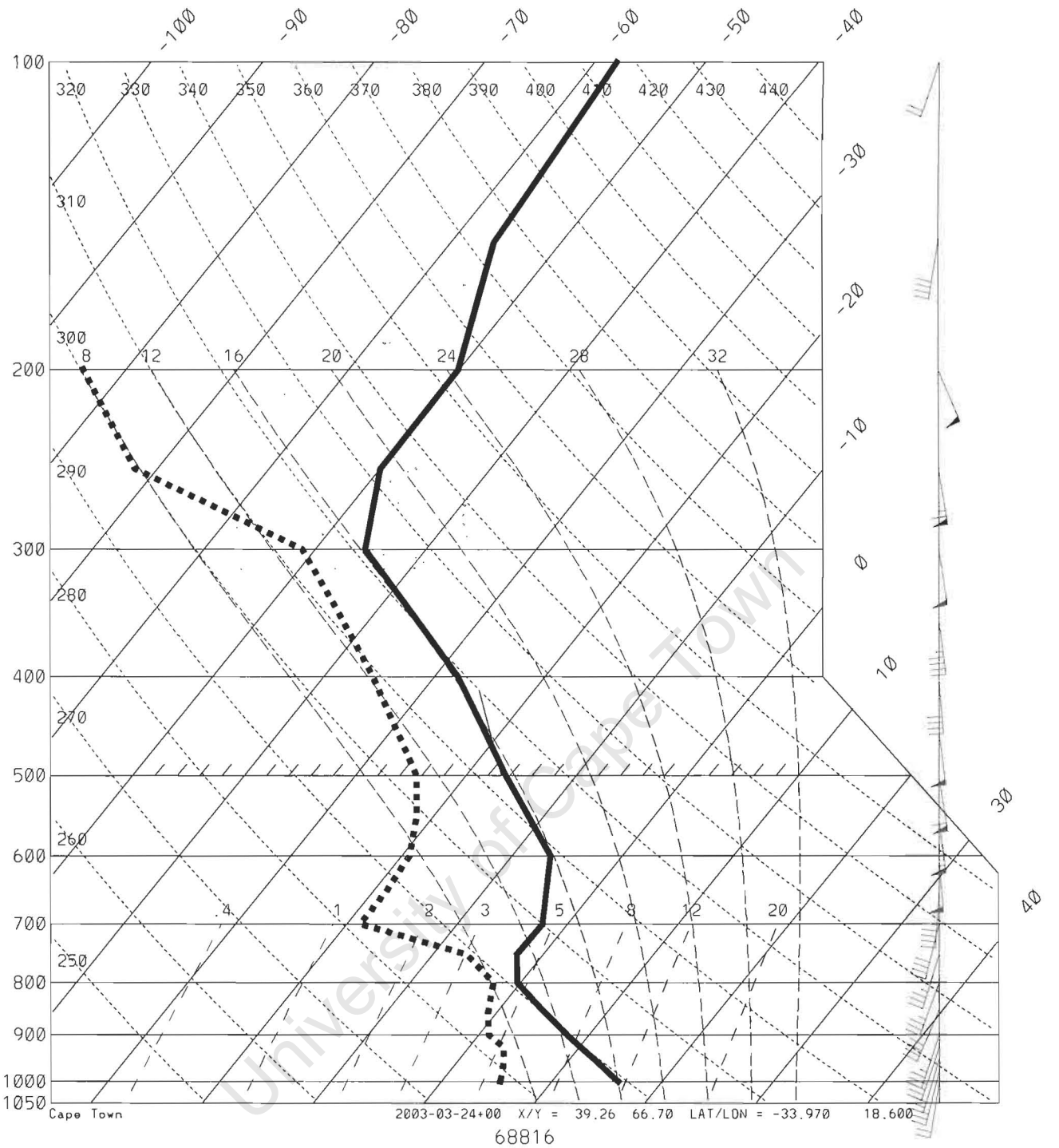

Figure 5.13 - Radiosonde ascent from Cape Town at 0000 UTC 24 March 2003.

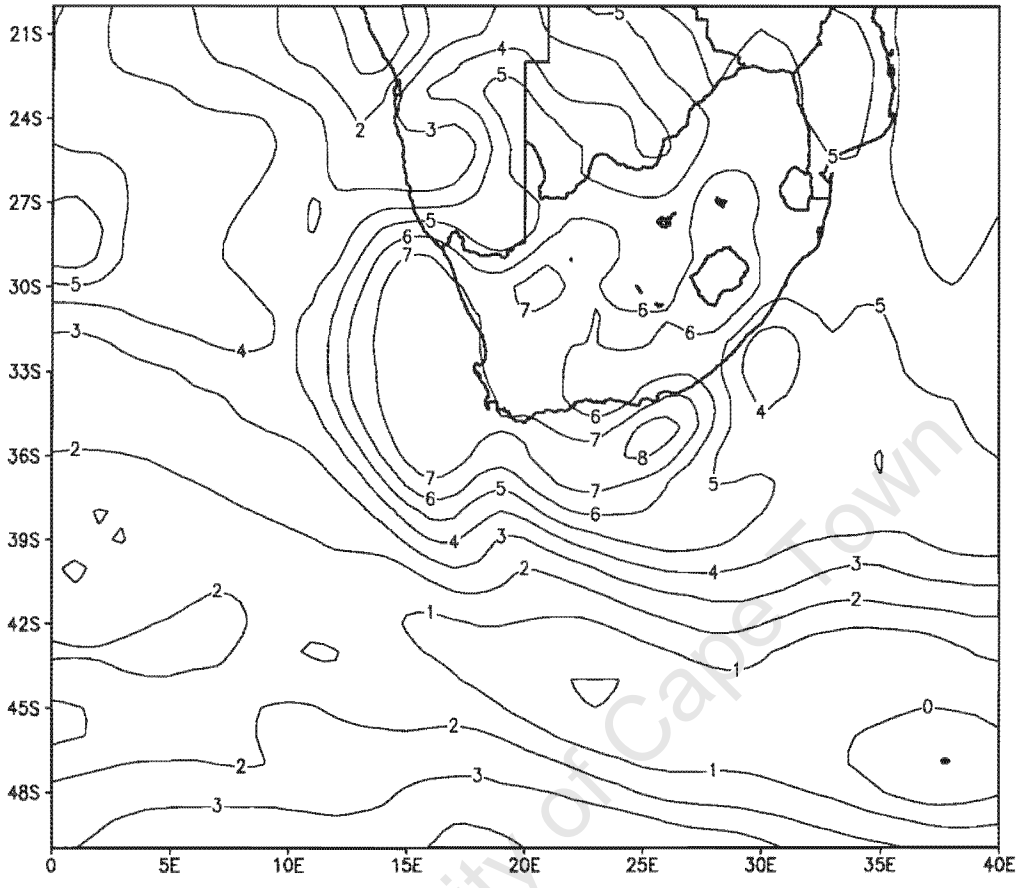

Figure 5.14 – Low level environmental lapse rate, taken as the temperature difference between the 1000- and 800-hPa levels from the MRF model analysis at 0000 UTC 24 March 2003.

University of Cape Town

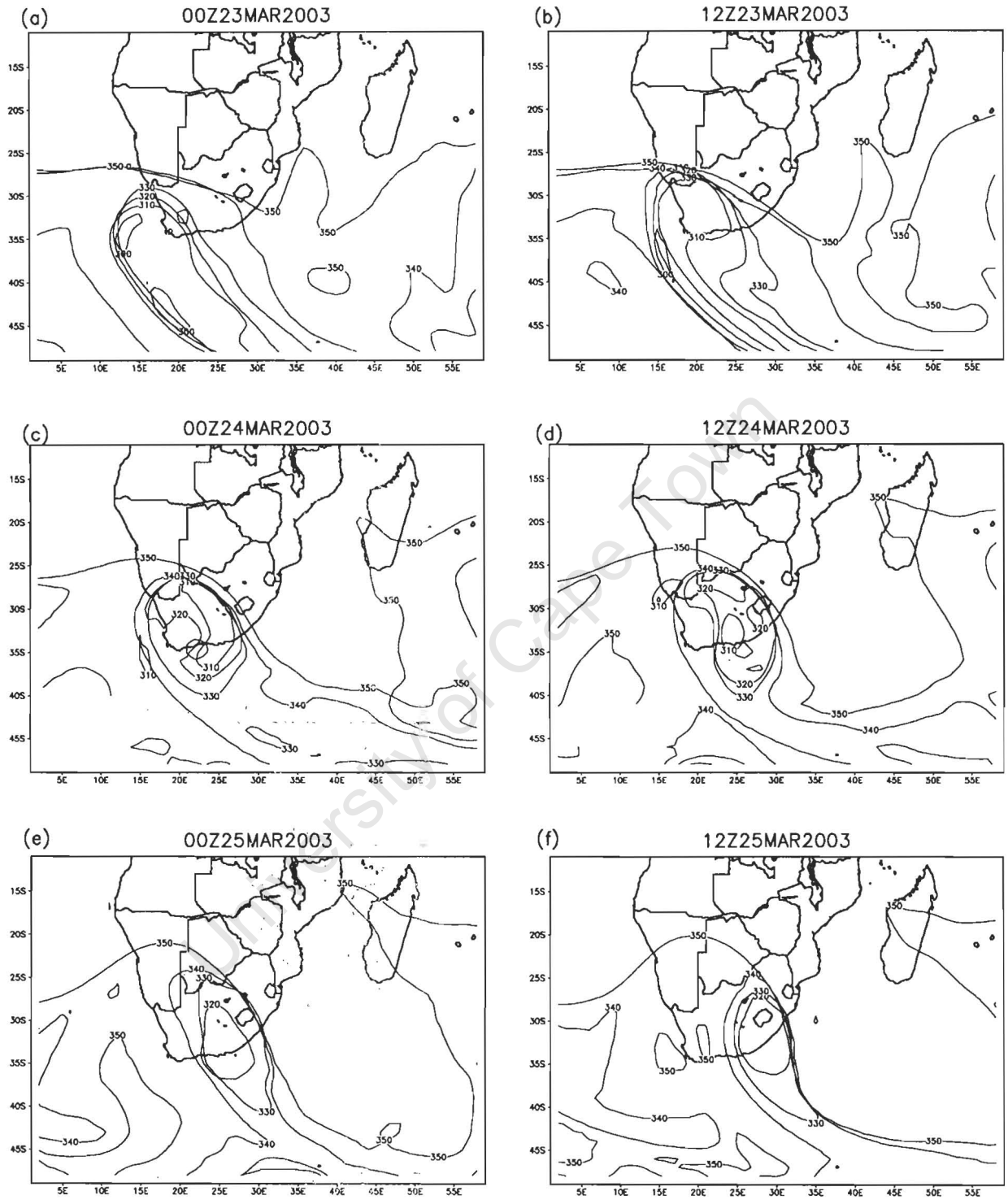

Figure 5.15 – Potential temperature superimposed onto the dynamic tropopause, defined as the -1.5 PVU surface, from the MRF model analyses at 12 hour intervals from (a) 0000 UTC 23 March to (f) 1200 UTC 25 March 2003. Contour interval is 10K.

University of Cape Town

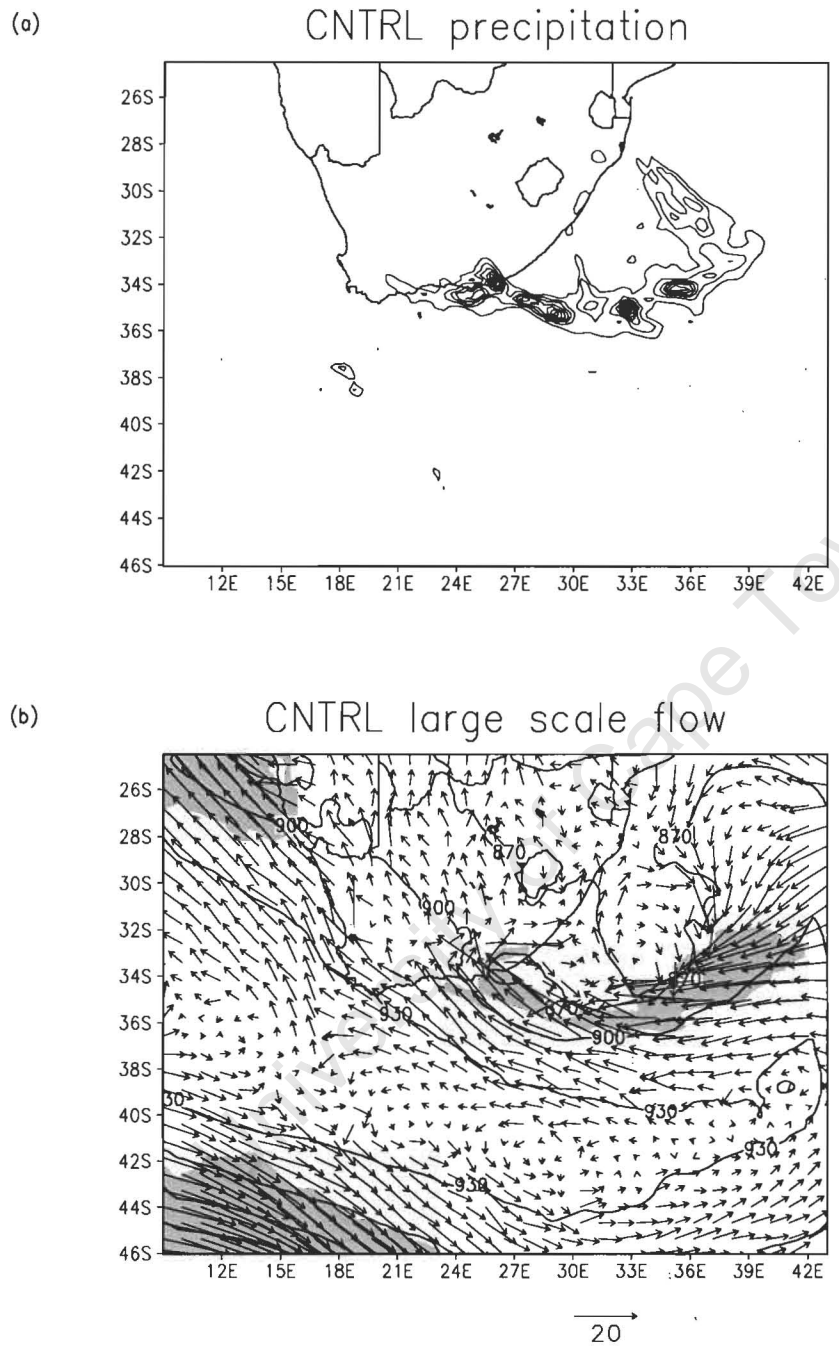

Figure 5.16 – (a) MM5 rainfall for the East London case for the 24-hour period to 0700 UTC 16 August 2002. Contour interval is 20mm starting at 20mm. (b) 925 hPa geopotential height (contour interval 30m) and wind speed greater than 15 $m.s^{-1}$ from the MM5 simulation of the East London case at 0000 UTC 16 August 2002.

University of Cape Town

(a)

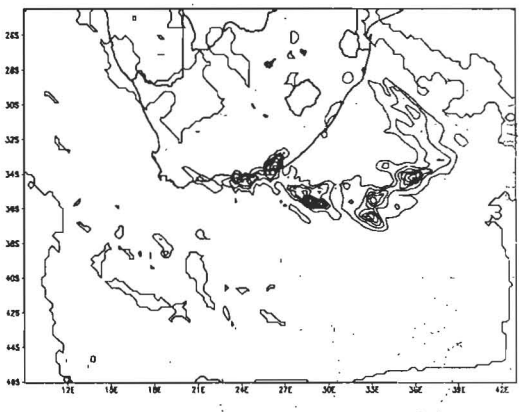

(b)

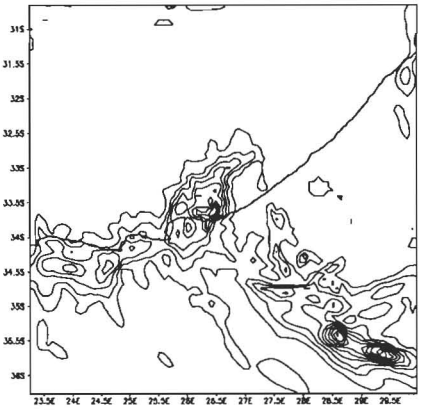

(c)

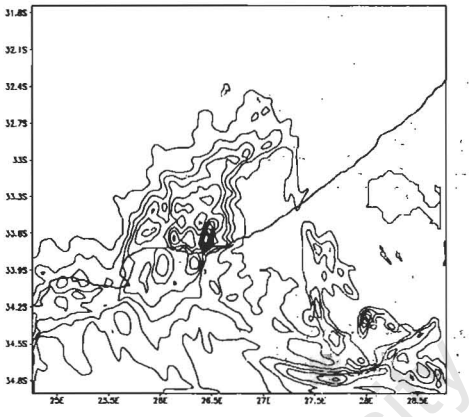

Figure 5.17 – 24-hour rainfall for the 24-hour period to 0700 UTC 16 August 2002 from the MM5 simulation of the East London case with three grids; (a) from the 27km resolution grid, (b) from the 9km resolution nested grid, (c) from the 3km resolution nested grid. For each of the panels the contour interval is 20mm.

University of Cape Town

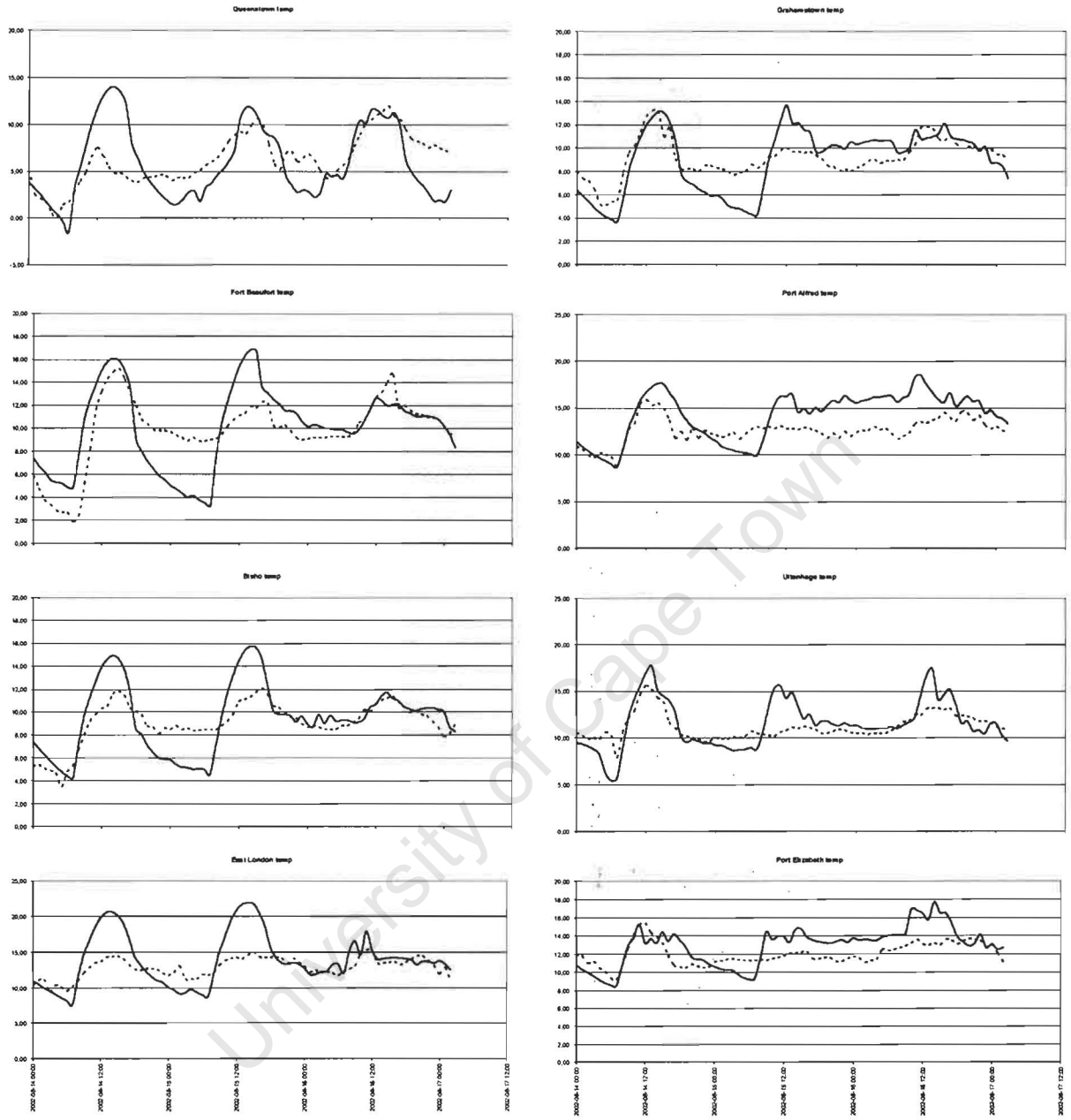

Figure 5.18 – Time series of 2m temperature at various weather stations for the East London case. The solid line is from the 3km grid of the MM5 simulation, and the dashed line is the observed temperature. Station names are given above each panel and locations are given in the text.

University of Cape Town

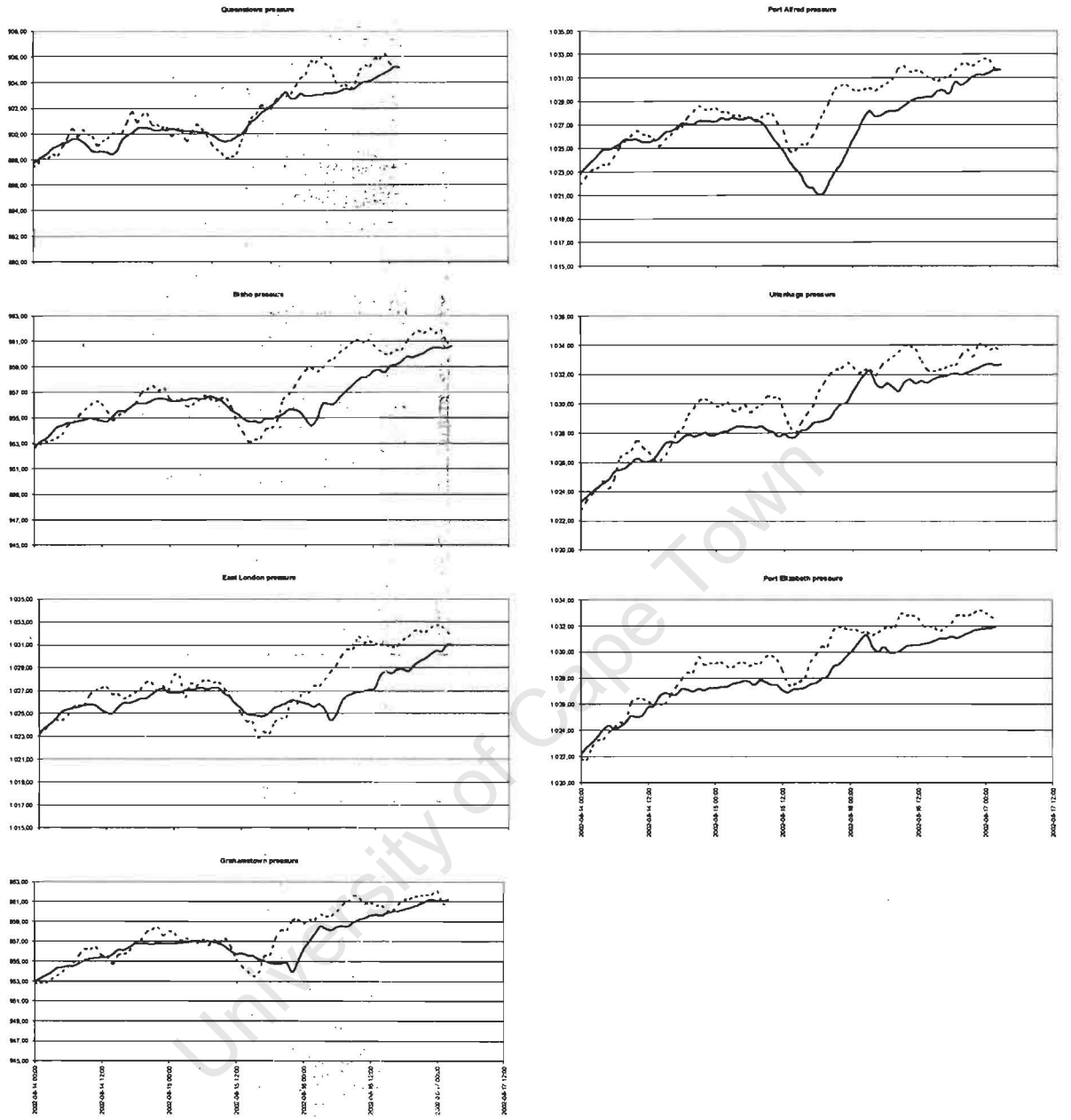

Figure 5.19 – As in Fig. 5.18 except for surface pressure.

University of Cape Town

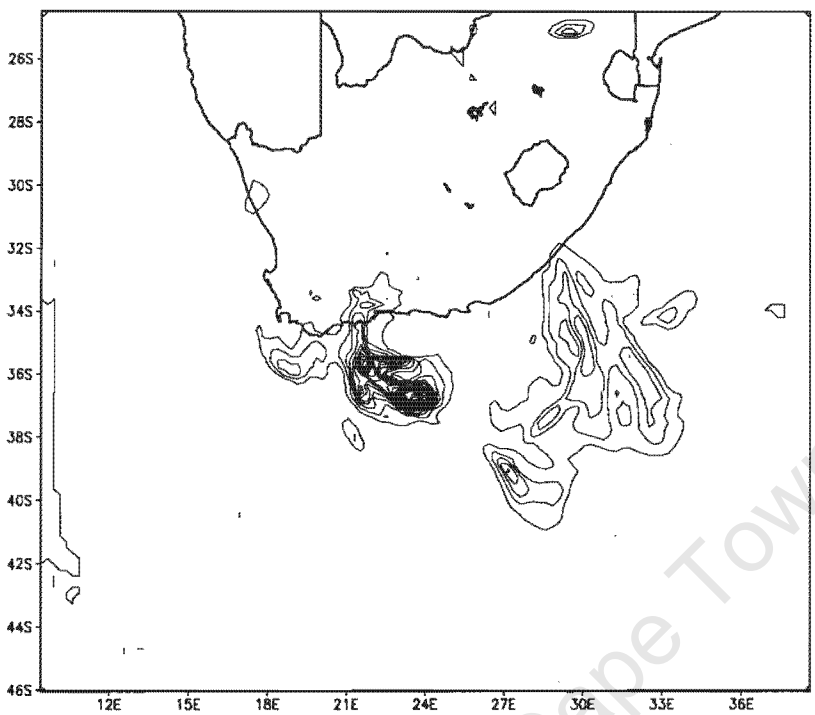

Figure 5.20 – MM5 simulated rainfall for the 24-hour period to 0600 UTC 24 March 2003 for the Montagu case. Contour interval is 20mm.

University of Cape Town

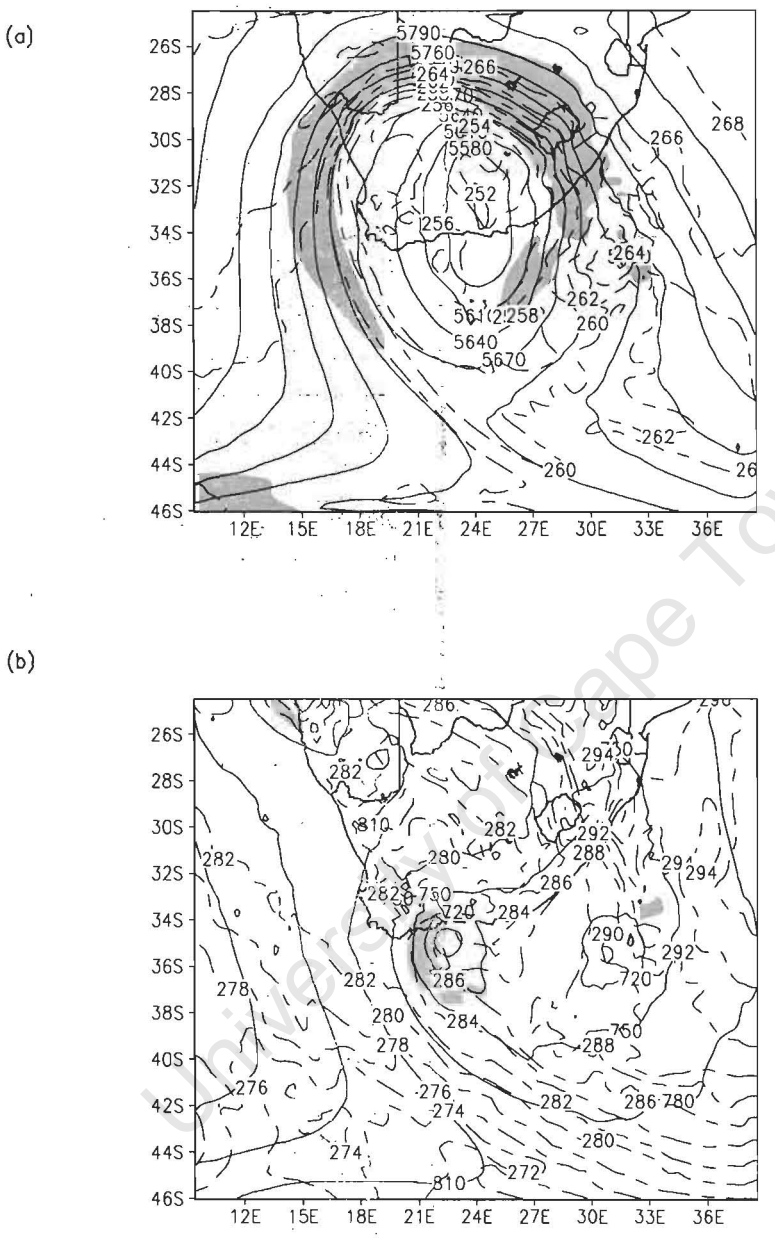

Figure 5.21 – (a) 500 hPa geopotential height (solid contours, interval 30m), temperature (dashed contours, interval 2K) and wind speed greater than 30 $m.s^{-1}$ (shaded); (b) 925 hPa geopotential height (solid contours, interval 30m), temperature (dashed contours, interval 2K) and wind speed greater than 20 $m.s^{-1}$ (shaded)

University of Cape Town

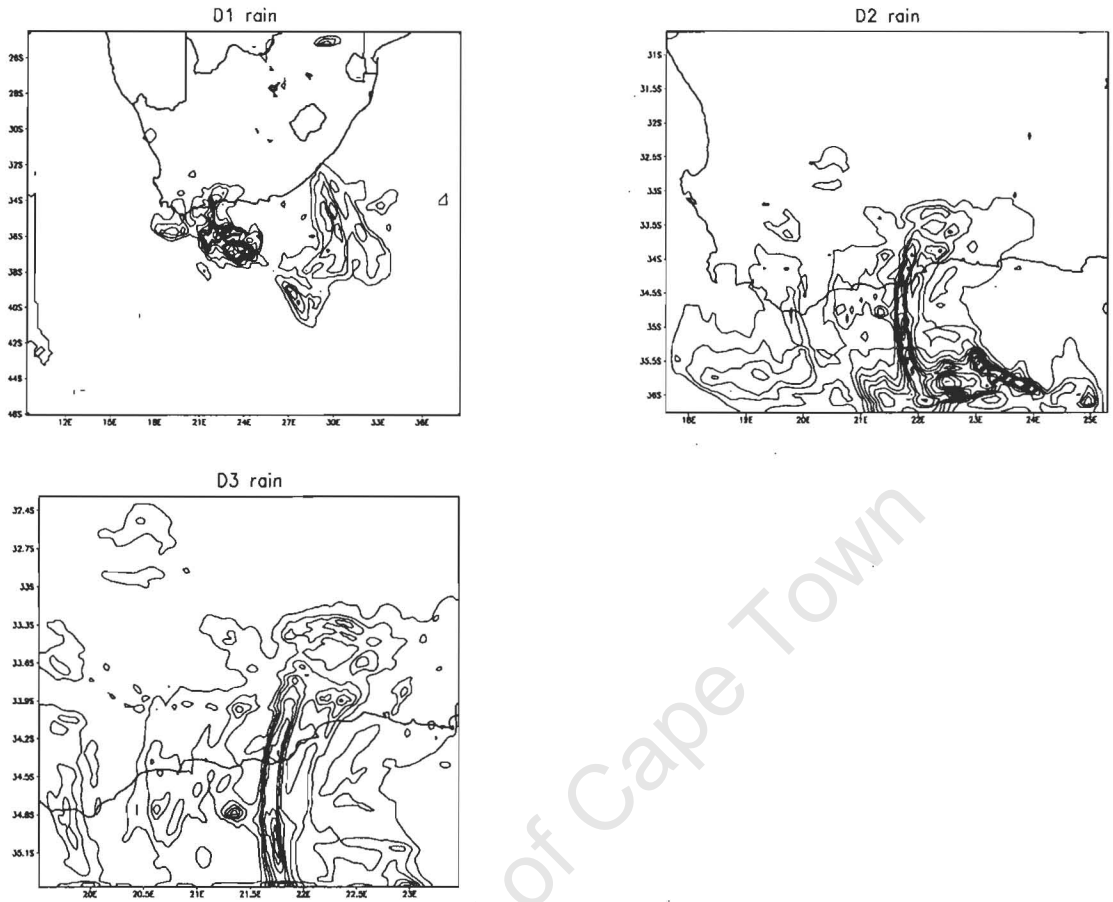

Figure 5.22 – 24-hour rainfall for the 24-hour period to 0600 UTC 24 March 2003 from the MM5 simulation of the Montagu case with three grids; (a) from the 27km resolution grid, (b) from the 9km resolution nested grid, (c) from the 3km resolution nested grid. For each of the panels the contour interval is 20mm.

University of Cape Town

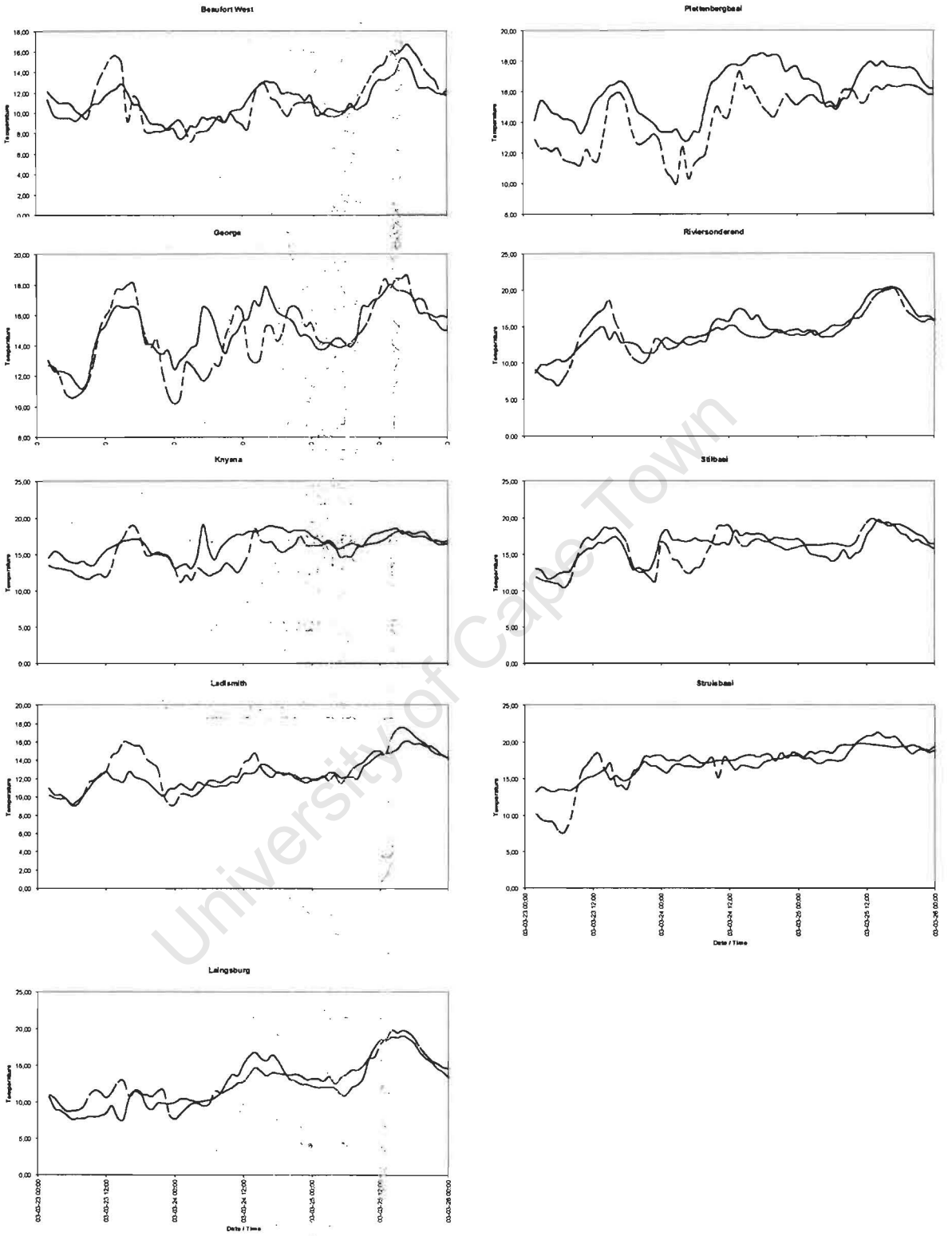

Figure 5.23 – Time series of 2m temperature at various weather stations for the Montagu case. The solid line is from the 3km grid of the MM5 simulation, and the dashed line is the observed temperature. Station names are given above each panel and locations are given in the text.

University of Cape Town

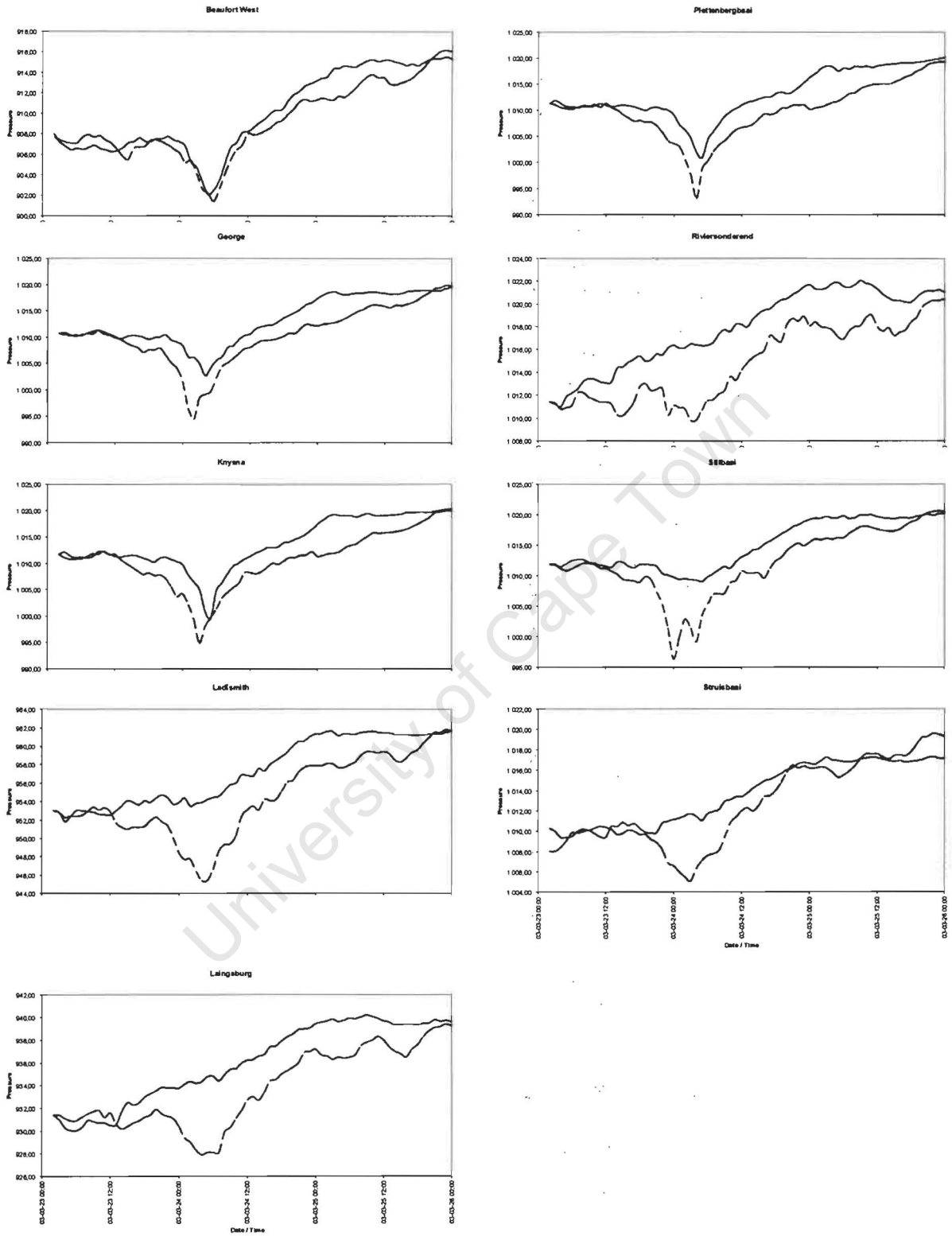

University of Cape Town

Figure 5.24 – As in Fig. 5.23, except for surface pressure.

University of Cape Town

Chapter 6

Diagnostics of the MM5 simulations

University of Cape Town

University of Cape Town

6.1. Introduction

This chapter presents analyses and diagnostics of the MM5 simulations of the East London and Montagu cases. The objective here is to identify mechanisms that led to the extreme amounts of precipitation observed during these events. Particular emphasis is placed on the development of the low-level flow and its interaction with the coastal topography.

As discussed in Chapter 5, a major feature of both of these cases was the development of an onshore LLJ, offshore of the location of the most intense precipitation. The analyses presented in this chapter will show the importance of the LLJ in the development of the convective environment. Convection is identified by locating areas in which the three ingredients necessary for convection, namely, low-level moisture, ascent and instability (Chapter 3; Doswell et al. 1996) are present. The interaction of the LLJ with the differing topography of the two cases is investigated. Additionally, the origin of air parcels arriving at the location of the most intense precipitation is investigated.

University of Cape Town

In addition to this introduction, this chapter comprises three main sections. Section 6.2 comprises a full analysis of the East London case, and section 6.3 contains a similar analysis for the Montagu case. Section 6.4 concludes the chapter by summarising the main findings.

6.2. The East London case

A brief summary of the synoptic environment of this event, described in detail in the previous chapter, follows. This event was characterised by a cold trough in the upper

atmosphere with a southeast-northwest orientation. A cut-off low pressure system developed within this trough over the Western Cape, while strong upper level jets existed on the western and eastern flanks of the trough. At the surface, a ridge of high pressure was present over the ocean to the south of South Africa with a trough over the ocean to the east of South Africa. An onshore LLJ developed due to the steep pressure gradient between the ridge and the trough.

6.2.1. Development of the convective environment

Here 0000 UTC 16 August 2002 has been chosen as the reference time for investigation since this is the time at which the heaviest rainfall was falling in both the observations and in MM5. Fig. 6.1 shows the large scale flow at this reference time. One of the most striking aspects of the large scale flow in MM5 was the formation of a meso-beta scale low pressure system off the coast of the Eastern Cape with cyclonic circulation over the coast at 26°–27.5°E. This feature did not appear to be present in the MRF analysis at this time (Fig. 5.3c), although there was some evidence of a cyclonic flow on the northern flank of the LLJ over the Eastern Cape coast (i.e. weak offshore flow at 33°S, 29°E in Fig. 5.3c). This suggests that the approximately 100km resolution of the MRF model was not sufficiently high to capture this feature, which was simulated in the 27km resolution MM5 simulation. This meso-beta scale low contributed to the strengthening of the LLJ in MM5 as it led to an increase in the pressure gradient there. The low-level wind showed a strong onshore component of southeasterly flow in the region of the LLJ, with strong wind shear on the cyclonic side (i.e. the right-hand side looking downstream, where pressure is lower) of the LLJ. Flow entering the LLJ consisted of air from north of

University of Cape Town

28°S, due to the trough east of South Africa, and air from south of 40°S being advected into the LLJ by the ridge to the south of South Africa.

In order to assess the influence of the pressure gradient on the LLJ, the pressure gradient force, PGF, was calculated following

$$PGF_x = -g\frac{\partial z}{\partial x} \qquad PGF_y = -g\frac{\partial z}{\partial y},$$

where the subscripts x and y denote the force in the x and y directions; g is the acceleration due to gravity; and z is the geopotential height. The calculation was performed in the region of the maximum wind speed of the LLJ and averaged over a 5 x 5 grid-point box in order to remove transitory waves. The time series of pressure gradient force (Fig. 6.2) shows an increasing y component from 1500 UTC 15 August to a maximum around 0000 UTC 16 August, when the wind speed of the LLJ was at a maximum. The x component had a maximum around 1800 UTC 15 August, and was at a minimum around 0000 UTC 16 August, suggesting a much more easterly component to the flow in the LLJ at this time. In addition, the low-level wind was found to be primarily geostrophic (not shown), suggesting that the pressure gradient was the main forcing mechanism.

Strong low level water vapour flux convergence was apparent at the leading edge of the LLJ where it impinged on the Eastern Cape coast (Fig. 6.3a). An additional area of low-level water vapour flux convergence was present on the cyclonic side of the LLJ extending eastwards from 29°E, 35.5°S. The ascent of moist air at the leading edge of the LLJ was due to the flow of the onshore LLJ impinging on a westerly flow ahead of it, which may have been as a result of the topography there, which is considered further in section 6.2.2. The convergence zone over the ocean was

University of Cape Town

related to the northwesterly flow due to the meso-beta scale low pressure system, and southeasterly flow being advected by the ridge interacting with the onshore flow of the LLJ.

The development of the convergence of the surface wind is shown in Fig. 6.4. There was initially, at 1400 UTC 15 August, a zonal band of convergence over the ocean between 23°-34°E at a latitude of 35°S, as a result of southeasterly flow coming into contact with easterly flow there (Fig. 6.4a-c). Additionally, convergence was strong where the meso-beta scale low led to flow being circulated into the LLJ. From 2000 UTC 15 August onwards (Fig. 6.4d), the convergence began to break down into several individual zones, and strengthened at the leading edge of the LLJ. By 0000 UTC 16 August, the convergence of the surface wind at the leading edge of the LLJ was at its highest, with a value of 40×10^{-5} s^{-1} (Fig. 6.4f). From 0200 UTC 16 August (Fig. 6.4g), the convergence at the leading edge of the LLJ weakened, but also spread to form a zonal band along the coast, which moved slowly to the north as time progressed (Fig. 6.4h-l). By 1200 UTC 16 August (Fig. 6.4l), the convergence of the surface wind had lessened considerably, and was confined to a weak band along the south coast of South Africa between 24°-28°E.

University of Cape Town

An examination of the convective instability at the reference time (0000 UTC 16 August) (Fig. 6.3b), inferred by the difference in equivalent potential temperature (i.e. the potential temperature of an air parcel if it was brought to full saturation) between the 1000- and 500-hPa levels[1], shows that the stratification was convectively unstable over the LLJ and on its cyclonic side. This convectively unstable

[1] $\theta e_{1000} - \theta e_{500}$

stratification just penetrated onto the land in the MM5 simulation slightly to the south of East London. With the ascent of moist air, indicated by zones of low-level water vapour flux convergence (Fig. 6.3a), occurring in a convectively unstable environment, air parcels were able to become buoyant resulting in convection.

The convective instability was a result of warm air extending down the east coast of South Africa towards the rainfall region (Fig. 6.3c), which led to a narrow tongue of high θe (equivalent potential temperature) air extending towards the coast between 26 – 30°E (Fig. 6.3d), approximately co-located with a tongue of low-level moisture (Fig. 6.3e). It therefore appears that the trough over the eastern seaboard of South Africa was responsible for advecting warm, moist air towards the location of heavy rainfall. This warm moist air was advected by the LLJ in a narrow band onto the coast of the Eastern Cape where it underwent vigorous ascent. Additionally, there were large values of surface latent heat fluxes (500 – 600 $W.m^{-2}$) from the ocean in the region of the LLJ (Fig. 6.3f), which indicates that the warm SST due to the Agulhas Current may have contributed to the low-level moisture supplying the rainfall, which is investigated further in section 6.2.3 and in Chapter 7.

A cross section along the axis of the LLJ where it impinged on the coast shows that there was strong ascent near the south coast, which appeared to form the upward branch of a convective cell with a weaker descending branch to the southeast (Fig. 6.5a), as well as farther offshore (not shown). An inspection of a time series of cross sections (not shown) showed that this cell was initially located over the ocean and approached the coast from the southeast. As it reached the south coast, the ascending arm was strengthened considerably, with upward velocities close to 50

University of Cape Town

$cm.s^{-1}$ (Fig. 6.5b), which is rather large for a simulation with this spatial resolution. This result suggests that the coastal topography played a role in enhancing the ascending branch of the convective cell, and this is discussed further in section 6.2.2.

The potential vorticity cross section shows a considerably lowering of the tropopause, as a result of the deep trough aloft, towards the northwest of the cross-section above the interior plateau of South Africa, and a plume of high potential vorticity air from the coastal mountain peak up to the tropopause (Fig. 6.5c). Since potential vorticity is conserved in adiabatic conditions (Hoskins et al. 1985), the generation of potential vorticity in the lower troposphere suggests that some diabatic process was taking place. In this convective environment, it is logical to assume that latent heat release due to condensation is responsible for the generation of potential vorticity in the lower troposphere, and comparison with Figs. 6.5a,b shows that this plume of potential vorticity is approximately co-located with the vigorous ascent. As shown by the relative humidity cross-section (Fig. 6.5d), the ascent took place in an almost fully saturated environment. Additionally, the lowering of the tropopause over the interior plateau is confirmed by a lowering of the region of low relative humidity air, indicative of stratospheric origins.

University of Cape Town

6.2.2. Interaction of the LLJ with topography

Here the interaction of the LLJ with the coastal topography of the Eastern Cape is considered at the reference time (0000 UTC 16 August). Fig. 6.4b clearly shows that, at this time, there was a plume of ascent just ahead of a topographic barrier. This peak is located approximately 70km inland and has a height of 1200m in MM5. The

ascent was most vigorous at around 750- and 600-hPa on the upstream side of the topographic barrier.

The influence the topography had on the LLJ impinging on it may be estimated in terms of the non-dimensional numbers, the Froude number, Fr, and the Rossby number, Ro (see Chapter 3 for a definition of these numbers). In this instance, the variables used to estimate Fr were as follows: h ~ 1200m, U ~ 16m.s^{-}1 and N ~ 0.007, yielding a value of Fr = 1.9. This value suggests that the flow will tend towards the 'flow over' regime, and therefore upslope flow, which is likely to enhance the ascent of moist air as the LLJ impinges on the slope. Additionally, since Fr < 5, it is also likely that there would have been a degree of blocking (Baines 1979; Smolarkiewicz and Rotunno 1990). For the Rossby number calculation, the mountain half width, L ~ 40km, and at this latitude f ~ 0.000073 s^{-1}, giving a value of Ro = 5.5. This value, Ro >> 1, suggests the development of vertically propagating gravity waves on the upstream side of the mountain (Trüb and Davies 1995), potentially resulting in increased cloud formation.

The above result suggests that as the LLJ impinged on this steep topography, the flow was sufficiently strong, and the stratification unstable enough, for upslope flow to occur. This upslope flow would have enhanced the convective ascent, which was already taking place at the leading edge of the LLJ before it impinged on the topography, resulting in the extreme rainfall rates observed at this time.

University of Cape Town

6.2.3. Air parcel back trajectories

The air parcels considered here are those that arrived at the location of the most intense precipitation in MM5 at the surface, 900- and 500-hPa levels. The location of most intense precipitation, taken from Fig 5.16a, was 26.8°E, 34°S. The trajectories were calculated from the model winds using a 600 second time step, and a release time of 0000 UTC 16 August.

Fig. 6.6 shows the trajectories for the air parcels arriving at the surface, 900- and 500-hPa levels, labelled A, B and C respectively. Parcel A had its origins to the south and at the model initialisation at 0000 UTC 14 August was at a height of 700 hPa (Fig. 6.7a). This suggests that the trajectory of this parcel was initially controlled by winds associated with the trough. Along its trajectory, the pressure of the parcel increased (Fig. 6.7a) indicating that it was in sinking air. As it sank below approximately the 850 hPa level, the relative humidity of the parcel increased considerably as it entered the moist low-level air.

Air parcel B appeared to have its trajectory governed by the ridge over the ocean to the south of South Africa (Fig. 6.6 cf Fig. 6.1). It was initially in sinking air (Fig. 6.7b) and then as it began to traverse a region of high latent heat flux (Fig. 6.6) it began to ascend to close to 700 hPa, before sinking again as it approached the land. For most of its trajectory, this parcel was in high relative humidity air. This result suggests that the region of high latent heat flux was associated with ascending air, suggesting that convection was taking place there over the relatively high SST of the Agulhas Current. This is consistent with the findings of Lutjeharms et al. (1986); Jury and Walker (1988); Jury and Courtney (1991); Jury (1993); Rouault et al (2003), who

University of Cape Town

have suggested that there is an increase in convection over the warm SST of the Agulhas Current. As air parcel B sank, it is likely that its trajectory was being influenced by the descending branch of a convective cell.

Air parcel C was clearly being advected by the jet streak of the trough that was present in the upper air (Fig. 6.6 cf Fig. 5.2c). For the initial part of its trajectory, it was in dry subsiding air (Fig. 6.7c), until it became part of the northwesterly jet at 500 hPa, when its humidity remained mostly constant. As it moved towards the area of extreme rainfall, its relative humidity increased as it entered the moist convective column.

The above analysis suggests that, for this event, low-level flow originated over the ocean to the south of South Africa, and was advected towards the continent by the enhanced wind due to the ridge. There appeared to be vigorous ascent associated with a region of high latent heat flux over the ocean just off the south coast of the Eastern Cape.

University of Cape Town

6.2.4. Summary

The MM5 simulation allowed an examination of the development of the convective system during this cut-off low event, and identified factors, such as the meso-beta scale surface low, that were not so apparent in the MRF analyses or observations. However, it is possible to have confidence in the simulation since MM5 was able to capture the salient, large scale features. The analysis of the MM5 simulation showed that convection developed on the right-hand, looking downstream, and leading edges of the LLJ, which back trajectories showed was advecting air from high latitudes to

the south of the rainfall region. The Froude and Rossby numbers greater than one suggest that the coastal topography enhanced the ascent of moist air at the leading edge of the LLJ.

6.3. The Montagu Case

Observations from this event suggest that precipitation was at its most intense between 0200 and 0800 UTC 24 March, and in the model it was heaviest at around 0400 UTC 24 March. Hence 0400 UTC 24 March was chosen as the representative time to further examine the factors contributing to the convective development of the system.

6.3.1. Development of the convective environment

At the representative time, a large area of low pressure extended over the ocean to the south and east of South Africa (with two mesoscale lows embedded within it, one near 32°, 28°S, and one near the rainfall region around 23°E, 34°S), which resulted in the flow of warm air (emanating from the southern Mozambique / subtropical Southwest Indian Ocean region) south over the Agulhas Current system, and then northwest towards the rainfall region in the Western Cape (Fig. 6.8). Over the south coast, the relatively steep pressure gradient on the west side of the depression provided forcing for the strong onshore LLJ, which impinged on the topography of the south coast. Animation sequences of the flow pattern showed that the time at which the LLJ began to impinge on the coast to be simultaneous with the onset of precipitation over land, and as the LLJ continued to impinge on the south coast, with wind speeds in excess of 20 $m.s^{-1}$, heavy precipitation continued to fall over this area.

University of Cape Town

A calculation of the pressure gradient force, using the method described for the East London case, shows that there was a considerable increase in the x component of the pressure gradient force from 2100 UTC 23 March to a maximum at 0100 UTC 24 March 2003 (Fig. 6.9). Since the flow was predominantly southerly in the LLJ, the y component of the force was almost an order of magnitude smaller.

At the reference time (0400 UTC 24 March), a distinct band of low-level water vapour flux convergence was apparent on the cyclonic side of the LLJ (Fig. 6.10a) where there was strong horizontal wind shear. This band of convergence was due to the cyclonic flow of the surface depression mixing with the onshore flow of the LLJ.

The development of surface wind convergence at two hour intervals on 23-24 March (Fig. 6.11) shows that convergence was initially strong with several zonal bands existing over the ocean south of the Western Cape before developing into a linear area of convection on 24 March extending northwestwards across the Agulhas Current to the coast where the convergence intensified. This pattern persisted in the simulation for approximately twelve hours suggesting that conditions favourable for heavy rainfall remained in the same area for an extended period, thus leading to the high rainfall totals observed on 23-24 March.

An examination of the convective instability at 0400 UTC 24 March showed that the ascent of moist air (Fig. 6.10a) at low levels was taking place in a convectively unstable environment (Fig. 6.10b). This instability was particularly strong over the ocean around 23°E, 37°S, but was relatively weak over the coastal region of the Western Cape. The near surface potential temperature at this time (Fig. 6.10c) showed a tongue of warm air extending over the ocean from the east with cooler air

University of Cape Town

on its onshore side. The warm tongue extended towards the coast on the eastern side of the LLJ. The equivalent potential temperature (Fig. 6.10d), and the mixing ratio (Fig. 6.10e) at 925 hPa showed that this tongue of warm air was also relatively moist. Therefore the band of low-level water vapour flux convergence on the cyclonic side of the LLJ can be attributed to the mixing of warm moist easterly flow originating from tropical latitudes with cooler, drier onshore flow from the southeast. Additionally, both the flow from the east and that from the southeast passed over regions of high latent heat flux from the ocean, particularly over the Agulhas retroflection region where fluxes greater than 700 $W.m^{-2}$ occurred, with strong gradients to the north of this maximum (Fig. 6.10f).

An additional feature of Fig. 6.8 is the mesoscale depression over the ocean to the southeast of South Africa near 37°S, 30°E. Unfortunately, validation of this feature is difficult since it does not exist in the coarser resolution MRF model (Fig. 5.11c) and there is a lack of sufficient observations over the ocean. However, an inspection of scatterometer winds derived from the QuikSCAT satellite (Fig. 5.4c) revealed that a signature of this feature was indeed apparent. This depression was maintained for more than twelve hours in the simulation and may have helped to accelerate the southerly flow of warm air coming from the east of South Africa towards the Western Cape.

A vertical cross-section through the axis of the LLJ at the representative time (Fig. 6.12a) reveals that there was considerable ascent as the onshore LLJ impinged on the coastal topography (Fig. 6.12a). A plume of vertical motion apparent up to the mid-levels of the troposphere (Fig. 6.12b), with ascent close to 100 $cm.s^{-1}$ was embedded in a layer of high relative humidity air that extended to the edge of the escarpment (Fig. 6.12d). Time sequences of this cross section showed that this

University of Cape Town

plume of vertical ascent remained rooted to the topography for several hours while the precipitation was at its most intense, suggesting that the topography here was important in aiding the ascent of moist air and thus convection. Additionally, the cross section of PV (Fig. 6.12c) shows two downward intrusions of high PV air into the troposphere. This is consistent with the tropopause map constructed from the MRF analyses at 0000 UTC 24 March (Fig. 5.15c), which showed that the PV anomaly in the troposphere was horseshoe shaped with higher anomalies over the ocean to the south of the Western Cape, and over the Northern Cape. There was also a plume of high PV rooted to the mountain peak at this time implying latent heat release due to condensation.

University of Cape Town

6.3.2. Interaction of the LLJ with topography

An investigation of the interaction of the LLJ with the coastal topography for the present case study follows. As in the East London case (section 6.2.2), the flow regime is investigated in terms of the non-dimensional numbers, Fr and Ro. In this instance, $U=25.87 m.s^{-1}$, $N=0.0075 s^{-1}$, and h=915m, giving a value of Fr=3.77, a value considerably greater than one, indicating that there was a tendency for the flow to go over rather than around the topography. Furthermore, this value of Fr>>1 indicates that there was strong upslope flow, which would have promoted ascent at the topographic barrier (Smith 1979). However, since Fr<5, there was still the potential for some degree of blocking (Baines 1979), and hence the ascent was confined to the upstream side of the mountain.

Additionally, in this instance, where the mountain half width is approximately 30km, the LLJ led to a value Ro=11.8. This value of Ro>>1 implies that the impingement of the LLJ on the coastal topography resulted in high amplitude vertically propagating gravity waves (Trüb and Davies 1995).

6.3.3. Air parcel back trajectories

This section presents an analysis of air parcel back trajectories for air parcels arriving in the region of the most intense precipitation in the MM5 simulation (21.6°E, 34.0°S in Fig. 5.20a). Trajectories arriving at this location at A, the surface; B, 850- and C, 500-hPa were calculated from the model winds using a 600 second time step and a release time equal to the representative time (0400 UTC 24 March).

Fig. 6.13 shows that air parcels arriving at various heights (the surface, 850 hPa and 500 hPa) at this location all had their origins to the south, with their trajectories traversing an area of surface latent heat flux in excess of 700W.m^{-2} to the south of the Western Cape, suggesting that the ocean here, in the region of the southern Agulhas Current, could have been an important source of moisture.

Closer examination of each of the trajectories in terms of the height (pressure) and the moisture content (relative humidity) of the parcels is presented in Fig. 6.14. Parcel A had its origins over the ocean to the south of the Western Cape, and was advected onto the coast by the LLJ near to the ocean surface in relatively moist air (Fig. 6.14a). When this air parcel arrived at the coast it underwent rapid ascent as it encountered the coastal topography, and its humidity increased.

University of Cape Town

Similarly, parcel B was advected onto the coast topography by the LLJ (Fig. 6.14). Its origins were similar to the location parcel A originated in, but was higher above the surface. It was advected towards the coast in a fully saturated layer (Fig. 6.14b), which is clearly seen in the cross section (Fig. 6.12d). The parcel then ascended into the dry layer above 800 hPa, and was advected towards the coast within this layer, where it entered moister air.

Parcel C was initially part of the northwesterly jet which was present at 500 hPa (Fig. 5.11) and extended down to approximately the 700 hPa level, before it descended towards the surface and was advected towards the land in the LLJ (Fig. 6.13, 6.14c). As the parcel underwent rapid descent it passed through a dry layer into moister air near the surface. The trajectory of this parcel here suggests that there may have been some momentum transfer between the upper northwesterly and low-level southerly jets. As parcel C approached the coastal topography, it underwent rapid ascent as part of the vertical ascent of moist air where convection occurred.

Examination of the boundary layer height (not shown), calculated in the boundary layer parameterization scheme of MM5, compared with the height of the air parcel trajectories showed that the air parcels arriving at the surface, 850 hPa and 500 hPa were all within the boundary layer when they passed over the area of highest latent heat fluxes. This suggests that not only was the ocean here likely to have added moisture to the passing air parcels, but there was also considerable ascent after passing over this area with air parcels ending up as high as 500 hPa when they reached the region of most intense convective activity.

University of Cape Town

6.3.4. Summary

The MM5 simulation of this case suggests that the LLJ formed as a result of a rapidly increasing pressure gradient force. Similar to the East London case, convection was apparent at the leading and right-hand edges of the LLJ, which back trajectories suggest was advected air from relatively high latitudes onto the south coast of the Western Cape. These air parcels passed over an area of high latent heat fluxes from the surface in the boundary layer, and ascended as they impinged on the coastal topography.

6.4. Summary

This chapter investigated the processes that led to the most intense rainfall over the land in the two case studies examined in this thesis. There are a number of distinct similarities between the two systems. Firstly, an onshore LLJ formed as a result of increasing pressure gradient force. In the Montagu case the LLJ was southerly, whereas in the East London case it was more easterly. Due to the change in orientation of the coastline between these locations, the LLJ was approximately perpendicular to the coastal topography in both cases, aiding uplift.

University of Cape Town

Secondly, important regions of convection were associated with the leading and cyclonic edges of the LLJ. At the leading edge of the LLJ, ascent was enhanced as the strong onshore winds impinged on the coastal topography. However, in the East London case, the LLJ was not as strong as in the Montagu case leading to a value of Fr closer to one and less vigorous ascent, but in terms of the scaling parameter, the Burger number, B, calculated from Ro / Fr, the two situations are very similar. In the Montagu case B=3.1, and in the East London case B=2.9. This suggests that in both

cases, the degree to which rotational effects dominated over stratification in the flow was approximately the same. In the Montagu case, ascent was evident as the LLJ impinged on the coastal topography for an extended length of time, whereas in the East London case, ascent was present at the leading edge of the LLJ before it began to impinge on the topography. However, in this case ascent appeared to be greatly enhanced when the LLJ began to interact directly with the topography just inland of the coast.

Additionally, both cases appeared to show similarities in terms of the source of low-level warm moist air. A tongue of low-level warm moist air was seen to extend over the ocean from the east towards the regions of convection. This warm moist air was likely to have played a part in destabilising the atmosphere allowing air parcels to become buoyant leading to severe convection. In both cases, a narrow tongue of this warm moist air penetrated a small distance onto the coast on the cyclonic side of the LLJ. The cyclonic side of the LLJ can thus be thought of as a mesoscale front between the cold air being advected by the surface ridge to the south of South Africa, and the warm moist tropical air being advected by the surface trough down the eastern seaboard of South Africa. The warm low-level air also appears to be associated with the warm SST of the Agulhas Current, which is evident from colder air on the inshore side of the warm tongue, approximately co-located with regions of cold upwelling in the SST distribution.

The origin of air parcels arriving at the point of most intense precipitation appeared to be from relatively high latitudes in both cases. This was especially the case for air parcels arriving at levels below 850 hPa. This appears to confirm the suggestion of

University of Cape Town

Taljaard (1985) that the low-level flow in cut-off low events is characterised by cold air from high latitudes 'undercutting' warm moist air from the tropics, leading to an environment favourable for deep moist convection to occur. In the Montagu case, there was evidence to suggest that the LLJ may have been enhanced due to momentum transfer from the upper level jet, as the trajectory of one of the air parcels showed that it descended from a northwesterly flow around 700 hPa towards the surface where it became part of the southeasterly flow into the onshore LLJ.

The analyses of these case studies therefore suggest a number of important factors which may have influenced the flow at low-levels. The increasing pressure gradient force led to an increase in the low-level wind speed and the formation of a LLJ. The topography appears to play an important role in enhancing the ascent of moist air and therefore the severity of convection. Additionally, the mesoscale front that is associated with the cyclonic side of the LLJ promotes convection. On the warm side of this front, the warm SST of the Agulhas Current and its retroflection zone may have been responsible for warming the low-levels of the atmosphere and thus helping to destabilise the stratification. Furthermore, air parcels passed over regions of high latent heat flux from the ocean, associated with the warm SST of the Agulhas Current, suggesting that this might be an important moisture source in cut-off low events. These factors are investigated in more detail in the following chapter through sensitivity experiments with the MM5 simulations.

University of Cape Town

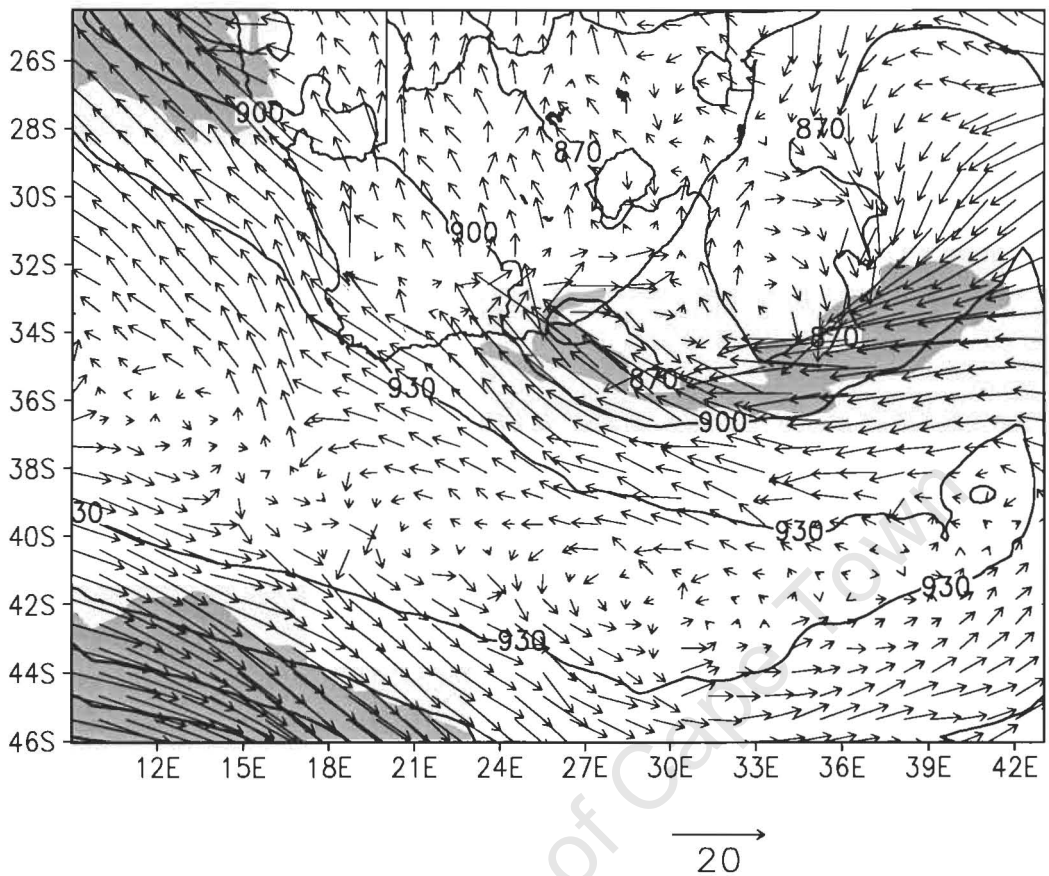

Figure 6.1 – 925 hPa geopotential height (solid contours, interval 30m), wind vectors, with a scale given to the bottom right of the panel, and wind speed greater than 15 $m.s^{-1}$ (shading) at 0000 UTC 16 August 2002 from the MM5 simulation of the East London case.

University of Cape Town

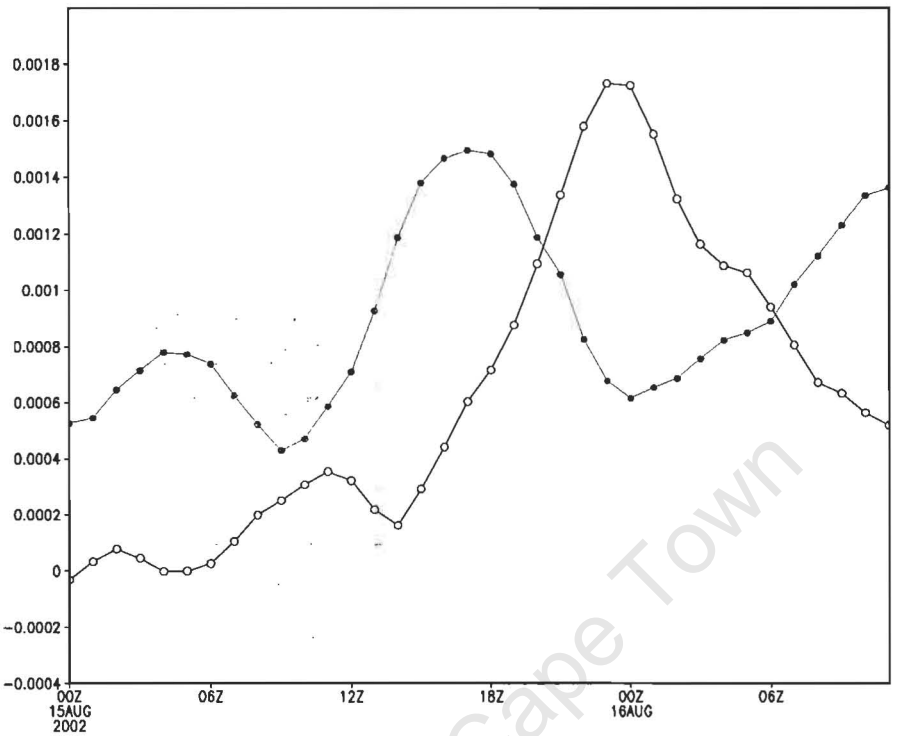

Figure 6.2 – Pressure gradient force over the region of maximum wind speed in the LLJ for the East London case. Green closed circles indicate the x-component and open circles indicate the y component

University of Cape Town

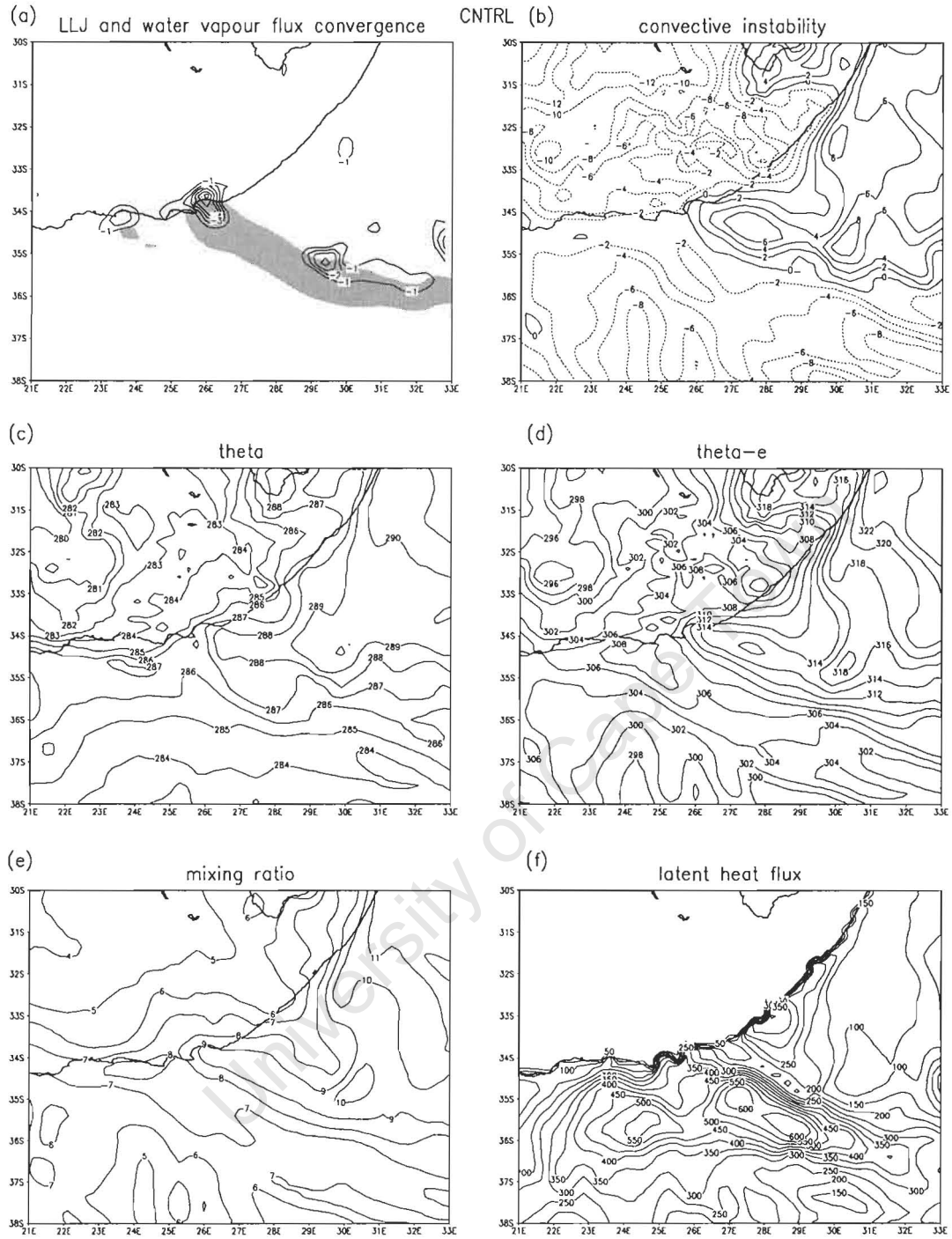

Figure 6.3 – Output from the MM5 simulation at 0000 UTC 16 August 2002. (a) 1000-850 hPa water vapour flux convergence, contour interval 1 $g.m^{-2}.s^{-1}$, with wind speed greater than 15 $m.s^{-1}$ shaded; (b) Convective instability taken as the difference in equivalent potential temperature between 1000- and 500-hPa, contour interval 5K; (c) 1000 hPa potential temperature, contour interval 1K; (d) 1000 hPa equivalent potential temperature, contour interval 2K; (e) 1000 hPa mixing ratio, contour interval 1 $g.kg^{-1}$; (f) surface latent heat flux, contour interval 50 $W.m^{-2}$.

University of Canterbury

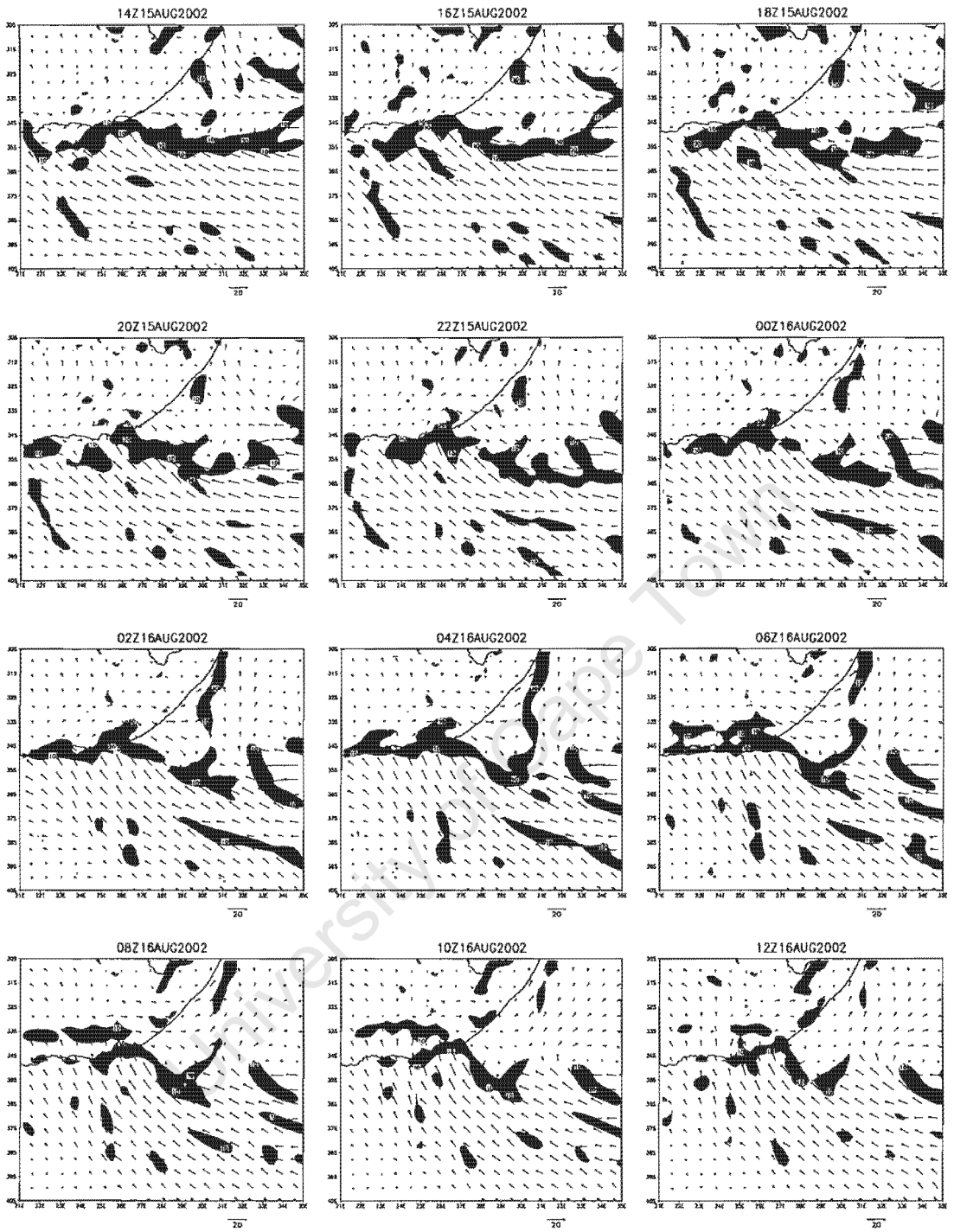

Figure 6.4 – Convergence of the surface wind (solid contours, interval 10 x 10^{-5} s^{-1}, from 10 x 10^{-5} s^{-1} and shading from 5 x 10^{-5} s^{-1}) and surface wind vectors (a scale is given to the bottom right of each panel) from the MM5 simulation of the East London case at 2-hour intervals from 1400 UTC 15 August to 1200 UTC 16 August.

University of Cape Town

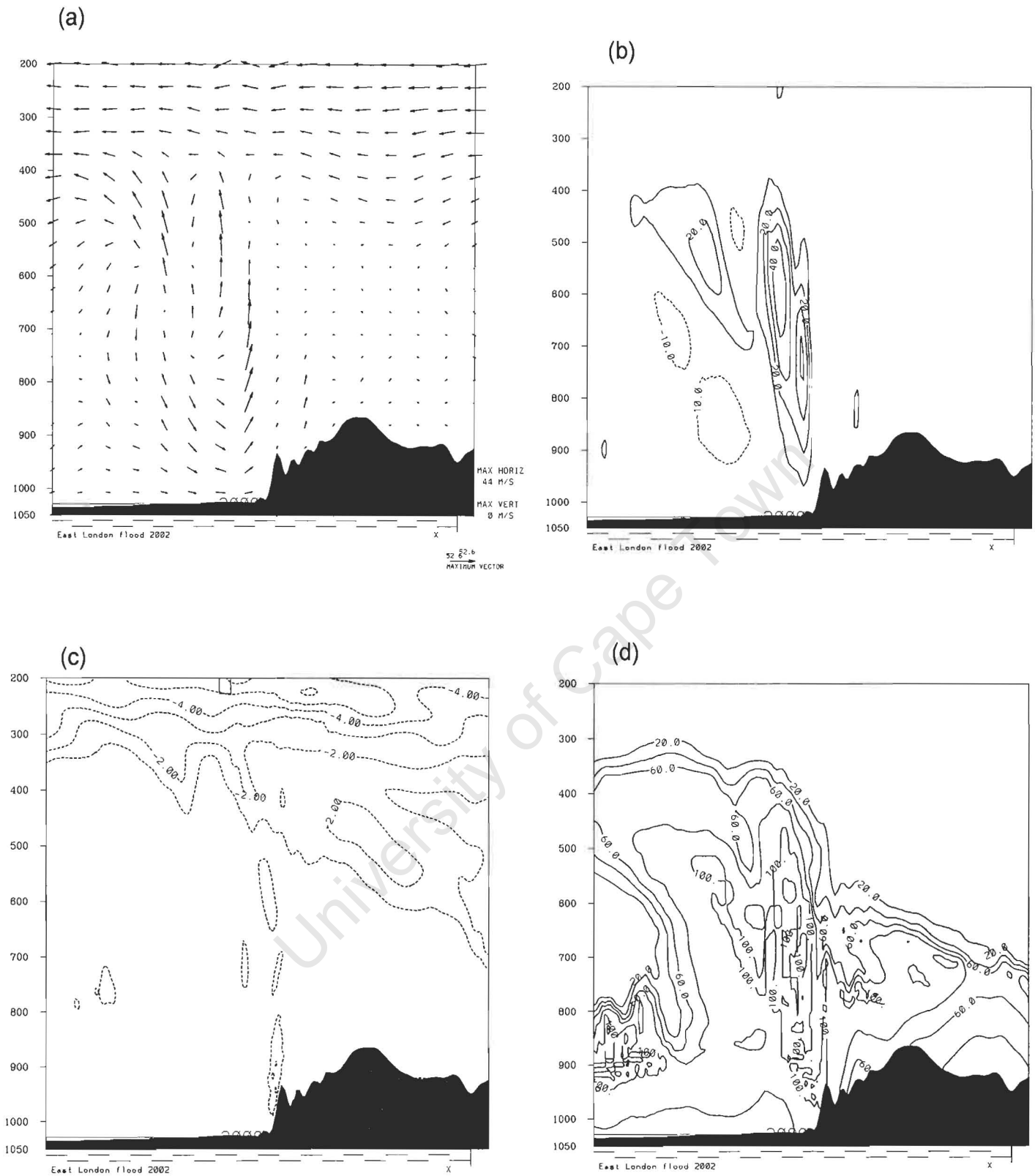

Figure 6.5- Cross sections AB through from CNTRL at 0000 UTC 16 August 2002. (a) Wind vectors in the plane of the cross-section; (b) vertical velocity (contour interval 20 cm.s $^{-1}$); (c) potential vorticity (contour interval 1 PVU); (d) relative humidity (contour interval 20%).

University of Cape Town

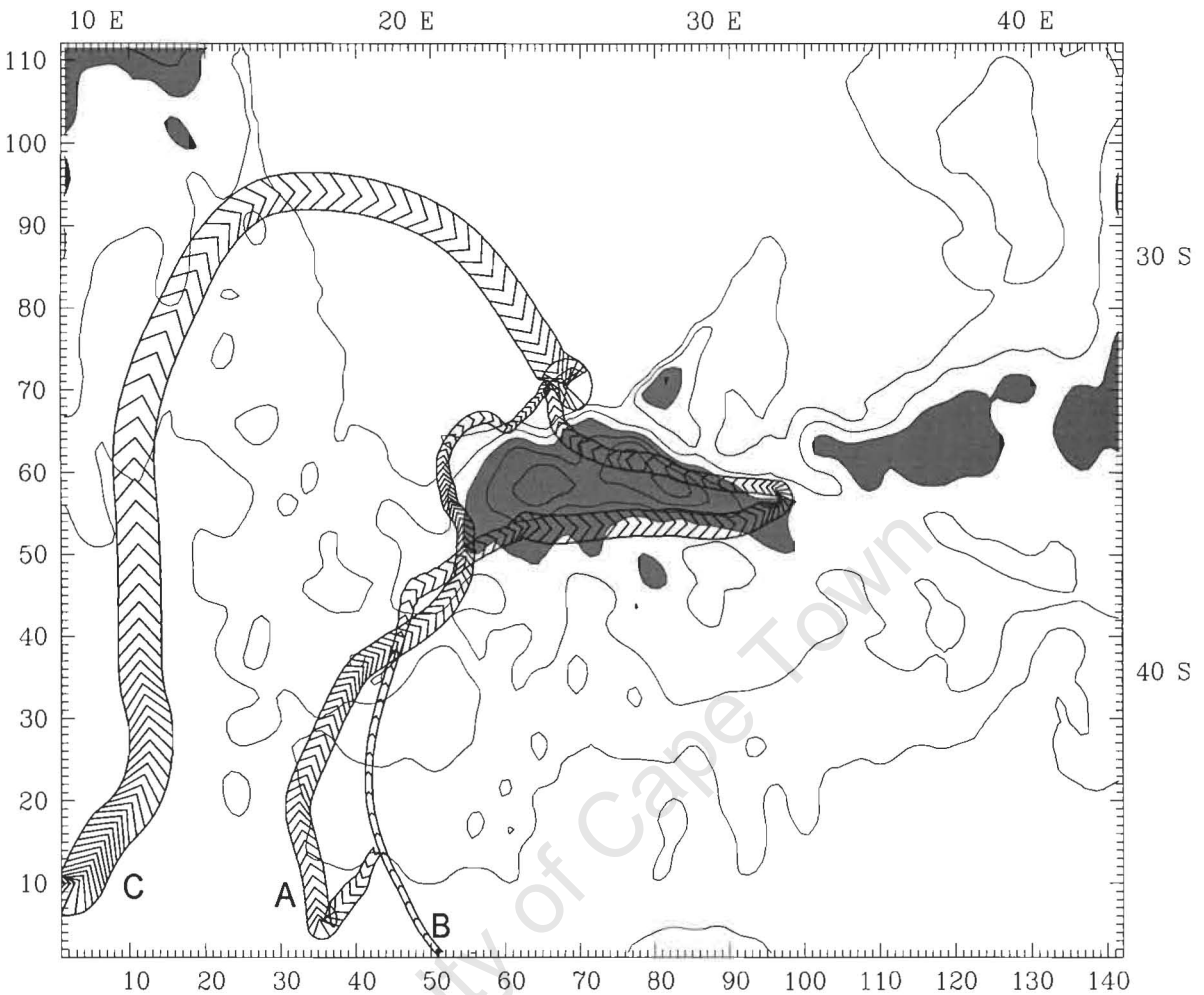

University of Cape Town

Figure 6.6 Backward trajectories from the MM5 simulation of the East London case for air parcels arriving at A, the surface; B, 850-; and C, 500 hPa. The release time of the trajectories is 0000 UTC 16 August 2002. Contours show the surface latent heat flux at an interval of 100 $W.m^{-2}$ and shading > 300 $W.m^{-2}$. Trajectory width is proportional to the height of the air parcel (wider = higher).

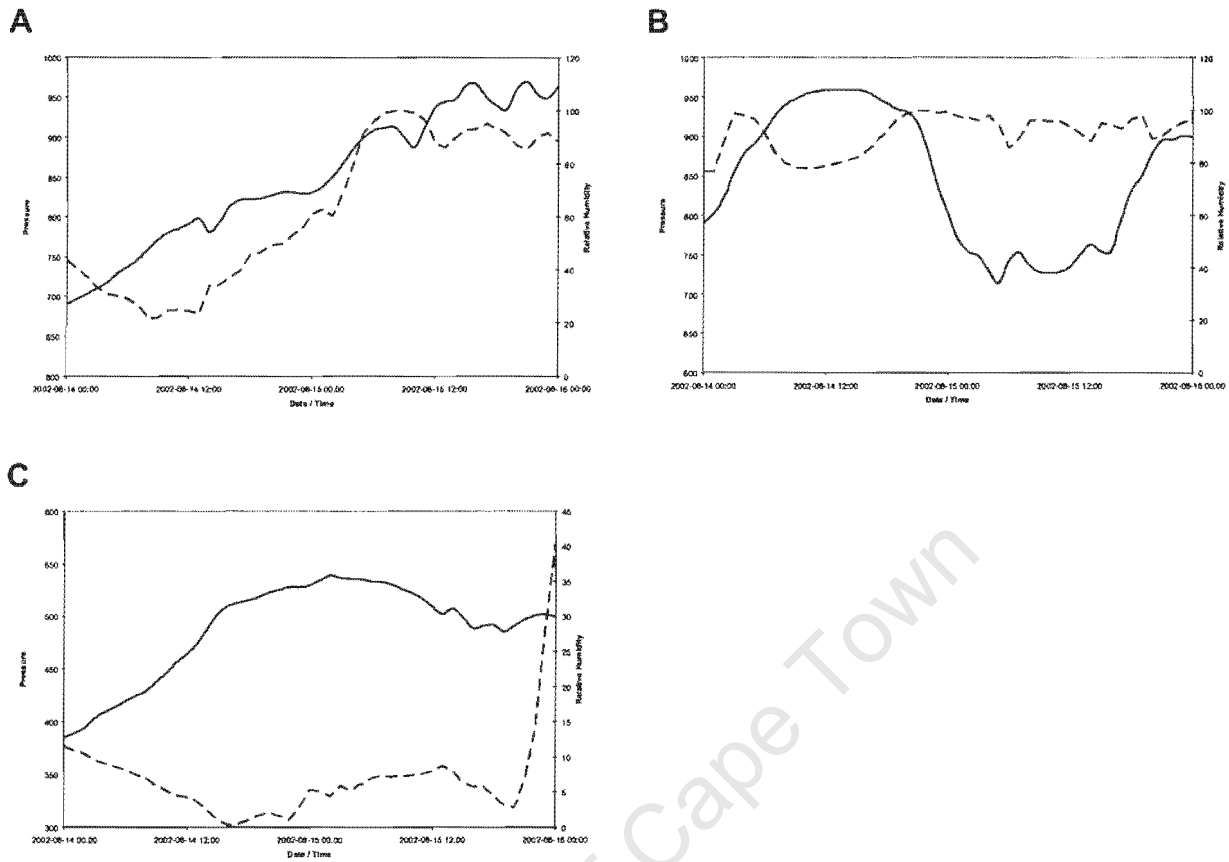

Figure 6.7 – Backward trajectory diagnostics for the trajectories shown in Fig. 6.5. The panels are labelled for trajectories A, B and C. Solid line is pressure (hPa) and the dashed line is relative humidity (%).

University of Cape Town

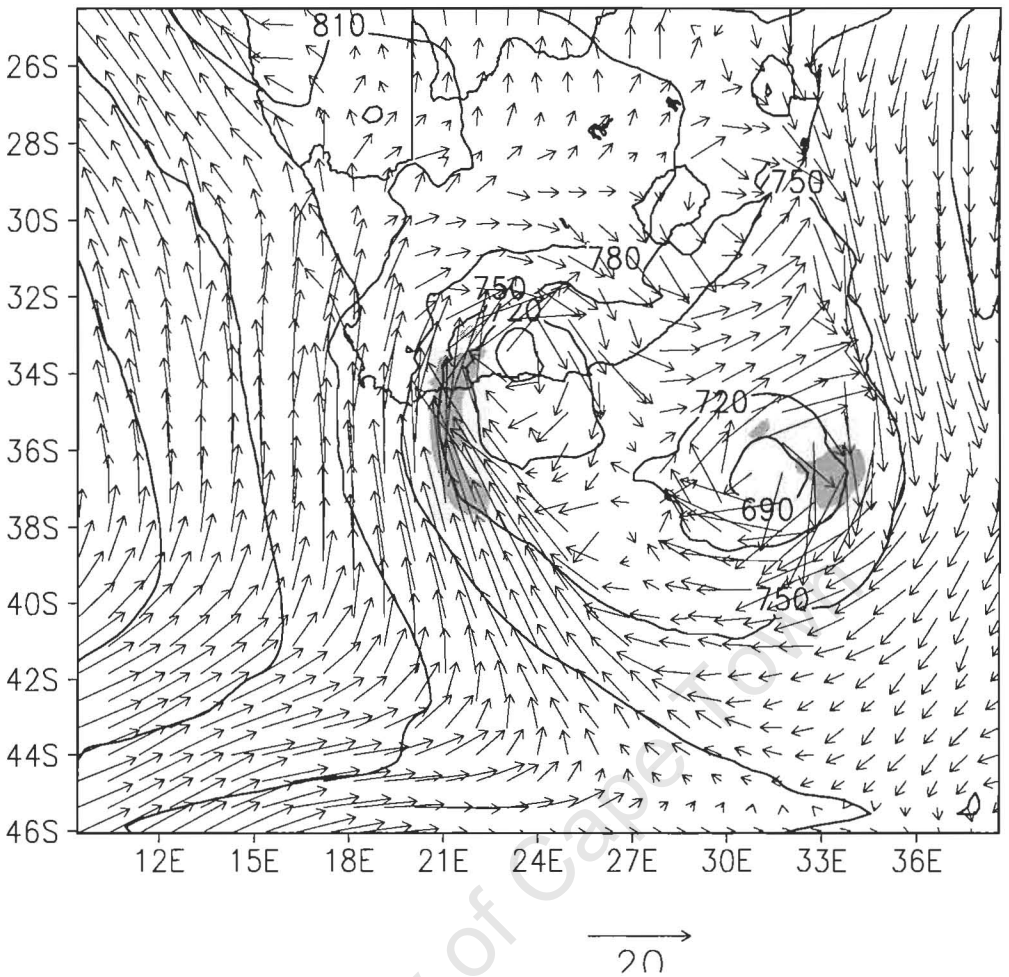

Figure 6.8 – 925 hPa geopotential height (solid contours, interval 30m), wind vectors, with a scale given to the bottom right of the panel, and wind speed greater than 20 $m.s^{-1}$ at 0400 UTC 24 March 2003 from the MM5 simulation of the Montagu case.

University of Cape Town

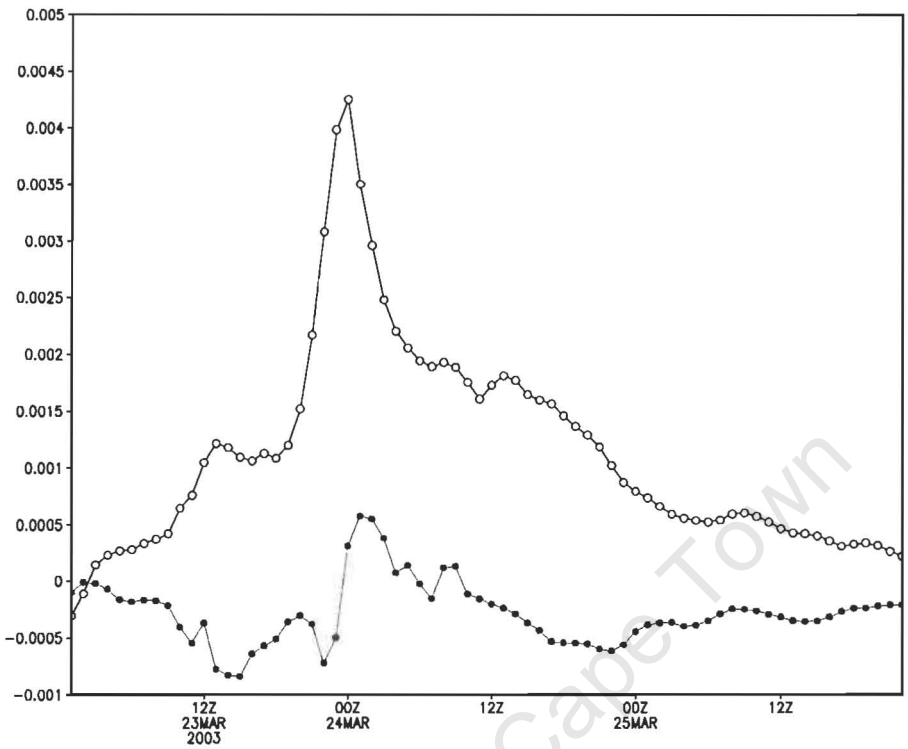

Figure 6.9 – Pressure gradient force averaged over the region of maximum wind speed of the LLJ for the Montagu case. Open circles indicate the x-component and green closed circles the y-component.

University of Cape Town

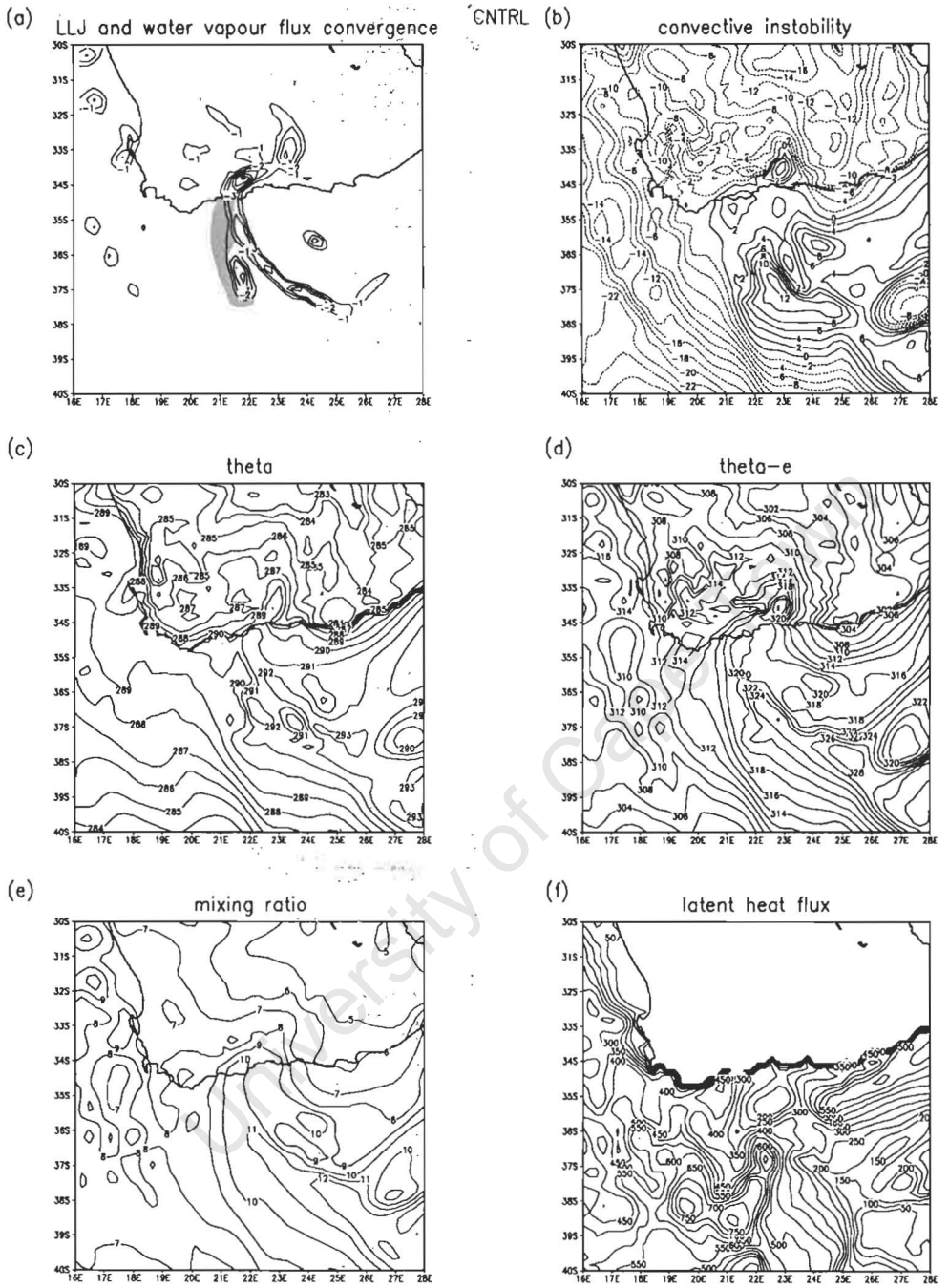

Figure 6.10 – Output from the MM5 simulation at 0400 UTC 24 March 2003. (a) 1000-850 hPa water vapour flux convergence, contour interval 1 $g.m^{-2}.s^{-1}$, with wind speed greater than 15 $m.s^{-1}$ shaded; (b) Convective instability taken as the difference in equivalent potential temperature between 1000- and 500-hPa, contour interval 5K; (c) 1000 hPa potential temperature, contour interval 1K; (d) 1000 hPa equivalent potential temperature, contour interval 2K; (e) 1000 hPa mixing ratio, contour interval 1 $g.kg^{-1}$; (f) surface latent heat flux, contour interval 50 $W.m^{-2}$.

University of Oxford

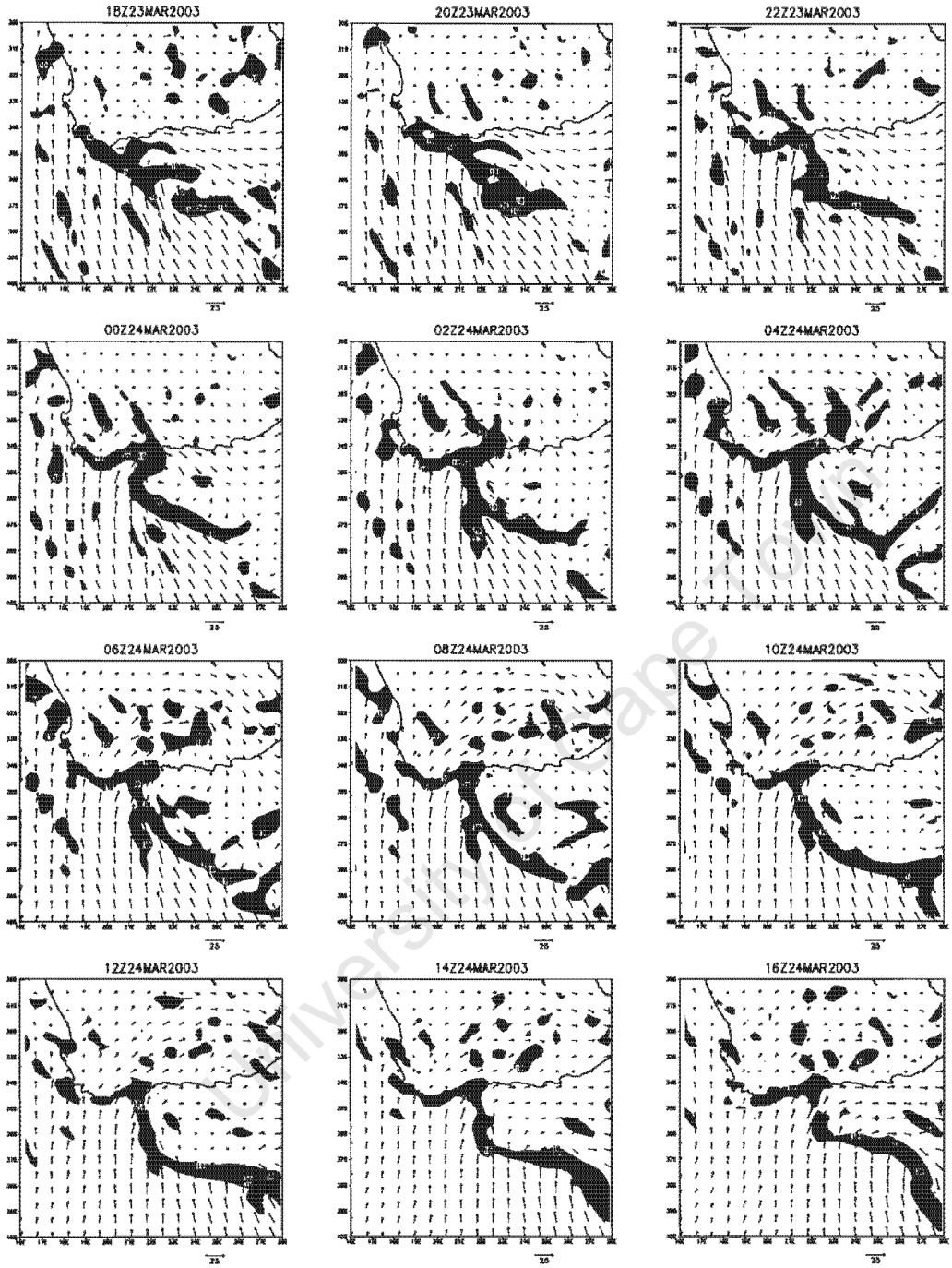

Figure 6.11 – Convergence of the surface wind (solid contours, interval 10 x 10^{-5} s^{-1}, from 10 x 10^{-5} s^{-1} and shading from 5 x 10^{-5} s^{-1}) and surface wind vectors (a scale is given to the bottom right of each panel) from the MM5 simulation of the Montagu case at 2-hour intervals from 1800 UTC 23 March to 1600 UTC 24 March 2003.

University of Cape Town

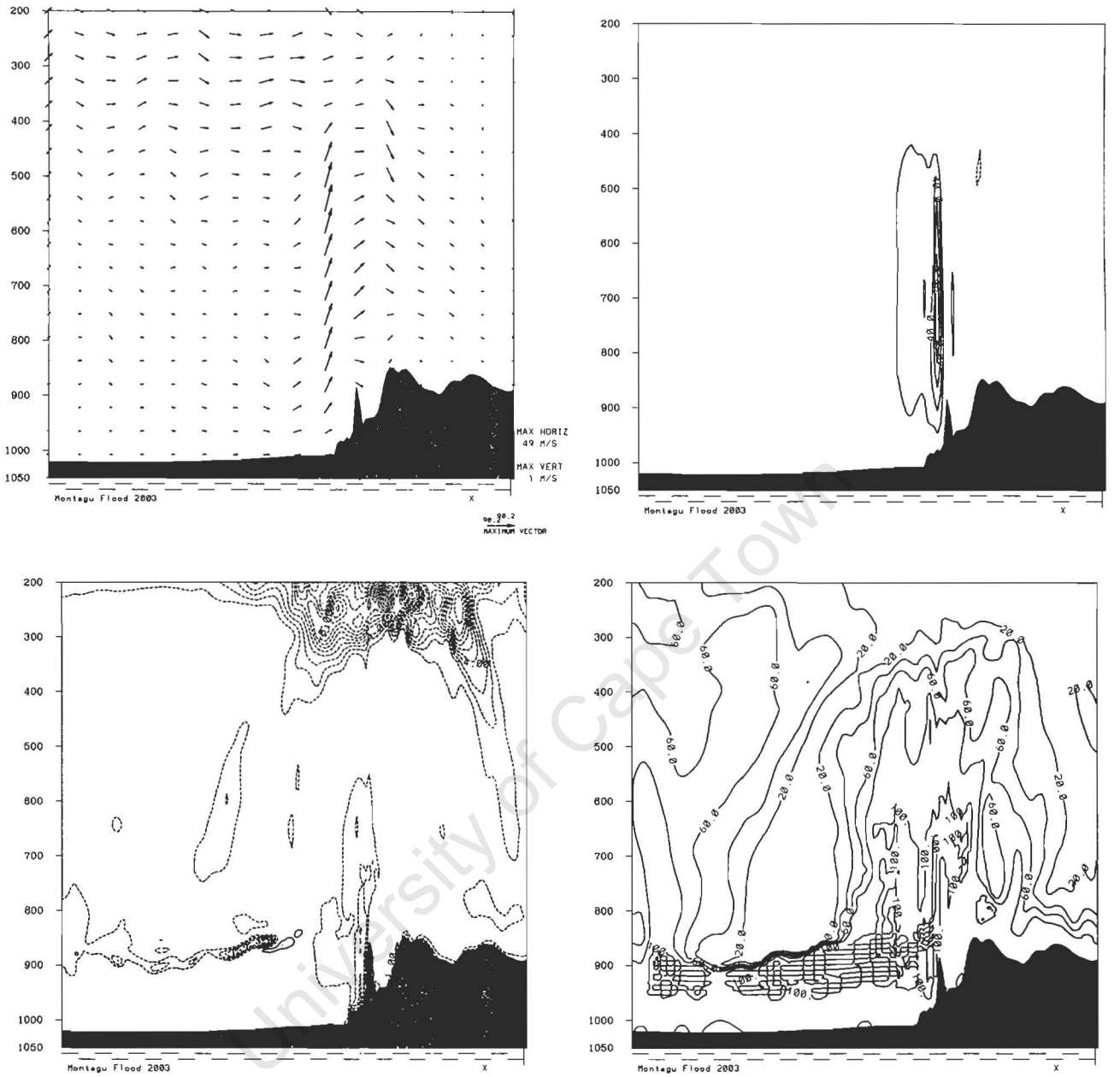

Figure 6.12 - Cross sections AB through from CNTRL at 0000 UTC 16 August 2002. (a) Wind vectors in the plane of the cross-section; (b) vertical velocity (contour interval 20 cm.s $^{-1}$); (c) potential vorticity (contour interval 1 PVU); (d) relative humidity (contour interval 20%).

University of Cape Town

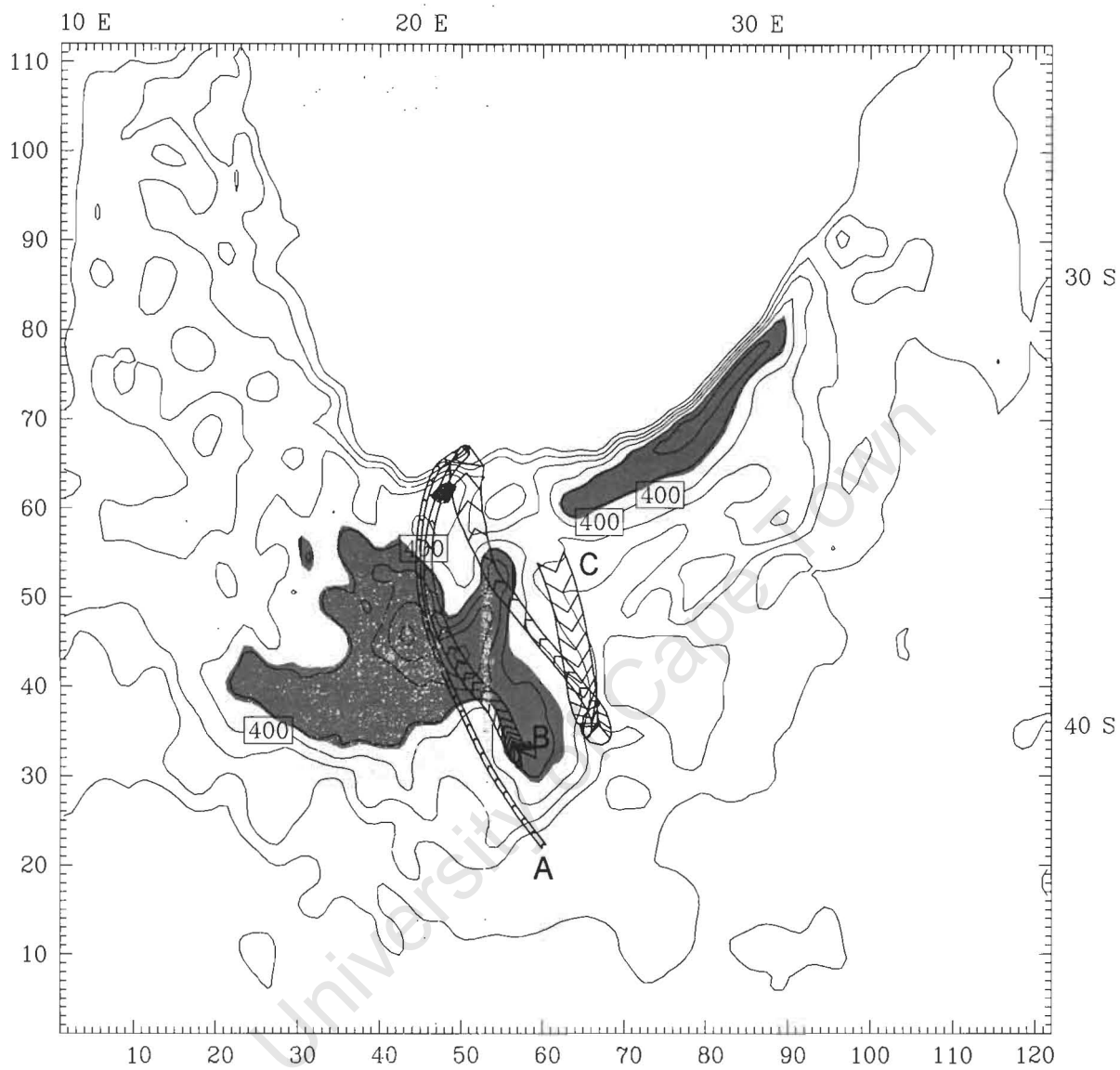

Figure 6.13- Backward trajectories from the MM5 simulation of the Montagu casefor air parcels arriving at A, the surface; B, 850-; and C, 500 hPa. The release time of the trajectories is 0400 UTC 24 March 2003. Contours show the surface latent heat flux at an interval of 100 W.m^{-2} and shading > 400 W.m^{-2}. Trajectory width is proportional to the height of the air parcel (wider = higher).

University of Cape Town

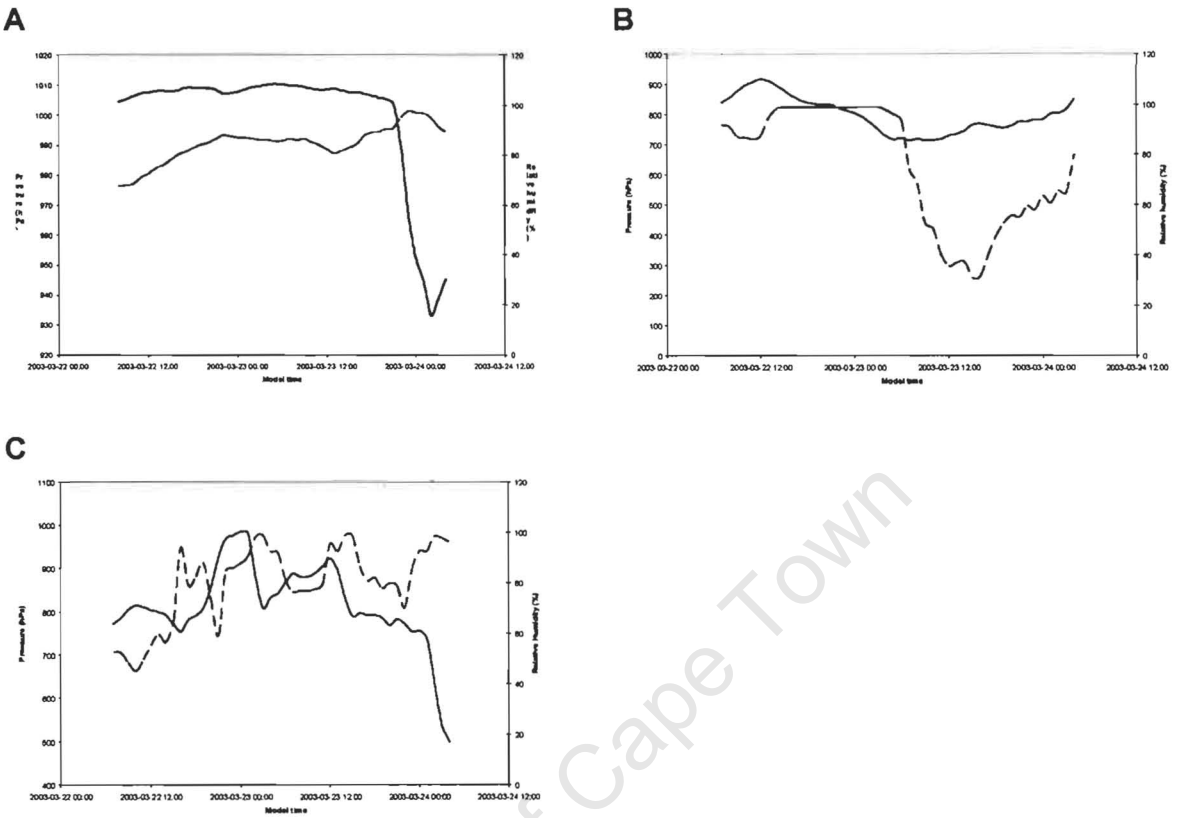

Figure 6.14 – Backward trajectory diagnostics for the trajectories shown in Fig. 6.11. The panels are labelled for trajectories A, B and C. Solid line is pressure (hPa) and the dashed line is relative humidity (%).

University of Cape Town

Chapter 7

Sensitivity studies and factor separation

University of Cape Town

University of Cape Town

7.1. Introduction

In the previous chapter, the processes contributing to the extreme precipitation totals of the cut-off low case studies considered in this thesis were identified. It was found that at the leading and right-hand edges of an onshore LLJ, there was ascent of moist air in convectively unstable stratification. At the leading edge, the topography further promoted the ascent where the LLJ impinged on it. On the right-hand side of the LLJ, convection occurred due to a mesoscale front between warm moist air originating from tropical latitudes and cool maritime air from higher latitudes to the south of South Africa. It was hypothesised that the warm low-level flow from the east was contributed to by the presence of the warm SST of the Agulhas Current.

In this chapter, sensitivity studies are undertaken in order to quantify the influences of topography, SST and surface heat fluxes on these weather events. Two suites of experiments were carried out for each case study. The first suite of experiments individually considers the effects of the mesoscale structure of the SST distribution, the presence of the Agulhas Current, the entire topography of South Africa, the topography where the LLJ impinges on the coast, and the surface heat fluxes. This was achieved by conducting the same simulations as discussed in the previous two chapters, but with one of the above factors removed. The second suite of experiments considers not only the individual contributions, but also the interactions between surface heat fluxes and the topography of South Africa. This was done using the factor separation method of Stein and Alpert (1993) described in Chapter 3.

The results of these experiments should not only help to quantify the contribution of particular factors (and / or their interactions with other factors) to these extreme

University of Cape Town

precipitation events, but may also help to identify possible reasons for the deficiencies in the model simulations described in chapter 5.

This chapter is divided into three main sections following this introduction. In section 7.2, the individual sensitivity studies are discussed for each of the case studies. Section 7.3 includes the factor separation experiments for both of the case studies. The findings of this chapter are summarised in section 7.4.

7.2. Sensitivity studies

A brief description of the sensitivity studies follows. Note that the full physics simulations described in chapters 5 and 6 represent the control experiments and shall hereafter be referred to as CNTRL. Two experiments were constructed to investigate the effects of SST on these events. In the first experiment, SST from the Optimal Interpolation Sea Surface Temperature (OISST) dataset, which has a resolution of 1° x 1° was used. This represents an approximately fivefold decrease in SST resolution compared to the full physics experiments of the previous two chapters, resulting in a loss of mesoscale detail in the SST distribution. In particular the steep gradients on the inshore side of the Agulhas Current, between its core and coastal upwelling, are reduced. This experiment is referred to as LRSST.

In the second SST experiment, the warm core of the Agulhas Current was removed by setting the SST within the current to a constant value, subjectively chosen as the contour that best represents the outer border of the Agulhas Current. This leads to reductions in the SST of up to 5°C over the warmest part of the Agulhas Current. This experiment is referred to as NOAGL.

University of Cape Town

Two sensitivity experiments were undertaken to investigate the role played by topography in the model for this event. In the first of the topography experiments, the height of the topography near to the coast was reduced prior to initialisation, by defining the topography as $h[exp\{[(x - x_0)^2 + (y - y_0)^2]/r_0\} - 1]$, where h is the topographic height in CNTRL, and x_0 and y_0 are the co-ordinates of the centre of the Gaussian. This Gaussian was chosen to be centred at approximately the location at which the LLJ impinged on the coast in CNTRL. The radius of influence, r_0, was chosen to be 500 km. In this way, part of the topography near to the coast is reduced without introducing any artificial steep gradients. This experiment is referred to as NOCOAST.

In the second topography experiment, the entire topography within the model grid was set to zero prior to initialisation. In this way, the pre-conditioning of the atmosphere due to the topography can be investigated. While there will be some signature of the topography in the initial and boundary conditions, it was considered that the initialisation times of the experiments were sufficiently earlier than the times of interest for the model simulation sufficiently to adjust to the lack of topography. The experiment with zero topography is referred to as NOTOP.

In the final sensitivity experiment, the effects of surface heat fluxes were considered. This is a sensitivity test built into the MM5 code, and is done by setting the surface heat fluxes to zero in the boundary layer parameterisation scheme. This experiment is referred to as NOFLX.

University of Cape Town

7.2.1. The East London case

In this case, the effects of the surface parameters were investigated at the reference time, 0000 UTC 16 August 2002, used in Chapter 6. Precipitation is for the 24-hour period to 0600 UTC 16 August 2002. For comparison of these sensitivity experiments with the CNTRL experiment, see the corresponding plots in Fig. 5.16a, for rainfall; Fig. 6.1, for the large scale flow; and Fig. 6.2, for the low-level diagnostics.

7.2.1.1. The effect of mesoscale SST patterns

The difference between the SST in LRSST and the 18km resolution NAVOCEANO SST in CNTRL is shown in Fig. 7.1a. LRSST does not include the cold upwelling south of Port Elizabeth seen in CNTRL and the core of the Agulhas Current is up to 2 K cooler. Furthermore, the upwelling near the Agulhas Bank is up to 1.5K weaker.

The precipitation pattern from the LRSST experiment (Fig. 7.2a) was broadly similar to that from CNTRL. The main differences are that the main precipitation maximum was further to the southeast of the coast in LRSST and was considerably less at 143 mm, with less inland penetration of rainfall. Farther to the west, between 23°–25°E, the precipitation was increased in LRSST and penetrated further inland (Fig. 7.2c). These differences in the precipitation pattern are reflected in the large scale flow for LRSST (Fig. 7.2b), with the meso-beta scale low pressure system being situated approximately 1° to the east, and smaller in its spatial extent, compared with CNTRL. As a result, the LLJ was located a similar distance to the east, with less inland penetration of the onshore flow. Farther to the west, where the rainfall was greater in LRSST, there was little appreciable difference in the large scale flow (Fig. 7.2d)

University of Cape Town

The low-level water vapour flux convergence at the leading edge of the LLJ in LRSST (Fig. 7.3a,g) was much weaker than in CNTRL at this time, with its maximum slightly to the south of the coast. However, the area of maximum convective instability in LRSST (Fig. 7.3b,h) was located closer to the coast than in CNTRL. This occurred because the tongue of warm air, which was considerably narrower and up to 2K cooler in LRSST (Fig. 7.3c,i), was closer to the land and farther to the east compared with CNTRL, due to the cooler SST in LRSST in this region. Additionally, the tongue of high θ_e air (Fig. 7.3d) and the associated high mixing ratio (Fig. 7.3e) was similarly located farther to the east in LRSST compared with CNTRL, and was cooler and less moist (Fig. 7.3j,k). As a result of the cooler SST, surface latent heat fluxes in this region (400 – 500 $W.m^{-2}$) were also as much as 250 $W.m^{-2}$ lower in LRSST (Fig. 7.3f,l) compared with CNTRL.

It therefore seems that the mesoscale structure of the SST to the south of the Eastern Cape coast, where there are large differences between the high resolution NAVOCEANO and the lower resolution OISST datasets, is important in determining the location of the LLJ. The warmer core of the Agulhas Current seen in the NAVOCEANO SST field extends farther to the west compared with the corresponding OISST SST field. However, the cooler SST to the south of Port Elizabeth in the CNTRL experiment appears to have had less impact on the event in this region. However, this may account for the smaller amount of precipitation simulated in CNTRL between 23°E – 25°E compared to LRSST.

University of Cape Town

7.2.1.2. The effect of the Agulhas Current

In the NOAGL experiment, the warm Agulhas Current present in the NAVOCEANO data used in CNTRL was removed by setting SST > 291 K south of 33°S and north of 38°S to 291 K. Some linear smoothing of the SST north of 33°S was applied to prevent unrealistic temperature gradients. This resulted in the SST anomaly shown in Fig. 7.1b, with a cold anomaly of up to 4K over the core of the Agulhas Current. In this experiment, the quantity of precipitation simulated (Fig. 7.4a,c) differed greatly from the CNTRL experiment (Fig. 5.16a), especially near to the coast, where only around 20 mm was simulated in NOAGL. However, the broad spatial extent of the precipitation field was similar in NOAGL and CNTRL. Correspondingly, the large scale flow at the reference time (0000 UTC 16 August) was characterised by much weaker onshore flow, with the LLJ not reaching the coast (Fig. 7.4b,d). Furthermore, there was no evidence of the meso-beta scale low in NOAGL (Fig. 7.4b) and thus the pressure gradient forcing near to the coast was much weaker.

University of Cape Town

As in CNTRL, areas of low-level water vapour flux convergence in NOAGL were associated with the cyclonic and leading edges of the LLJ (Fig. 7.5a). Since the LLJ did not impinge on the coast in NOAGL, the moist ascent there was removed (Fig. 7.5a,g). However, a larger portion of the ocean to the south of the Eastern Cape displayed convective instability in NOAGL (Fig. 7.5b,h), albeit slightly weaker than in CNTRL. The cooler SST in NOAGL led to the low-level temperature (Fig. 7.5c) being cooler than in CNTRL (Fig. 6.2c,i), with no evidence of a warm tongue. There was some evidence of a tongue of relatively high θ_e air in NOAGL (Fig. 7.5d), which appeared to be approximately co-located with the LLJ in this experiment (Fig. 7.5a). However, the maximum temperature of 310 K was 6K cooler than this high θ_e tongue

in CNTRL (Fig. 7.5j). This high θ_e tongue in NOAGL did not, however, appear to be reflected in a tongue of low-level moisture (Fig. 7.5e,k). As a result of the cooler SST, the surface latent heat flux in NOAGL (Fig. 7.5f,l) was much less than that simulated in CNTRL, suggesting less evaporation from the ocean and reduced low-level moisture supplied to the system.

The significantly reduced quantity of rainfall generated in NOAGL was due to the LLJ not impinging on the coast. The much cooler air at low-levels did not provide sufficient heating of the boundary layer for the formation of the meso-beta scale low; this factor combined with the lower latent heat flux not adding sufficient low-level moisture to the evolving weather system meant that the conditions for deep moist convection to occur were not satisfied.

7.2.1.3. The effect of coastal topography

In NOCOAST, there was little generation of precipitation around the coastline where the topography was reduced (Fig. 7.6a,c). The removal of the coastal topography led to a complex response of the flow in this region, probably due to the introduction of unrealistic topographic gradients. The meso-beta scale low associated with the LLJ was situated over the ocean centred at approximately 35°S, 29°E with the onshore portion of the LLJ on its western side, while a second meso-beta scale low was generated over the land centred near 33.5°S, 25°E (Fig. 7.6b,d). This led to a secondary onshore LLJ, which impinged on the coast at 34°S, 23.5°E, where there was some low-level water vapour flux convergence, and the moist ascent associated with the topography in CNTRL was reduced to zero (Fig. 7.7a,g). Associated with the second mesoscale low and LLJ was an area of convectively unstable stratification

University of Cape Town

(Fig. 7.7b,h) penetrating onto the land. The low-level potential temperature had a narrow tongue of warm air extending westwards over the ocean south of Port Elizabeth and a warm pool extending onto the land in the vicinity of the secondary LLJ (Fig. 7.7c,i). There was a more noticeable tongue of high θ_e air (Fig. 7.7d,j) and low-level moisture (Fig. 7.7e,k) here as the secondary LLJ advected warm moist air onto the land. In response to the secondary LLJ, surface latent heat flux was increased by up to 150 $W.m^{-2}$ next to the coast between 22°-25°E (Fig. 7.7f,l)

It is difficult to draw any concrete conclusions from the NOCOAST experiment since a secondary meso-beta scale low and LLJ formed as a result of the unrealistic topographic gradients in this experiment. However, one may tentatively suggest that that the coastal topography here had an influence in the location of the LLJ as it trapped the meso-beta scale low in its position over the coast in CNTRL.

7.2.1.4. The effect of South African topography

In the NOTOP experiment, the precipitation pattern over the ocean was spatially similar to that in CNTRL, but shifted to the west (Fig. 7.8a,c). However, towards the coast, there was no major peak in the simulated precipitation, which in this case was concentrated between 22°–25°E, with a maximum around 23.5°E. The large scale flow was characterised by the LLJ covering a much larger spatial area extending all the way up western South Africa towards Namibia (Fig. 7.8b,d). The meso-beta scale low was located over the land and to the west compared with CNTRL, as a result of the low-level trough which was located off the east coast of South Africa in CNTRL being situated over the whole of eastern South Africa in NOTOP. This would suggest that the 2.5 km – 3 km high topography of the Drakensberg and Maloti mountain

University of Cape Town

ranges over eastern South Africa and Lesotho was responsible for maintaining the position of this trough off the east coast of South Africa, and thus having an influence on the location of the meso-beta scale low and the LLJ.

The low-level water vapour flux convergence in NOTOP was clearly associated with the cyclonic circulation of the meso-beta scale low converging with the onshore flow of the LLJ just to the south of Port Elizabeth (Fig. 7.9a). At the coast, the topographic ascent in CNTRL was reduced to zero in NOTOP (Fig. 7.9g). Convectively unstable stratification was mostly concentrated over the ocean (Fig. 7.9b) slightly to the south of the main area of convective instability in CNTRL. In addition, the stratification over land became more stable west of 25°E (Fig. 7.9h). Although warm moist air was apparent at low-levels in NOTOP (Figs. 7.9c-e,i-k), it did not form into a narrow tongue penetrating onto the coast as seen in CNTRL (Figs. 6.2c-e), and a wide tongue of moist air, not seen in CNTRL, extended over the land from the north in NOTOP (Figs. 7.9d,e,j,k). The maximum surface latent heat flux in NOTOP (Fig. 7.9f) was as high (500 – 600 $W.m^{-2}$) as in CNTRL, but was located to the west in NOTOP (Fig. 7.9l) and appeared to be mostly associated with the high wind speeds of the LLJ.

University of Cape Town

7.2.1.5. The effect of surface heat fluxes

With the surface heat fluxes switched off, the NOFLX experiment resulted in very little precipitation over the entire model grid (Fig. 7.10a,c) for the 24-hour period to 0600 UTC 16 August. The large scale flow was characterised by a broadening of the ridge over the ocean to the south of South Africa, and there was little evidence of the surface trough extending down the eastern seaboard of South Africa (Fig. 7.10b,d).

As a result, there was no formation of an onshore LLJ due to the absence of a sufficient pressure gradient.

The non-formation of the LLJ in the NOFLX experimented resulted in a lack of a forcing mechanism for the ascent of moist air over the ocean to the south of the Eastern Cape (Fig. 7.11a,g). Additionally, the fact that in this experiment, the surface ridge pushed farther to the north than in CNTRL, and the easterly trough did not extend to the south meant that the stratification remained stable over the region (Fig. 7.11b,h), as there was not sufficient warming of the lower atmosphere. In fact, a cold pool existed over the ocean to the southeast of the Eastern Cape in NOFLX (Fig. 7.11c,i). There was also very little moisture in the lower atmosphere (Fig. 7.11d,e,j,k), meaning that none of the ingredients required for deep moist convection to occur were present in the absence of surface heat fluxes (Fig. 7.11f,l).

7.2.1.6. Summary

Therefore, the fluxes of heat from the ocean surface were vital in generating an environment conducive to the extreme rainfall observed. They were responsible for the advection of warm moist tropical air down the eastern seaboard of South Africa through the extension of a surface trough to the south. Additionally, the extension of this surface trough was important in providing the necessary pressure gradient forcing for the formation of the LLJ, which has been shown in Chapter 6 to have made a key contribution to the rainfall observed during this cut-off low event. In addition, the SST distribution, and in particular the warm core of the Agulhas Current, were important, not only in providing low-level moisture, but also in developing the low-level circulation that led to the location of the extreme rainfall. The topography of

University of Cape Town

South Africa has also been shown to be responsible for enhancing moist ascent and influencing the low-level circulation pattern.

7.2.2. The Montagu case

For this event, the results of the sensitivity experiments are presented for the reference time, 0400 UTC 24 March 2003, used in Chapter 6. Precipitation is for the 24-hour period to 0600 UTC 24 March 2003. For comparison of these sensitivity experiments with the CNTRL experiment, see the corresponding plots in Fig. 5.20, for rainfall; Fig. 6.7, for the large scale flow; and Fig. 6.8, for the low-level diagnostics.

7.2.2.1. The effect of mesoscale SST patterns

The difference between the SST forcing used in the LRSST experiment and the CNTRL experiment for the Montagu case study is shown in Fig. 7.12a. LRSST does not capture the high temperature of the warm core of the Agulhas Current, being cooler by up to 4K near 24°E, 36°S. Additionally, the upwelling over the Agulhas bank to the south of the Western Cape around 21°E, 36°S is not fully represented in LRSST and is 1.5K warmer. Inshore of this, LRSST is cooler than the SST in CNTRL by 1K. Small coastal areas near Port Elizabeth, and on the west coast near Cape Town are also warmer since coastal upwelling is not well represented in LRSST.

University of Cape Town

The response of the precipitation to the lower resolution SST pattern in LRSST is shown in Fig. 7.13a. The inland structure of the rainfall was similar in LRSST compared to CNTRL (Fig. 5.16a), but the rainfall at the coast was reduced by approximately 20mm in LRSST, and a second band was generated slightly to the east. This reduced coastal rainfall was probably due to the slightly cooler SST next to

the coast in this experiment. Over the ocean, the precipitation became a narrower zonal band approximately co-located with the area where there was little difference between the LRSST SST and the CNTRL SST in Fig. 7.12a. There appeared to be very little difference in the large scale flow between LRSST (Fig. 7.13b), other than an increase in the onshore flow near to the second rainfall band and a slightly less deep surface depression (Fig. 7.13d)

There was an eastward shift in the band of moist ascent in LRSST (Fig. 7.13a,g) and stratification became more stable over the Western Cape (Fig. 7.13b,h). The more stable stratification was a result of the tongue of warm air extending towards the coast being up to 2K cooler and not penetrating onto the land in LRSST (Fig. 7.13c,i). Additionally, the maximum θ_e over land was 2-4K cooler in LRSST than in CNTRL (Fig. 7.14d,j), and the low-level moisture did not extend so far onto the land (Fig. 7.14e,k). This slight difference in the degree of penetration of the warm moist tongue onto the land probably explains the slightly reduced precipitation there through less low-level moisture availability. Furthermore, the structure of the latent heat flux in LRSST was not as complex as in CNTRL (Fig. 7.14f). Additionally, the maximum latent heat flux in LRSST was 200 $W.m^{-2}$ less than the mesoscale maxima in CNTRL (Fig. 7.14f,l)

In this case, the reduction in resolution of the SST field only had a small effect on the model simulation. However, there was some difference in the quantity of the coastal precipitation simulated, and the structure of the precipitation over the ocean was altered as a result of reduced temperature and moisture at low-levels.

University of Cape Town

7.2.2.2. The effect of the Agulhas Current

In the NOAGL experiment, the Agulhas Current was removed by setting SST>294K to 294K south of 33°S. This had the effect of reducing the SST of the Agulhas Current by 4K (Fig. 7.12b). The response of the precipitation was similar to that from the LRSST experiment, with a less narrow band penetrating onto the land in NOAGL (Fig. 7.15a) in comparison to CNTRL. Additionally, the coastal precipitation was approximately 20mm less and precipitation maxima over the ocean were reduced (Fig. 7.15a,c). There was little difference in the low-level large scale flow between NOAGL and CNTRL, apart from a less deep surface depression in NOAGL with a central geopotential height of 720m (Fig. 7.15b), 30m higher than in CNTRL Fig. 7.15d).

The ascent of moist air at the leading edge of the LLJ in NOAGL (Fig. 7.16a) was weaker than in CNTRL, and was shifted to the east (Fig. 7.16g). The stratification was less convectively unstable near the coast, but stability was reduced further inland (Fig. 7.16b,h). The tongue of warm air extending northwards onto the coast in CNTRL was similar, but slightly cooler and wider in NOAGL (Fig. 7.16c,i), and there was no θ_e maximum at the coast (Fig. 7.16d,j). Furthermore θ_e was increased over the west coastal regions of South Africa, which was responsible for less stable stratification there. Similar to the tongue of warm air, the band of moisture penetrating onto the land was not so narrow, with a slightly increased mixing ratio in NOAGL (Fig. 7.16e,k). The cooler SST of NOAGL resulted in a greatly reduced latent heat flux over the Agulhas Current, and an increase over the Agulhas Bank, presumably as a result of the less steep SST gradient between the coastal upwelling and the region of the Agulhas Current.

University of Cape Town

The effects of removing the Agulhas Current were therefore fairly small in this case, as there was only a small difference in the precipitation compared with CNTRL, and small differences in the advection of warm moist air from the east, suggesting that in this case the warm SST of the Agulhas Current was not so influential for coastal rainfall as in the East London case.

7.2.2.3. The effect of coastal topography

With the coastal topography removed in the NOCOAST experiment, the maximum precipitation over the coastal region of the Western Cape was reduced to 40mm. (Fig. 7.17a,c). There appeared to also be some effect on the precipitation upstream of the coast as the spatial structure of the precipitation maxima was slightly altered compared to CNTRL. The surface depression over the coast was located in the same area in NOCOAST (Fig. 7.17b) as in CNTRL, with a slight deepening (Fig. 7.17d). On the western flank of the depression, the LLJ extended much further inland in NOCOAST.

The reduced rainfall over the coast in the NOCOAST experiment can be attributed to reduced ascent of moist air, as indicated by the greatly reduced low-level water vapour flux convergence there (Fig. 7.18a,g). However, the band of moist ascent in NOCOAST penetrated further inland in association with the LLJ, before being deflected to the east. The stratification (Fig. 7.18b) was broadly similar to that in CNTRL, except that the convectively unstable zone over the coastal region of the Western Cape at around 23°E, 34°S in CNTRL was not simulated in NOCOAST. The low-level temperature was also broadly similar in NOCOAST (Fig. 7.18c) to that in CNTRL, except that the gradient over the ocean just off the coast between 23°-28°E

University of Cape Town

was not as steep in NOCOAST as the low-level temperature was cooler there (Fig. 7.18i). Furthermore, in NOCOAST, the tongue of moisture extended farther onto the land in a northeastward direction (Fig. 7.18d,e,j,k), but the θ_e maximum near 23°E, 34°S, which was responsible for the convective instability there was not simulated in NOCOAST. The spatial structure of the latent heat flux was very similar in NOCOAST (Fig. 7.18f) to that in CNTRL, although upstream of the reduced topography there was a 50-100 $W.m^{-2}$ reduction in the latent heat flux.

The above suggests that the influence of the coastal topography was substantial in the generation of coastal rainfall in this event. Moist ascent in the coastal region was greatly reduced by removing the topography there. In addition, the topography near to the coast appeared to be responsible for some blocking of the onshore flow, deflecting it to the east.

7.2.2.4. The effect of South African topography

The effect of removing the topography from the simulation prior to initialisation of the model on the precipitation is shown in Fig. 7.19a. The overall spatial structure of the 24-hour precipitation was spatially similar to the CNTRL simulation. However, the coastal rainfall was greatly affected in the NOTOP experiment. Here, there were two coastal maxima of order 40mm, compared to around 80mm in CNTRL, with the second coastal maximum to the west of that in CNTRL (Fig. 7.19c). This suggests that the coastal topography played an important role in generating the large quantity of precipitation observed there.

University of Cape Town

The large scale flow was greatly affected over the south coast of South Africa in NOTOP (Fig. 7.19b). The spatial extent of the surface depression was greatly increased and the strong onshore flow of the LLJ extended much further inland (Fig. 7.19d). This confirms that there was some degree of blocking of the flow by the topography in CNTRL. Additionally, the surface depression that was over the ocean to the southeast of South Africa around 32°E, 37°S in CNTRL appeared to be located much further to the west in NOTOP around 25°E, 37°S, suggesting that the high topography of the Drakensberg and Maloti Mountains over the eastern interior of South Africa and Lesotho may have influenced the track of this depression.

The low-level water vapour flux convergence from NOTOP (Fig. 7.20a) shows that moist ascent was reduced greatly over the land by the lack of topography, and over the ocean, upstream of the coast, there was a shift in the band of moist ascent (Fig. 7.20g). The convective instability was stronger towards the coast near 21°E, 35°S in NOTOP (Fig. 7.20b) than in CNTRL, but more stable near 23°E, 34°S, probably as a result of the warm moist tongue penetrating onto the land slightly to the west (Fig. 7.20c-e,i-k). The moisture extended farther inland in NOTOP (Fig. 7.20d,e,j,k), suggesting that this moisture was being advected onto the land by the LLJ and deflected to the right by the topography in CNTRL. The spatial structure of the surface latent heat flux was very similar in NOTOP (Fig. 7.20f) compared with CNTRL, but there was a 50-250 $W.m^{-2}$ decrease upstream of the coast, and an increase over the ocean to the west of South Africa (Fig. 7.20l) as wind speeds were increased there (Fig. 7.19d).

University of Cape Town

The NOTOP experiment therefore suggests that the topography of South Africa played a part in both promoting ascent near the coast and in blocking the onshore flow. Despite the large Fr (3.77) in CNTRL, it is clear that the topography was responsible for deflecting the onshore flow to the right, consistent with Baines (1979) who suggested that there is some degree of topographic blocking for flows with Fr<5. In addition, the high value of Ro (11.8) suggests that strong Coriolis deflection may have contributed to the blocking of the flow here. Indeed the Burger number, B=3.1, in this case suggests that rotational effects dominated the stratification in response to the flow impinging on the topography.

7.2.2.5. The effect of surface heat fluxes

In the NOFLX experiment, only a small amount of precipitation was generated over the ocean, with none over the land (Fig. 7.21a,c). The surface depression was located much further to the east in NOFLX near 30°E, 36°S (Fig. 7.21b) and was not as deep compared to CNTRL (Fig. 7.21d). Moreover, there was only one surface depression compared to the two simulated in CNTRL. At 500 hPa (not shown), the cut-off low was situated far to the southeast of its position in CNTRL, indicating that the surface depression in NOFLX was a downward extension of the cyclone in the upper air. Surface heat fluxes appeared to have little effect on the ridge that extended to the east at 45°S in CNTRL.

As a result of the very different flow over the ocean south of South Africa in NOFLX, there were no mechanisms forcing the ascent of moist air (Fig. 7.22a,g), and the stratification was more stable (Fig. 7.22b,h). Indeed, the south coastal region of the Western Cape was characterised by a cold pool (Fig. 7.22c,i), probably due to the

University of Cape Town

southerly flow into this region originating at relatively high latitudes (Fig. 7.21b).. Not only was the air over the Western Cape and the adjoining ocean much cooler than in CNTRL, it was also considerably drier (Fig. 7.22d,e,j,k), due to a lack of both moisture advection from the east and evaporation from the ocean (Fig. 7.22f,l).

The results of the NOFLX experiment suggest that surface heat fluxes were responsible for the position of the surface depression in this event. As a result they also had an important influence on the formation of the LLJ by providing the pressure gradient forcing. Additionally, the surface heat fluxes were likely responsible for adding low-level moisture to the system.

7.2.2.6. Summary

In the Montagu case, the sensitivity studies have shown that topography and surface heat fluxes both had a strong influence on the development of the surface flow in this event. The surface heat fluxes helped the pressure gradient to develop and led to the formation of the strong onshore low-level jet, and the topography blocked the onshore flow and provided additional forcing for the ascent of moist air. However, unlike the East London case, SST appeared to not be as important for coastal rainfall. This is likely due to the large area of cooler SST of the Agulhas Bank south of the Western Cape coast.

University of Cape Town

7.3. Factor separation experiments

In this section, further quantitative illustration of the *individual* and *synergistic* contributions of the topography of South Africa and surface heat fluxes are presented. These two factors were chosen since the sensitivity studies showed that

they both played a significant role in generating convection of the coastal areas of intense precipitation. SST effects were excluded from the factor separation study since, by definition, they contribute to the surface heat fluxes. Additionally, the effect of coastal topography was not included because the artificial topographical gradients induced spurious effects.

The factor separation technique (Stein and Alpert 1993) is described in detail for experiments with *n* factors in Chapter 3. Here, the objective is to determine the individual and combined effects of two factors; namely, topography and surface heat fluxes. Therefore, a total of four simulations are required: f_0, in which both topography and surface heat fluxes are removed; f_1, with surface heat fluxes set to zero and full topography; f_2, with zero topography and full surface heat fluxes; and f_{12}, with full topography and full surface heat fluxes. f_{12} represents the CNTRL simulation, so for each case study, three further simulations were required.

University of Cape Town

The results of the four simulations were then combined algebraically following the technique described in Chapter 3 to give the desired contributions:

- effect of topography, $f_1^* = f_1 - f_0$
- effect of surface heat fluxes, $f_2^* = f_2 - f_0$
- combined effect of topography and surface heat fluxes, $f_{12}^* = f_{12} - (f_1 + f_2) + f_0$.

For an evaluation of the individual factors, one must first consider the simulation with all of the factors under investigation removed, f_0, which provides a reference state.

The interpretation of the combined factors is, however, more complex and requires comparison with the state in all of the other experiments.

7.3.1. The East London case

In the reference simulation, f_0, very little precipitation was generated, with only a small area of rain over the KwaZulu Natal coast (Fig. 7.23a). The low-level flow was dominated by a ridge of high pressure near the surface (7.23b) giving rise to southeasterly winds onto the coast of South Africa. The stratification was entirely stable throughout the domain.

The addition of topography to the reference state, f_1*, had the effect of suppressing the small amount of rainfall that was generated over the KwaZulu Natal coast (Fig. 7.24a). High pressure was generated over the eastern coastal region of South Africa and the adjoining ocean (Fig. 7.24b). Accordingly, the onshore flow was reduced over the coastal regions. The high pressure anomaly appeared to be confined to the coastal side of the high topography of the interior plateau of South Africa, suggesting that this topography had the effect of 'steering' the ridge along the south coast, and up the east coast of South Africa. In addition the stability was reduced over much of South Africa, particularly inland of the high pressure anomaly.

The effect of the surface heat fluxes, regardless of the topography, f_2*, is shown in Fig. 7.25. A band of precipitation with a northwest-southeast orientation was generated off the south coast of South Africa (Fig. 7.25a). This precipitation pattern is similar to that generated in the CNTRL experiment (Fig. 5.16a), except that the main

University of Cape Town

band of rainfall is to the west of that in CNTRL, suggesting that surface heat fluxes played a very important role in generating the precipitation in this case.

The influence of the surface heat fluxes on the low-level flow was to reduce pressure over much of the model domain, centred around 24°E, 34°S (Fig. 7.25b). This led to a strengthening of the onshore flow to the west of 24°E, and offshore flow to the east. In addition, the stability of the atmosphere was reduced over much of the model domain. This suggests that surface heat fluxes were an important contributor to the southwestward advancement of the surface trough down the eastern seaboard of South Africa.

The combined influence of topography and surface heat fluxes, f_{12}*, shown in Fig. 7.26, led to a rather complex response. In terms of the rainfall, it seems that the combined influence was to shift the precipitation generated by the surface heat fluxes to the east, as well as increasing the quantity, leading to the precipitation maximum seen in CNTRL at 26°E, 34°S (Fig. 7.26a).

In addition, the synergistic effects of the topography and surface heat fluxes appear to have been responsible for the generation of the onshore LLJ, as shown by the narrow band of high wind speed vectors penetrating onto the coast around 26.5°E, 34°S. The reason for this was the pressure gradient generated by a 20m increase in 925 hPa geopotential height to the west of 26°E, and a slightly weaker reduction to the east. Furthermore there was increased flow of warm moist tropical air down the eastern seaboard of South Africa. As a result, the stratification became more convectively unstable in this area.

University of Cape Town

This factor separation study suggests that surface heat fluxes were responsible for producing a large proportion of the rainfall for this event through the generation of convective instability, while their interaction with topography was responsible for the location and enhancement of precipitation due to the creation of a LLJ.

7.3.2. The Montagu case

Consider first the reference state, f_0, for this case at 0400 UTC 24 March, shown in Fig. 7.27. The near surface flow was characterised by a spatially large depression centred over the south coast of South Africa. Strong cyclonic flow existed around the perimeter of the depression, with strong southerly flow over the ocean to the south of the Western Cape which extended well onto the southern African landmass. The land area was entirely within stable stratification, as was the ocean west of 25°E and polewards of 40°S. In addition, there was negligible precipitation in f_0 for the 24-hour period to 0600 UTC 24 March (Fig. 7.27a).

The effect of southern African topography, regardless of surface heat fluxes, f_1*, is shown in Fig. 7.28. The introduction of topography to the reference state had little effect on the rainfall (Fig. 7.28a). However, there was an increase in pressure over much of the area covered by the depression in the reference state (Fig. 7.28b cf Fig. 7.27). Accordingly, the topography weakened the onshore flow over the Western Cape, and led to reduced stability over much of South Africa as the low-level air there did not originate from such high latitudes. Therefore, one can conclude that, acting individually, the topography of South Africa was responsible for blocking the onshore flow and had a considerable upstream influence.

University of Cape Town

Conversely, acting individually, the surface heat fluxes, f_2^* (Fig. 7.29), led to a considerable quantity of precipitation, particularly over the ocean to the south of the Western Cape (Fig. 7.29a). This precipitation pattern is very similar to that from the CNTRL experiment (Fig. 5.20), except that there are two bands of rainfall penetrating onto the coast, very much like in the NOTOP experiment (Fig. 7.19a). This suggests that surface heat fluxes alone were mainly responsible for the rainfall within the synoptic cut-off low environment.

In addition, surface heat fluxes had the effect of decreasing the near surface pressure, particularly over the Western Cape (Fig. 7.29b). The maximum negative contribution was centred over southern South Africa some 200km to the north of the south coast, near 23°E, 32°S. The onshore flow was increased at the Western Cape coast west of 21°E, but decreased to the east of this. These results suggest that the surface depression in the reference state (Fig. 7.27) was located to the northwest on account of the introduction of surface heat fluxes. In addition, as the surface heat fluxes warmed the lower troposphere, the stratification became less stable.

The interaction of topography and surface heat fluxes, f_{12}^*, is shown in Fig. 7.30. The interaction led to an increase in rainfall in a narrow band penetrating onto the Western Cape coast near 22°E, and suppression of rainfall to the west of this (Fig. 7.30a). This suggests that the two coastal bands of rainfall that occured as a result of the surface heat fluxes alone (Fig. 7.29a) combined into a single band. Indeed, by considering the eastern band in Fig. 7.29a in addition to the increased rainfall there in Fig. 7.30a, the band of coastal rainfall is approximately equivalent to that from CNTRL (Fig. 5.20).

University of Cape Town

The response of the low-level atmosphere to the interaction of topography and surface heat fluxes included a reduction in pressure of about the same magnitude as that seen from the contribution of surface fluxes alone (Fig. 7.29b), but centred over the south coast, at approximately the same location as the depression in CNTRL (Fig. 6.7). Accompanying the reduction in sea level pressure was a strong enhancement of the onshore low-level flow and the formation of the LLJ to the south of the Western Cape. The coastal region of the Western Cape also experienced reduced stability as a result of this interaction.

To summarise, the factor separation experiments have shown that the surface heat fluxes were responsible for the generation of the rainfall for this event through the generation of instability and enhanced surface cyclogenesis. The topography, on the other hand, was responsible for modulating the low-level flow through blocking the onshore flow. Therefore, one can conclude that the surface heat fluxes were responsible for generating the rainfall and that the topography was responsible for its location.

University of Cape Town

7.4. Summary

The objective of this chapter was to identify factors which made a contribution to these rainfall events and to analyse the mechanisms through which they made their influence. The sensitivity studies showed that, in the East London case, the SST of the Agulhas Current region of the South West Indian Ocean was very important, both in terms of its mesoscale structure and its warm core. The mesoscale structure was important in that the warm core of the Agulhas Current did not extend so far to the west influencing the position of the mesolow and therefore the LLJ. In addition, the

cold upwelling south of Port Elizabeth was not fully captured in the low resolution SST data and therefore spurious rainfall was generated there. Furthermore, the warm Agulhas Current appeared to be responsible for maintaining the high wind speed of the LLJ through the formation of a meso-beta scale low pressure system near the surface. Without the additional pressure gradient forcing of this meso-beta scale low, the LLJ was not able to penetrate onto the coast, and thus coastal rainfall was greatly reduced. Additionally, the low-level moisture appeared to be related to the warm SST of the Agulhas Current, suggesting that the large fetch of the onshore LLJ over warm water was influential in providing moisture to the system.

On the other hand, in the Montagu case, the SST appeared to be less important. Both the warm core of the Agulhas Current and the mesoscale structure of the SST were responsible for about 20mm of the rainfall simulated at the coast, by providing warm moist air near to the surface. The fact that the region of heavy coastal rainfall in the Montagu case was adjacent to a region of cold SST, due to inshore upwelling, probably reduced the influence of the warm Agulhas Current on the system; whereas in the East London case, the warm SST of the Agulhas Current was adjacent to the coast. This is consistent with the findings of Jury et al. (1993), who found that there was a strong correlation between coastal rainfall and the distance to the warm core of the Agulhas Current, with a shorter distance being associated with increased rainfall. During onshore wind conditions, such as in these cases, they suggest that increased moisture due to high latent heat fluxes from the ocean leads to increased rainfall over land when the distance to the warm SST is short. Indeed, in the Montagu case, the majority of the precipitation was simulated to occur over the ocean near to the region of warm SST. In addition, the NOAGL experiment for the East London case not only

University of Cape Town

confirms the hypothesis of Jury et al. (1993) for onshore wind conditions, it also shows that the Agulhas Current was important in forcing these onshore winds.

In addition, the air-sea temperature difference may have played an important role. The Montagu case was in late summer, when a smaller temperature difference can be expected between the warm SST of the Agulhas Current and the air, and therefore less influential than in the East London case, which was in mid-winter, when a much larger air-sea temperature difference would be expected in this region.

In both cases, topography had a strong influence on the rainfall produced in these cut-off low weather systems. Unfortunately, the unrealistic gradients introduced by removing the coastal topography in the East London case led to a simulation that was difficult to interpret, as phenomena associated with the new gradients were introduced. However, in the Montagu case, the NOCOAST sensitivity test showed that the coastal topography enhanced moist ascent considerably, as well as deflected the onshore flow to the east, confining the moist maritime air to the coastal regions.

University of Cape Town

In addition, the South African topography as a whole was important in determining the location of the mesoscale bands of rainfall in both cases within the synoptic system. The sensitivity tests showed that topography was important for blocking onshore flow, which was confirmed in the factor separation studies. In addition, the factor separation studies showed that the topography was important in determining the location of the dominant ridge over the ocean to the south of South Africa in the

East London case, which played a role in providing the necessary forcing for the onshore LLJ.

Furthermore the factor separation studies indicates that a coherent set of processes led to the rainfall and its location within the environment of a cut-off low aloft, and may be described as follows:

- *Surface heat fluxes add heat and moisture to the lower atmosphere leading to the extension of a trough down the eastern seaboard of South Africa.*
- *As the surface fluxes warm the lower atmosphere, it becomes convectively unstable and considerable precipitation is generated.*
- *The South African topography blocks onshore flow leading to a steep pressure gradient between a ridge over the ocean to the south of South Africa and the aforementioned trough, and thus the formation of a LLJ.*
- *This LLJ advects moist air onto the coast of South Africa where its ascent is enhanced by the coastal topography.*

University of Cape Town

The above therefore presents a conceptual model of the development of the low-level flow that leads to extreme rainfall when there is a cut-off low in the upper atmosphere. This may be of use in forecasting applications for South Africa, since the important factors have been identified. It is therefore essential that forecast models contain a good representation of the South African topography, and the heat fluxes

from the ocean, which requires accurate representation of the mesoscale SST structure in the vicinity of the Agulhas Current System.

University of Cape Town

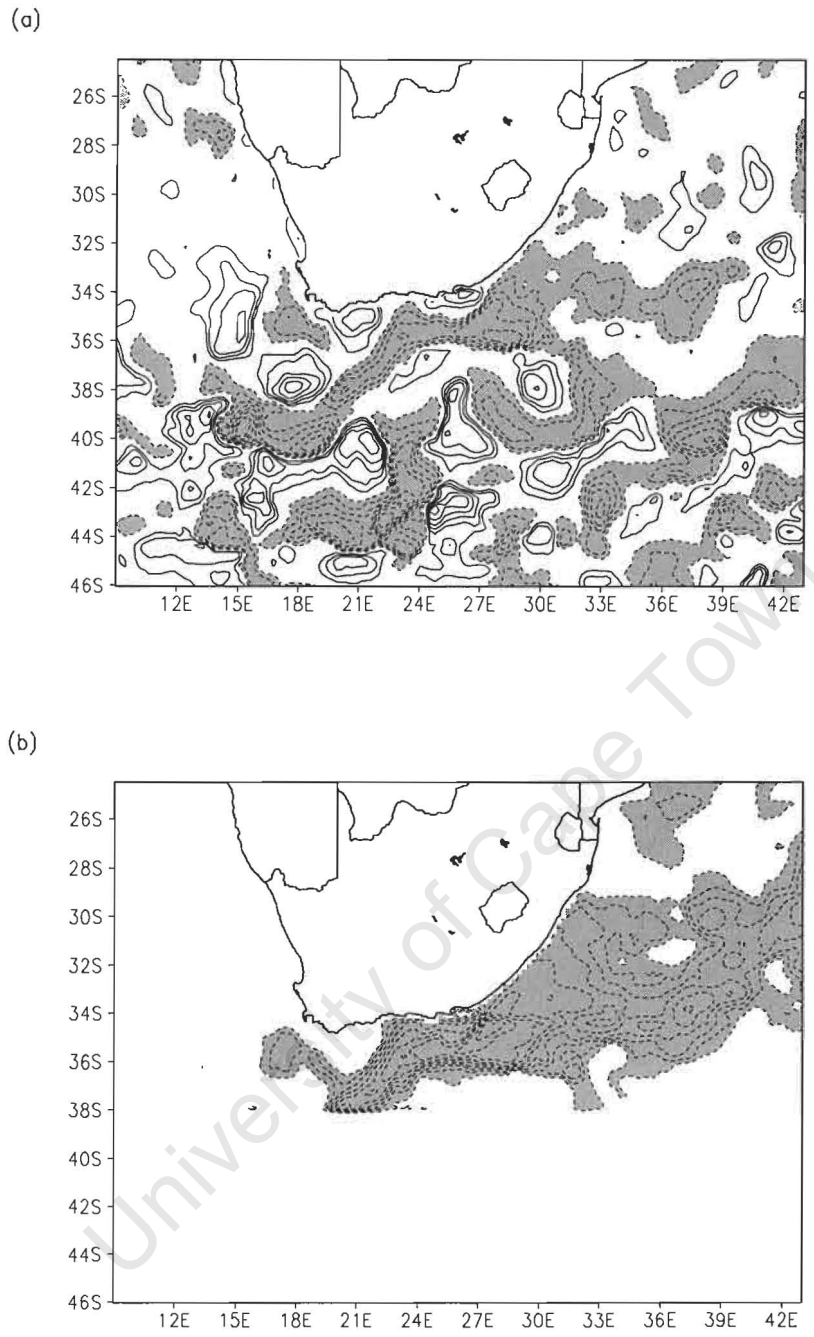

University of Cape Town

Figure 7.1 – SST anomalies from CNTRL for (a) LRSST and (b) NOAGL. Solid (dashed and shading) contours show a warm (cold) anomaly. Contour interval is 0.5K.

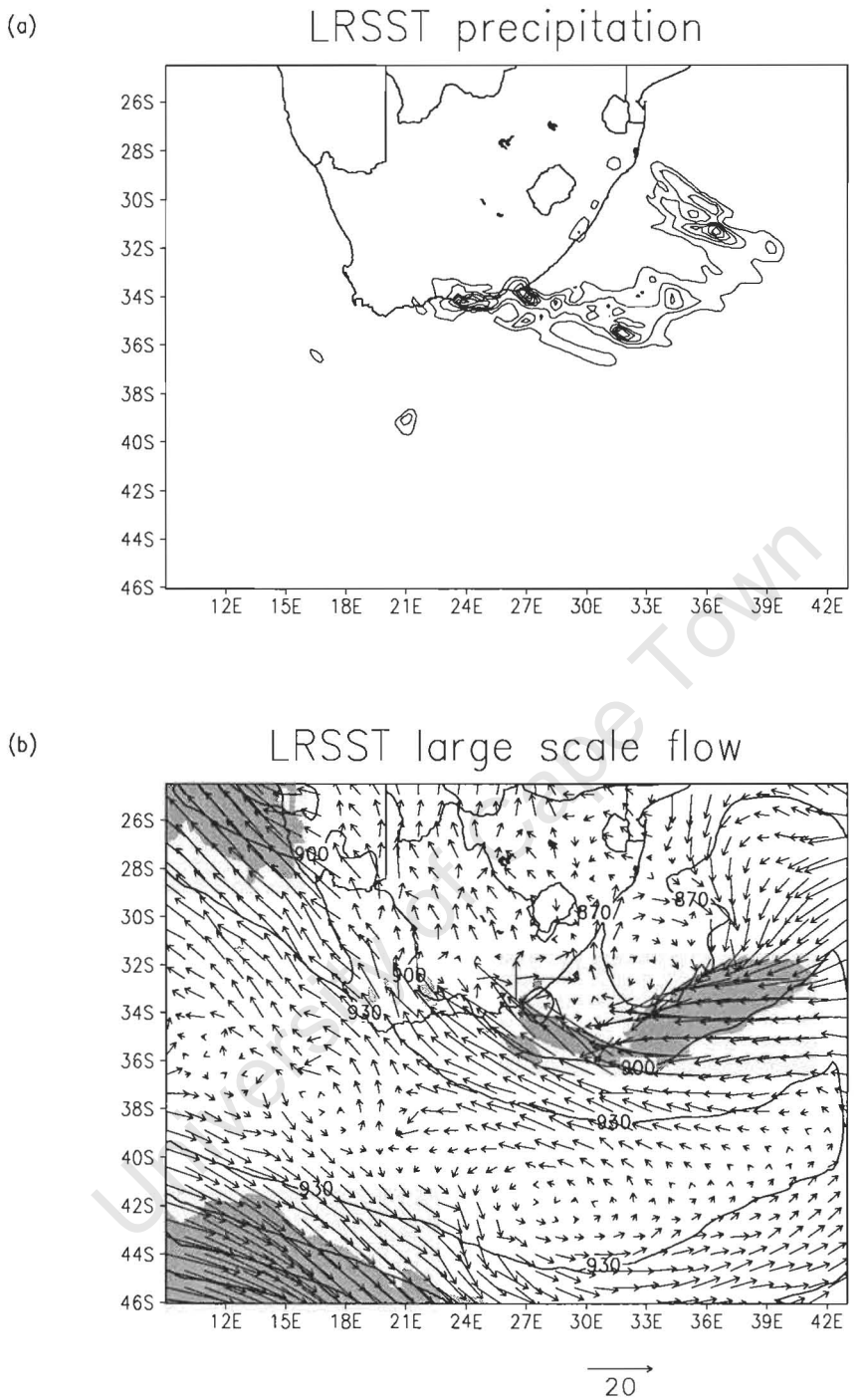

University of Cape Town

Figure 7.2 – Output of the LRSST simulation for the East London case. (a) Precipitation for the 24-hour period to 0600 UTC 16 August 2002. Contour interval is 20mm starting at 20mm; (b) 925 hPa geopotential height (solid contours, interval 30m), wind vectors (with a vector scale given to the bottom right of the panel), and wind speed greater than 15 $m.s^{-1}$ shaded, at the reference time 0000 UTC 16 August 2002. (c) and (d) as in (a) and (b) except for difference plots between LRSST and CNTRL, with solid (dashed) contours showing a positive (negative) difference.

(c)

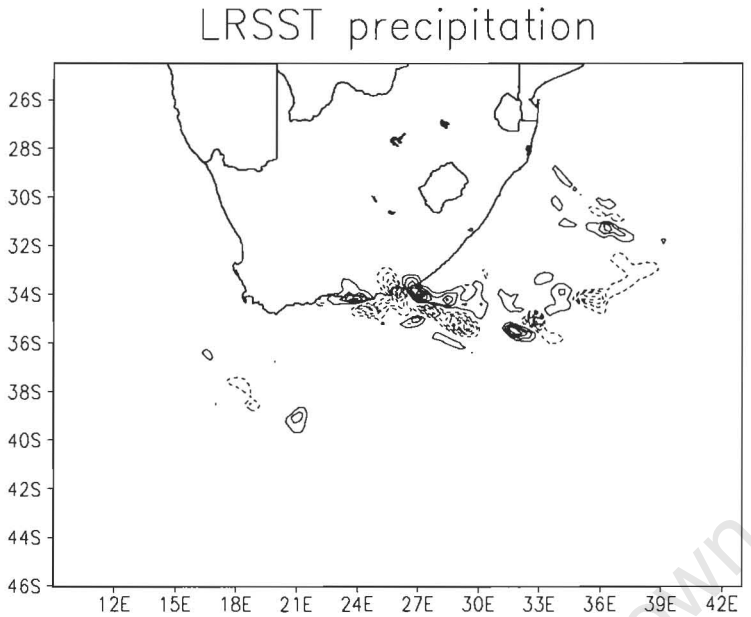

(d)

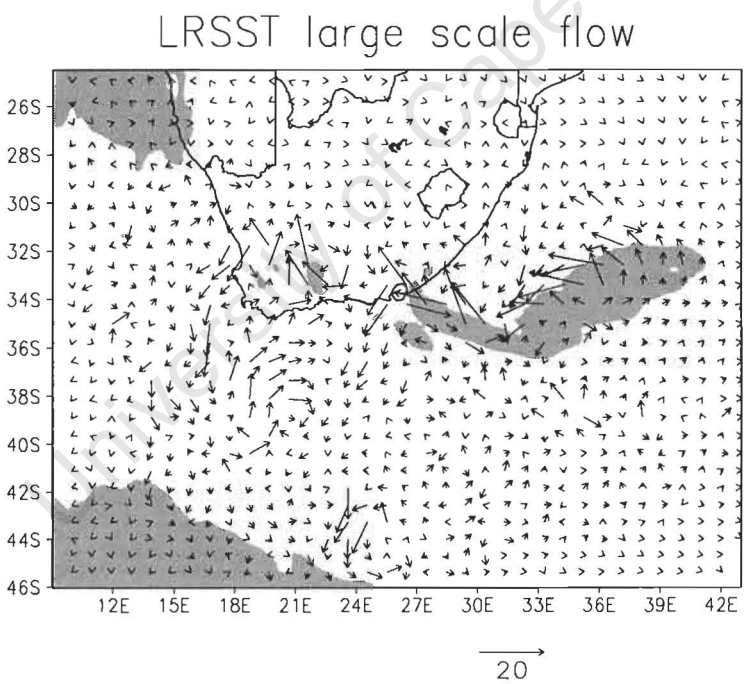

University of Cape Town

Figure 7.2 - *continued*

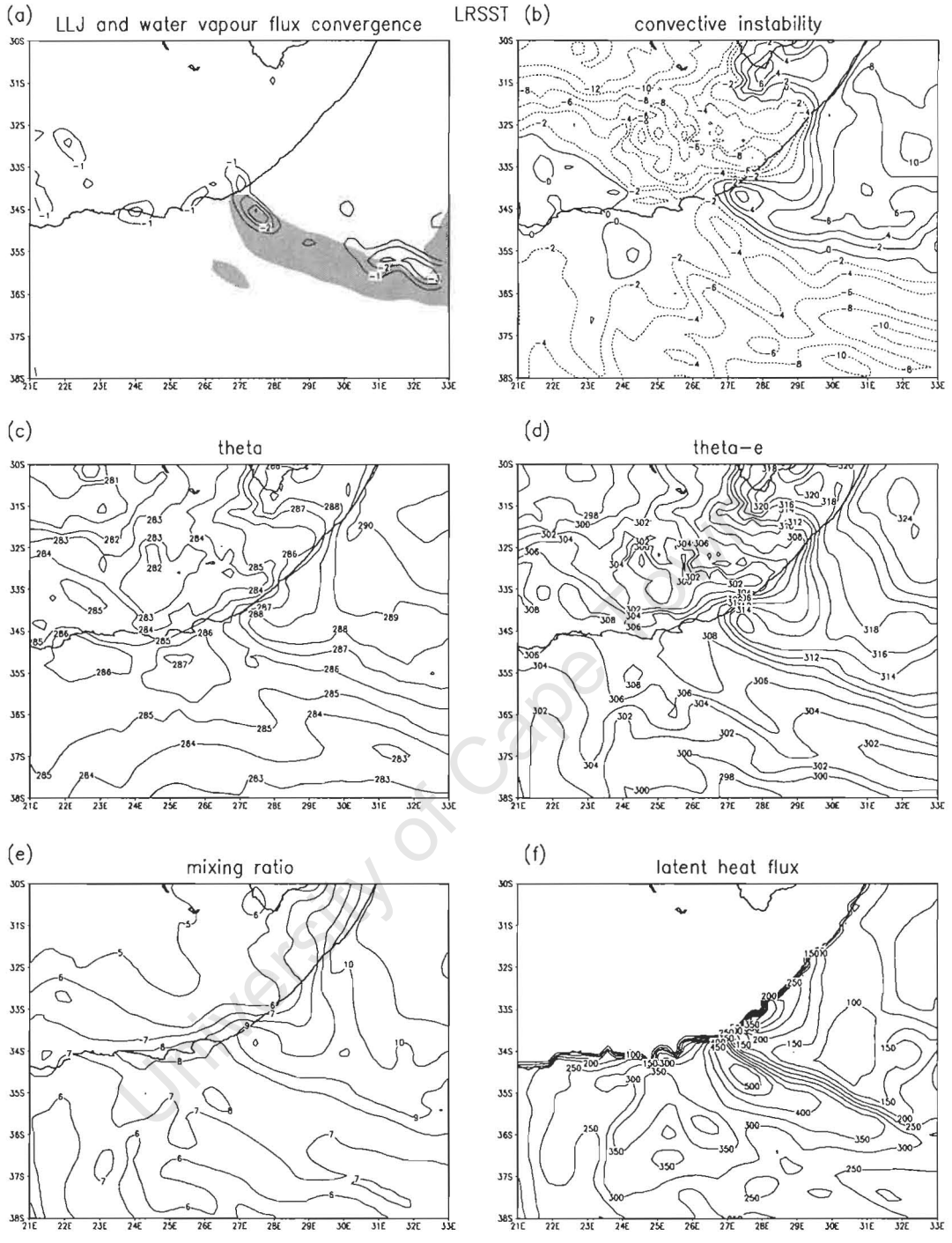

Figure 7.3 - Output from the LRSST simulation at 0000 UTC 16 August 2002. (a) 1000-850 hPa water vapour flux convergence, contour interval 1 $g.m^{-2}.s^{-1}$, with wind speed greater than 15 $m.s^{-1}$ shaded; (b) Convective instability taken as the difference in equivalent potential temperature between 1000- and 500-hPa, contour interval 5K; (c) 1000 hPa potential temperature, contour interval 1K; (d) 1000 hPa equivalent potential temperature, contour interval 2K; (e) 1000 hPa mixing ratio, contour interval 1 $g.kg^{-1}$; (f) surface latent heat flux, contour interval 50 $W.m^{-2}$. (g) – (l) as in (a) – (f), except for difference between LRSST and CNTRL. Solid (dashed) contours indicate a positive (negative) difference.

University of Cape Town

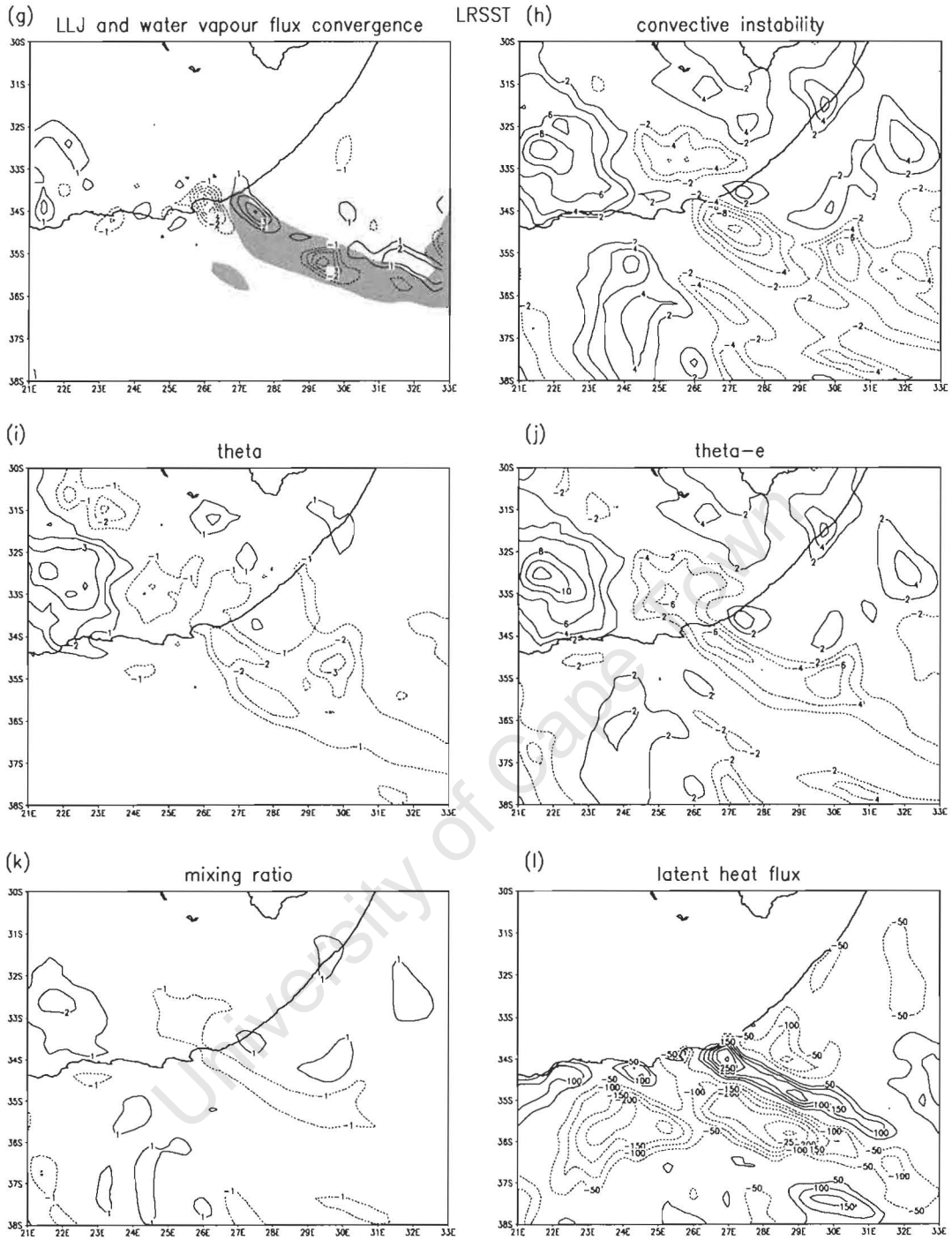

Figure 7.3 *-continued*

University of Cape Town

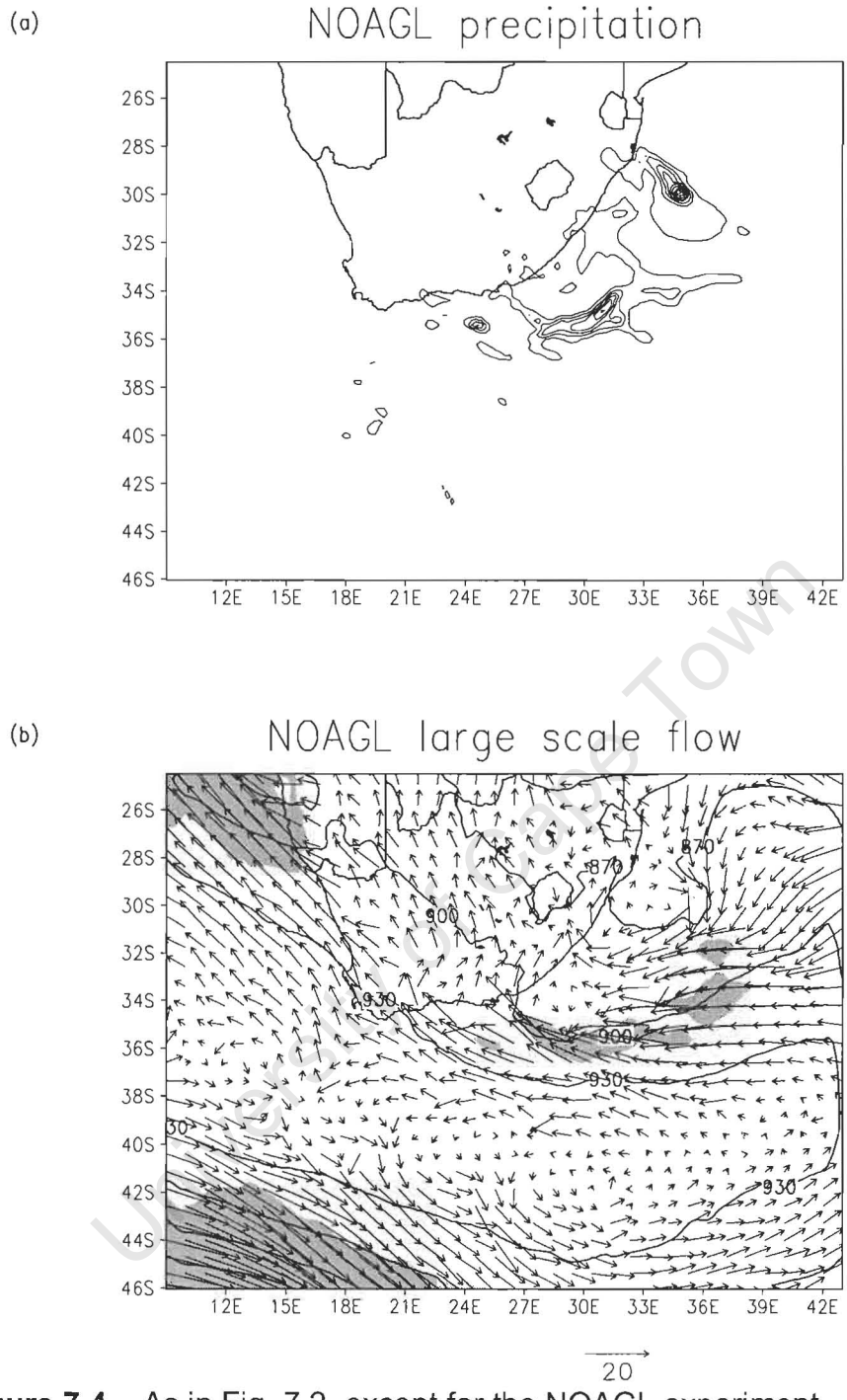

Figure 7.4 – As in Fig. 7.2, except for the NOAGL experiment

University of Cape Town

(c)

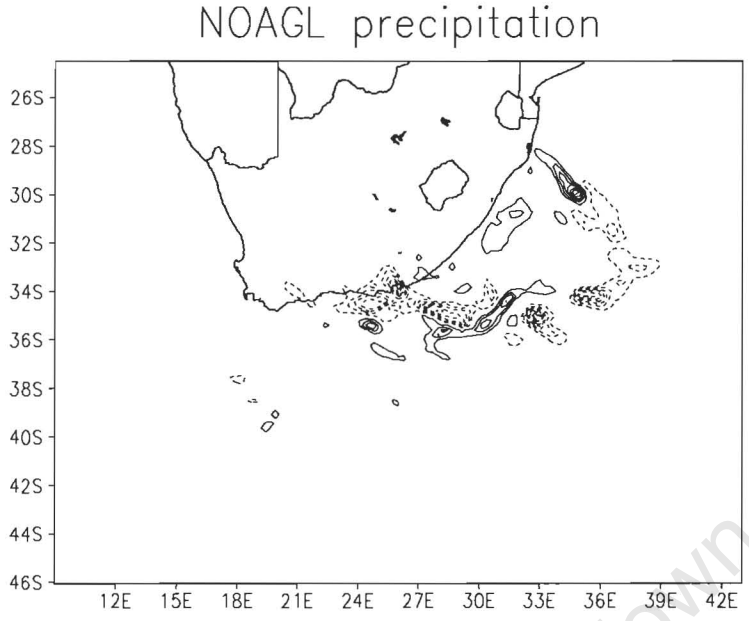

(d)

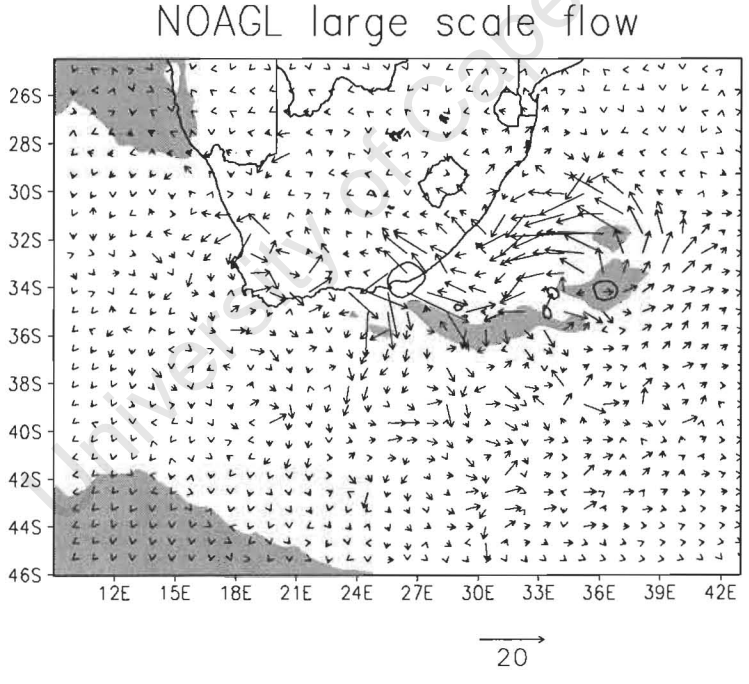

University of Cape Town

Figure 7.4 - *continued*

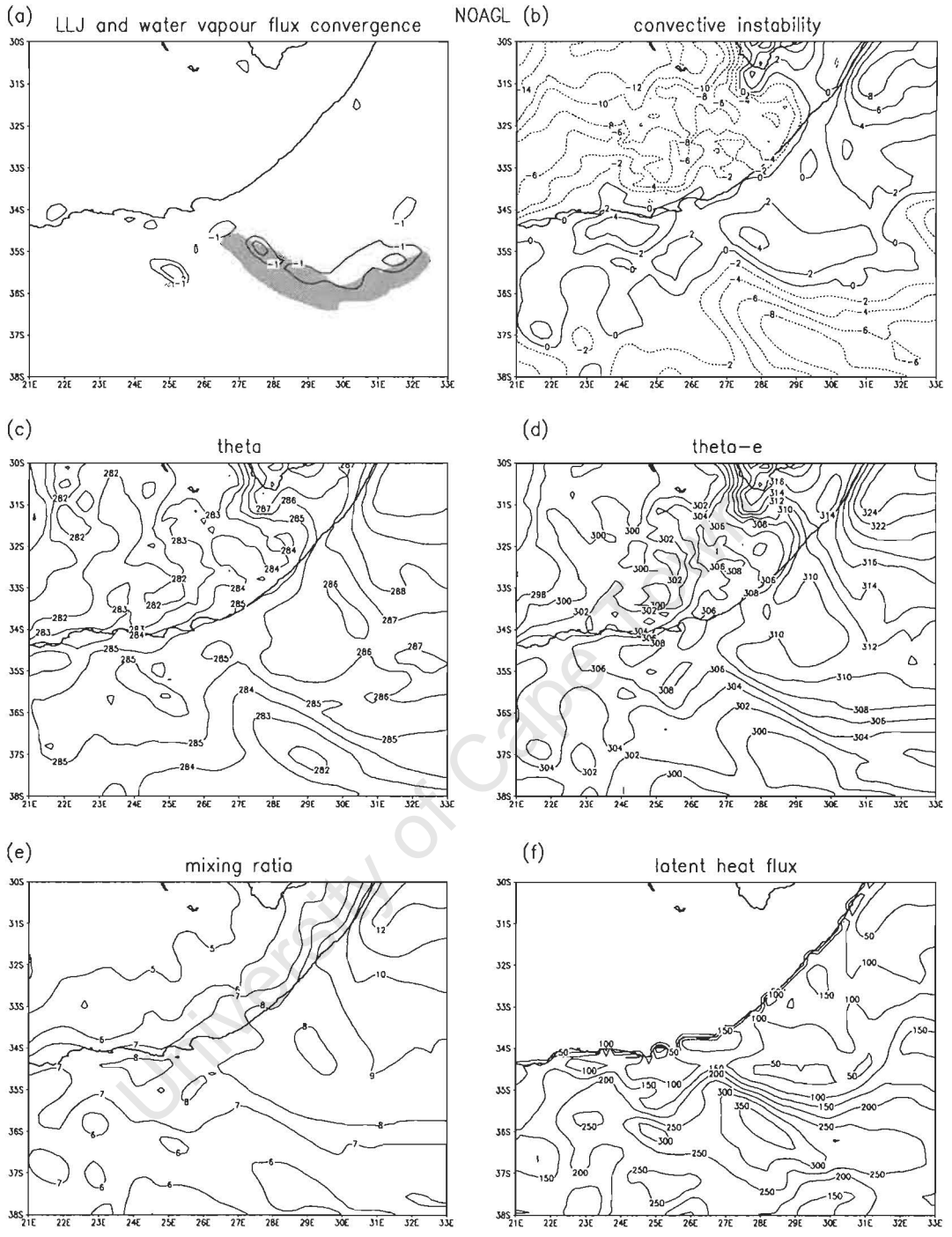

Figure 7.5 – As in Fig.7.3, except for the NOAGL experiment

University of Cape Town

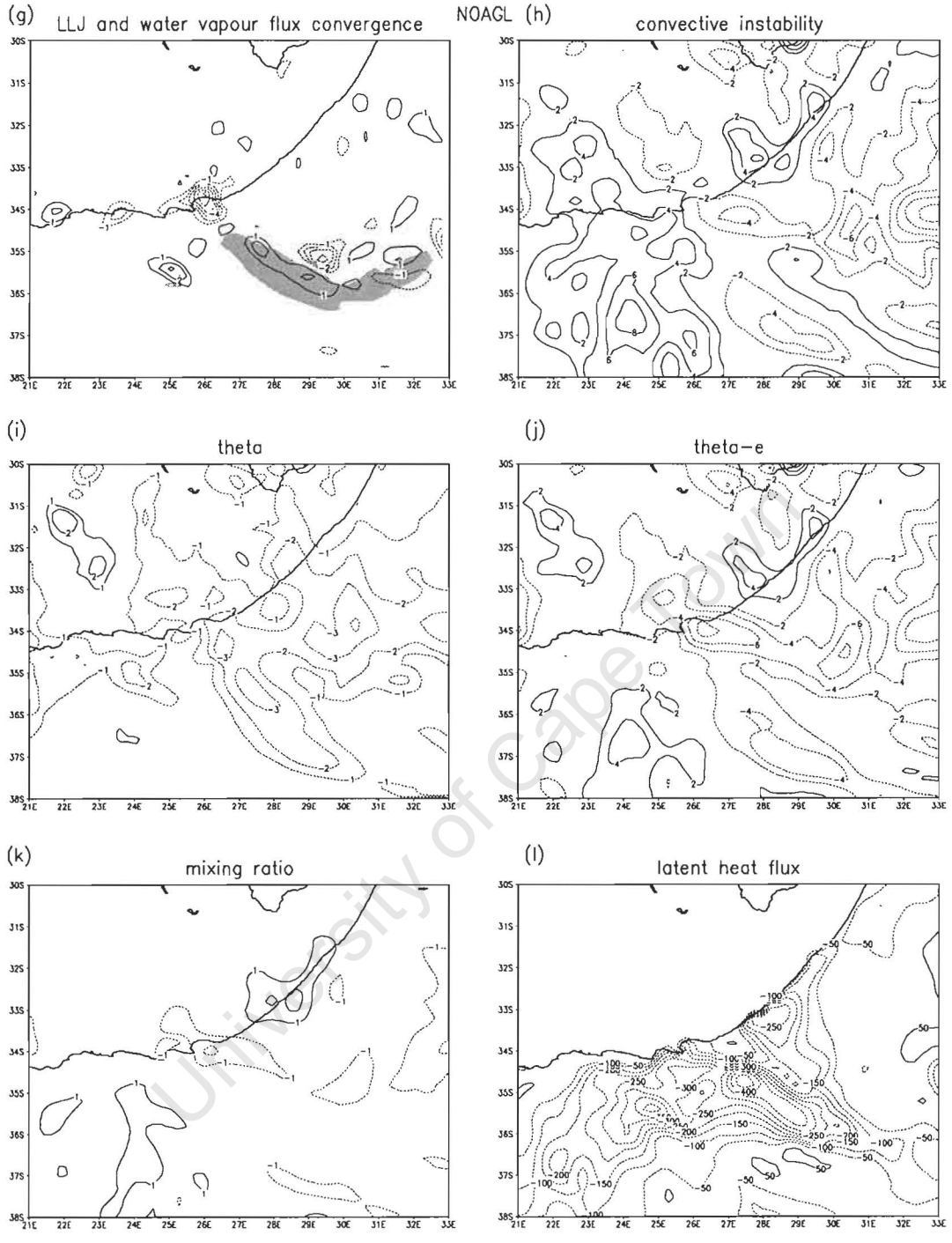

Figure 7.5 – *continued*

University of Cape Town

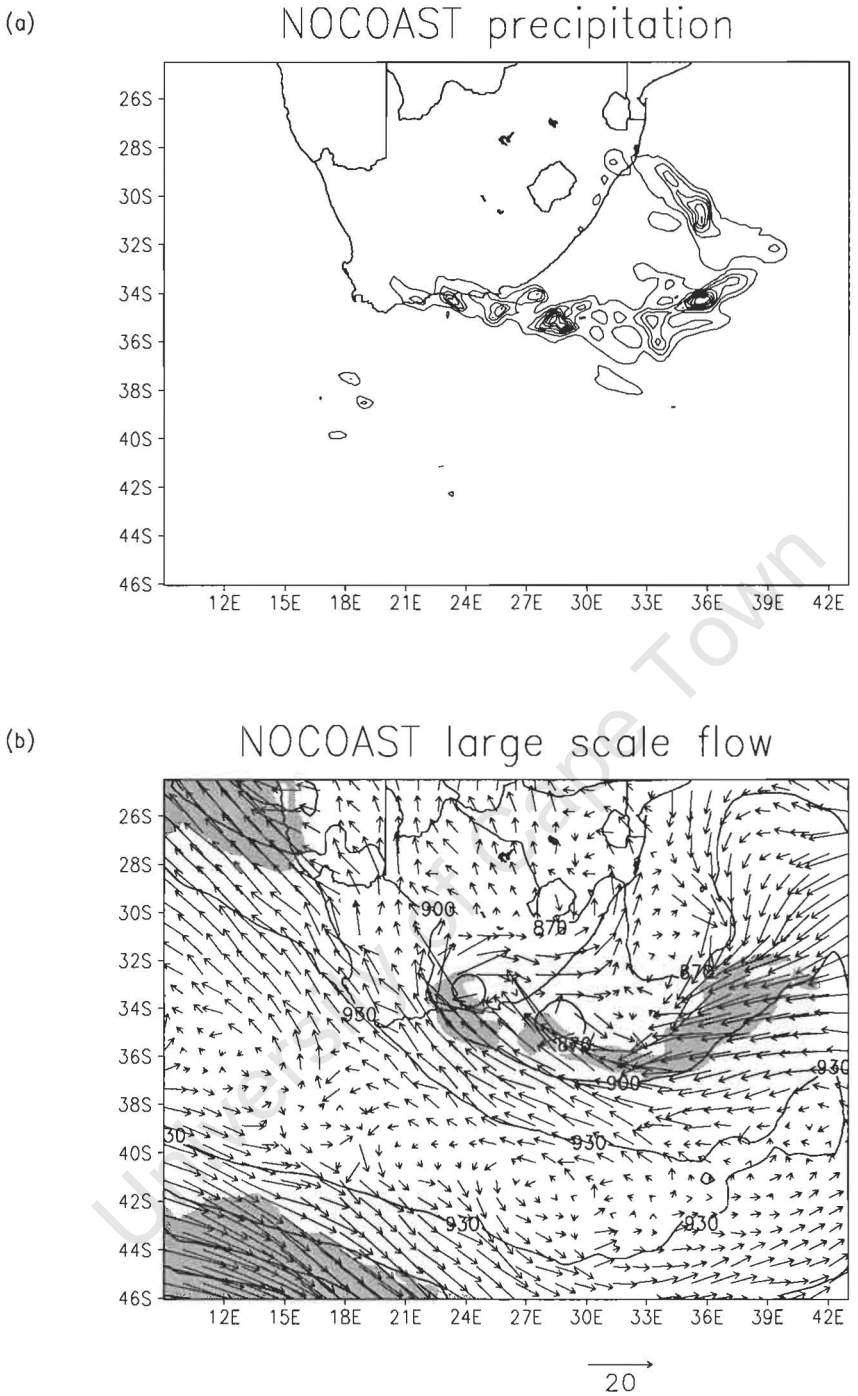

Figure 7.6 – As in Fig. 7.2, except for the NOCOAST experiment

University of Cape Town

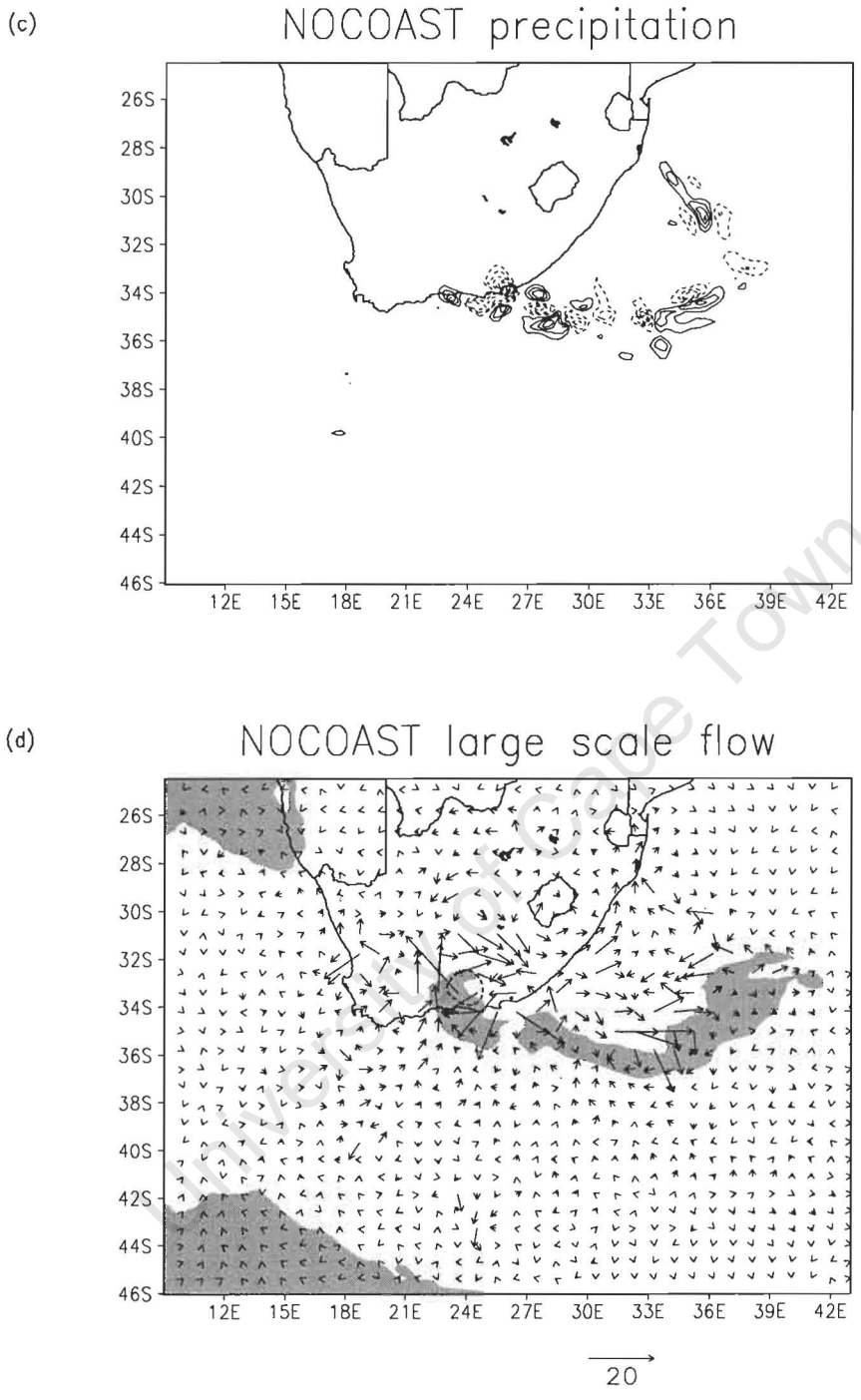

University of Cape Town

Figure 7.6 – *continued*

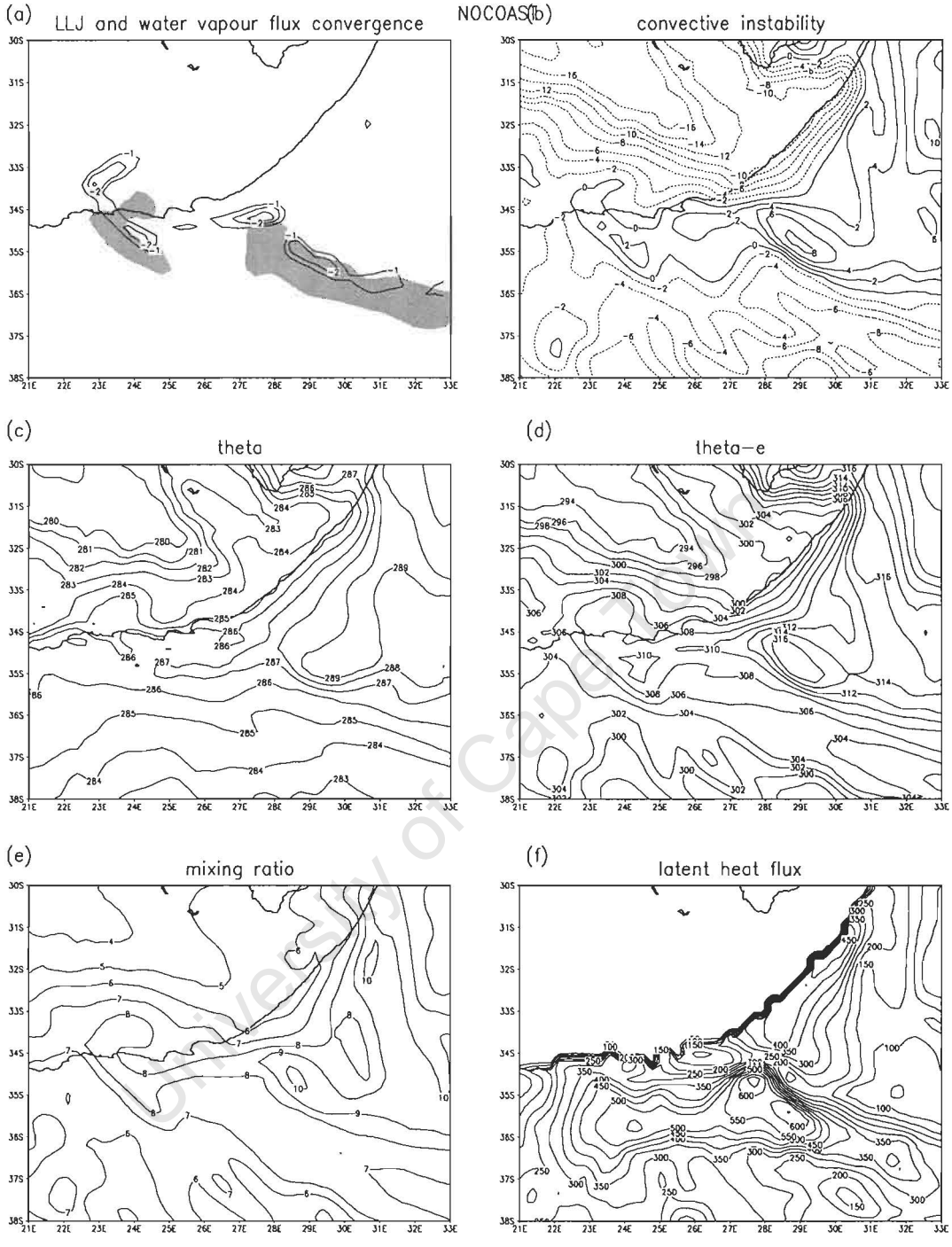

Figure 7.7 – As in Fig. 7.3, except for the NOCOAST experiment

University of Cape Town

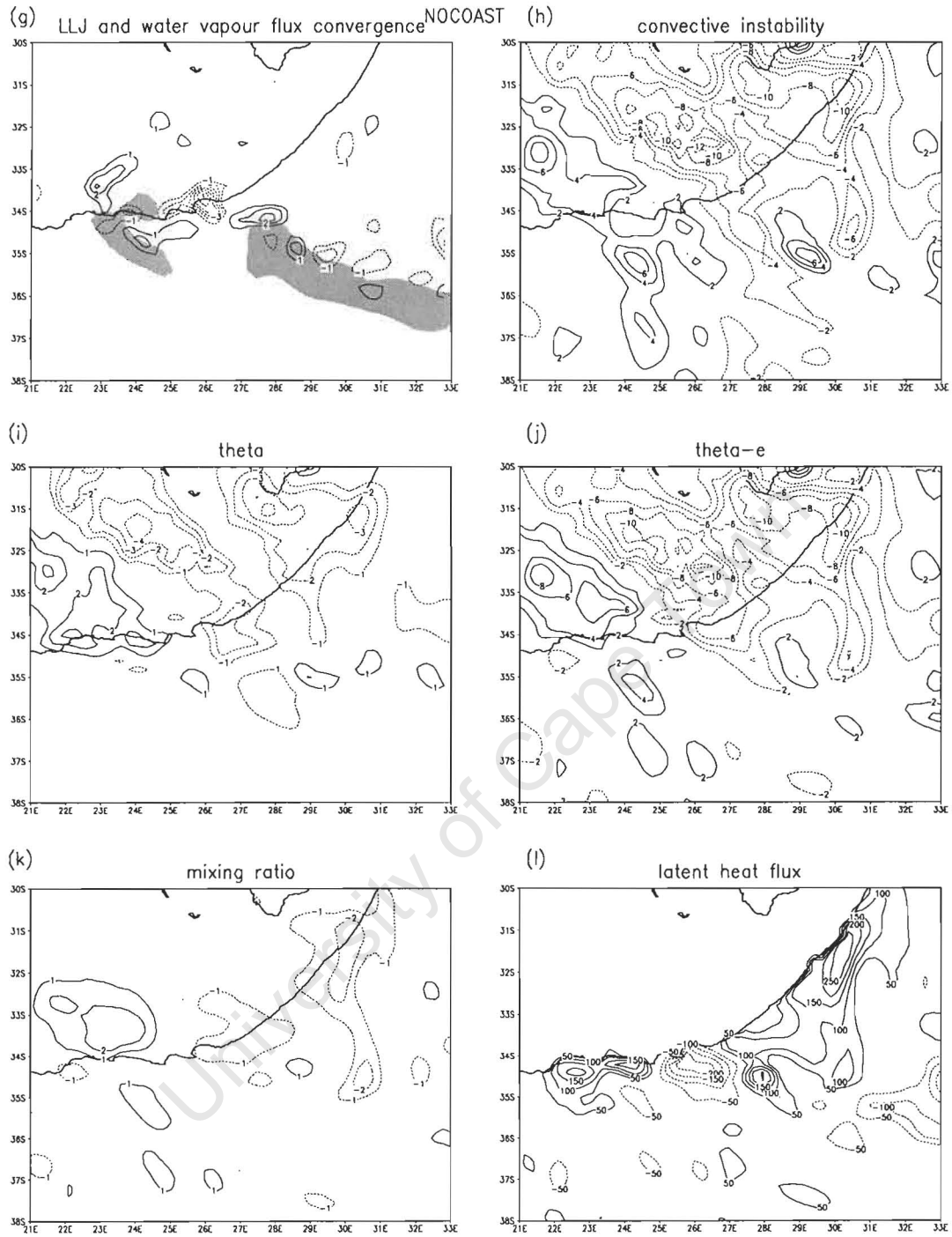

Figure 7.7 – *continued*

University of Cape Town

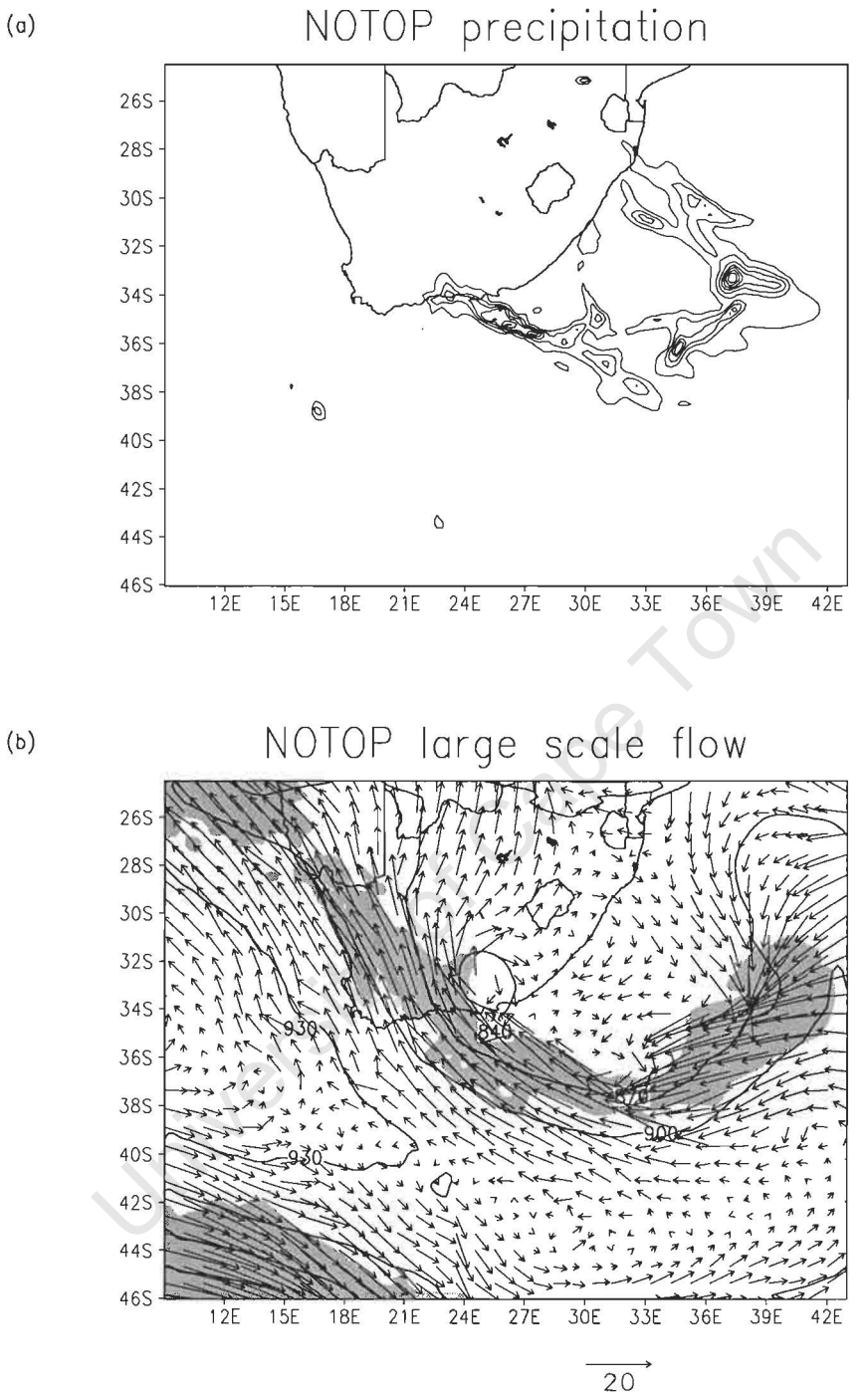

Figure 7.8 – As in Fig. 7.2, except for the NOTOP experiment

University of Cape Town

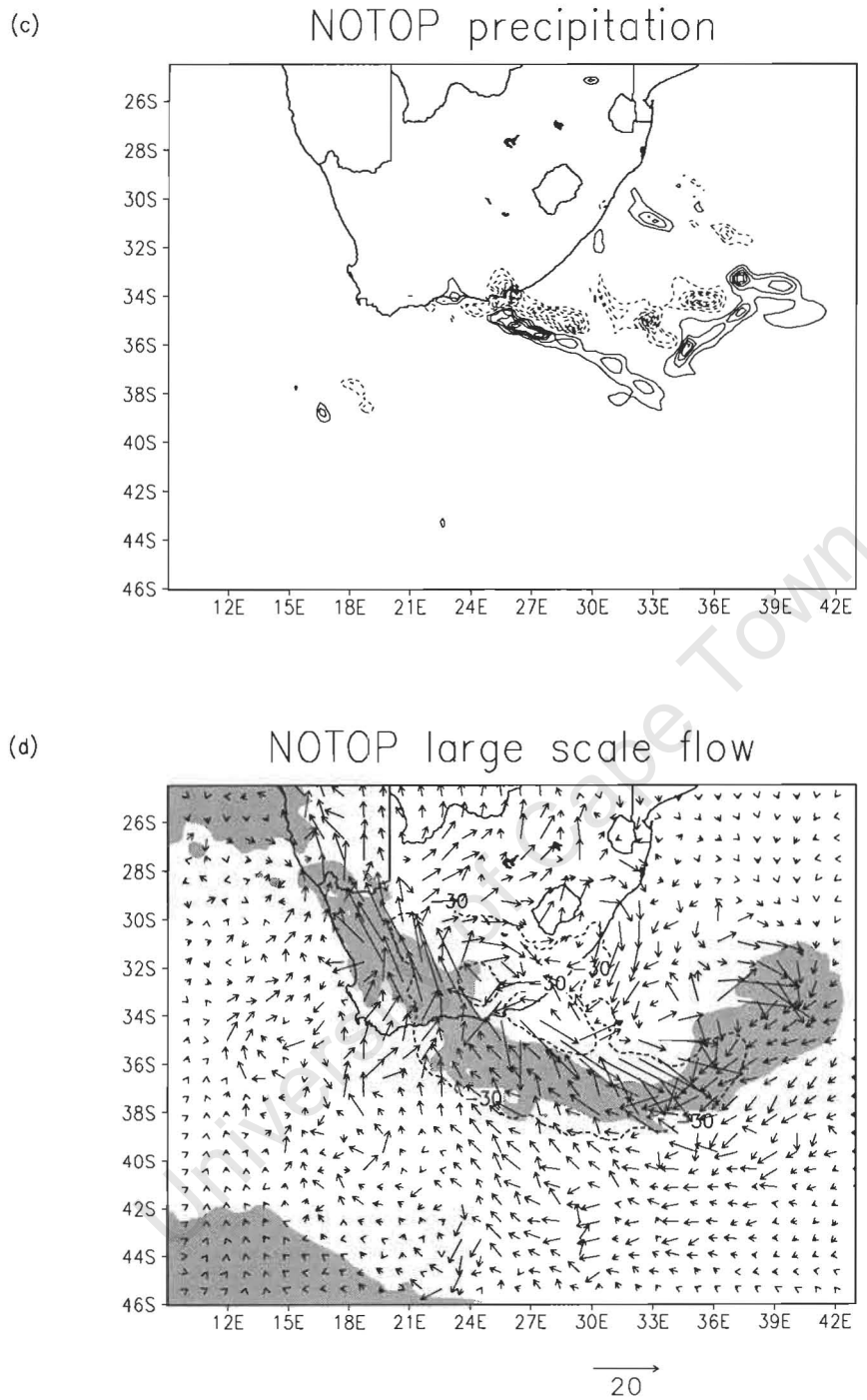

University of Cape Town

Figure 7.8 – *continued*

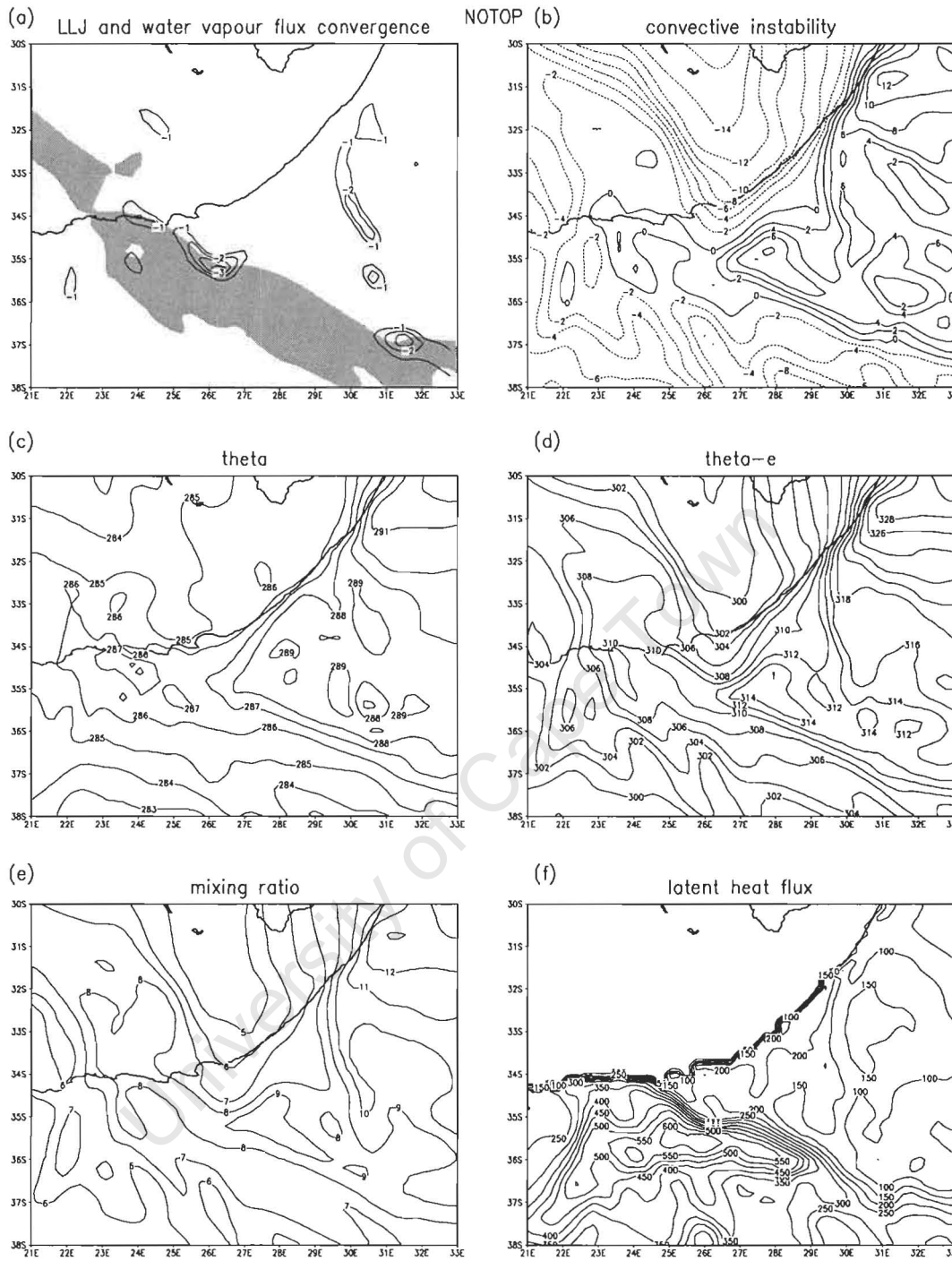

Figure 7.9 – As in Fig. 7.3, except for the NOTOP experiment

University of Cape Town

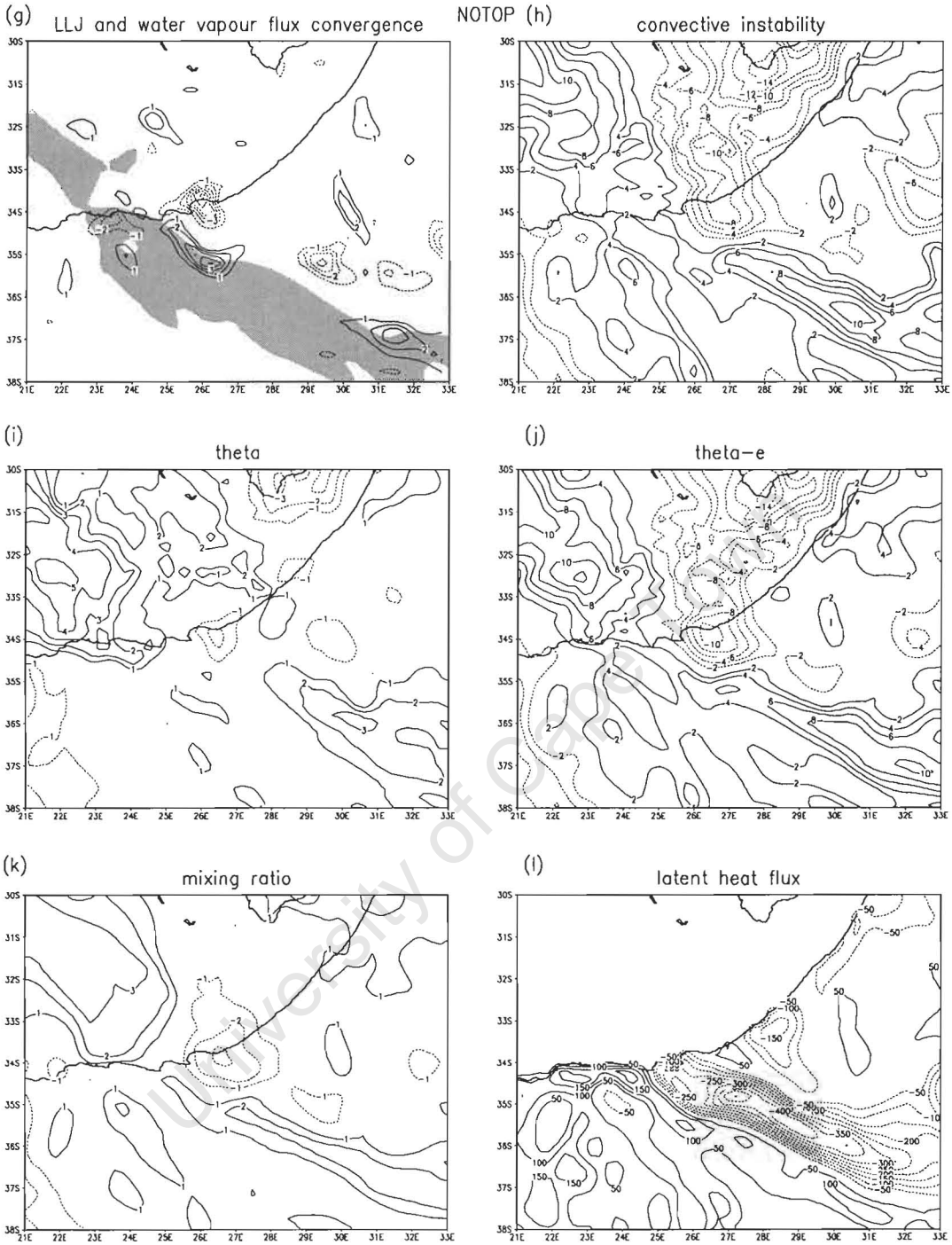

Figure 7.9 – *continued*

University of Otago

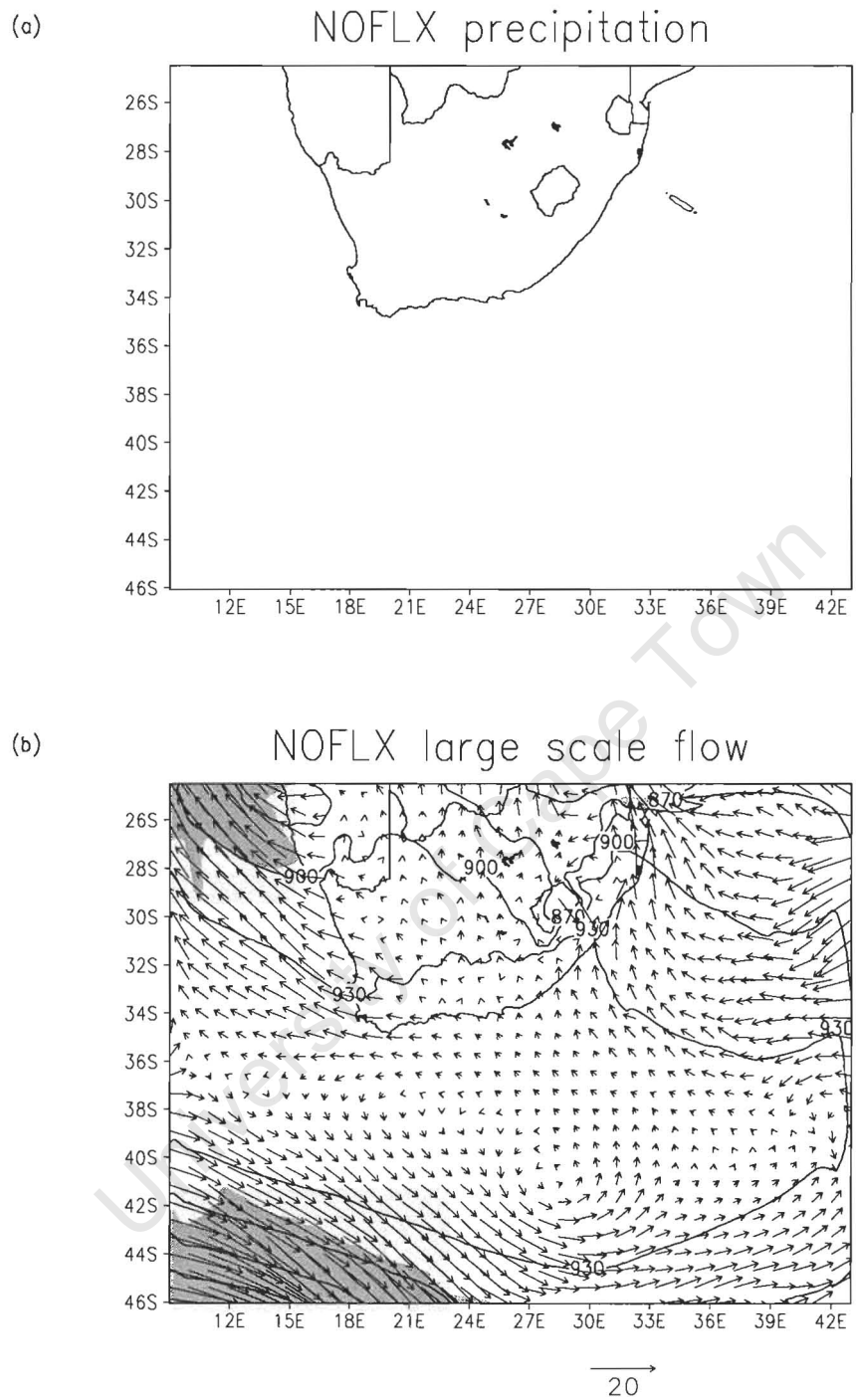

Figure 7.10 – As in Fig. 7.2, except for the NOFLX experiment

University of Cape Town

(c)

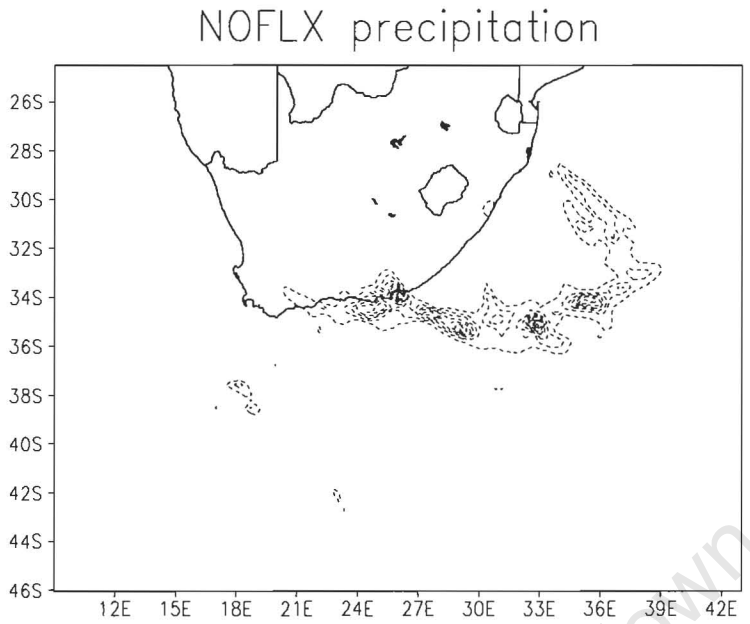

(d)

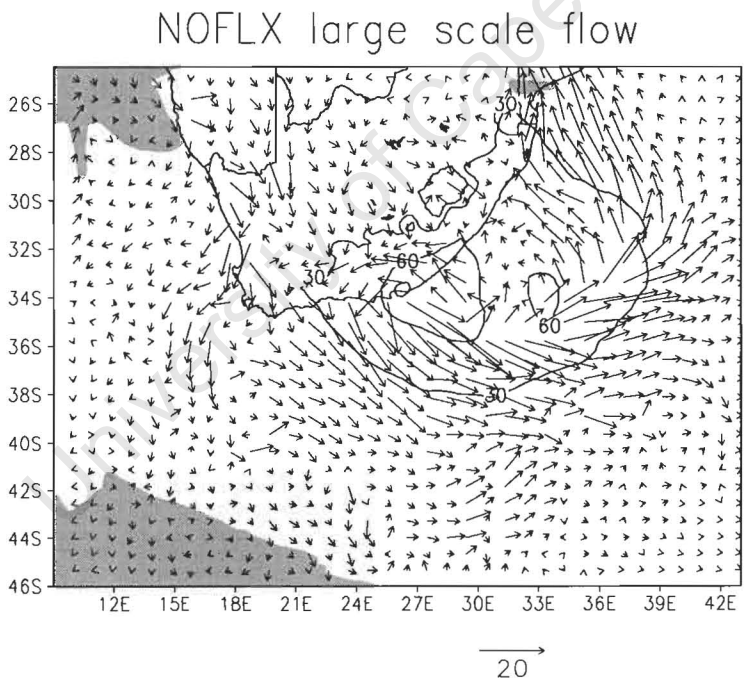

Figure 7.10 – *continued*

University of Cape Town

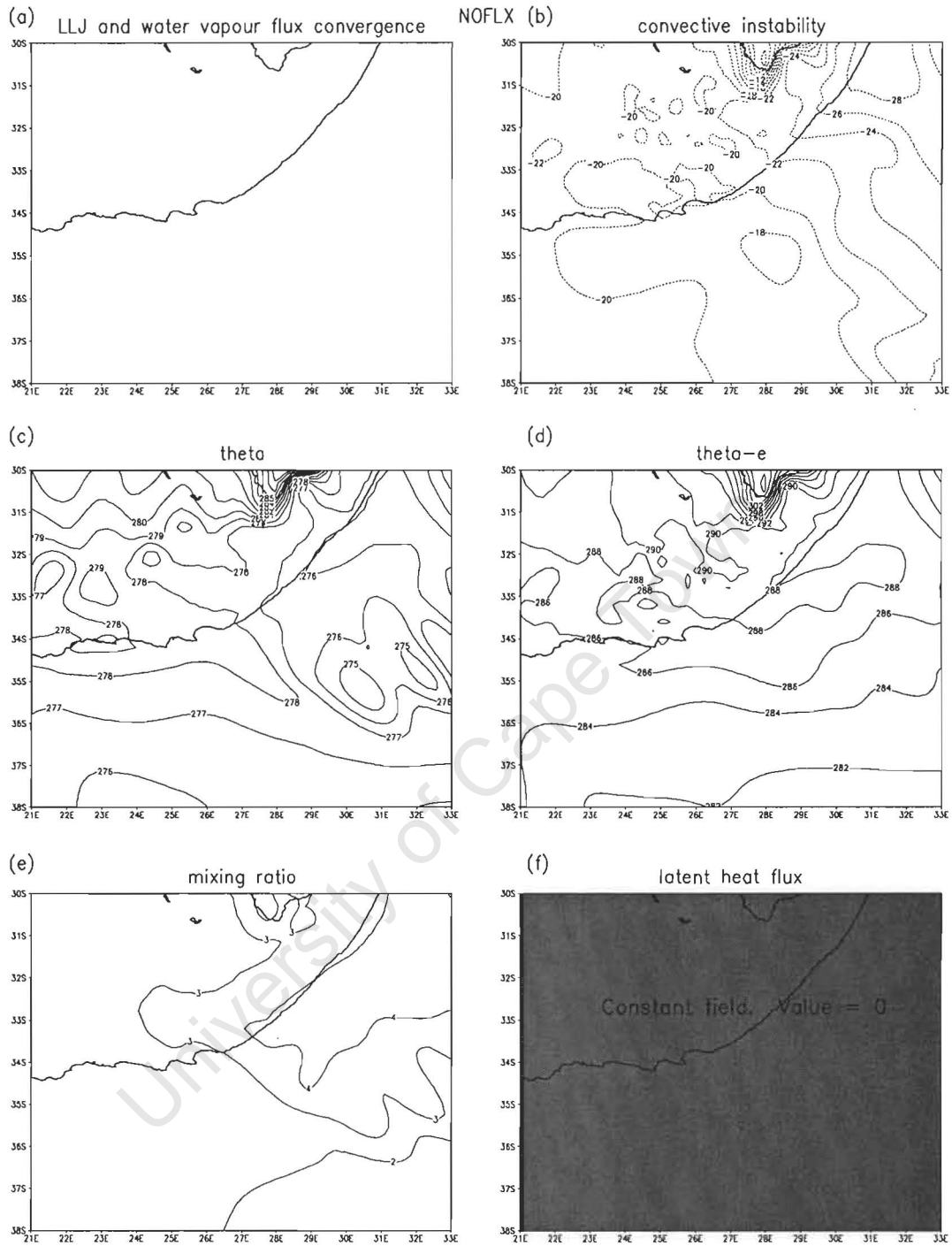

Figure 7.11 – As in Fig. 7.3, except for the NOFLX experiment

University of Cape Town

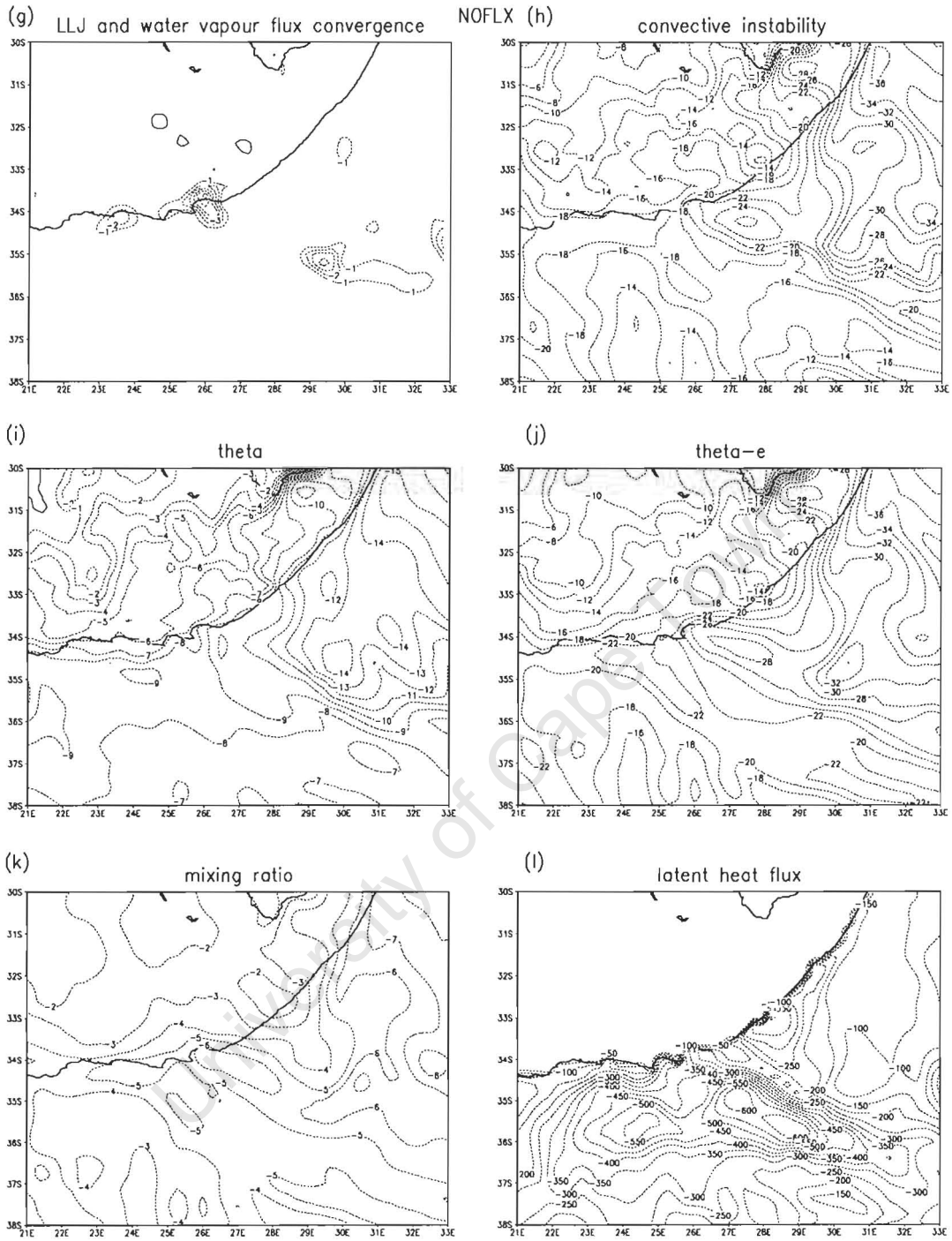

Figure 7.11 - *continued*

University of Cape Town

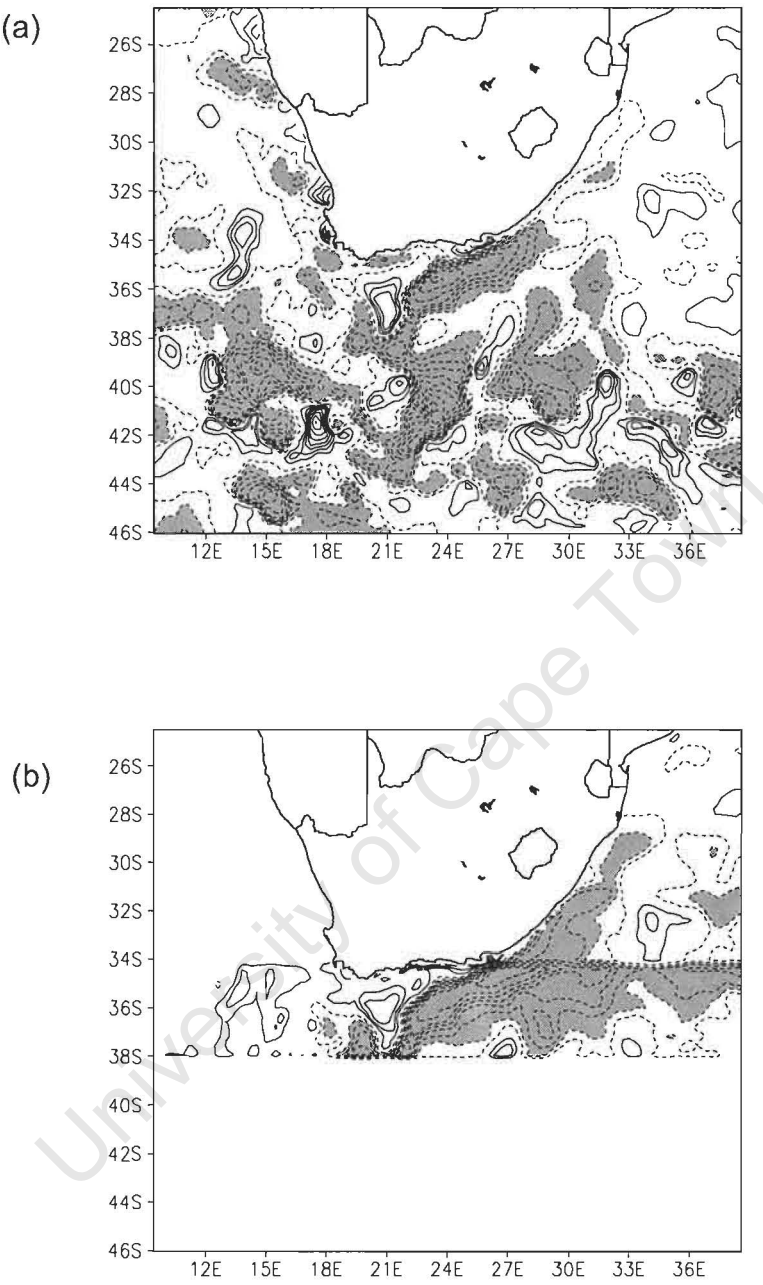

University of Cape Town

Figure 7.12 – As in Fig. 7.1, except for the Montagu case

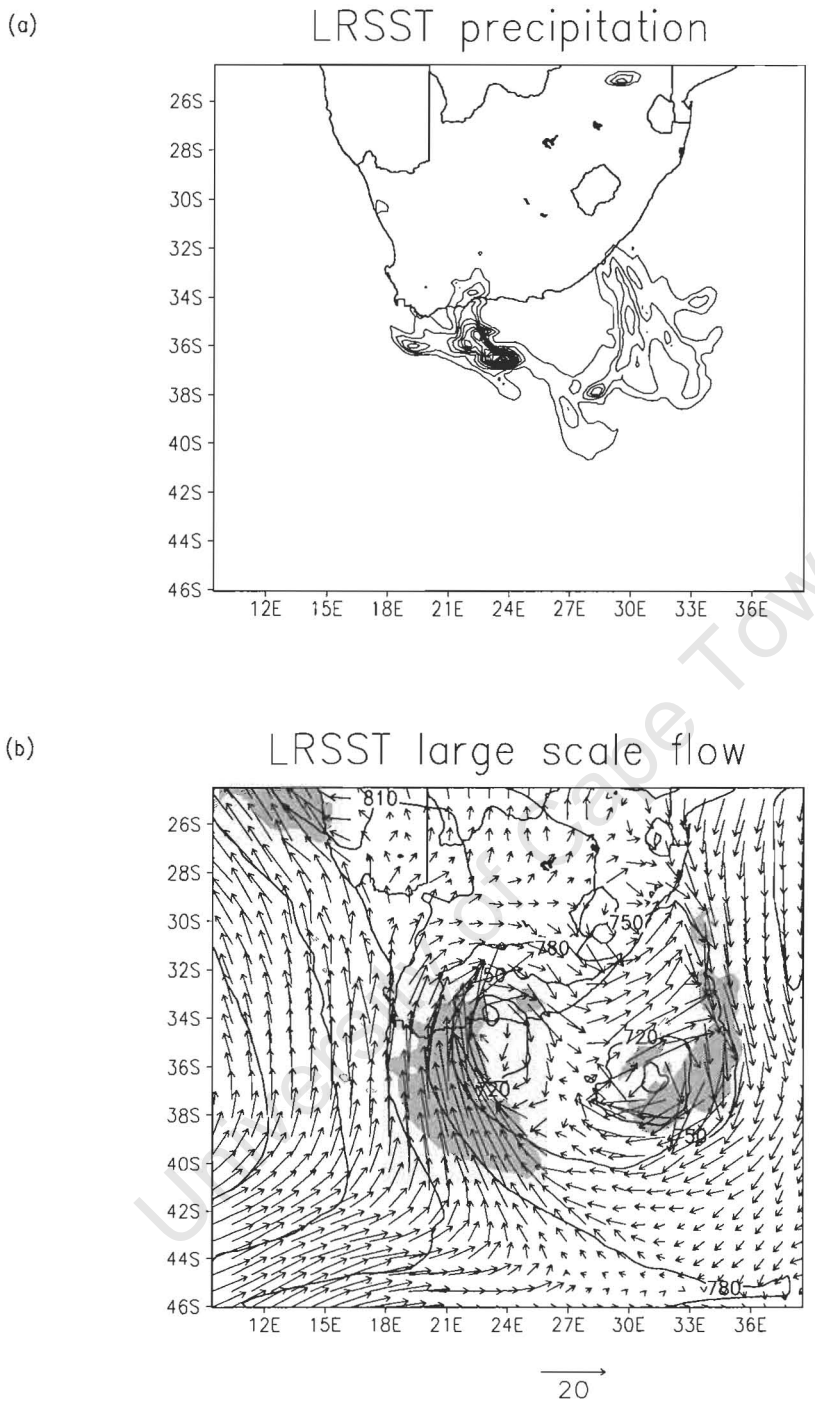

Figure 7.13 - Output of the LRSST simulation for the Montagu case. (a) Precipitation for the 24-hour period to 0600 UTC 24 March 2003. Contour interval is 20mm starting at 20mm; (b) 925 hPa geopotential height (solid contours, interval 30m), wind vectors (with a vector scale given to the bottom right of the panel), and wind speed greater than 15 $m.s^{-1}$ shaded, at the reference time 0400 UTC 24 March 2003. (c) – (d) as in (a) – (b), except for the difference between LRSST-CNTRL, with solid (dashed) contours representing a positive (negative) difference.

University of Cape Town

(c)

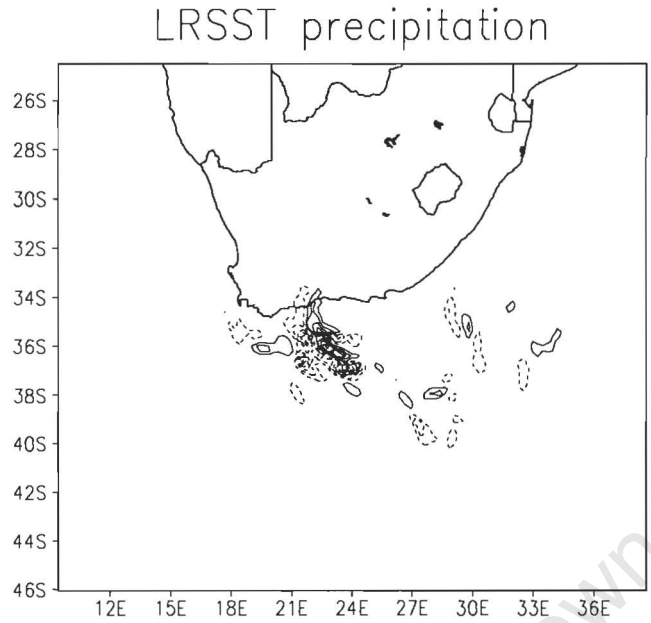

(d)

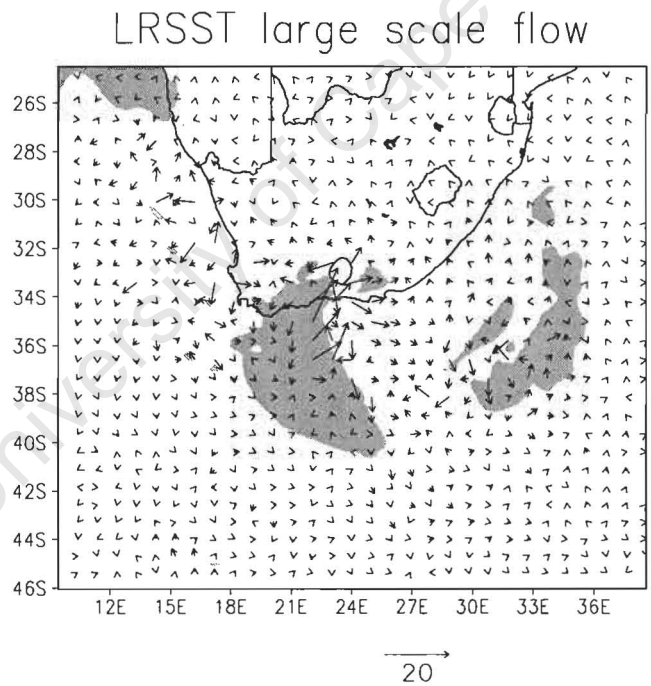

University of Cape Town

Figure 7.13 - *continued*

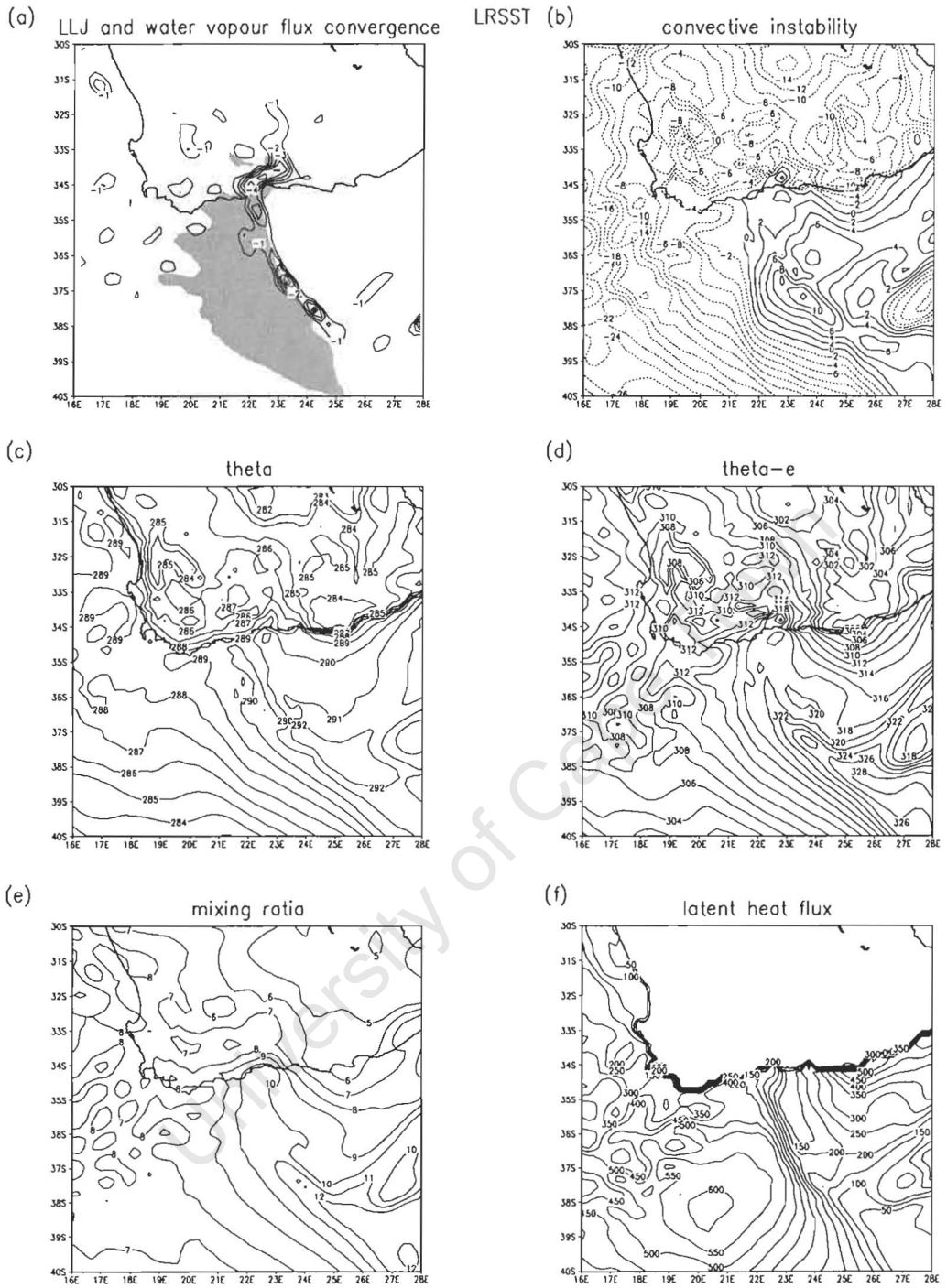

Figure 7.14 - Output from the LRSST simulation at 0400 UTC 24 March 2003. (a) 1000-850 hPa water vapour flux convergence, contour interval 1 $g.m^{-2}.s^{-1}$, with wind speed greater than 15 $m.s^{-1}$ shaded; (b) Convective instability taken as the difference in equivalent potential temperature between 1000- and 500-hPa, contour interval 5K; (c) 1000 hPa potential temperature, contour interval 1K; (d) 1000 hPa equivalent potential temperature, contour interval 2K; (e) 1000 hPa mixing ratio, contour interval 1 $g.kg^{-1}$; (f) surface latent heat flux, contour interval 50 $W.m^{-2}$. (g) – (l) as in (a) – (f), except for the difference between LRSST-CNTRL, with solid (dashed) contours representing a positive (negative) difference.

University of Ca

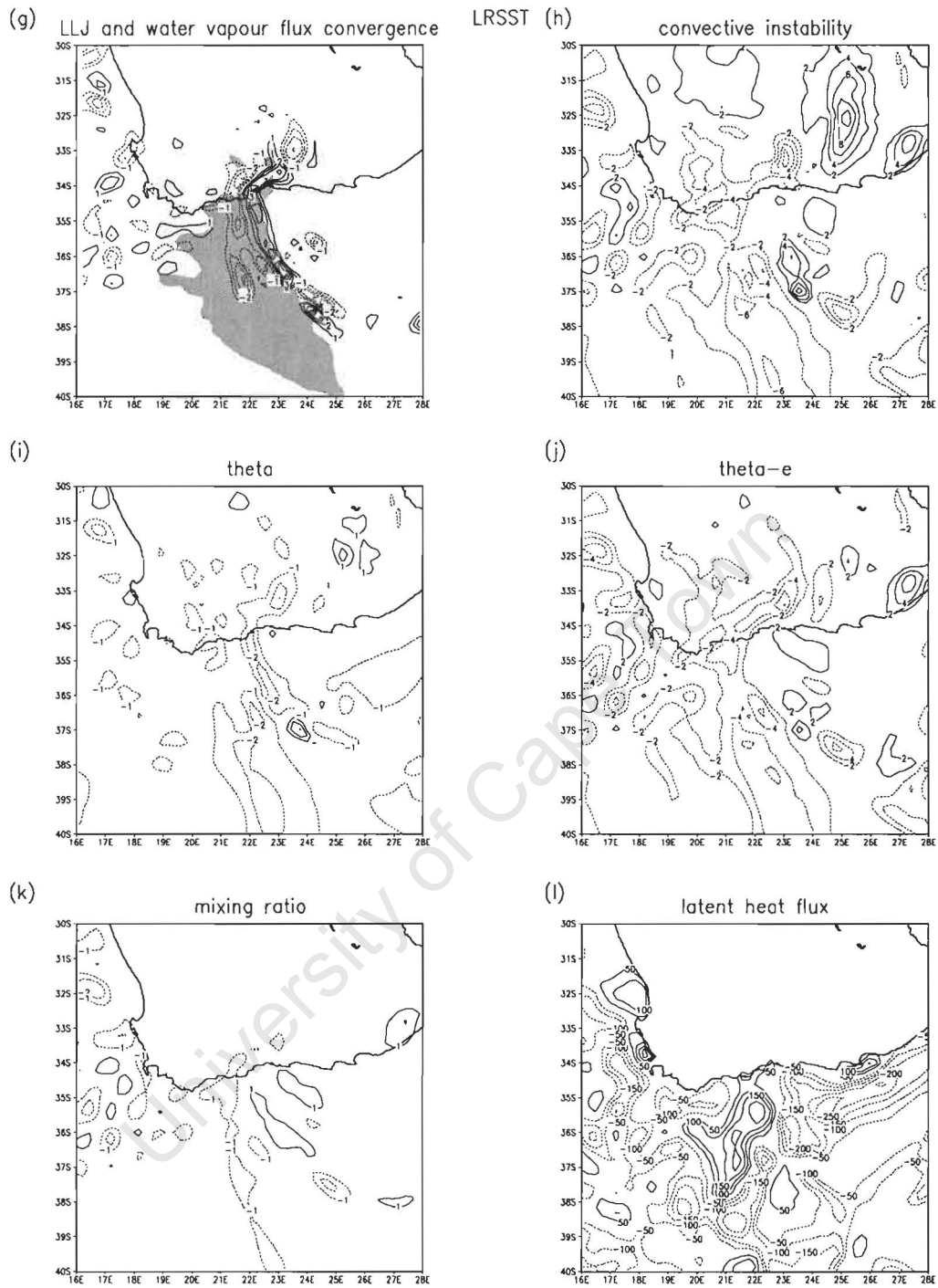

Figure 7.14 - *continued*

University of Cape Town

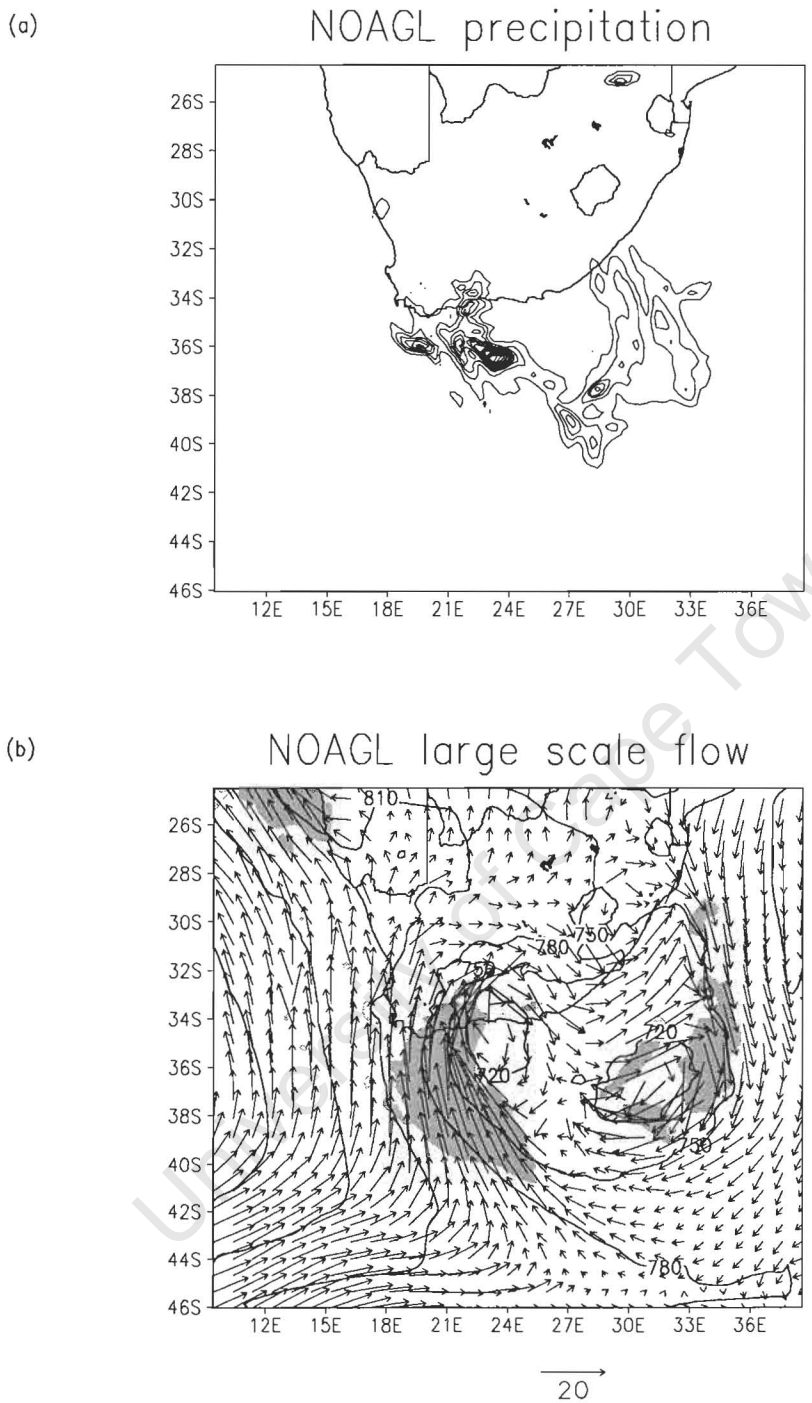

Figure 7.15 – As in Fig. 7.13, except for the NOAGL experiment

University of Cape Town

(c)

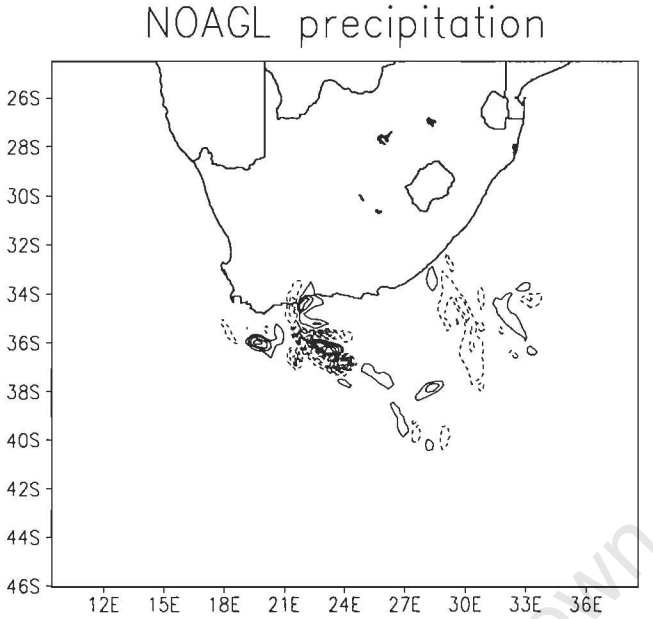

(d)

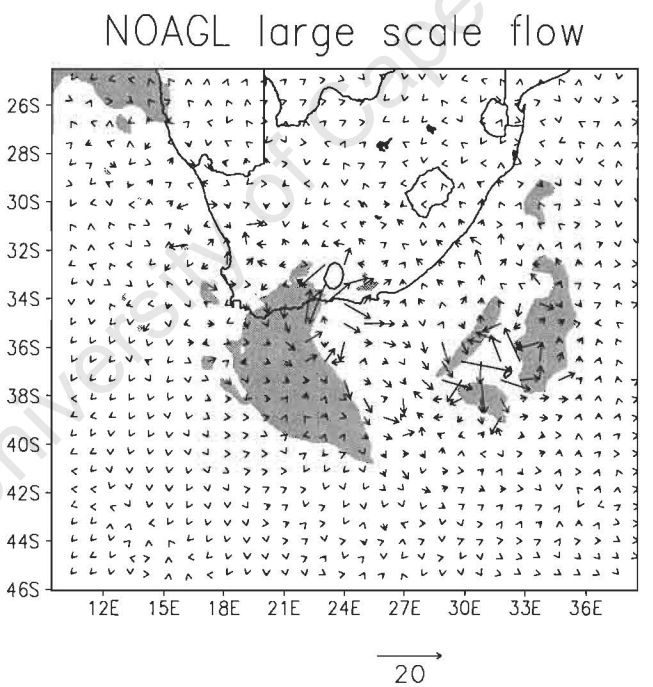

University of Cape Town

Figure 7.15 – *continued*

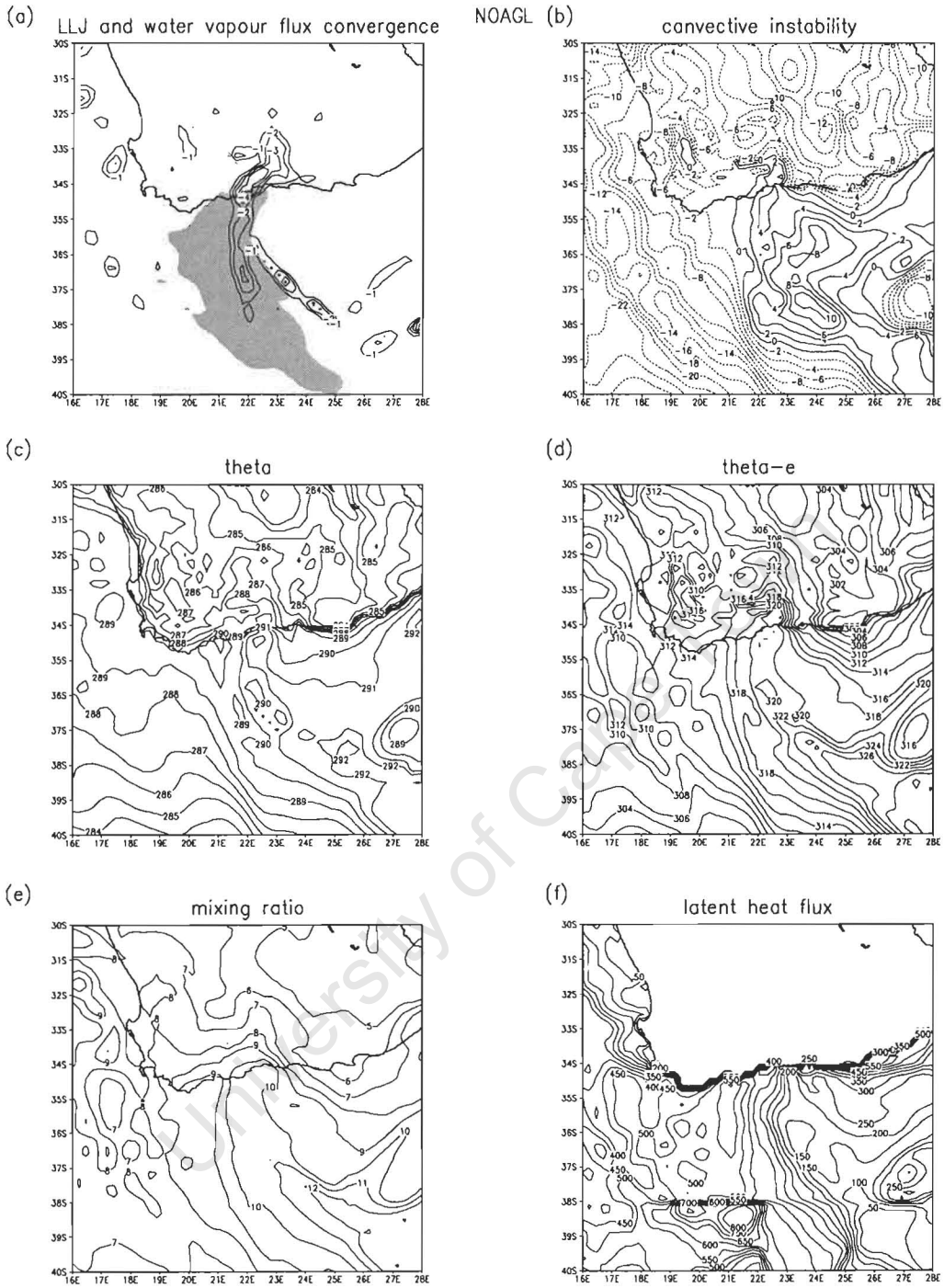

Figure 7.16 – As in Fig. 7.14, except for the NOAGL experiment.

University of Cape Town

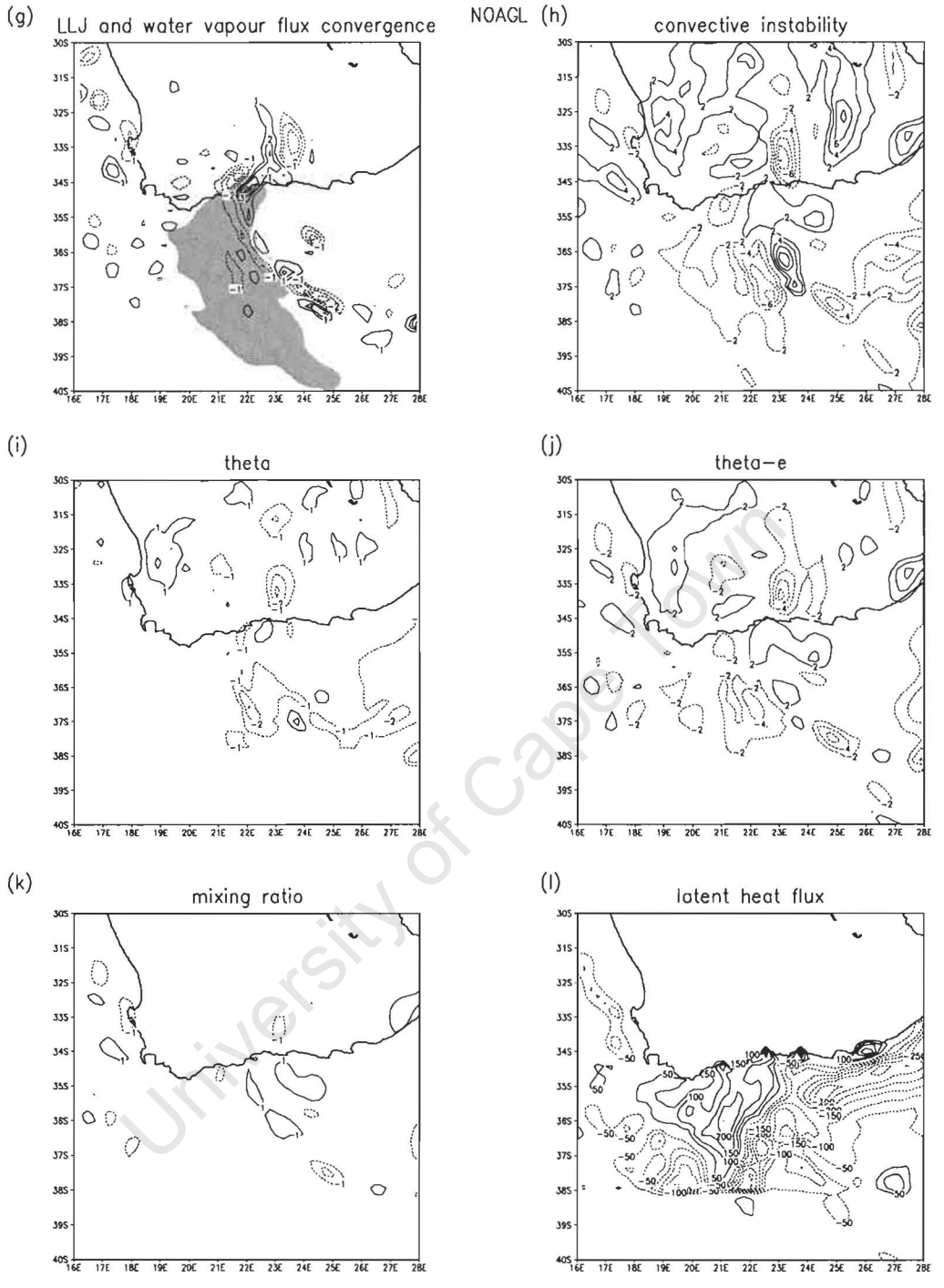

Figure 7.16 - *continued*

University of Cape Town

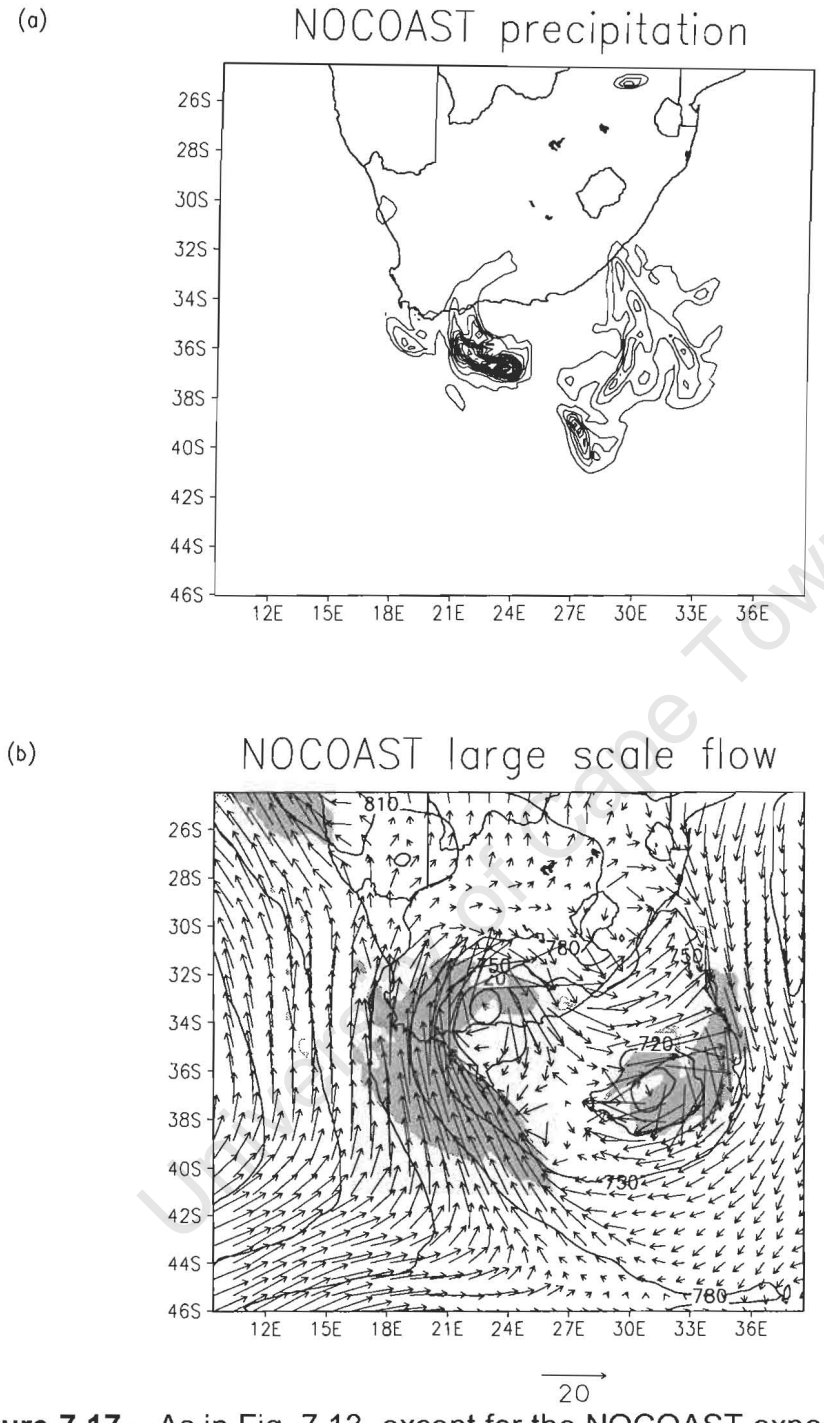

Figure 7.17 – As in Fig. 7.13, except for the NOCOAST experiment

University of Cape Town

(c)

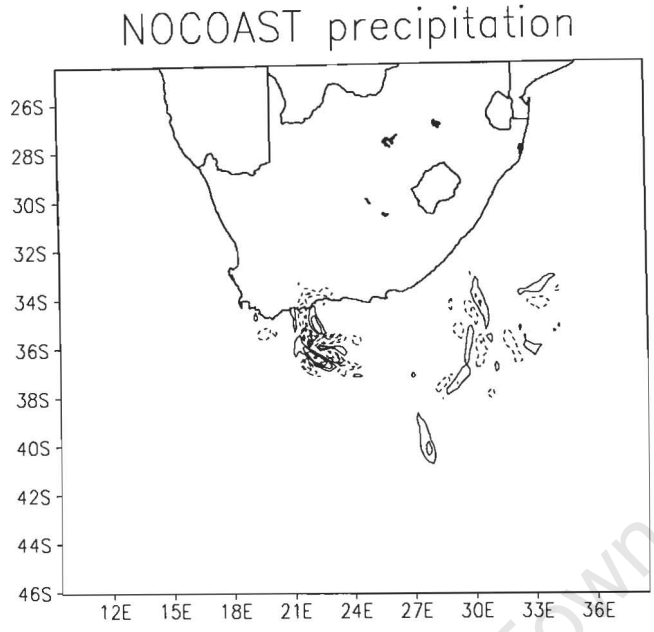

(d)

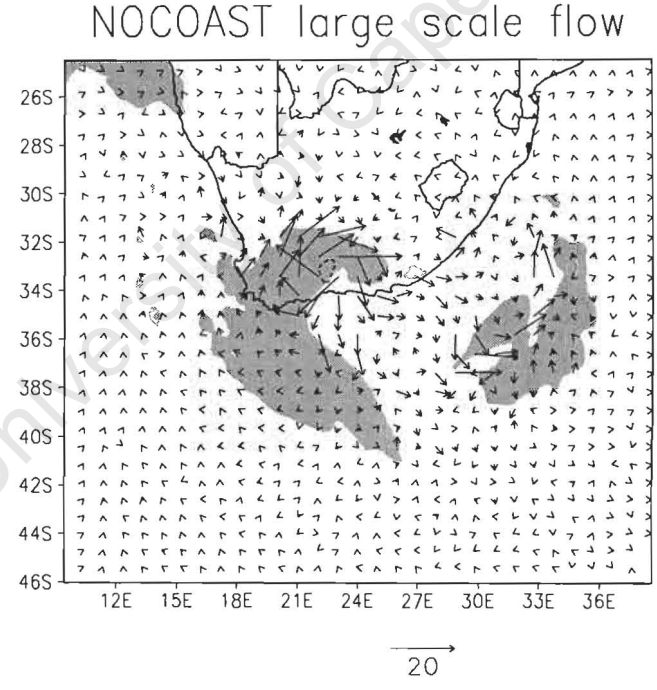

University of Cape Town

Figure 7.17 – *continued*

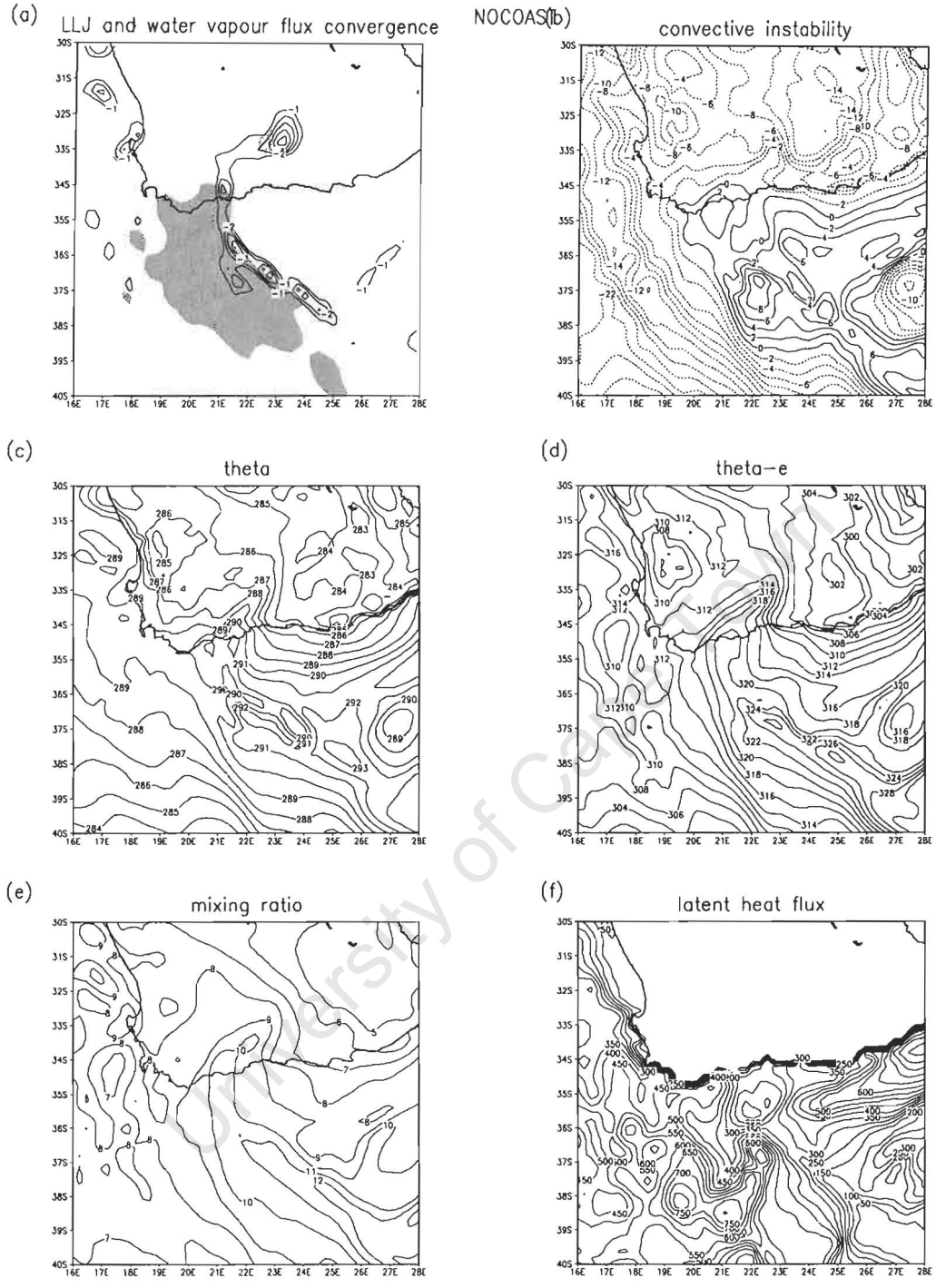

Figure 7.18 – As in Fig. 7.14, except for the NOCOAST experiment

University of Cape Town

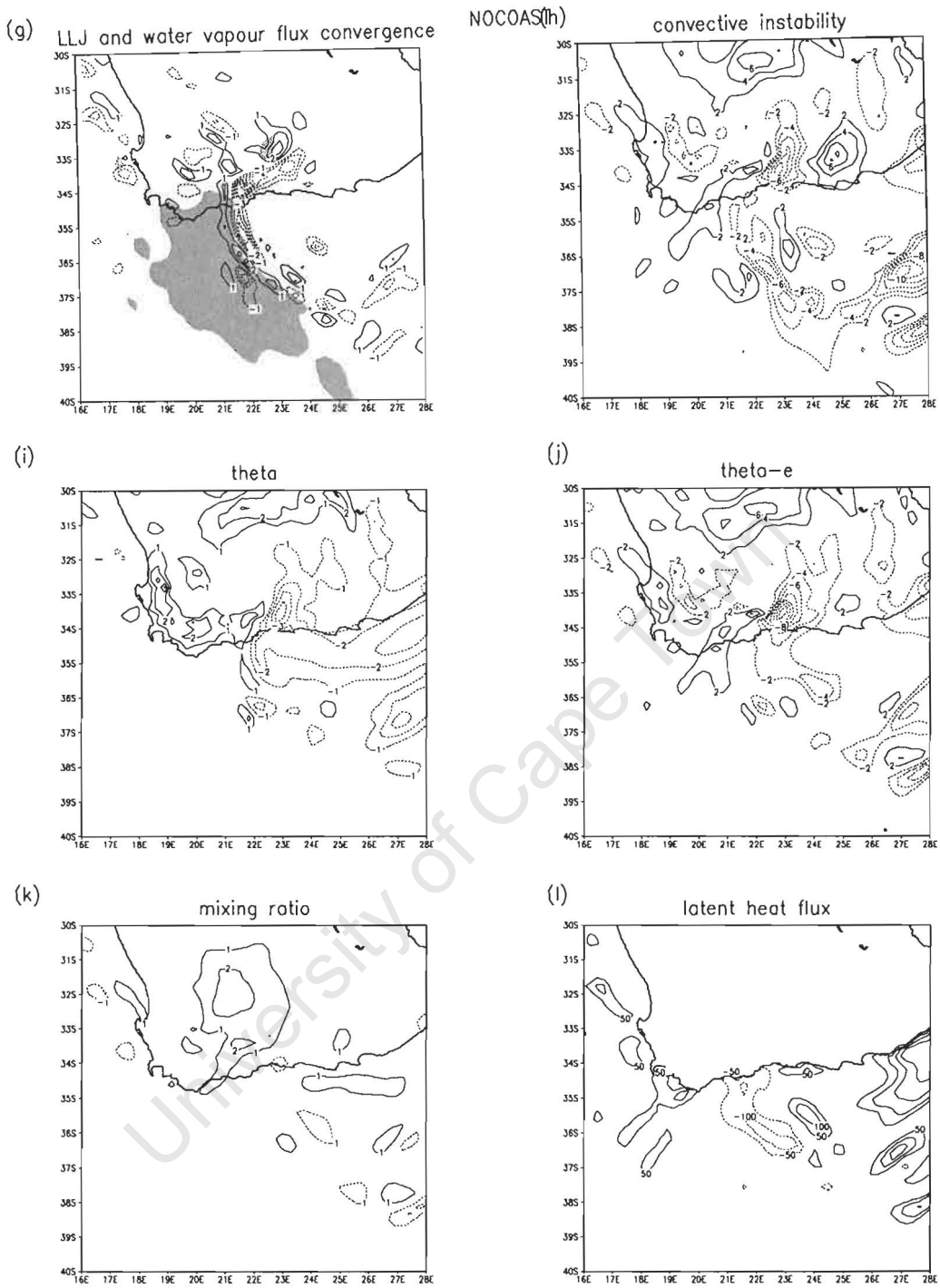

Figure 7.18 - *continued*

University of Cape Town

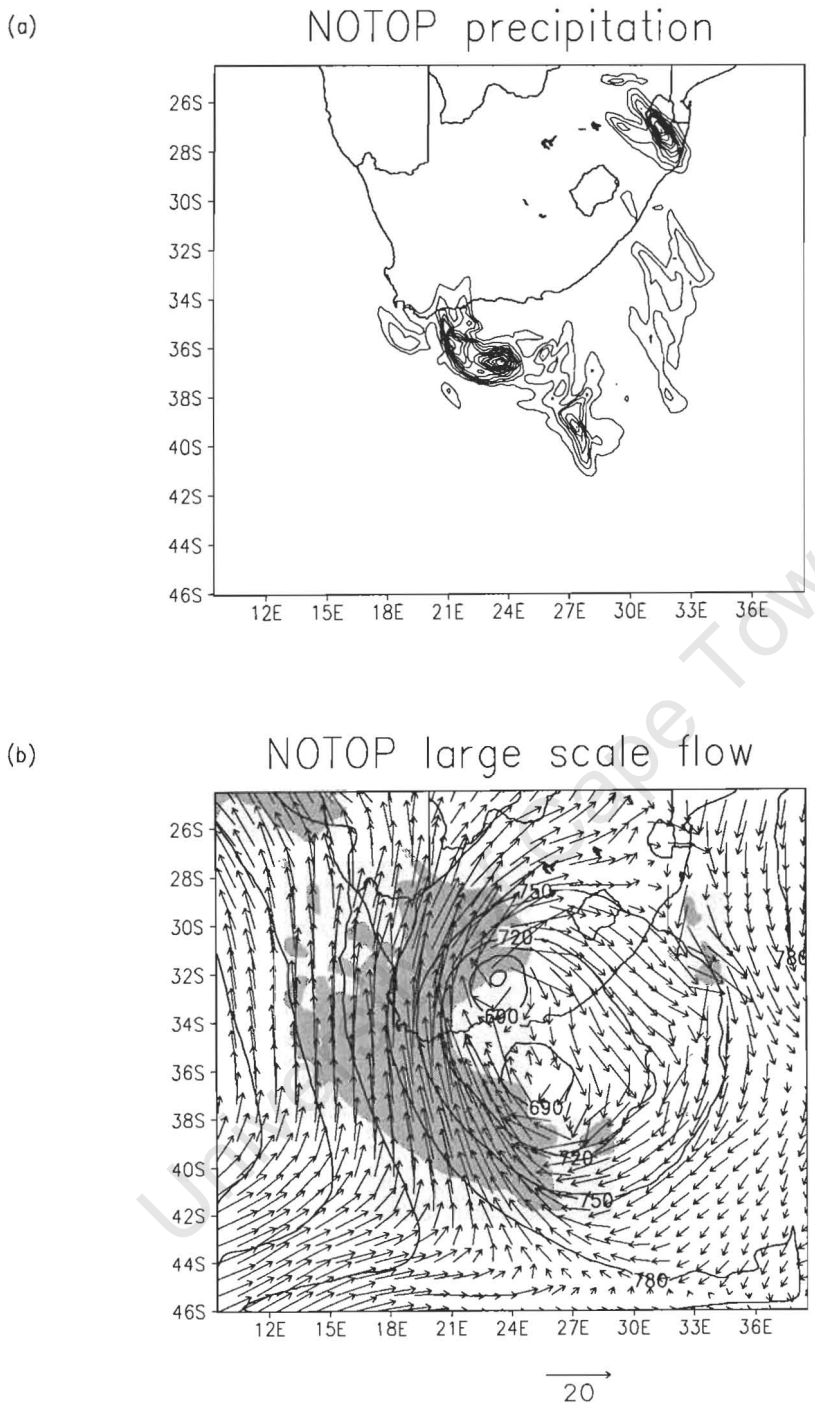

Figure 7.19 – As in Fig. 7.13, except for the NOTOP experiment

University of Cape Town

(c)

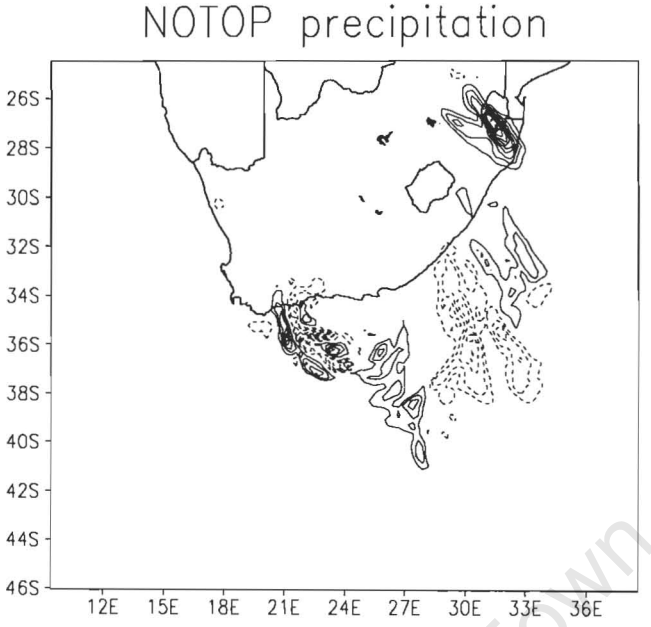

(d)

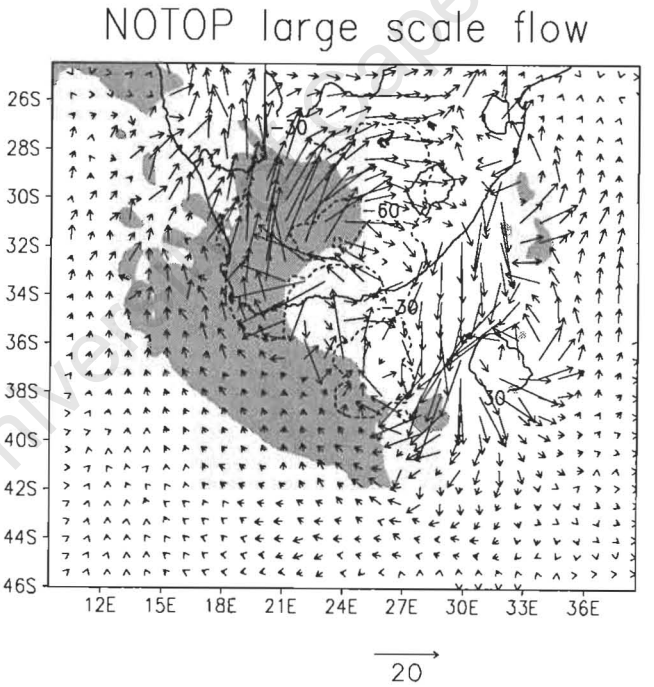

Figure 7.19 - *continued*

University of Cape Town

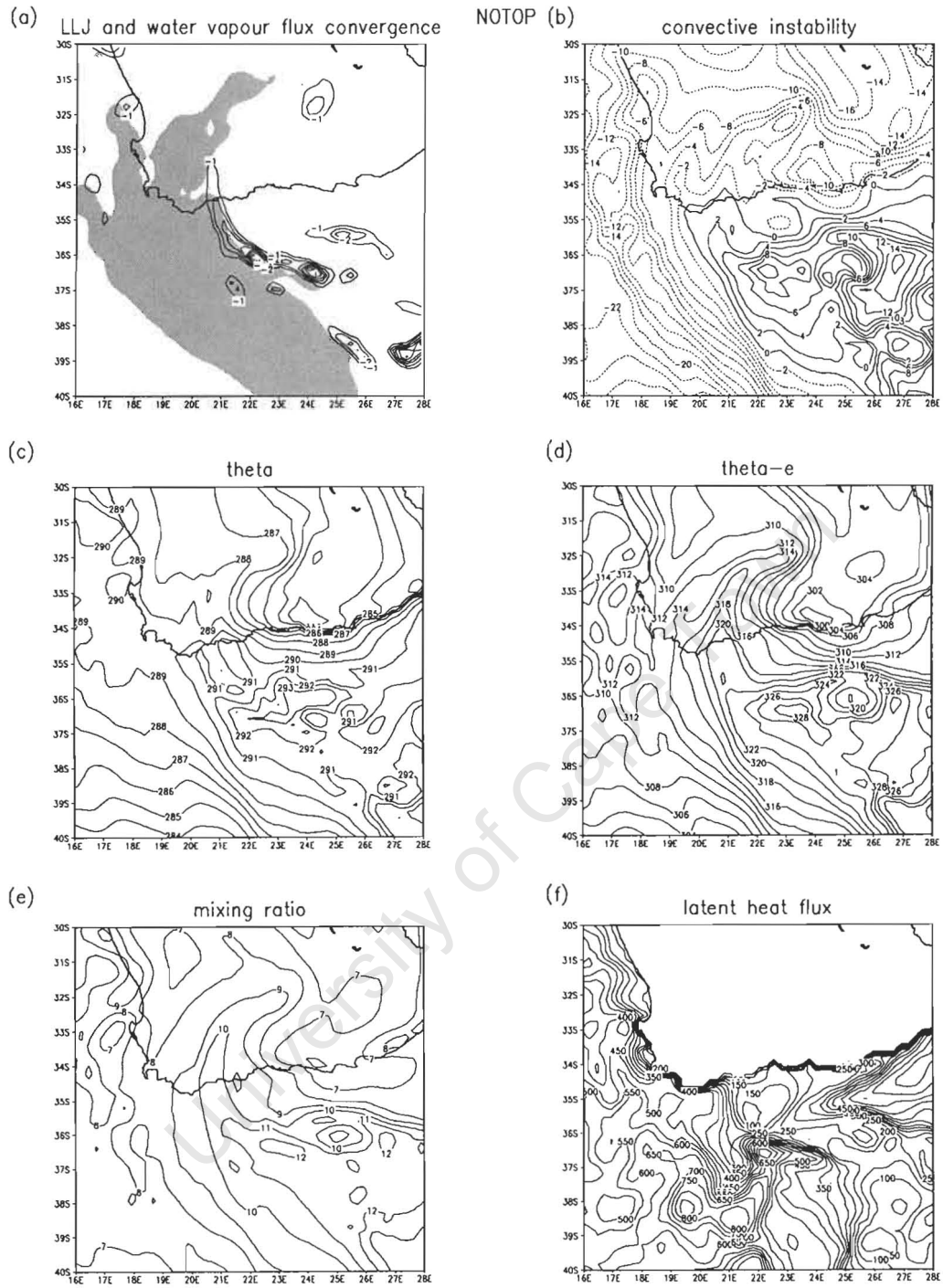

Figure 7.20 – As in Fig. 7.14, except for the NOTOP experiment

University of Canterbury

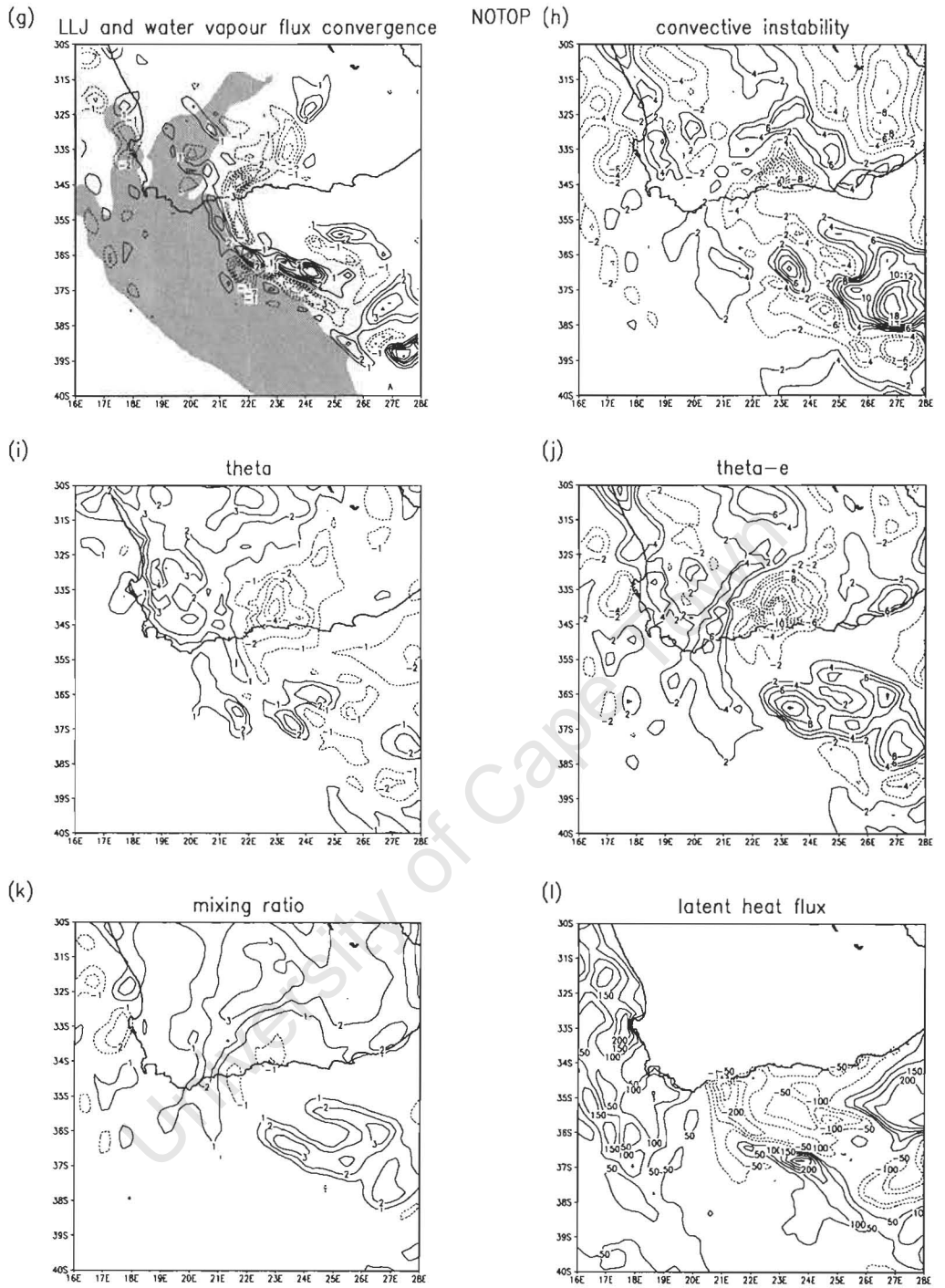

Figure 7.20 - *continued*

University of Cape Town

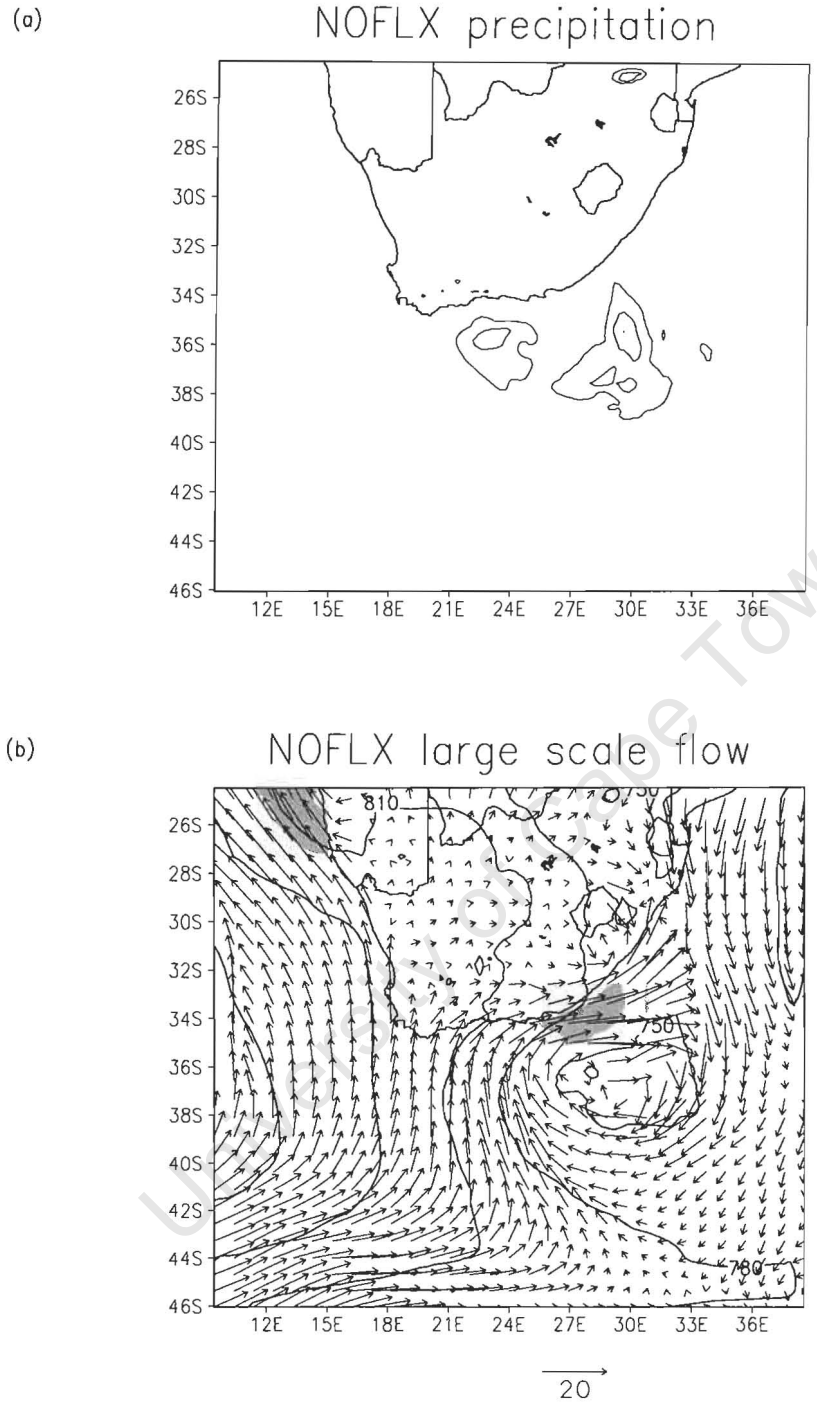

Figure 7.21 – As in Fig. 7.13, except for the NOFLX experiment

University of Cape Town

(c)

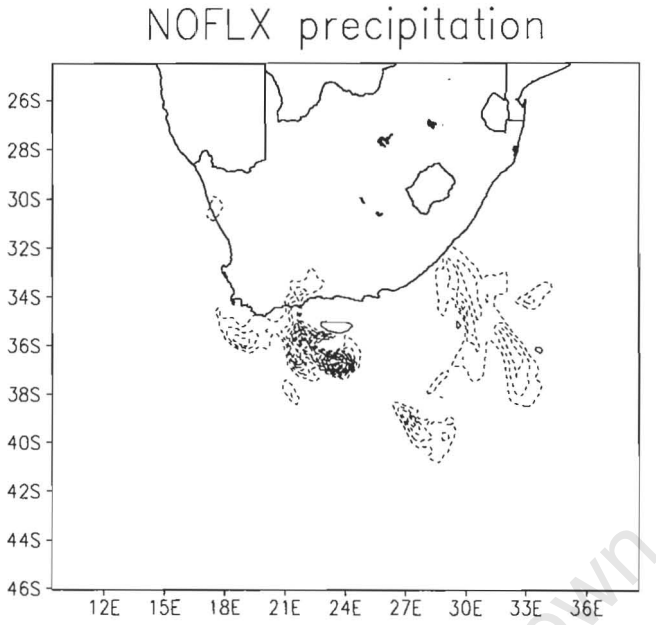

(d)

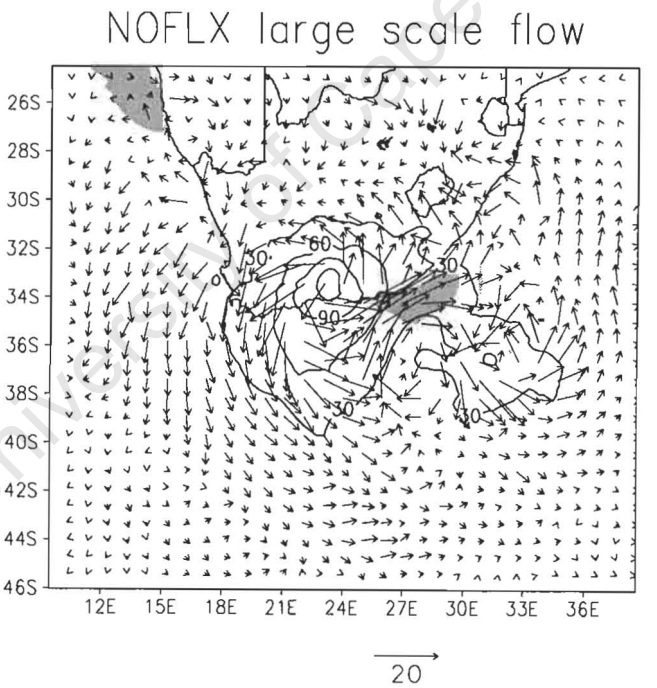

University of Cape Town

Figure 7.21 - *continued*

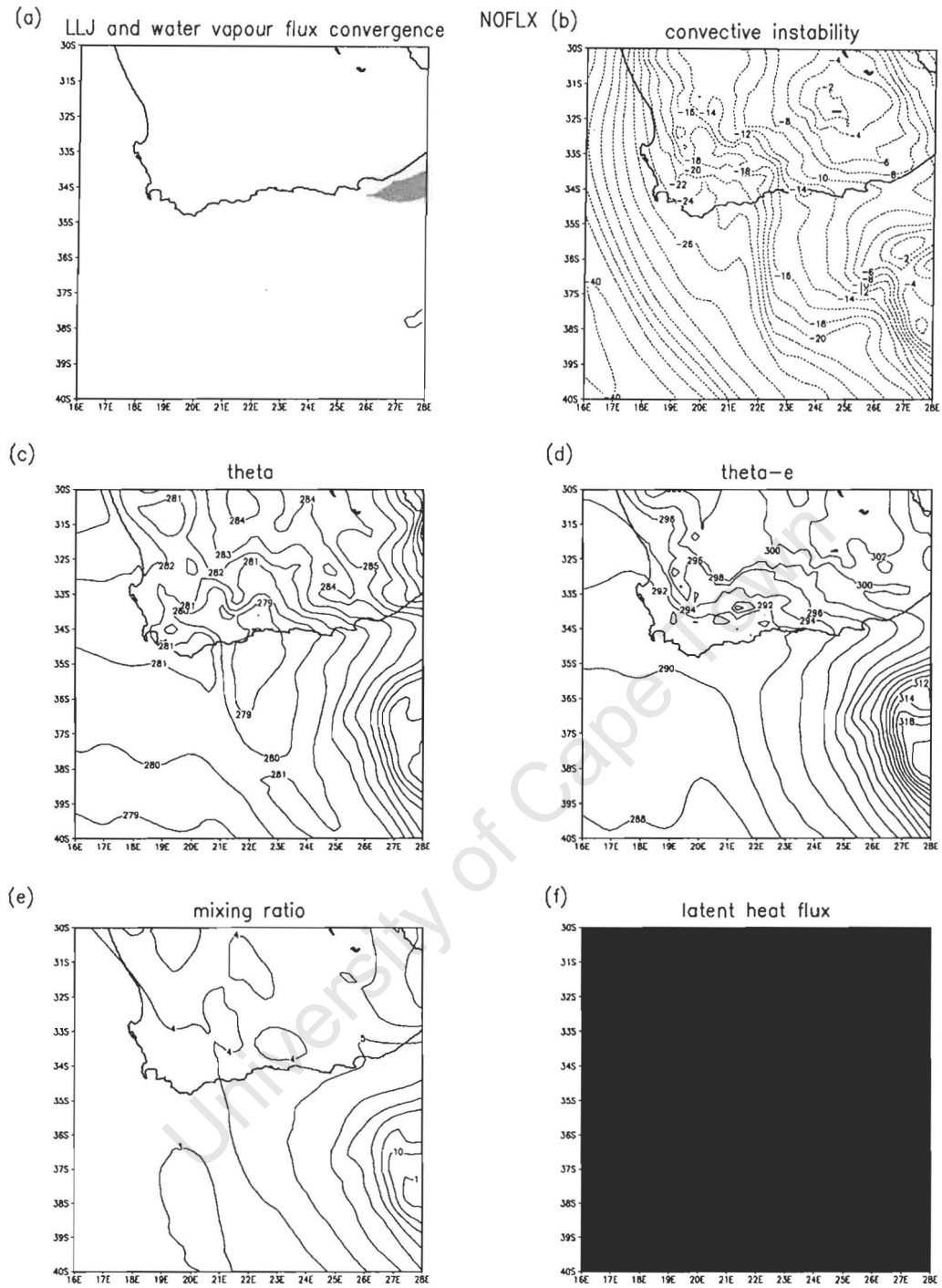

Figure 7.22 – As in Fig. 7.14, except for the NOFLX experiment

University of Cape Town

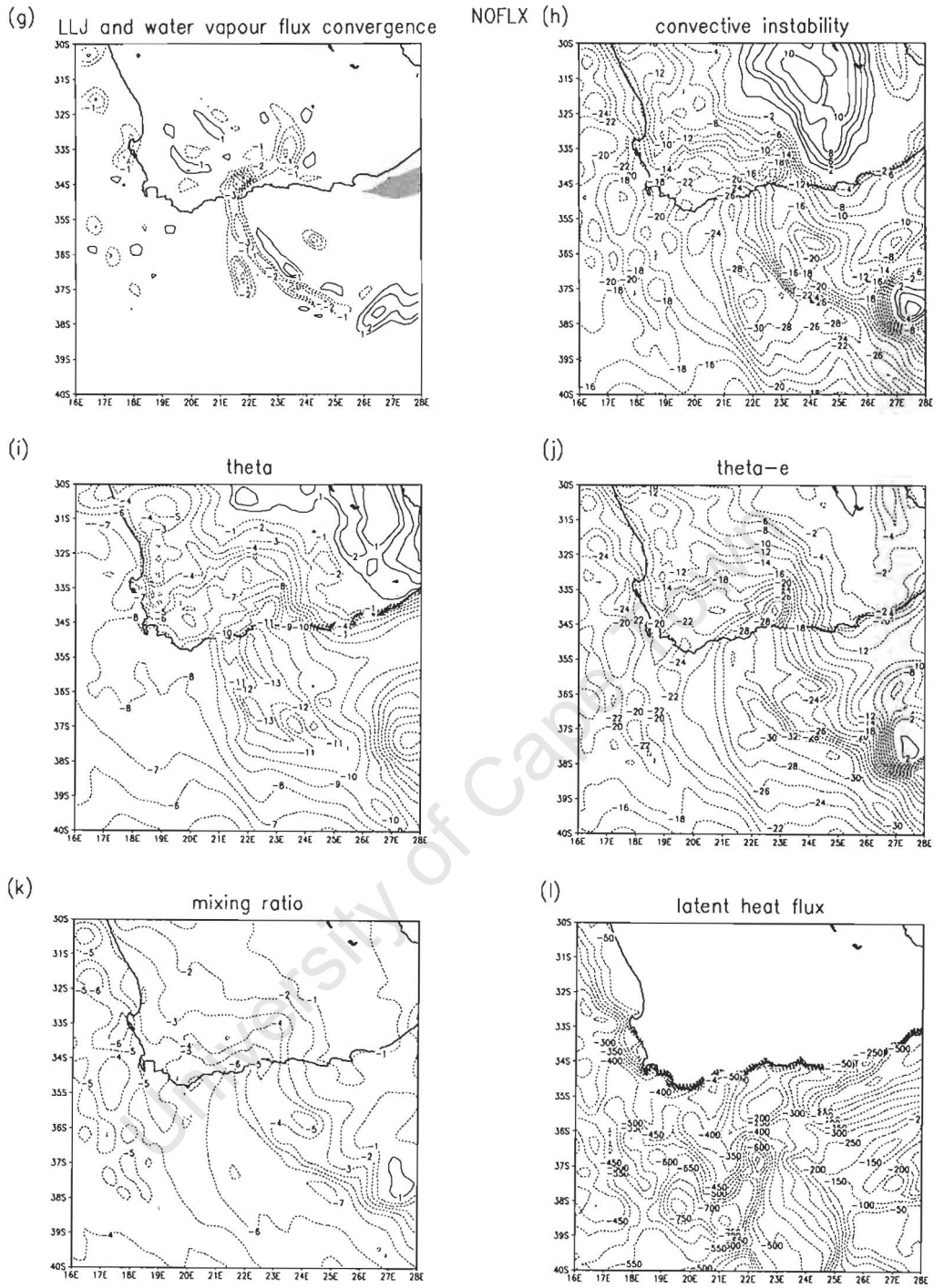

Figure 7.22 - *continued*

University of Cape Town

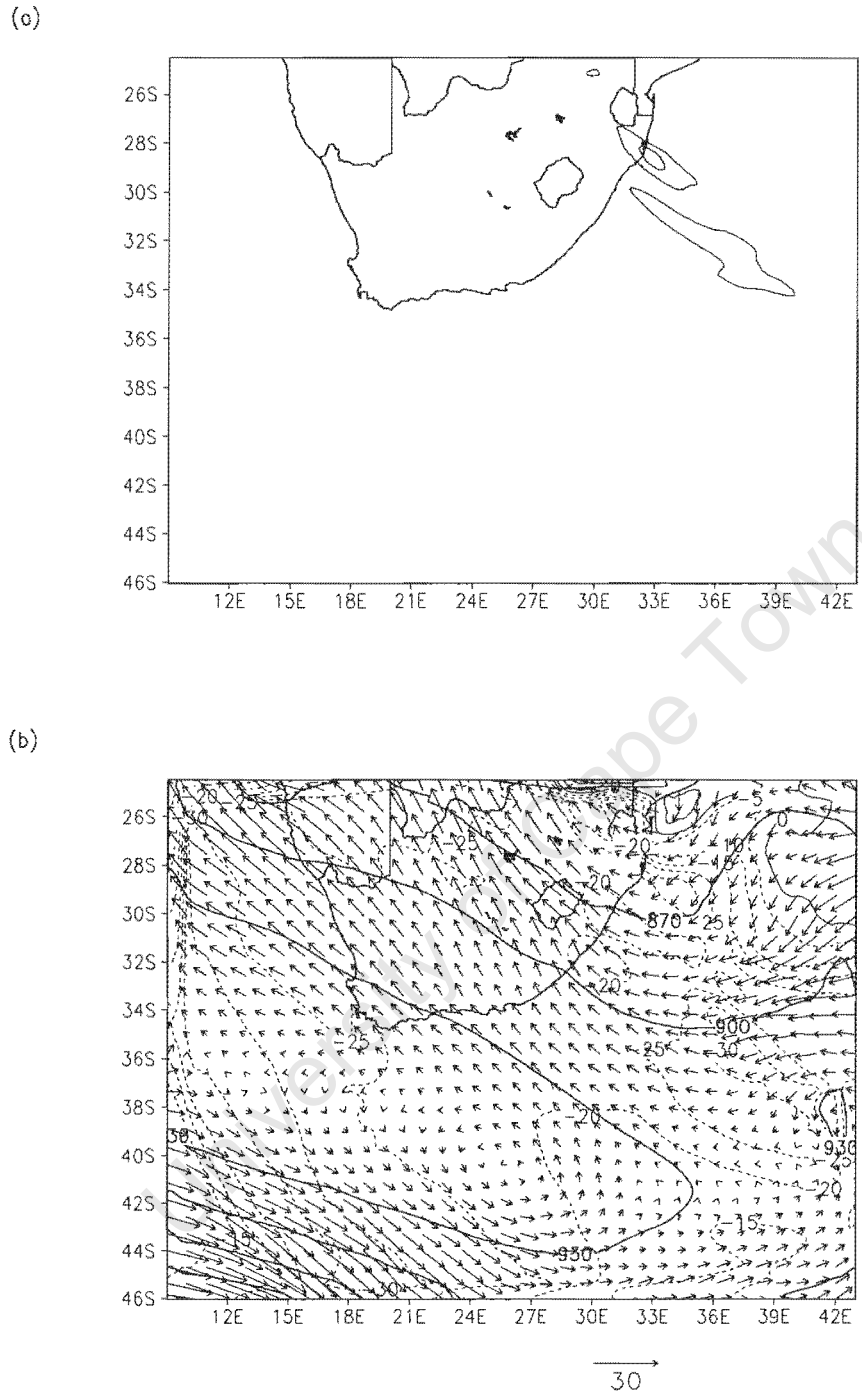

Figure 7.23 – Output of the reference experiment, f_o, for the East London case (a) Rainfall for the 24-hour period to 0600 UTC 16 August 2002, contour interval 20mm starting at 20mm; (b) 925 hPa geopotential height (thick contours, interval 30m); wind vectors, with a vector scale given to the bottom right of the panel; and convective instability, taken as the difference in equivalent potential temperature between the 1000- and 500-hPa levels (thin contours, interval 5K, with solid (dashed) contours representing convectivel unstable (stable) stratification, at the reference time, 0000 UTC 16 August 2002.

University of Cape Town

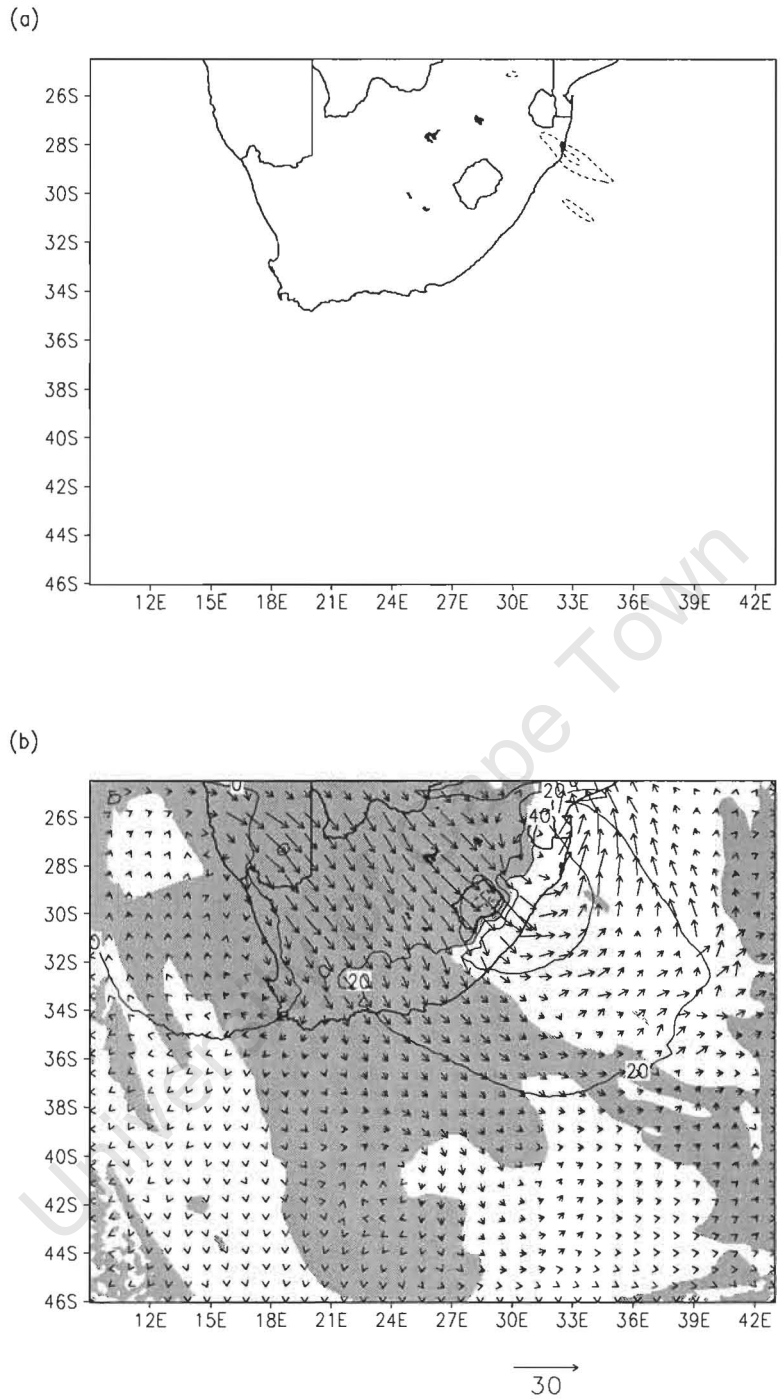

Figure 7.24 – Contribution of topography, f_1^* to (a) rainfall for the 24-hour period to 0600 16 August 2002 (contour interval 20mm, with solid (dashed) contours representing a positive (negative) contribution); and to (b) 925 hPa geopotential height anomaly (contour interval 20m, with solid (dashed) contours representing a positive (negative) contribution. Wind vector anomalies at 925 hPa, with a vector scale given to the bottom right of the panel. Shading represents an increase in convective instability, at the reference time, 0000 UTC 16 August 2002, for the East London case.

University of Cape Town

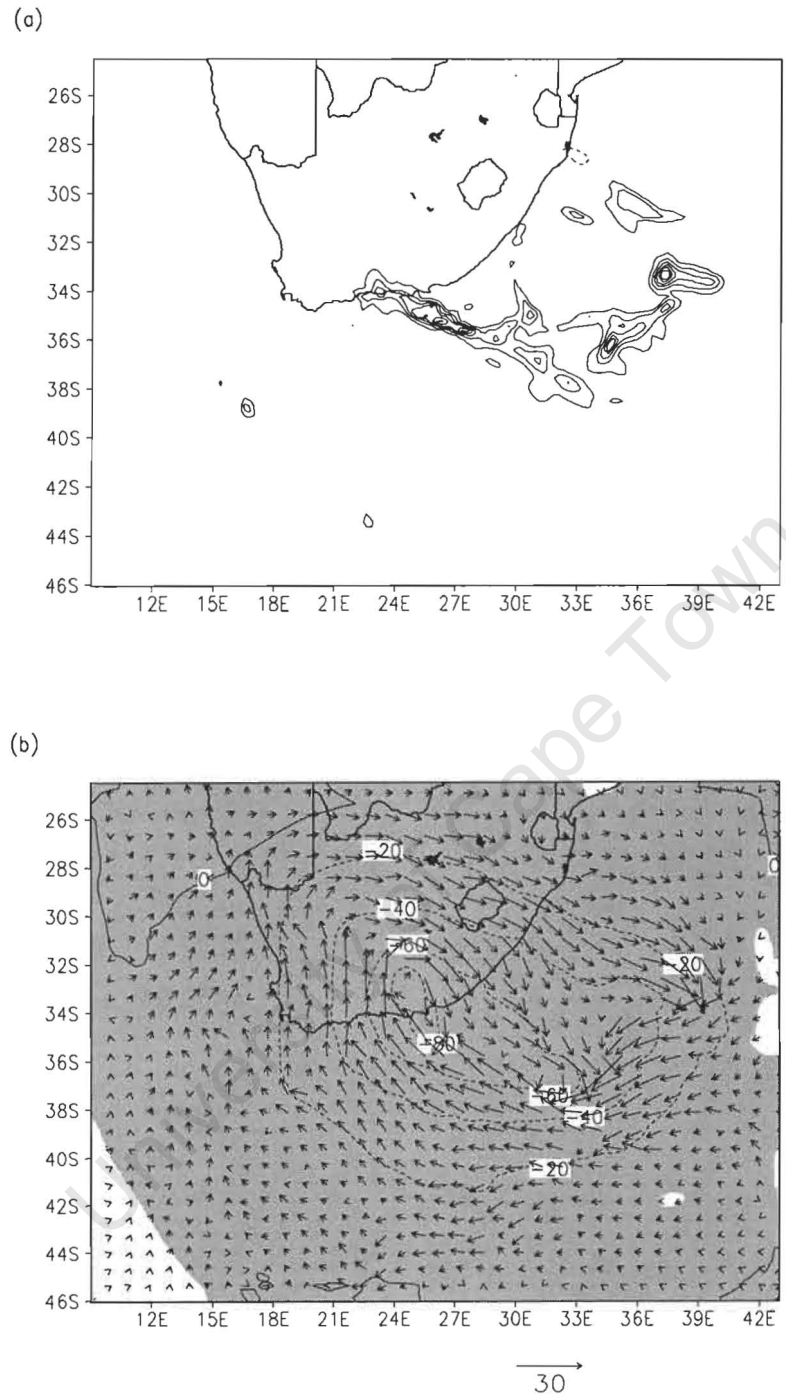

Figure 7.25 – As in Fig. 7.24, except for the contribution of surface heat fluxes, f_2*

University of Cape Town

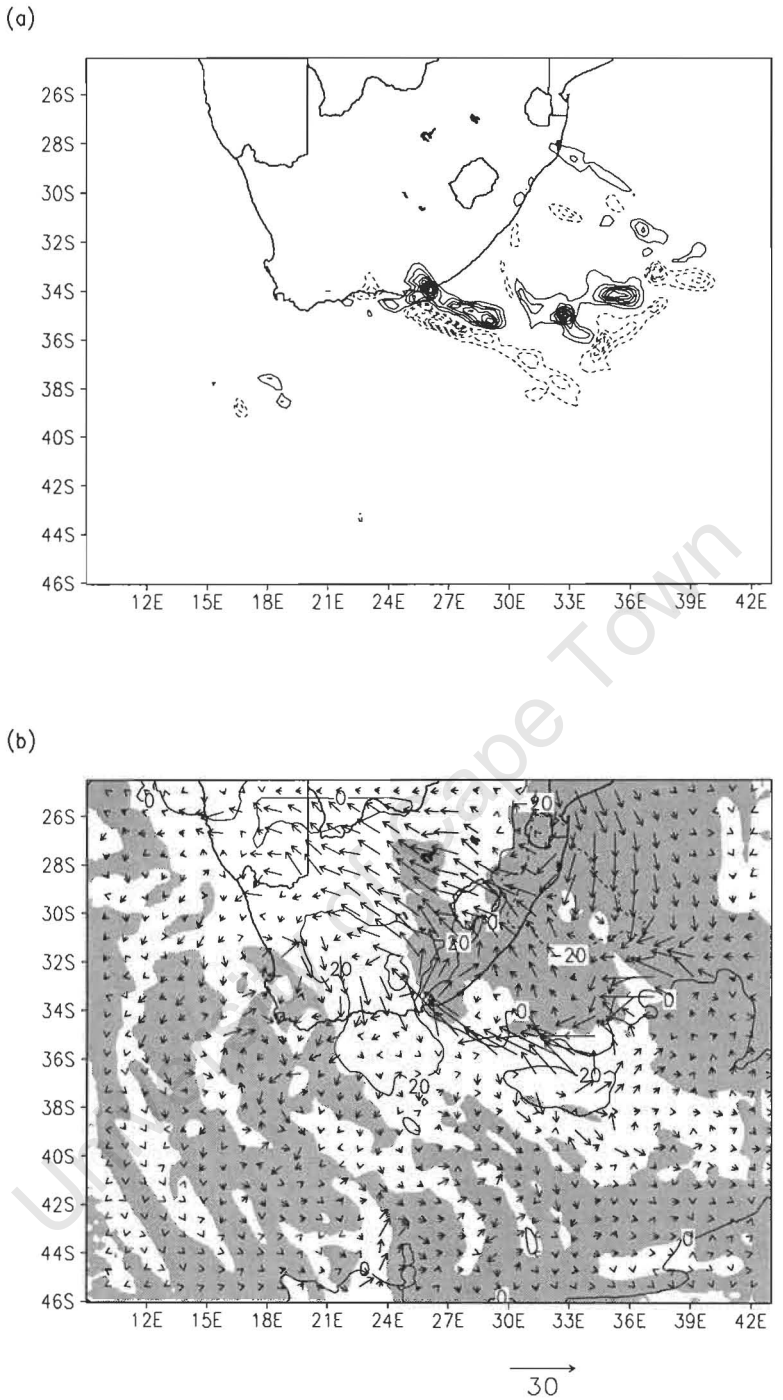

Figure 7.26 – As in Fig. 7.24, except for the combined contribution of topography and surface heat fluxes, f_{12}*

University of Cape Town

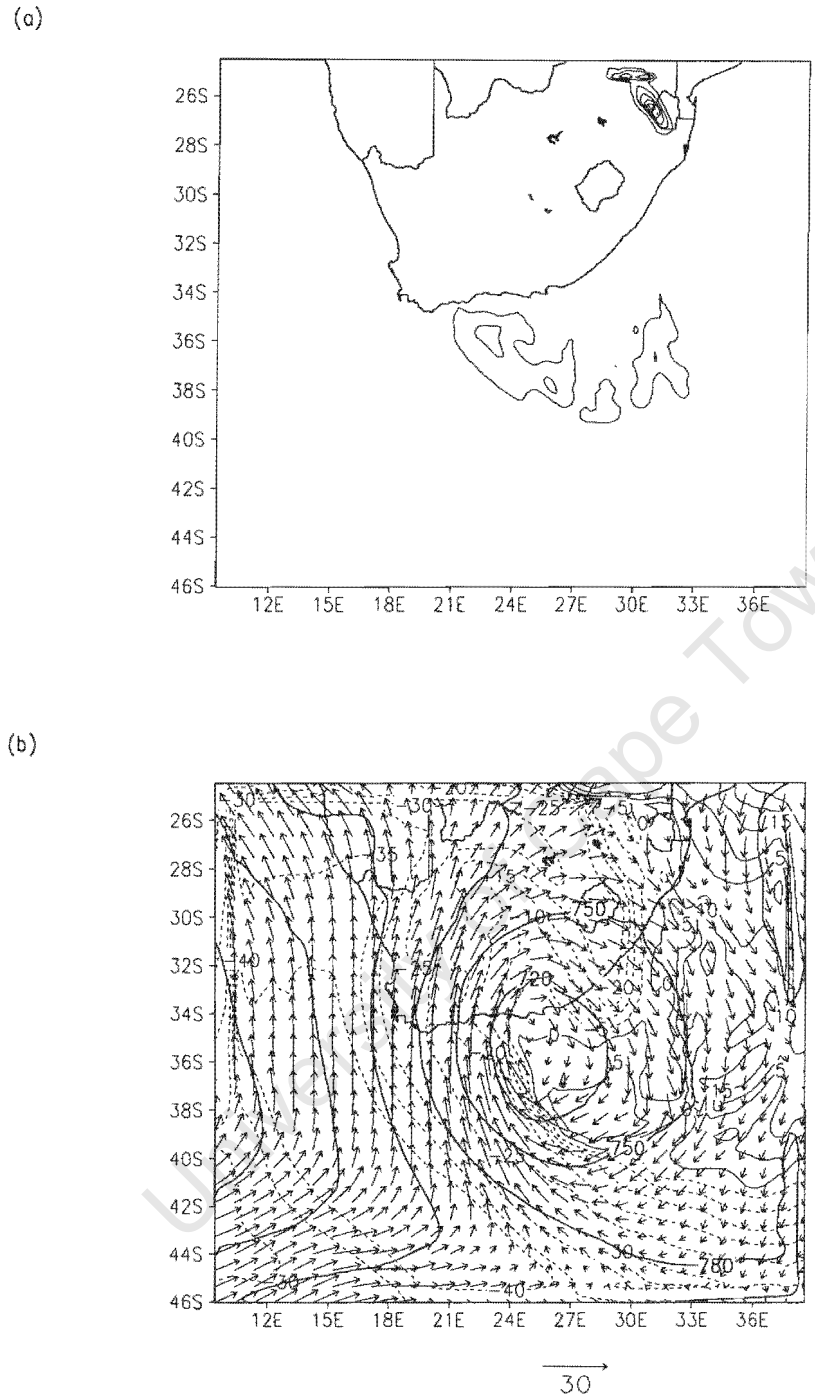

Figure 7.27 - Output of the reference experiment, f_o, for the Montagu case (a) Rainfall for the 24-hour period to 0600 UTC 24 March 2003, contour interval 20mm starting at 20mm; (b) 925 hPa geopotential height (thick contours, interval 30m); wind vectors, with a vector scale given to the bottom right of the panel; and convective instability, taken as the difference in equivalent potential temperature between the 1000- and 500-hPa levels (thin contours, interval 5K, with solid (dashed) contours representing convectivel unstable (stable) stratification, at the reference time, 0400 UTC 24 March 2003.

University of Cape Town

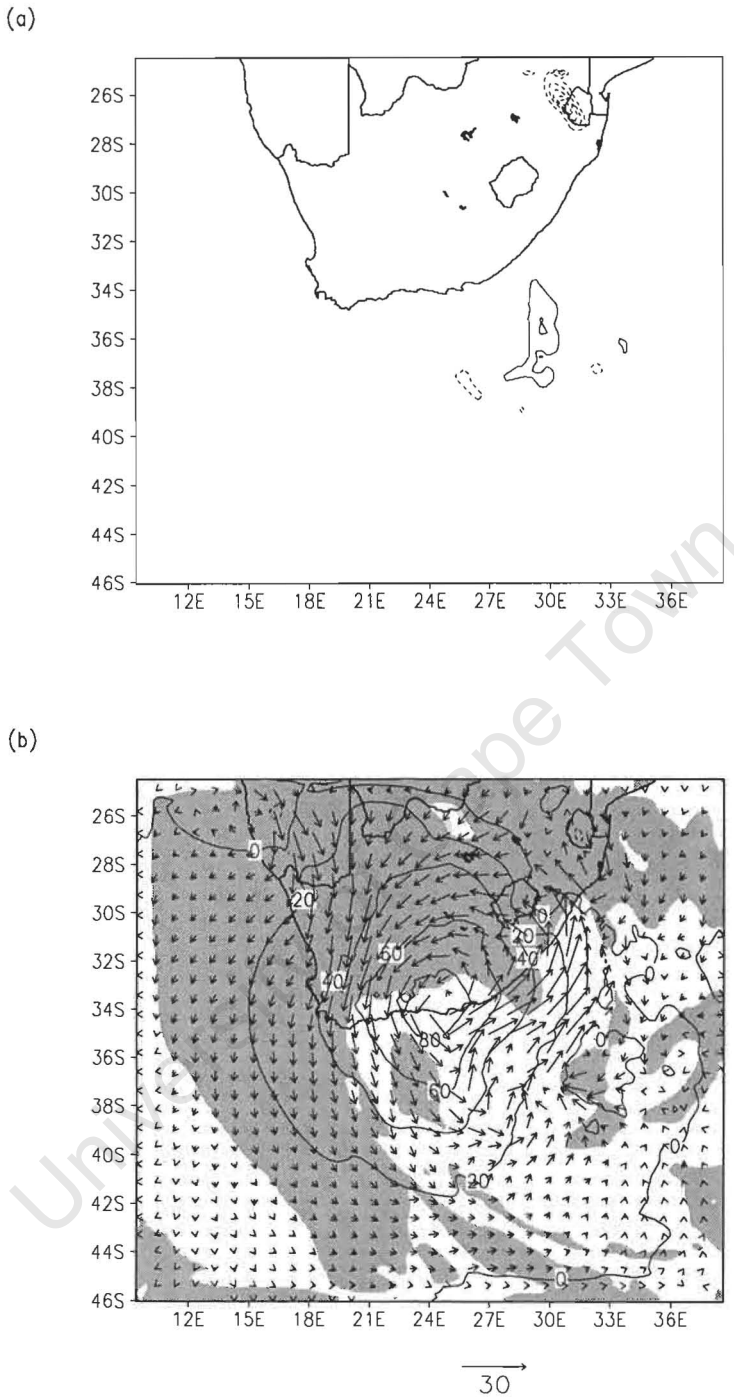

Figure 7.28 - Contribution of topography, f_1* to (a) rainfall for the 24-hour period to 0600 UTC 24 March 2003 (contour interval 20mm, with solid (dashed) contours representing a positive (negative) contribution); and to (b) 925 hPa geopotential height anomaly (contour interval 20m, with solid (dashed) contours representing a positive (negative) contribution. Wind vector anomalies at 925 hPa, with a vector scale given to the bottom right of the panel. Shading represents an increase in convective instability, at the reference time, 0400 UTC 24 March 2003, for the Montagu case.

University of Cape Town

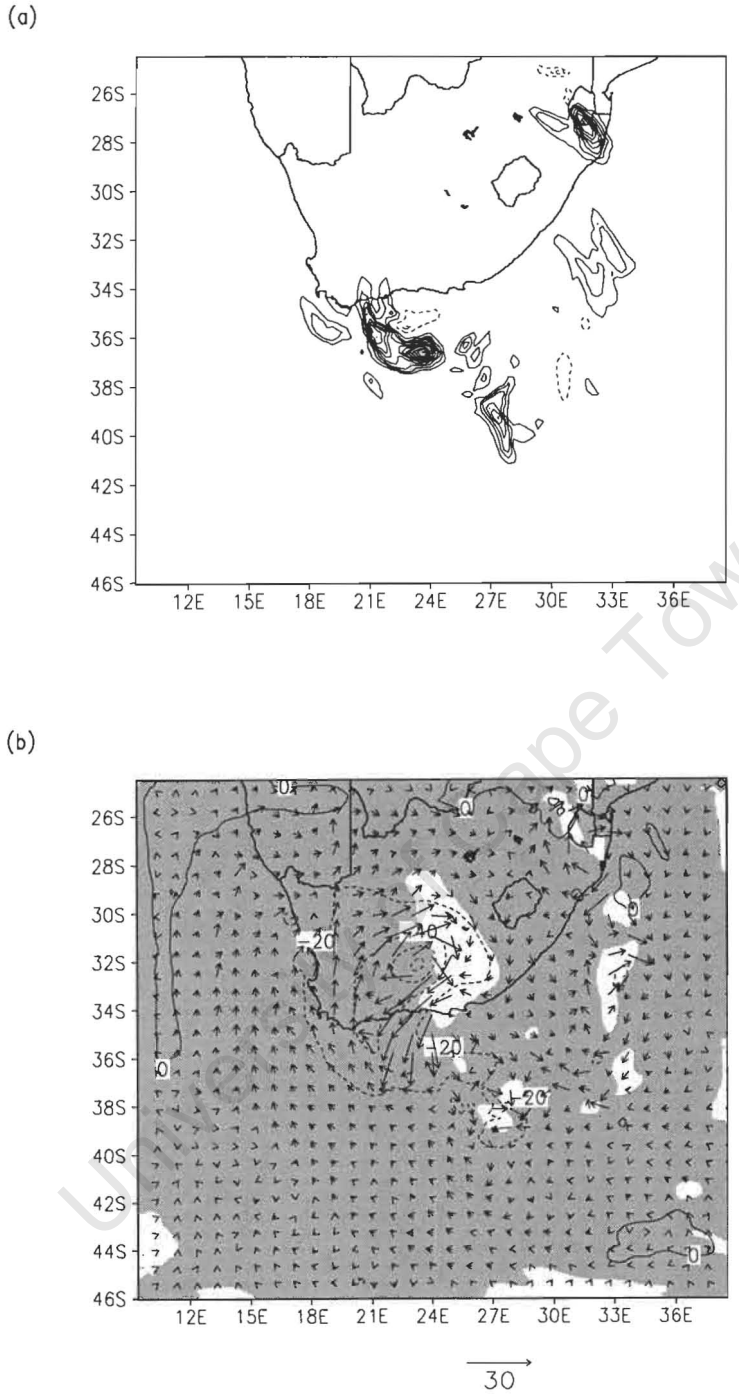

Figure 7.29 – As in Fig. 7.28, except for the contribution of surface heat fluxes, f_2*

University of Cape Town

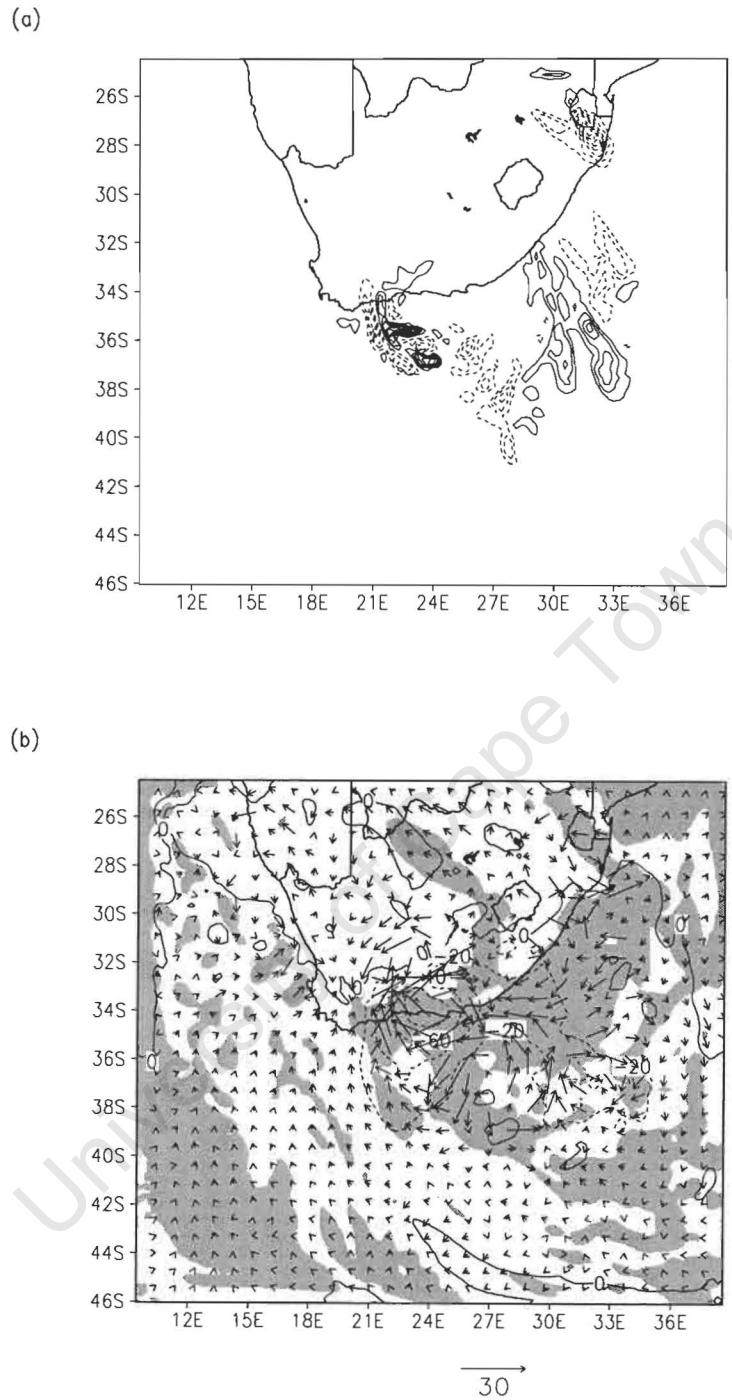

Figure 7.30 – As in Fig. 7.28, except for the combined contribution of topography and surface heat fluxes

University of Cape Town

Chapter 8

Conclusions

University of Cape Town

University of Cape Town

8.1. Introduction

This thesis has presented an examination of cut-off low pressure systems over South Africa. These systems have been shown to be responsible for extreme rainfall events over South Africa over recent decades (e.g. Haywood and van den Berg 1968, 1970; Estié 1981; Triegaardt et al. 1988). In this thesis, various aspects of cut-off low pressure systems over South Africa have been examined. Their seasonality, interannual variability and associations with large scale modes in the Southern Hemisphere were investigated in Chapter 4. Chapters 5-7 presented case studies of two recent cut-off low events, both of which resulted in extreme amounts of rainfall over coastal regions of South Africa. These case studies were diagnosed through an examination of analysis fields from the MRF model in Chapter 5, and further investigated in Chapters 6 and 7 through simulations using the MM5 limited area model.

Important aspects concerning possible associations of cut-off lows with large scale modes in the Southern Hemisphere, which were hitherto unknown, are summarised in section 8.2 of this chapter. Important characteristics of the development of the low-level flow during extreme rainfall producing cut-off lows, which were identified in the MM5 simulations, are discussed in section 8.3 of this chapter. Section 8.4 presents a summary of this chapter, and of the thesis as a whole, in relation to its implications for forecasting over South Africa.

University of Cape Town

8.2. Seasonality, interannual variability and associations with large scale modes in the Southern Hemisphere

A 30-year (1973-2002) climatology of cut-off lows over subtropical southern Africa and the surrounding oceans was developed in this thesis. This represented an extension of the work of Taljaard (1985), which examined 10 years of data (1973-1982), and is widely used as a reference for cut-off low studies over South Africa. There were several similarities between the 30-year climatology and Taljaard's (1985) 10-years of data. These included an average of approximately 11 systems per year over the region, and relative peaks in the frequency of the spring and autumn seasons.

The interannual variability of cut-off lows appears to have no coherent trend over the 30 years of data examined. However, a possible relationship to ENSO was identified. Mature phase La Niña years appeared to be associated with high occurrences of cut-off lows over subtropical southern Africa. To some extent, the opposite El Niño association was also true, but the association was much less robust.

The 30-year climatology also revealed a possible association between the Semi-Annual Oscillation (SAO) in the Southern Hemisphere, and the frequency and location of cut-off lows over subtropical southern Africa. The relative peaks in cut-off frequencies in spring and autumn suggested a phasing similar to that of the SAO, and so possible relationships with changes in the SAO were investigated. It was found that a well documented weakening of the SAO after 1979 (van Loon et al. 1993; Hurrell and van Loon 1994; van Loon and Tourpali 1995; Chen and Yen 1997; Meehl et al. 1998),

University of Cape Town

approximately coincided with a change in the most common location and preferred season for cut-off low occurrences over subtropical southern Africa.

During the 1970s, cut-off lows were most common over the southwest of South Africa (region A in Chapter 4), and MAM was the preferred season. In the 1980s, however, the most common location for cut-off lows moved to the northeast South Africa area (region D in Chapter 4), and JJA became the preferred season. This happened as a result of increased meridional flow to the west of South Africa, and a strengthening of the ridge to the southeast of South Africa in JJA, favouring both the formation of meridionally extensive troughs and cutting-off over the northeast of South Africa. Conversely, in MAM, there was a strengthening of the zonal flow to the west of South Africa, leading to less favourable conditions for the formation of troughs that may become cut-off over subtropical southern Africa.

These results present new evidence of relationships between cut-off lows over subtropical southern Africa and large scale modes in the Southern Hemisphere. In particular, changes in the SAO appear to strongly influence the location and seasonality of cut-off lows over this region.

8.3. Cut-off lows and extreme rainfall

Two recent cut-off low events that resulted in extreme rainfall over coastal regions of South Africa were chosen as case studies for this thesis. These two cases are in some senses at opposite ends of the spectrum in terms of their seasonality and size. The first case study was the "East London" event in August 2002 (winter), which resulted in more than 300mm (approximately four

University of Cape Town

times the monthly average) of rainfall measured at East London over a single 24-hour period. The second case study was the "Montagu" event in March 2003 (late summer), which resulted in extreme amounts of rainfall over much of the south coast of the Western Cape and flash flooding at Montagu, some 150km inland of the coast, where 178mm of rain fell in 24 hours (compared to the climatological average for March of 19.5mm).

Analysis fields from the MRF model highlighted the differences and similarities between the two events. The Montagu case was characterised by a spatially large cut-off low that extended from the upper air down to the surface, and tracked east along the south coast of South Africa. In contrast the East London case was characterised by much smaller cut-off low, which was situated over the southwest of South Africa, and split into two systems, with the second cut-off becoming situated off the west coast of Namibia. For this case, the construction of tropopause maps of potential temperature proved to be particularly useful in following the evolution of the upper air, and the splitting of the cut-off low into two systems. In addition, in the East London case, the cut-off low did not extend down to the surface in the MRF analysis fields. Despite these differences, both systems resulted in extreme rainfall.

University of Cape Town

At the surface, both cases were characterised by strong ridging of high pressure over the ocean to the south of South Africa, which has been shown to be typical of these systems (Taljaard 1985). In addition, both cases were characterised by a strong onshore low-level jet (LLJ) impinging onto the coast where rainfall was most intense. While strong onshore flow has been identified in the past as a characteristic of cut-off low events resulting in

extreme rainfall, the relationship of this onshore flow with the extreme rainfall has not been fully examined. This thesis has attempted to examine this relationship by simulating these two events using a limited area model, MM5.

In both cases, there were some discrepancies in the MM5 simulations in reproducing the exact location of the extreme rainfall maxima and the LLJ. However, MM5 was able to capture the salient large scale features of these events. Running the model with increased horizontal resolution led to only small improvements in the location of the precipitation maxima, but it was felt that the massive increase in computational expense this required did not justify further experiments at high resolution for the purposes of this thesis.

The model simulations showed that areas of vigorous convection were present at the leading edge of the LLJ, and its right-hand edge looking downstream. On the right-hand edge of the LLJ, convection was a result of a strong airmass contrast between cold, relatively high latitude, air being advected by the ridge from the south, and warm moist tropical air being advected down the eastern seaboard of South Africa by a surface trough. Associated with the LLJ was a tongue of warm moist air, which extended onto the land where convection occurred at the leading edge of the LLJ. Convection there was enhanced as the LLJ impinged on the coastal topography.

In addition, back trajectories calculated from the MM5 simulations suggested that the warm SST of the Agulhas Current, and in the Montagu case its retroflection region, may have contributed to the low-level moisture for these

University of Cape Town

events as high latent heat fluxes were present there. Furthermore, in the Montagu case, these back trajectories suggested that the LLJ may have been enhanced by momentum transfer from flow at upper levels.

In order to evaluate the factors that influenced these extreme rainfall cut-off low events, a series of sensitivity experiments were constructed. The influence of SST, topography and surface heat fluxes were examined. It was found that these factors were all important, to varying degrees, for both cases.

In the East London case, both the warm SST of the Agulhas Current, and the mesoscale structure of the SST were particularly influential. The warm SST of the Agulhas Current enhanced the low-level winds over it through secondary cyclogenesis, allowing the LLJ to advect warm moist air onto the coast. In addition, the mesoscale structure of the SST had an influence on the location of the secondary cyclogenesis and therefore the LLJ and the convection associated with its leading edge. In the Montagu case, however, the warm SST of the Agulhas Current appeared to be much less important. It is likely that this was due to the cooler SST of the Agulhas Bank directly to the south of the region of extreme coastal rainfall, resulting in a smaller fetch of the LLJ over warm SST. Experiments with heat fluxes from the surface set to zero showed that heat fluxes were vital in generating the convective environment necessary for the extreme rainfall to occur in both cases.

Topography was found to be a very important contributing factor in both cases. The coastal topography was shown to be particularly important in enhancing moist ascent, and confining the moist maritime air to coastal

University of Cape Town

regions in the Montagu case. Unfortunately, it was difficult to draw any conclusions with regard to the influence of the coastal topography in the East London case due to the introduction of spurious circulations in this experiment. The topography of South Africa as a whole was shown to be particularly important in blocking synoptic scale onshore flow, which helped to provide the necessary pressure gradient forcing for the LLJ.

A factor separation study was done to isolate the individual and combined effects of the topography of South Africa and heat fluxes from the surface. This study enabled the construction of a conceptual model which describes the evolution of the low-level flow during these extreme rainfall cut-off low events. Although only two case studies were examined, the results seem sufficiently robust for such a conceptual model to be applied to all severe rainfall inducing cut-off lows. This conceptual model is described below.

- *Surface heat fluxes add heat and moisture to the lower atmosphere leading to the extension of a trough down the eastern seaboard of South Africa.*
- *As the surface fluxes warm the lower atmosphere, it becomes convectively unstable and considerable precipitation is generated.*
- *The South African topography blocks onshore flow leading to a steep pressure gradient between a ridge over the ocean to the south of South Africa and the aforementioned trough, and thus the formation of a LLJ.*

University of Cape Town

- *This LLJ advects moist air onto the coast of South Africa where its ascent is enhanced by the coastal topography.*

This thesis has therefore culminated in a conceptual model that describes some of the processes that influence the evolution of the low-level flow during cut-off low events over South Africa. Of course it must be borne in mind that this conceptual model only considers a proportion of those factors that influence the development of the low-level flow, and other factors not considered here in any detail, such as the upper level forcing, may also have played an important role.

8.4. Implications and recommendations

This thesis has led to a number of conclusions that may be of use to the meteorological community in South Africa. Firstly, by identifying potential relationships between cut-off lows and large scale modes in the Southern Hemisphere, an indication of cut-off low occurrences over South Africa may be obtained from changes in these large scale modes. With further research, it may be possible to incorporate these relationships into, for example, seasonal forecasts. Given the vulnerability of the region's large and poor rural population to the impacts of severe weather, further investigation into the possibility of seasonally forecasting cut-off low occurrences would be of great importance.

Secondly, in terms of individual cut-off low events resulting in extreme rainfall, this thesis has highlighted the importance of an onshore LLJ and its relationship with vigorous convection. This LLJ has been shown to form as a

University of Cape Town

result of an interaction between surface heat fluxes and the topography of South Africa. This suggests that is important that these factors be properly included into forecast models. This is especially important in that has been shown that surface heat fluxes over the Agulhas Current tend to be strongly underestimated in NCEP and ECMWF (European Centre for Medium-range Weather Forecasting) analyses (Rouault et al. 2003). Moreover, the SST of the Agulhas Current has been shown to be influential, particularly in the East London case, where the warm core of the current was near to the coast. This result suggests that it is very important that forecast models used for South African applications have an accurate, high resolution representation of the SST in the Agulhas Current region, particularly in areas where the warm SST is near to the coast. In addition, further insight into to the processes leading to extreme rainfall in these events may be gained by investigating cut-off lows that did not result in large quantities of precipitation.

Furthermore, this thesis has demonstrated the usefulness of the MM5 model for investigating severe weather systems. While mesoscale modelling rarely yields perfect results, it is possible to gain considerable understanding of these events, especially in areas such as South Africa where the observational network near the coast is sparse. With only four daily coastal radiosonde ascents, and relatively few inland, it is impossible to fully investigate mesoscale details of the evolution of cut-off low events from observations alone. Ideally, one would combine a field program with a modelling study for a more complete picture.

University of Cape Town

There are also a number of avenues that may be explored to shed further light on cut-off low events. For example, an ensemble of model simulations may be undertaken with some perturbations applied to the initial conditions. This may prove to be useful in further determining the role played by the SST in the Agulhas Current region. In terms of relationships between cut-off lows and large scale modes of the Southern Hemisphere circulation, a spectral analysis that isolates zonal wave number 3 may provide further insight into any influence that the SAO has on cut-off low events over South Africa.

University of Cape Town

References

University of Cape Town

University of Cape Town

Baines, P., 1979: Observations of stratified flow past three-dimensional barriers. *J. Geophys. Res.*, **84,** 7834-7837.

Barnes, S.L., and C.W. Newton, 1986: Thunderstorms in the synoptic setting. *Thunderstorm Morphology and Dynamics,* 2d ed., E. Kessler, Ed., University of Oklahoma Press, 75-112.

Barsby, I. and R.D. Diab, 1995: Total ozone and synoptic weather relationships over southern Africa and surrounding oceans. *J. Geophys. Res.,* **100,** 3023-3033.

Bell, G.D., and L.F. Bosart, 1993: A case study diagnosis of the formation of an upper level cyclonic circulation over the eastern United States. *Mon. Wea. Rev.*, **121,** 1635-1655.

Bell, G.D. and D. Keyser, 1993: Shear and curvature vorticity and potential vorticity interchanges: Interpretation and application to a cut-off cyclone event. *Mon. Wea. Rev.,* **121,** 76-102.

Binder, P., and A. Rossa, 1995: The Piedmont flood: Operational prediction by the Swiss model. *MAP Newsl.,* **2,** 12-16.

Blackadar, A.K., 1957: Boundary layer wind maxima and their significance for the formation of nocturnal inversions. *Bull. Amer. Meteor. Soc.,* **38,** 283-290.

University of Cape Town

Buzzi, A., N. Tartaglione, C. Cacciamani, T. Paccanella, and P. Patruno, 1995: Preliminary meteorological analysis of the Piedmont flood of November 1994. *MAP Newsl.,* **2,** 2-6.

Chen, C., W.-K. Tao, P.-L. Lin, G.S. Lai, S.F. Tseng, and T.-C. Chen, 1998: The intensification of the low-level jet during the development of mesoscale convective systems on a Mei-Yu front. *Mon. Wea. Rev.,* **126,** 349-371.

Chen, F., and J. Duddhia, 2001a: Coupling an advanced land-surface / hydrology model with the Penn State / NCAR MM5 modeling system. Part I: Model implementation and sensitivity. *Mon. Wea. Rev.,* **129,** 569-585.

Chen, F., and J. Duddhia, 2001b: Coupling an advanced land-surface / hydrology model with the Penn State / NCAR MM5 modeling system. Part II: Preliminary model validation. *Mon. Wea. Rev.,* **129,** 587-604.

Chen, G.T.-J., and C.-C. Yu, 1988: Study of low-level jet and extremely heavy rainfall over northern Taiwan in the Mei-Yu season. *Mon. Wea. Rev.,* **116,** 884-891.

Chen, Q., 1982: The instability of the gravity inertia wave and its relationship to low-level jet and heavy rainfall. *J. Meteorol. Soc. Jpn.,* **60,** 1041-1057.

Chen, S.-J. Y.-H. Kuo, W. Wang, Z.-Y. Tao, and B. Cui, 1998: A modeling case study of heavy rainfall along the Mei-Yu front. *Mon. Wea. Rev.,* **126,** 2330-2351.

University of Cape Town

Chen, T.-S. and M.-C. Yen, 1997: Interdecadal variation of the Southern Hemisphere circulation. *J. Clim.,* **10,** 805-812.

Chen, Y.-L., X.-A. Chen, S. Chen, and Y.-H. Kuo, 1997: A numerical study of the low-level jet during TAMEX IOP5. *Mon. Wea. Rev.,* **125,** 2583-2604.

Colberg, F., C.J.C. Reason, and K. Rodgers, 2004: South Atlantic response to ENSO induced climate variability in an OGCM. *J. Geophys. Res.*, **109,** 10.1029/2004JC002301.

Colle, B.A., and A.F. Mass, 2000: The 5-9 February 1996 flooding event over the Pacific Northwest: Sensitivity studies and evaluation of the MM5 precipitation forecast. *Mon. Wea. Rev.,* **128,** 593-617.

Cressman, G., 1959: An operational analysis system. *Mon. Wea. Rev.,* **87,** 367-374.

Crimp, S.J., J.R.E. Lutjeharms, and S.J. Mason, 1998: Sensitivity of a tropical temperate trough to sea surface temperature anomalies in the Agulhas retroflection region. *Water SA,* **24,** 93-100.

Crimp, S.J., and S.J. Mason, 1999: The extreme precipitation event of 11 to 16 February 1996 over South Africa. *Meteor. Atmos. Phys.,* **70,** 29-42.

University of Cape Town

Darbyshire, J., 1964: A hydrological investigation of the Agulhas Current area. *Deep Sea Res.*, **11,** 781-815.

Davidson, N.E., K. Kurihara, T. Kato, G. Mills, and K. Puri, 1998: Dynamics and prediction of a mesoscale extreme rain event in the Baiu front over Kyushu, Japan. *Mon. Wea. Rev.*, **126,** 1608-1629.

Dickinson, R.B.B., and H.H. Neumann, 1982: The occurrence of nocturnal low-level jets in New England and the Canadian Maritimes. *Atmos.-Ocean,* **20,** 287-300.

Dirks, R.A., J.P. Kuettner, and J.A. Moore, 1988: Genesis of Atlantic Lows Experiment (GALE): Overview. *Bull. Amer. Meteor. Soc.*, **69,** 148-160.

Doswell, C.A. III, H.E. Brooks and R.A. Maddox, 1996: Flash flood forecasting: An ingredients based methodology. *Wea. Forecasting,* **11,** 560-581.

Doyle, J.D., 1997: The influence of mesoscale orography on a coastal jet and rainband. *Mon. Wea. Rev.*, **125,** 1465-1488.

Doyle, J.D., and T.T. Warner, 1991: A Carolina coastal low-level jet during GALE IOP 2. *Mon. Wea. Rev.*, **119,** 2414-2428.

University of Cape Town

Doyle, J.D., and T.T. Warner, 1993a: The impact of the sea surface temperature resolution on mesoscale coastal processes during GALE IOP 2. *Mon. Wea. Rev.,* **121,** 313-334.

Doyle, J.D., and T.T. Warner, 1993b: A numerical investigation of coastal frontogenesis and mesoscale cyclogenesis during GALE IOP 2. *Mon. Wea. Rev.,* **121,** 1048-1077.

Estié, K.E., 1981: The Laingsburg flood disaster of January 1981. *South African Weather Bureau Newsletter,* **383,** 19-32.

Fehlmann, R., C. Quadri, and H.C. Davies, 2000: An Alpine rainstorm: Sensitivity to mesoscale upper level structure. *Wea. Forecasting,* **15,** 4-28.

Grell, G.A., 1993: Prognostic evaluation of assumptions used by cumulus parameterizations. *Mon. Wea. Rev.,* **121,** 764-787.

Grell, G.A., J. Dudhia, and D.R. Stauffer, 1994: A description of the fifth generation Penn State/NCAR mesoscale model (MM5). NCAR Tech. Note NCAR/TN-398 + STR. 122pp.

Haywood, L.Q. and H. Van den Berg, 1968: Die Port Elizabeth storeëns van 1 September 1968. *South African Weather Bureau Newsletter,* **234,** 157-169.

Haywood, L.Q. and H. Van den Berg, 1970: The Eastern Cape floods of 24-28 August 1970. *South African Weather Bureau Newsletter,* **257,** 129-141.

University of Cape Town

Holton, J.R., 1967: The diurnal boundary layer wind oscillation above sloping terrain. *Tellus,* **19,** 199-205.

Hong, S.-Y., and H.-L. Pan, 1996: Nonlocal boundary layer vertical diffusion in a medium-range forecast model. *Mon. Wea. Rev.,* **124,** 2322-2339.

Hoskins, B.J., M.E. McIntyre, and A.W. Robertson, 1985: On the use and significance of isentropic potential vorticity maps. *Quart. J. Roy. Met. Soc.,* **111,** 877-946.

Hseih, Y.-P., 1949: An investigation of a selected cold vortex over North America. *J. Meteorol.,* **6,** 401-410.

Hurrell, J.W. and H. van Loon, 1994: A modulation of the atmospheric annual cycle in the Southern Hemisphere. *Tellus,* **46A,** 325-338.

Jury, M.R., 1993: A thermal front within the marine atmospheric boundary layer over the Agulhas Current south of Africa: Composite aircraft observations. *J. Geophys. Res.,* **99,** 3297-3304.

Jury, M.R., and S. Courtney, 1991: A transition in weather over the Agulhas Current. *S. Afr. J. Mar. Sci.,* **10,** 159-171.

Jury, M.R., H.R. Valentine, and J.R.E. Lutjeharms: Influence of the Agulhas Current on summer rainfall along the southeast coast of South Africa. *J. Appl. Meteor.,* **32,** 1282-1287.

University of Cape Town

Jury, M.R., and N.D. Walker, 1988: Marine boundary layer modification across the edge of the Agulhas Current. *J. Geophys. Res.*, **93,** 647-654.

Kalnay, M. Kanamitsu, and W.E. Baker, 1990: Global numerical weather prediction at the National Meteorological Center. *Bull. Amer. Meteor. Soc.*, **71,** 1410-1428.

Kalnay, E., M. Kanamitsu, R. Kistler, W. Collins, D. Deavan, L. Gandin, M. Iredell, S. Sarah, G. White, K. Woollen, Y. Zhu, M. Chelliah, W. Ebisuzaki, W. Higgens, J. Janowiak, K.C. Mo, C. Ropolewski, J. Wang, A. Leetmaa, R. Reynolds, R. Jenne, and D. Joseph, 1996: The NCEP/NCAR 40-year reanalysis project. *Bull. Amer. Meteor. Soc.*, **77,** 437-471.

Kanamitsu, M., 1989: Description of the NMC global data assimilation and forecast system. *Wea. Forecasting,* **4,** 335-342.

Kanamitsu, M., J.C. Alpert, K.A. Campana, P.M. Caplan, D.G. Deaven, M. Iredell, B. Katz, H.-L. Pan, J. Sela, and G.H. White, 1991: Recent changes implemented into the global forecast system at NMC. *Wea. Forecasting,* **6,** 425-435.

Karoly, D.J., 1995: Observed variability of the Southern Hemisphere atmospheric circulation. *Natural Climate Variability on Decade-Century Time Scales,* D.G. Martinson et al., Eds., National Research Council, 111-119.

University of Cape Town

Kidson, J.W. 1988: Interannual variations in the Southern Hemisphere circulation. *J. Climate*: **1**, 1177–1198

Kleinshmidt, E., 1950a: Uber aufbau und entstehung von zyklonen I. Teil. *Meteor. Rundschau.* **3,** 1-7.

Kleinshmidt, E., 1950b: Uber aufbau und entstehung von zyklonen II. Teil. *Meteor. Rundschau.* **3,** 54-61.

Lee-Thorpe, A.M., M. Rouault, and J.R.E. Lutjeharms, 1998: Cumulus cloud formation above the Agulhas Current. *S. Afr. J. Sci.,* **94,** 351-354.

Lee-Thorpe, A.M., M. Rouault, and J.R.E. Lutjeharms, 1999: Moisture uptake in the boundary layer above the Agulhas Current. *J. Geophys. Res.,* **104,** 1423-1430.

Lutjeharms, J.R.E., R. Catzel, and H.R. Valentine, 1989: Eddies and other border phenomena of the Agulhas Current. *Cont. Shelf. Res.,* **9,** 597-616.

Lutjeharms, J.R.E., J. Cooper, and M. Roberts, 2000: Upwelling at the inshore edge of the Agulhas Current. *Cont. Shelf Res.,* **20,** 737-761.

Lutjeharms, J.R.E., R.D. Mey, and I.T. Hunter, 1986: Cloud lines over the Agulhas Current. *S. Afr. J. Sci.,* **82,** 635-640.

Lutjeharms, J.R.E., and R.C. van Ballegooyen, 1988: The retroflection of the Agulhas Current. *S. Afr. J. Sci.,* **94,** 351-354.

University of Cape Town

Mason, S.J., 1995: Sea surface temperature – South African rainfall associations, 1910-1989. *Int. J. Climatol.,* **15,** 119-135.

Matsuomo, S., 1972: Unbalanced low-level jet and solenoidal circulation associated with heavy rainfalls. *J. Meteorol. Soc. Jpn.,* **50,** 194-203.

Matsuomo, S., 1973: Lower tropospheric wind speed and precipitation activity. *J. Meteorol. Soc. Jpn.,* **51,** 101-107.

McNider, R.T., and R.A. Pielke, 1981: Diurnal boundary layer development over sloping terrain. *J. Atmos. Sci.,* **38,** 2198-2212.

Meehl, G.A., J.W. Hurrell, and H. van Loon, 1998: A modulation of the mechanism of the semi-annual oscillation in the Southern Hemisphere. *Tellus,* **50A,** 442-450.

Mey, R.D., N.D. Walker, and M.R. Jury, 1990: Surface heat fluxes and marine boundary layer modification in the Agulhas retroflection region. *J. Geophys. Res.,* **95,** 15997-16015.

Mizzi, A.P., and R.A. Pielke, 1984: A numerical study of the mesoscale atmospheric circulation observed during a coastal upwelling event on 23 August 1972. Part I: Sensitivity studies. *Mon. Wea. Rev.,* **112,** 76-90.

Morgan, M.C., and J.W. Neilsen-Gammon, 1998: Using tropopause maps to diagnose midlatitude weather systems. *Mon. Wea. Rev.,* **126,** 2555-2579.

University of Cape Town

Ninomiya, K., and T. Akiyama, 1974: Band structure of mesoscale clusters associated with low-level jet stream. *J. Meteorol. Soc. Jpn.*, **52,** 300-313.

Palmén, E., 1949: On the origin and structure of high level cyclones south of the maximum westerlies. *Tellus,* **1,** 22-31.

Palmén, E., and K.M. Nagler, 1949: The formation and structure of a large scale disturbance in the westerlies. *J. Meteorol.,* **6,** 227-242.

Palmén, E., and C. Newton, 1969: *Atmospheric circulation systems.* Academic Press, New York, 603pp.

Peagle, J., and G.E. Rasch, 1973: Three dimensional characteristics of diurnally varying boundary layer flow. *Mon. Wea. Rev.,* **101,** 746-756.

Pierrehumbert, R.T., and B. Wyman, 1985: Upstream effects of mesoscale mountains. *J. Atmos. Sci.,* **42,** 977-1003.

Preston Whyte, R.A., and P.D. Tyson, 1988: *The Atmosphere and Weather of Southern Africa.* Oxford University Press, 347 pp.

Price, J.D. and G. Vaughan, 1992: Statistical studies of cut-off low systems. *Ann. Geophys.*, **10,** 96-102.

University of Cape Town

Ramaswamy, V., M.D. Schwarzkopf and K.P. Shine, 1992: Radiative forcing of climate from halocarbon induced global stratospheric ozone loss. *Nature*, **355,** 810-812.

Reason, C.J.C., 1998: Warm and cold events in the Southeast Atlantic / Southwest Indian Ocean region and potential impacts on circulation and rainfall over South Africa. *Meteor. Atmos. Phys.,* **69,** 49-65.

Reason , C.J.C., 2001: Evidence for the influence of the Agulhas Current on regional atmospheric circulation patterns. *J. Clim.,* **14,** 2769-2778.

Reason, C.J.C., R.J. Allan, J.A. Lindesay and T.J. Ansell, 2000: ENSO and climatic signals across the Indian Ocean basin in the global context: Part I, interannual composite patterns. *Int. J. Climatol.,* **20,** 1285-1327.

Reason, C.J.C., and H. Mulenga, 1999: Relationships between South African rainfall and SST anomalies in the southwest Indian Ocean. *Int. J. Climatol.,* **19,** 1651-1673.

Reynolds, R.W. and T.M. Smith, 1994: Improved global sea surface temperature analyses using optimum interpolation. *J. Clim.,* **7,** 929-948.

Romero, R., C.A. Doswell III, and C. Ramis, 2000: Mesoscale numerical study of two cases of long-lived quasi-stationary convective systems over eastern Spain. *Mon. Wea. Rev.,* **128,** 3731-3751.

University of Cape Town

Rouault, M., A.M. Lee-Thorpe, I. Ansorge, and J.R.E. Lutjeharms, 1995: The Agulhas Current Air-Sea Exchange Experiment. *S. Afr. J. Sci.,* **91,** 493-496.

Rouault, M., Lee-Thorpe, A.M., and J.R.E. Lutjeharms, 2000: The atmospheric boundary layer above the Agulhas Current during alongcurrent winds. *J. Phys. Oceanogr.,* **30,** 40-50.

Rouault, M., C.J.C. Reason, J.R.E. Lutjeharms, and A.C.M. Beljaars, 2003: Underestimation of latent and sensible heat fluxes above the Agulhas Current in NCEP and ECMWF analyses. *J. Clim.,* **16,** 776-782.

Rouault, M., S.A. White, C.J.C. Reason, J.R.E. Lutjeharms and I. Jobard, 2002: Ocean-atmosphere interaction in the Agulhas Current region and a South African extreme weather event. *Wea. Forecasting,* **17,** 655-669.

Schumann, E.H., L.-A. Perrins, and I.T. Hunter, 1982: Upwelling along the south coast of the Cape Province, South Africa. *S. Afr. J. Sci.,* **78,** 238-242.

Smith, R.B., 1979: The influence of mountains on the atmosphere. *Advances in Geophysics,* Vol. 21, Academic Press, 87-230.

Smolarkiewicz and Rotunno 1990: Low Froude number flow past three-dimensional obstacles. Part II: Upwind flow reversal zone. *J. Atmos. Sci.,* **47,** 1498-1511.

University of Cape Town

Stein, U., and P. Alpert, 1993. Factor separation in numerical simulations. *J. Atmos. Sci.*, **50,** 2107-2115.

Stramma, L., and J.R.E. Lutjeharms, 1997: The flow field of the subtropical gyre of the South Indian Ocean. *J. Geophys. Res.*, **102,** 5513-5530.

Szeredi, I., and D.J. Karoly, 1987: The vertical structure of monthly fluctuations of the Southern Hemisphere troposphere. *Aust. Meteor. Mag.*, **35,** 19-30.

Taljaard, J.J., 1985: Cut-off lows in the South African region. *South African Weather Bureau Tech. Paper,* **14,** 153pp.

Tennant, W., 2004: Considerations when using pre-1979 NCEP/NCAR reanalyses in the southern hemisphere. *Geophys. Res. Lett.*, **31,** 10.1029/2004GL019751.

Tennant, W.J., and J. van Heerden, 1994: The influence of orography and local sea-surface temperature anomalies on the development of the 1987 Natal floods: a general circulation model study. *S. Afr. J. Sci.*, **90,** 45-49.

Triegaardt, D.O., D.E. Terreblanche, J. van Heerden, and M.V. Laing, 1988: The Natal floods of September 1987. *South African Weather Bureau Tech. Paper,* **19,** 62pp.

University of Cape Town

Trüb, J., and H.C. Davies, 1995: Flow over a mesoscale ridge.: Pathways to regime transition. *Tellus,* **47A,** 502-524.

Uccellini., L.W., 1980: On the role pf upper tropospheric jet streaks and leeside cyclogenesis in the development of low-level jets in the Great Plains. *Mon. Wea. Rev.,* **108,** 1689-1696.

Uccellini, L.W., and D.R. Johnson, 1979: The coupling of upper and lower tropospheric jet streaks and implications for the development of severe convection. *Mon. Wea. Rev.,* **107,** 682-703.

Uccellini, L.W., R.A. Peterson, K.F. Brill, P.J. Kocin, and J.J. Tuccillo, 1987: Synergistic interactions between an upper level jet stream and diabatic processes that influence the development of a low-level jet and a secondary coastal cyclone. *Mon. Wea. Rev.,* **115,** 2227-2261.

Van Delden, A., and R. Neggers, 2003: A case study of tropopause cyclogenesis. *Meteorol. Appl.,* **10,** 197-209.

van Loon, H., 1967: The half-yearly oscillations in middle and high southern latitudes and the coreless winter. *J. Atmos. Sci.*, **24**, 472-486.

van Loon, H., J.W. Kidson and B. Mullan, 1993: Decadal variation of the annual cycle in the Australian Dataset. *J. Clim.,* **6,** 1227-1231.

University of Cape Town

van Loon, H. and J.C. Rogers. 1984: Interannual variations in the half yearly cycle of pressure gradients and zonal wind at sea level in the Southern Hemisphere. *Tellus,* **36A,** 76-86.

van Loon, H. and K. Tourpali, 1995: Antarctic ozone and trends in the troposphere of the Southern Hemisphere. *Meteorologica*, **22,** 101-107.

Walker, N.D., 1990: Links between South African summer rainfall and temperature variability of the Agulhas and Benguela Current systems. *J. Geophys. Res.,* **95,** 3297-3319.

Walker, N.D., and J.A. Lindesay, 1989: Preliminary observations of oceanic influences on the February-March 1998 floods in central South Africa. *S. Afr. J. Sci.,* **85,** 164-169.

Yeh, H.-C., and Y.-L. Chen, 2002: The role of offshore convergence on coastal rainfall during TAMEX IOP 3. *Mon. Wea. Rev.,* **130,** 2709-2730.

Zeman, O., 1979: Parameterization of the dynamics of stable boundary layers and nocturnal jets. *J. Atmos. Sci.,* **36,** 792-804.

University of Cape Town

University of Cape Town

Appendix A

Cut-off low dates over sub-tropical southern Africa

University of Cape Town

University of Cape Town

YEAR	MONTH	DAY	DURATION (hours)	REGION	SIZE (km)
1973	2	8	24	C	560
1973	2	16	78	D	1770
1973	3	12	42	D	890
1973	3	19	18	A	670
1973	4	11	42	B	1110
1973	4	20	48	B	780
1973	5	10	36	C	330
1973	7	22	78	D	1500
1973	8	24	60	D	1330
1973	9	28	24	C	220
1973	11	22	48	C	1000
1974	1	4	30	C	330
1974	2	12	60	D	1000
1974	3	17	24	A	610
1974	3	19	66	A	1390
1974	4	19	30	D	780
1974	4	29	78	D	1990
1974	5	4	54	A	1110
1974	5	10	24	D	780
1974	5	17	36	B	1330
1974	6	2	60	B	1220
1974	6	25	24	A	1000
1974	7	2	66	D	1110
1974	8	16	84	A	1770
1974	9	4	30	B	670
1974	12	13	24	C	1110
1975	1	30	48	A	1110
1975	2	13	48	C	670
1975	2	17	24	C	440
1975	2	20	42	C	1060
1975	3	17	78	B	670
1975	3	28	36	C	1220
1975	4	26	24	A	670
1975	6	26	24	A	830
1975	9	27	30	B	560
1976	1	28	60	A	280
1976	2	21	24	B	1000
1976	3	20	48	A	780
1976	4	5	24	D	220
1976	4	29	36	A	780
1976	5	2	54	A	830
1976	5	28	42	A	1550
1976	9	21	30	A	1330
1976	10	3	24	A	560
1976	11	4	30	A	890
1977	1	1	42	B	560
1977	1	26	30	A	440
1977	2	19	30	A	560
1977	3	16	36	B	330
1977	3	30	66	C	780
1977	4	8	48	C	1550

University of Cape Town

YEAR	MONTH	DAY	DURATION (hours)	REGION	SIZE (km)
1977	4	30	30	D	440
1977	5	7	90	A - B	1440
1977	6	16	24	C	440
1977	8	12	42	D	1220
1977	11	30	54	A	1330
1977	12	30	30	A	670
1978	1	2	54	C	670
1978	2	28	84	D	1990
1978	3	17	54	D	1110
1978	3	31	60	A	1000
1978	4	20	90	A	1000
1978	5	2	30	B	560
1978	6	2	30	C	780
1978	8	21	30	B	110
1978	10	4	42	A	670
1979	2	2	60	D	560
1979	3	4	24	B	780
1979	5	22	138	A - B	890
1979	5	24	42	A	1770
1979	7	20	48	A	890
1979	8	19	60	A	560
1979	9	7	90	D	1000
1979	10	20	42	A	780
1980	3	25	48	D	1440
1980	4	26	114	A - B	1330
1980	6	4	48	C	1330
1980	6	21	30	A	440
1980	7	23	132	C	1550
1980	7	30	72	A	1110
1980	8	20	30	C	720
1980	9	8	36	B - D	940
1980	9	23	72	A	1170
1980	11	2	30	C	780
1980	11	27	72	A	1440
1981	1	5	42	A	220
1981	1	24	66	A	1330
1981	3	19	24	C	560
1981	3	24	42	A	890
1981	4	26	42	A	1000
1981	4	29	72	D	1220
1981	5	16	54	D	670
1981	5	28	66	A - B	1330
1981	8	21	84	A	1000
1981	8	28	42	A	1000
1981	9	11	42	B	560
1981	10	16	24	A	220
1981	10	19	24	A	220
1981	12	3	66	A	1110
1982	3	23	36	A - B	440
1982	4	17	54	B	1440
1982	4	22	48	A	1110

University of Cape Town

YEAR	MONTH	DAY	DURATION (hours)	REGION	SIZE (km)
1982	4	28	48	B	670
1982	5	5	36	D	440
1982	7	7	48	D	440
1982	7	23	36	A	440
1982	9	1	42	A	440
1982	10	15	66	C	890
1982	11	2	48	A - B	560
1982	11	14	48	A	780
1983	2	15	24	B	330
1983	3	14	24	C	670
1983	4	6	48	C	1220
1983	4	11	48	B	780
1983	4	24	72	D	1660
1983	5	27	54	D	890
1983	6	5	30	D	780
1983	6	7	78	C	1000
1983	6	12	66	B	1110
1983	7	2	42	D	780
1983	7	25	66	B	890
1983	8	24	36	D	1000
1983	9	21	96	A - B	1440
1983	10	12	54	A -D	220
1983	10	26	60	D	890
1984	2	17	30	D	890
1984	3	14	72	C	1220
1984	4	2	66	A	440
1984	6	20	36	B	560
1984	6	23	36	D	1000
1984	7	8	72	C	1500
1984	7	21	48	D	1060
1984	7	24	54	D	500
1984	11	2	24	C	500
1984	11	6	48	A	670
1984	11	7	78	D	560
1985	2	8	48	A	1550
1985	4	1	48	C	560
1985	4	20	42	A	890
1985	5	26	30	B	330
1985	6	4	84	C	1330
1985	6	23	84	A	1330
1985	8	18	42	D	1220
1985	8	30	42	A	670
1985	9	5	42	D	330
1985	10	30	90	A	1220
1985	11	27	186	C	1770
1985	12	1	54	D	670
1986	4	17	78	C	1000
1986	6	2	48	A	890
1986	6	7	48	B	560
1986	7	3	42	A	330
1986	7	7	24	A	780

University of Cape Town

YEAR	MONTH	DAY	DURATION (hours)	REGION	SIZE (km)
1986	7	23	24	A	610
1986	8	21	36	D	390
1986	8	28	66	A	1000
1986	10	11	84	D	1330
1986	10	22	48	D	1170
1986	11	23	48	D	670
1986	12	21	36	D	1000
1987	2	11	54	A	780
1987	3	26	54	B	330
1987	5	27	90	C	1330
1987	6	8	24	B	560
1987	6	12	24	A	330
1987	6	25	48	D	1220
1987	7	21	30	D	670
1987	8	25	54	B	1110
1987	9	21	42	A	890
1987	9	27	72	A - C - D	1220
1987	10	23	48	D	1000
1988	2	10	102	C	1220
1988	3	10	54	A	670
1988	4	3	66	A	1660
1988	4	16	36	C	670
1988	4	30	72	C	1440
1988	6	12	30	A	560
1988	6	26	114	A -D	1110
1988	8	27	36	A	1110
1988	9	2	24	A	220
1988	10	13	30	A	670
1988	11	25	60	C	560
1989	2	16	30	A	720
1989	3	13	60	A - B	1000
1989	4	12	36	C	1000
1989	4	18	48	B	440
1989	4	21	42	A	780
1989	4	23	78	C	1000
1989	5	10	60	D	1110
1989	6	16	60	D	1000
1989	7	16	48	D	780
1989	7	21	24	D	440
1989	8	6	60	D	1770
1989	11	15	24	A	670
1989	11	29	60	B	1110
1989	12	12	18	B	670
1990	1	10	48	B	1390
1990	2	3	48	D	1220
1990	2	7	60	B	1000
1990	2	12	42	A	780
1990	2	21	42	B	890
1990	3	20	48	B	1330
1990	4	12	48	A	1220
1990	4	21	36	A	670

University of Cape Town

YEAR	MONTH	DAY	DURATION (hours)	REGION	SIZE (km)
1990	5	14	84	D	1330
1990	10	18	60	B	830
1991	3	16	48	A	1500
1991	5	12	48	D	780
1991	6	8	48	C	1170
1991	10	10	54	D	1110
1991	10	20	36	A	1060
1992	2	27	42	A	610
1992	3	3	120	B	1330
1992	6	12	78	D	1110
1992	8	1	126	A -B - D	1330
1992	10	16	42	A	610
1992	10	23	60	A	720
1992	10	30	72	A	1110
1993	1	31	66	B	670
1993	2	28	60	D - C	1220
1993	3	23	54	B	1110
1993	4	4	36	A	890
1993	4	11	42	A	1330
1993	4	18	48	B	890
1993	4	22	48	A	1000
1993	6	11	102	B	1660
1993	7	1	114	C	1330
1993	9	2	42	D	390
1993	9	7	90	D	1440
1993	9	23	48	A	890
1994	3	6	102	A - B	1000
1994	3	20	54	B	1000
1994	4	1	36	C	1220
1994	4	19	90	A - B	1170
1994	6	10	36	A	830
1994	6	30	66	D	940
1994	7	25	30	A	1110
1994	8	4	42	B	560
1994	10	15	66	D	1110
1994	10	31	48	C	1330
1995	1	11	60	A	1330
1995	1	19	42	A	890
1995	3	16	66	D	1220
1995	3	25	30	A	440
1995	3	28	24	A	670
1995	4	6	72	D	1500
1995	5	5	66	A	1550
1995	6	15	60	B	1110
1995	9	14	42	C	940
1995	10	29	60	A	1110
1995	11	19	72	A	1170
1995	12	16	66	A	1220
1995	12	23	108	A	1330
1996	2	15	36	A	1060
1996	4	3	72	A - D	670

University of Cape Town

YEAR	MONTH	DAY	DURATION (hours)	REGION	SIZE (km)
1996	4	19	54	D	1330
1996	4	28	78	C - D	1110
1996	5	19	96	D	1990
1996	5	27	66	B	670
1996	7	7	72	B	1110
1996	7	23	78	A	1440
1996	8	3	42	A	890
1996	10	22	48	A	1330
1996	11	20	42	A	1220
1996	12	28	54	A	1110
1997	3	14	72	A	890
1997	3	26	42	A	890
1997	4	1	36	A	890
1997	4	6	96	B - C	1330
1997	5	8	72	B - D	890
1997	5	17	48	C	1110
1997	5	24	48	C	1550
1997	5	28	96	B	1220
1997	6	11	60	B	1000
1997	7	18	42	A	780
1997	8	28	30	A	1330
1997	9	13	36	B	1220
1997	10	17	36	D	330
1997	10	19	108	D	1220
1998	2	13	48	C	1390
1998	2	18	36	B	560
1998	3	26	54	A	1000
1998	11	18	30	A	1220
1999	1	26	78	D	1220
1999	4	17	54	A	890
1999	5	14	48	C	1610
1999	5	31	42	C	1500
1999	7	8	36	D	1550
2000	1	17	138	C	1000
2000	3	2	24	A	1110
2000	4	5	30	B	220
2000	4	18	72	A	890
2000	5	5	24	B	560
2000	5	12	78	A	1000
2000	5	13	24	B	560
2000	6	4	84	D	1110
2000	9	14	30	C	220
2000	10	31	72	B	1550
2000	11	14	72	B - D	1220
2000	11	16	24	A	1440
2000	11	19	66	D	890
2000	12	9	48	C	1110
2001	1	1	42	B	670
2001	4	6	24	A	610
2001	4	8	60	A	780
2001	4	12	48	D	1000

University of Cape Town

YEAR	MONTH	DAY	DURATION (hours)	REGION	SIZE (km)
2001	6	19	48	D	1220
2001	6	22	30	C	440
2001	7	20	36	B	670
2001	7	23	24	B	670
2001	8	30	24	A	560
2001	9	14	42	A	1110
2001	9	17	114	A - C	1220
2001	10	25	96	A	1880
2001	11	13	36	C	670
2001	11	19	24	A	110
2002	5	17	54	C	1110
2002	6	11	48	A	1390
2002	7	18	114	B	720
2002	8	9	60	D	1000
2002	8	16	42	A	780
2002	9	9	72	B	1500
2002	11	7	30	C	560
2002	12	5	96	D	670
2002	12	20	48	A	1060

University of Cape Town

University of Cape Town

Appendix B

Additional data and figures for the East London case

University of Cape Town

University of Cape Town

WESTERN CAPE / WES-KAAP	
BEAUFORT-WES DORP	27
BEAUFORT-WES e	20
BUFFELSFONTEIN	4
CAPE ST BLAZE	22
DE RUST	14
GEORGE WK	32
HEIDELBERG (W.Cape)	14
KNYSNA e	46
LADISMITH	7
LADISMITH e	7
MERWEVILLE	12
MOSSELBAAI/BAY	22
OUDTSHOORN	16
PLETTENBERGBAAI/BAY e	40
RIVERSDAL	23
STILBAAI	5
TSITSIKAMMA e	25
TYGERHOEK e	2
UNIONDALE	16
VAN WYKSDORP	5
VYEBOOM e	1

EASTERN CAPE / OOS-KAAP	
ADDO	79
ADELAIDE	15
ALEXANDRIA-POL	64
BATHURST	78
BISHO LUGHAWE e	14
CAPE/KAAP ST FRANCIS	46
CRADOCK	2
DOHNE	7
FORT BEAUFORT e	34
GRAAFF-REINET e	23
GRAAFF-REINET - GOODS	14
GRAHAMSTOWN e	69
GRAHAMSTOWN/STAD	84
HUMANSDORP	47
JOUBERTINA e	19
KAREEDOUW	34
KEI MOUTH/KEIMOND	19
KIDD'S BEACH	269
KIRKWOOD	69
KOMGA	8
OOS-LONDEN WK	317
PATENSIE e	60
PORT ELIZABETH WK	69
PORT ST JOHNS	2
SWARTKOPS (PE)	89
UITENHAGE e	81
WILLOWMORE	19

KWAZULU-NATAL	
CAPE/KAAP ST LUCIA	3
CATHEDRAL PEAK HOTEL	40
CEDARA	3
DURBAN WK	3
EMPANGENI	1
ESHOWE	5
ESTCOURT	7
GREYTOWN e	11
MANDINI	24
MARGATE e	2
MATATIELE	1
MT EDGECOMBE e	4
MTUNZINI e	6
PADDOCK e	2
PIETERMARITZBURG	2
PIETERMARITZBURG e	2
PORT EDWARD e	3
RICHARDS BAY e	1
ROYAL NATIONAL PARK	10
SCOTTBURGH	3
ULUNDI e	2
VAN REENEN e	7
VIRGINIA e	2
VRYHEID e	9
ZIETOVER	4

University of Cape Town

Table B1 – Rainfall totals (mm) for SAWS weather stations for the 24-hour period to 0600 UTC 16 August 2002

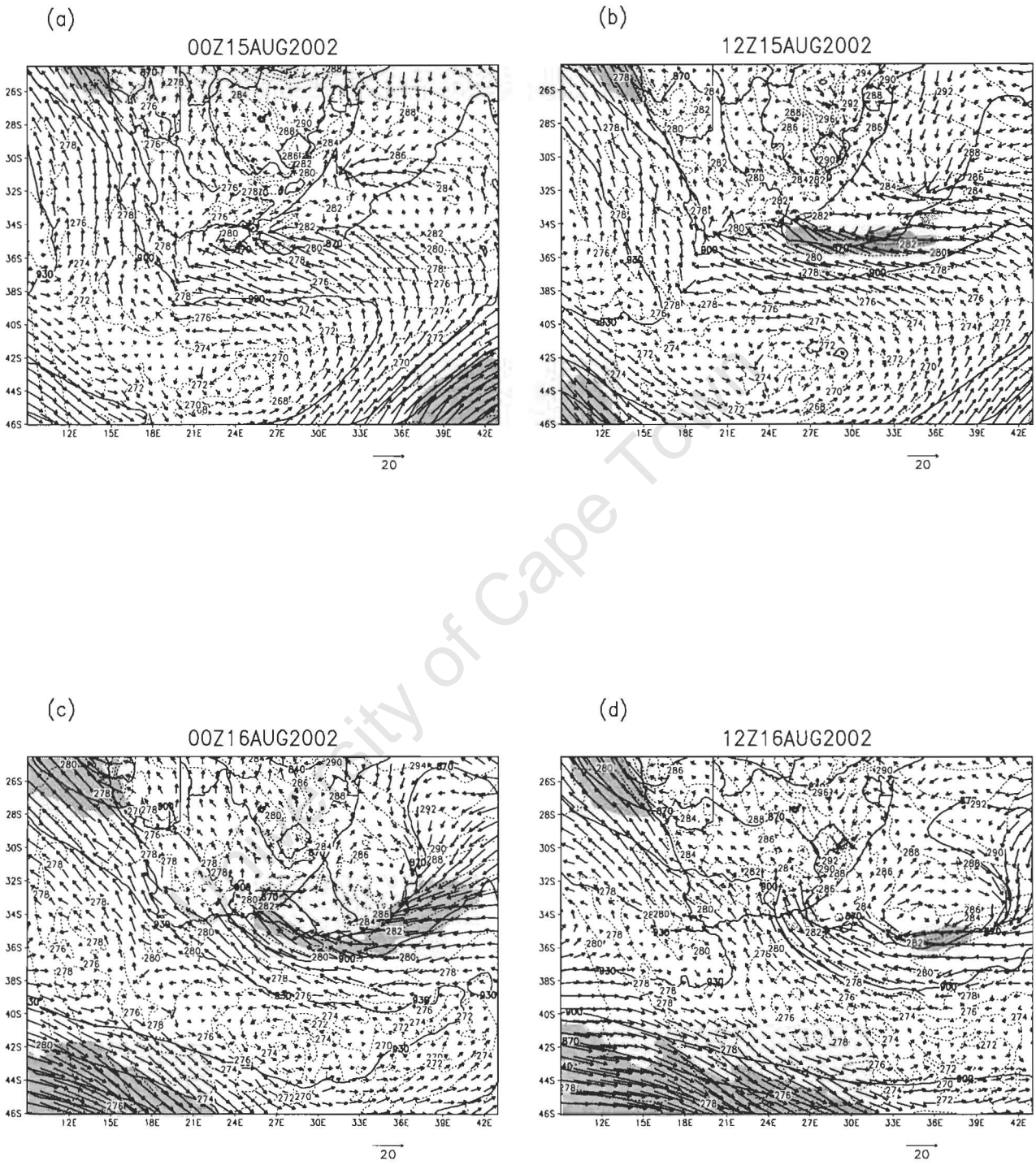

Figure B1 - 925 hPa geopotential height (solid contours, interval 30m), temperature (dashed contours, interval 2K), wind vectors (with a vector scale given to the bottom right of each panel in $m.s^{-1}$), and wind speed greater than $15m.s^{-1}$ (shading), from MRF model analyses at 12 hour intervals from (a) 0000 UTC 15 August to (d) 1200 UTC 16 August 2002

University of Cape Town

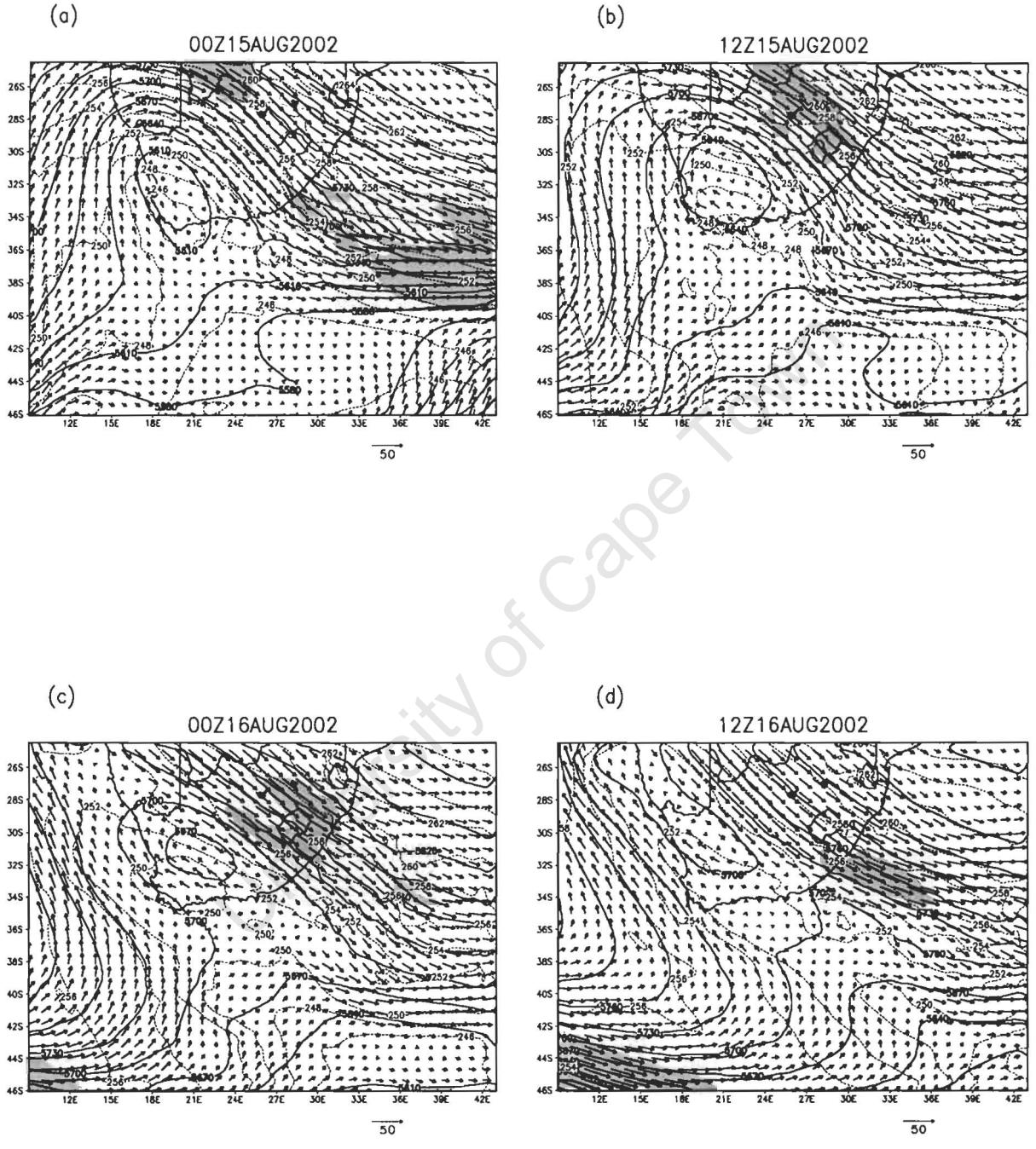

Figure B2 – As Fig. B1, except at 500 hPa, and wind speed greater than 30 $m.s^{-1}$ shaded

University of Cape Town

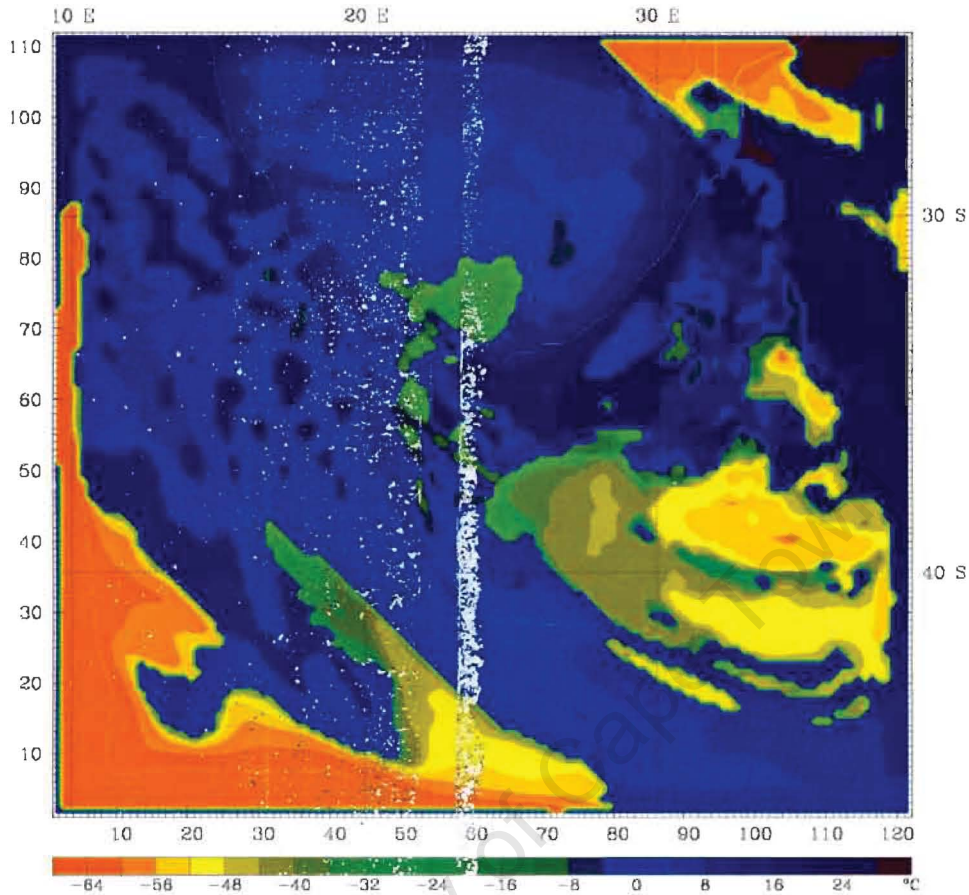

Figure C3 – cloudtop temperature from the MM5 simulation, at 0400 UTC 24 March 2003. A colour scale is given in °C below the panel.

University of Cape Town

Appendix C

Additional data and figures for the Montagu case

University of Cape Town

University of Cape Town

WESTERN CAPE / WES-KAAP	
ALGERIA FORESTRY/BOSBOU	21
BEAUFORT-WES e	17
CAPE/KAAP AGULHAS	14
CAPE POINT/KAAPPUNT	2
CAPE ST BLAZE	19
CAPE TOWN-GROOTE SCHUUR	15
CERES	2
DARLING	2
DE RUST	62
EENDEKUIL	1
GEORGE WK	128
HEIDELBERG (W.Cape)	49
HERMANUS e	12
KAAPSTAD WK	3
KLEINMOND	10
KNYSNA e	85
LADISMITH e	29
LAINGSBURG	8
LAINGSBURG e	5
LANGEBAAN	1
MALMESBURY e	2
MCGREGOR	29
MONTAGU	178
MOSSELBAAI/BAY	19
OUDTSHOORN	23
PAARL e	3
PIKETBERG	1
PLETTENBERGBAAI/BAY e	13
PORTERVILLE e	2
RIVERSDAL	34
ROBERTSON	36
SIMON'S TOWN/SIMONSTAD	4
SOMERSET-WES	10
STELLENBOSCH	20
STILBAAI	8
STRAND e	16
STRUISBAAI e	10
SWELLENDAM	54
TSITSIKAMMA e	31
TULBAGH	1
TYGERHOEK e	24
UNIONDALE	29
VAN WYKSDORP	26
VILLIERSDORP	26
VREDENBURG	3
VYEBOOM e	24
WORCESTER	12

EASTERN CAPE / OOS-KAAP	
ADDO	12
ALEXANDRIA-POL	3
ALIWAL-NOORD/NORTH	2
CAPE/KAAP ST FRANCIS	55
CRADOCK	6
GRAAFF-REINET e	5
GRAAFF-REINET - GOODS	15
HUMANSDORP	48
JOUBERTINA e	13
MIDDELBURG TNK	5
PATENSIE e	26
PORT ELIZABETH WK	19
STERKSTROOM	4
UITENHAGE e	10
WILLOWMORE	28

University of Cape Town

Table C1 – Rainfall totals (mm) for SAWS weather stations for the 24-hour period to 0600 UTC 24 March 2003.

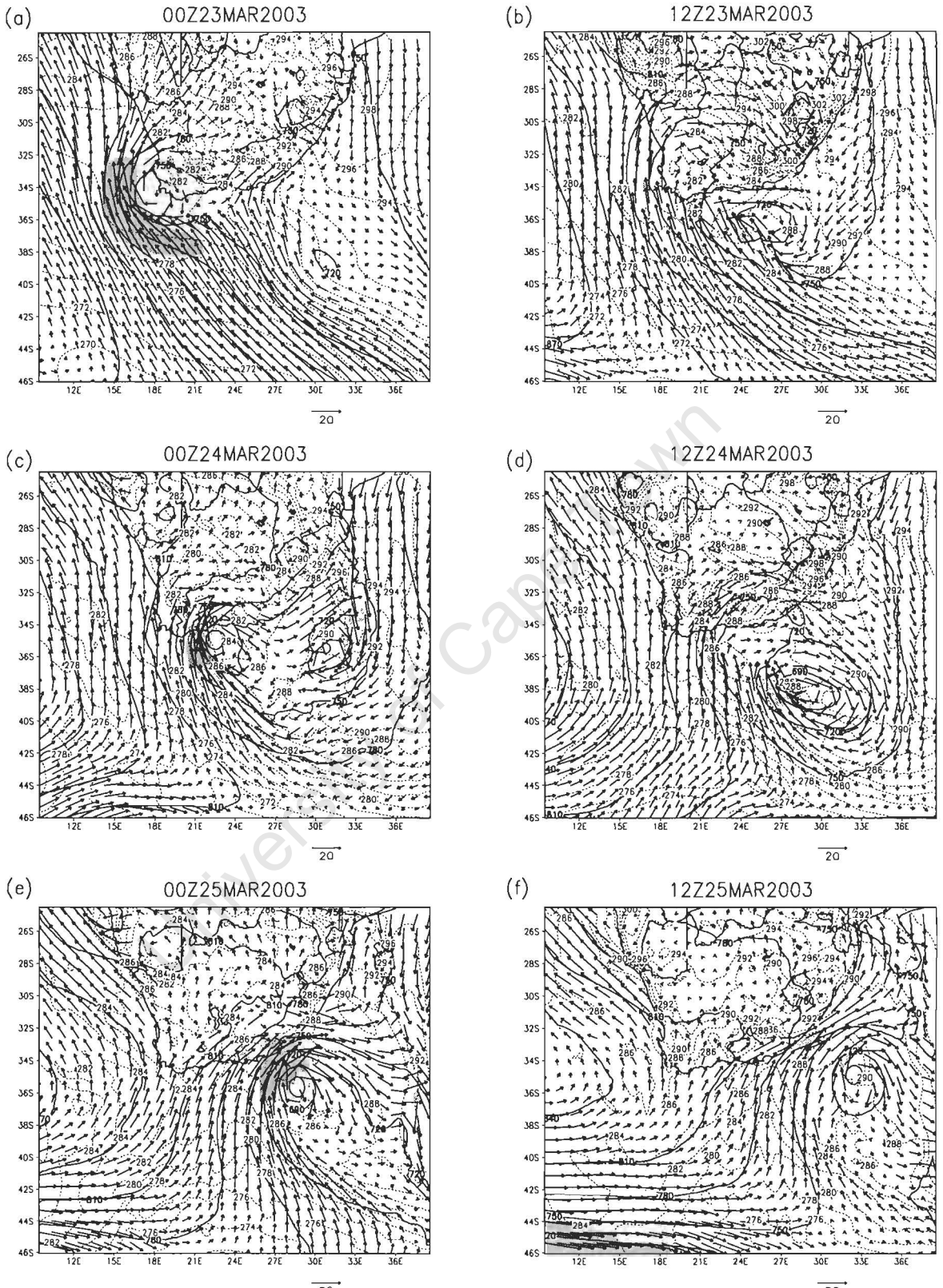

Figure C1 - 925 hPa geopotential height (solid contours, interval 30m), temperature (dashed contours, interval 2K), wind vectors (with a vector scale given to the bottom right of each panel in $m.s^{-1}$), and wind speed greater than 20 $m.s^{-1}$ (shading), from MRF model analyses at 12 hour intervals from (a) 0000 UTC 23 March to (f) 1200 UTC 25 March.

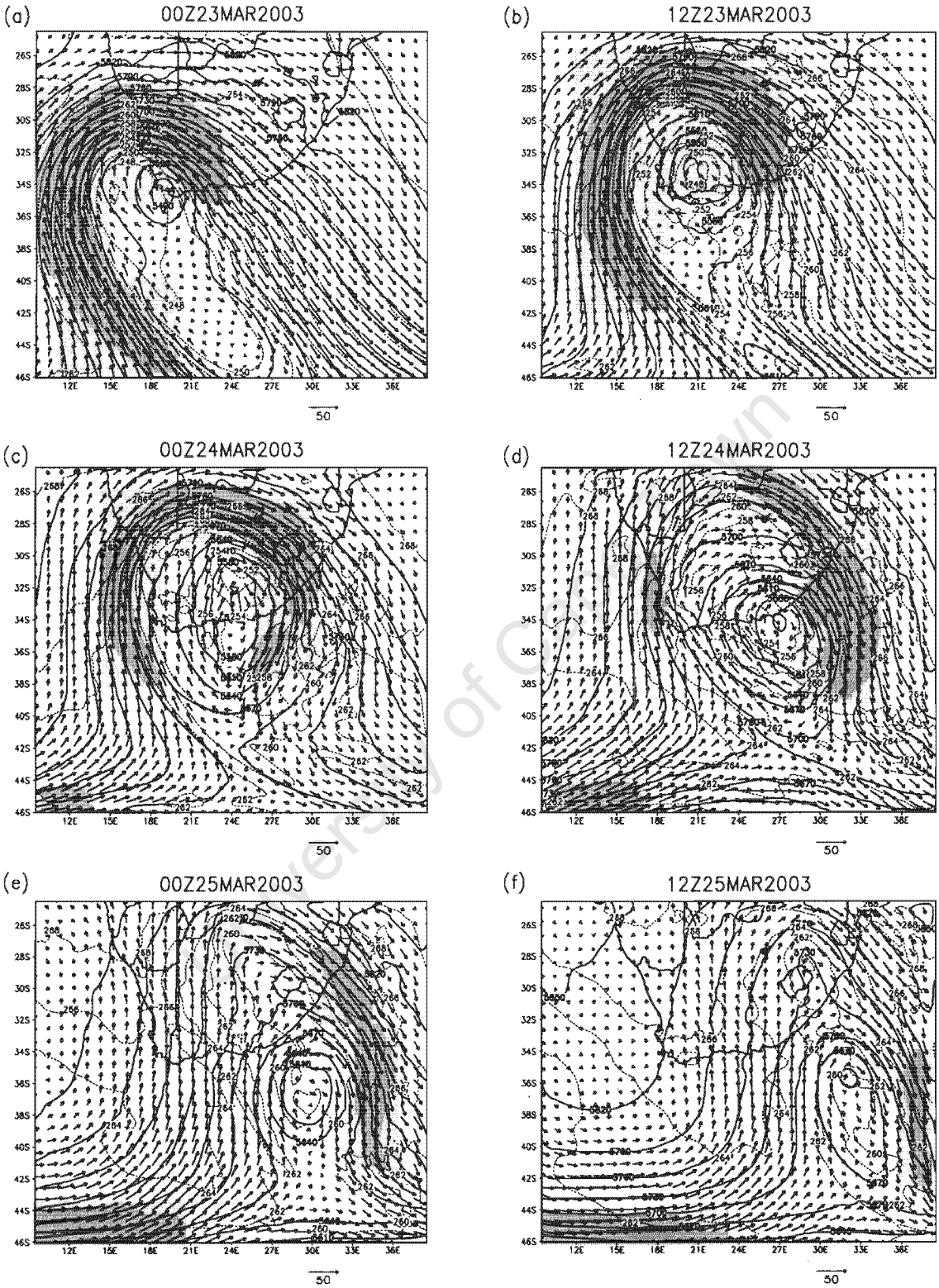

Figure C2 – As Fig. C1, except at 500 hPa, and wind speed greater than 30 $m.s^{-1}$ shaded

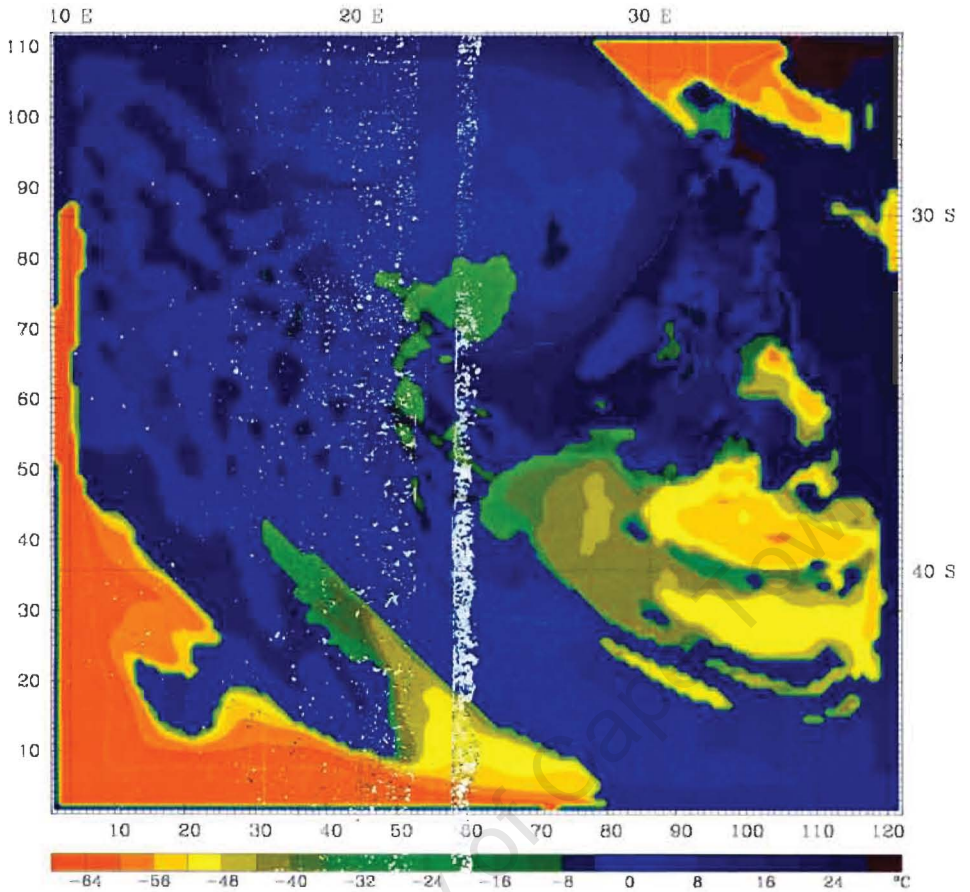

Figure C3 – cloudtop temperature from the MM5 simulation, at 0400 UTC 24 March 2003. A colour scale is given in °C below the panel.

University of Cape Town

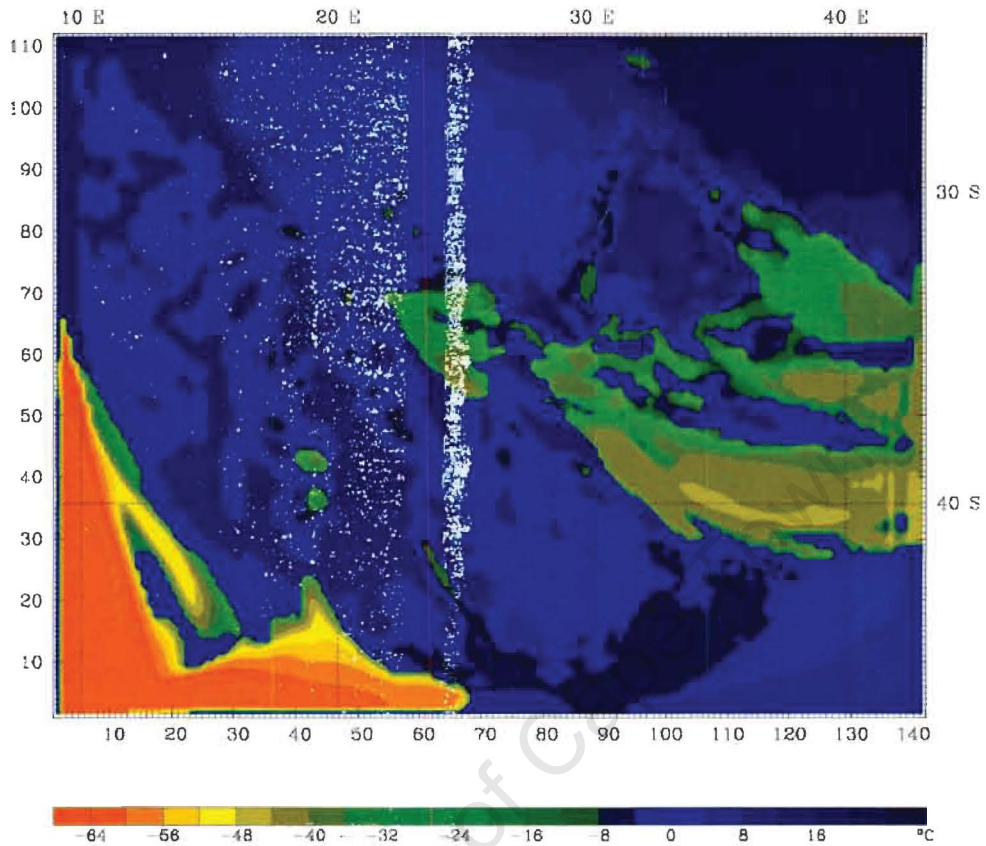

Figure B3 – cloudtop temperature from the MM5 simulation, at 0000 UTC 16 August 2002. A colour scale in °C is given below the panel.

University of Cape Town